Per Anders Eidem

Electrical Resistivity of Coke Beds

Thesis for the degree of Philosophiae Doctor

Trondheim, October 2008

Norwegian University of Science and Technology
Faculty of Natural Sciences and Technology
Department of Materials Science and Engineering

NTNU
Norwegian University of
Science and Technology

NTNU
Norwegian University of Science and Technology

Thesis for the degree of Philosophiae Doctor

Faculty of Natural Sciences and Technology
Department of Materials Science and Engineering

ISBN 978-82-471-1257-1 (printed ver.)
ISBN 978-82-471-1258-8 (electronic ver.)
ISSN 1503-8181
IMT-Report 2008:104

Doctoral theses at NTNU, 2008:279

Printed by NTNU-trykk

Preface

This work was carried out mainly at the Department of Material Science and Engineering (IMT) at the Norwegian University of Science and Technology between September 2004 and September 2008.

This work had not been possible without the support from and collaboration with a number of people and institutions to which I am forever grateful.

First of all I would like to express my gratitude towards my supervisor, Professor Merete Tangstad. From the lecture in April 2003, when she asked me if I would like to cooperate with Eramet Norway AS for my project and master thesis work, to this day she has believed in me and my work. She has inspired me and taught (or rather tried to teach) me the way of the process metallurgist and the researcher. I would also like to acknowledge her great patience, particularly during the last part of my thesis work.

After the mentioned lecture in April 2003, I went looking for a worthy supervisor. Professor Jon Arne Bakken said *yes* (although not quite that brief!). During the PhD work, Professor Em. Bakken continued as part of the steering committee. I greatly appreciated the discussions we have had, the many advices and comments he has given me. I would also like to recognize my co-supervisor Professor II Magne Runde, who introduced me to the complications of the electrical contacts, and Dr. Stein Wasbø, who also supported my work from early on and participated in the steering committee.

The cooperation with Professor Aibing B. Yu and Dr. Zongyan Zhou at Centre for Simulation and Modelling of Particulate Systems, School of Materials Science and Engineering at the University of New South Wales was very interesting. The warm welcome and good discussions during my stay at UNSW really contributed to the work.

During the PhD work the other PhD candidates, both at the department and members of DION, have contributed to my work through social gatherings and scientific discussions. I would especially like to thank Dr. Viktor Myrvågnes for the "short" coffee breaks.

Without the support form the staff and researchers at NTNU and SINTEF, particularly the experimental work would have been difficult, if not impossible. I would particularly like to give thanks to Mr. Jan Arve Baatnes, Dr. Sean Gall (SINTEF) and Mr. Steinar Prytz (SINTEF).

This work would not have been possible without the financial support from the CarboMat and ROMA projects. Through these projects SINTEF, the Norwegian Ferroalloy Producers Research Association (FFF), the Research Council of Norway and the Norwegian aluminum industry has contributed. Representatives from both Eramet Norway AS and Tinfos Jernverk AS have show support through interesting discussions.

Eramet Norway AS has, in particular, been helpful through the four years. This is gratefully acknowledged. I would also like to thank Mr. Dan Hedkvist at SSAB Tunnplåt AB for supplying large coke, and Rio Doce Manganese Norway for supplying raw materials for a pilot scale furnace experiment.

I would like to thank Ingrid Page for proofreading this thesis.

Finally I would like to thank Lina. Without your support through ups and downs, this would never have happened. I look forward to many years with time together!

Trondheim, September 2008

Per Anders Eidem

Summary

Several dig-outs of industrial submerged arc furnaces have confirmed that there is a coke bed present when producing ferromanganese (FeMn), sillicomanganese (SiMn) and ferrocromium (FeCr). The coke bed is here defined as the coke enriched area around and below the electrode tip. The coke bed is a high temperature zone, that is heated due to ohmic heating by the current flowing through the coke bed.

In the last few years, the price of metallurgical coke has increased dramatically. The ferroalloy industry, which traditionally has used only a few stable suppliers of metallurgical coke, has been forced to change the raw materials more often. As a result, there has been an increasing demand for knowledge concerning characterization of the new raw materials, and the ability to quantify the differences between them. The increased knowledge can be used to predict the effects that changing, e.g. the coke, will have on the operation of the furnace. The electrical resistivity of metallurgical coke has been the property of interest studied in this work.

The electrical resistivity of coke can be studied on several levels. The electrical resistivity of a coke bed is dependent upon the material resistivity of the coke, the particle-to-particle contact resistance and the electrical resistivity of the slag. In this work, the main focus has been on studying the dry coke bed and the fundamental mechanisms influencing the resistivity of a dry coke bed through experimental work. This has been done by developing an apparatus where the *material resistivity* and *contact resistance* of metallurgical coke can be measured at elevated temperatures. In addition, measurements were done in an established apparatus for measuring the bulk resistivity of coke, and three experiments were done in a 150 kVA one phase pilot scale furnace, studying the influence of particle size and slag on the resistivity of a coke bed.

The measurements show the general trend to be that the material resistivity, the contact resistance and the bulk resistivity decrease from room temperature to 1600°C.

The experiments show that the contact resistance is a major contributor to the bulk resistivity of a dry coke bed. The measurements show that the contact resistance contribution to the total resistance when two particles are in contact is 70-95 % at temperature up to 1400°C and approximately 50 % at 1600°C. Simulations indicate that the presence of slag reduces the particle-to-particle contact resistance. It can also be seen that the difference in bulk resistivity between different metallurgical cokes is probably due to differences in the contact resistance and not due to the material resistivity of the respective cokes. This is due to the statistical analysis not finding any significant difference between the material resistivities of the different cokes, but that there was a statistically significant difference in contact resistance. At 1600°C the typical material resistivity of the metallurgical cokes is measured as 130-150 μΩ·m. By comparison, the material resistivity of Preussang anthracite was measured as 485μΩ·m, and the material resistivity of graphite was measured to be 8.6 μΩ·m at 1600°C.

It can also be seen that the particle size is the one parameter with the strongest influence on the bulk resistivity. This is found both for the dry coke bed and for the coke bed where slag is present. The porosity analyses of the metallurgical coke indicate that the porosity of the coke increases with increasing particle size. Through literature it is known that an increasing porosity decreases the strength of the particles. A weaker particle probably leads to further crushing of the particle-to-particle contact point. A larger contact area decreases the particle-to-particle contact resistance, thus decreasing the bulk resistivity.

The results also indicate that if similar particle sizes of metallurgical cokes are compared, the bulk resistivity decreases with increasing ordering of the materials, i.e. more graphite-like material.

It can also be seen that the resistivity of a coke bed with slag can have a lower resistivity compared to a dry coke bed, depending on the electrical resistivity of the slag. The resistivity of the coke bed in the two FeMn experiments were estimated to be 1.71 - 2.2 mΩ·m and 0.95 - 1.62 mΩ·m for the experiment where Corus coke 5 - 10 mm and Corus coke 15 - 20 mm was used, respectively. By comparison, the bulk resistivity of the dry coke bed at 1600°C was measured as 4.2 mΩ·m and 3.9 mΩ·m, for the Corus coke 5 - 10 mm and 15 - 20 mm size fractions, respectively. For the SiMn experiment the coke bed resistivity was estimated to be 3.9 - 4.1 mΩ·m, which is the same as measured for the dry coke bed. The main difference between the SiMn and FeMn experiments is the electrical resistivity of the slag, which is much higher for the SiMn experiment. Simulations show that this may be due to the slag decreasing the particle-to-particle contact resistance.

Summary

Nomenclature

Symbol	Name	Notation
α	Holm's radius	m
δ	Skin depth	m
ρ	Electrical resistivity	Ω·m
ρ_{bulk}	Bulk resistivity	Ω·m
ρ_{cb}	Coke bed resistivity	Ω·m
ρ_{m}	Material resistivity	Ω·m
$\rho_{solution}$	Resistivity of a conducting solution	Ω·m
μ	Number of particle-to-particle contacts per unit area	
A,B,H	Dimensions of modelled coke bed	m
a	Coke bed shape parameter	
a_2	Material dependent parameter	
A_{cb}	Cross section area of the coke bed	m^2
$A_{conducting}$	Cross section area of the current path	m^2
A_{neck}	Cross section area of neck of sample	m^2
A_{sample}	Sample area	m^2
b	Material dependent parameter	
d	Particle diameter	m
d_{neck}	Diameter of the sample neck	m
d_{002}	Interplanar distance	Å
d_{50}	Median particle size	m
F	Force	N
f_c	Force on one particle-to-particle contact point	N
h	Height	m
h_{cb}	Electrode tip position/ distance electrode tip - metal	m
h_{sample}	Sample height	m
I	Current	A
$\mathbf{J}$	Current density vector	A
L_c	Stacking height of carbon crystal	Å

n_{array}	Number of particles in a conducting array	
N_p	Number of particle-to-particle contact points	
n'_{part}	Number of particles per unit area of mixture	
$N_{parallel}$	Number of parallel conductors in coke bed	
p	Coke bed shape parameter	
p_{bulk}	Bulk pressure	$\mathrm{kg/m^3}$
r	Particle radius	m
R_{array}	Resistance of an array of conducting particles	Ω
R'_{array}	R_{array} per unit length	$\Omega\cdot\mathrm{m^{-1}}$
R_c	Contact resistance	Ω
R_{cb}	Coke bed resistance	Ω
$R_{contact}$	Sum of contact resistances in coke bed	Ω
R_{div}	Resistance of a divided sample	Ω
r_{el}	Electrod radius	m
$R_{i,\ slag+gas}$	Resistance of the slag and gas layer i	Ω
$R_{i,coke+\ slag+gas}$	Resistance of the coke, slag and gas layer i	Ω
R_m	Resistance of one particle due to material resistivity	Ω
$R_{material}$	Sum of material resistances in coke bed	Ω
$R_{mixture}$	Resistance of a charge mixture	Ω
R_{sample}	Measured resistance of a sample	Ω
R_{tot}	Coke bed resistance	Ω
T	Temperature	°C
$type$	Type of coke (variable in regression)	
$V,\ U$	Electrical potential	V

List of Publications

P.A. Eidem, M. Tangstad, J.A. Bakken, *Measurement of Material Resistivity and Contact Resistance of Metallurgical Coke*, INFACON XI, New Delhi, India, February 18-21, 2007.

P.A. Eidem, M. Tangstad, J.A. Bakken, *Determination of Electrical Resistivity of Dry Coke Beds*, Metallurgical and Materials Transactions B, Vol. 39B, 2008.

P.A. Eidem, M. Tangstad, J.A. Bakken, *Influence of Coke Particle Size on the Electrical Resistivity of Coke Beds*, Third Nordic Symposium for Young Scientists in Metallurgy, TKK, Espoo, Finland, May 14-15, 2008.

P.A. Eidem, M. Runde, M. Tangstad, J.A. Bakken, Z.Y. Zhou and A.B. Yu, *Effect of Contact Resistance on Bulk Resistivity of Dry Coke Beds*, Accepted for publication in Metallurgical and Materials Transactions B, July 2008

Contents

Chapter 1 Introduction and Background

1.1 Background

During the production of ferromanganese (FeMn), silicomanganese (SiMn) and ferrochromium (FeCr) in a submerged arc furnace (SAF) a coke enriched area, often called the *coke bed*, is present below and around the electrode tips. The coke bed consists mostly of coke, slag, metal droplets and gas. The better part of the current passes through the coke bed where, due to the electrical resistance of the coke bed, thermal energy is developed through ohmic heating. The high temperature enables energy consuming processes to take place.

Traditionally, the Norwegian producers have used the same carbon materials over time, metallurgical coke being the most important one. Over the years, the various plants have tuned the furnace operations to a low number of steady suppliers of metallurgical coke.

Over the last few years, however, the markets have changed and the coke prices have risen, from a stable level around $ 70 to a price between $ 170 and now in the first quarter of 2008 (Q1 2008) exceeding $ 500 per tonne coke, free on

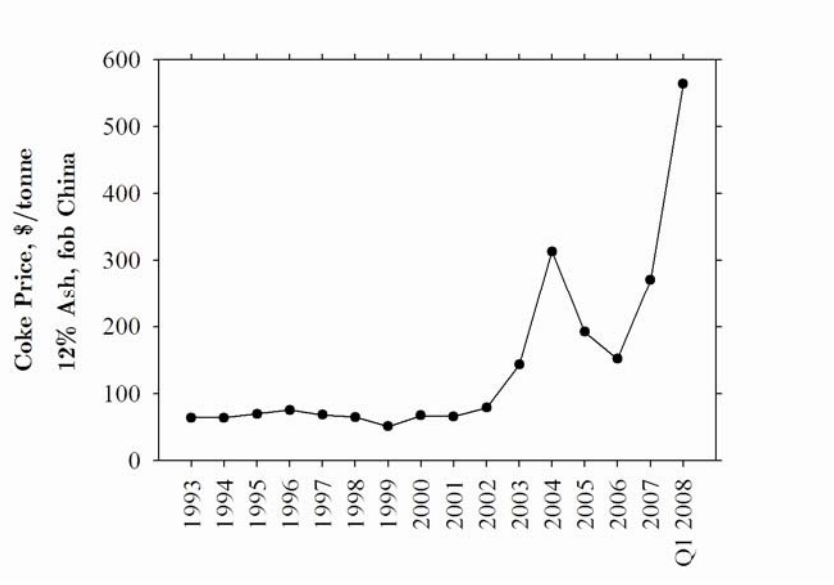

Figure 1-1: The average annual price of metallurgical coke is shown (Resource-Net 2007).

board (fob) China, see Figure 1-1. One of the main reasons for this price increase is the strong demand in developing economies such as India and China. China, which is the largest exporter of metallurgical coke in the world with a market share of approximately 50 %, controls the export of metallurgical coke through export licenses. A lack of available export licenses was accountable for the price peak observed in 2004. Other factors, such as a shortage of coking coal and increased domestic demands in Russia and the Ukraine have also influenced the coke price (Resource-Net 2007).

As a result of rising prices, the industry started to use a wider selection of carbon materials, and more knowledge was needed:

- Knowledge about properties of the materials, and the ability to specify the characteristics when buying, e.g. sizing.
- Knowledge of the effect on furnace performance when changing carbon materials.

More specifically, a knowledge of the fundamental mechanisms that determines the total resistance of an industrial coke bed was needed.

When this work started in the early 90's neither material resistivity, nor contact resistance in the high temperature region could be found in the literature, and few studies had been done on bulk resistivity of metallurgical coke. Hence, a major part of the work was developing apparatus and measuring the material resistivity and contact resistance.

1.2 Production of FeMn in a submerged arc furnace

Although a coke bed is also present in the SiMn and FeCr processes, the focus in this thesis will, for simplicity, be the FeMn process. However, the results will in most cases be relevant for all SAF processes involving a coke bed.

Previously FeMn was mainly produced in blast furnaces. But due to increasing prices and decreasing availability of metallurgical coke, more and more are produced in electrical furnaces. The size and capacities varies from small furnaces of only 3 - 8 MVA up to larger furnaces with capacities up to 90 MVA. Smaller furnaces give a more flexible production, compared to larger furnaces. The shape varies some, but in Norway the main furnace design is a circular furnace shell with three electrodes. Over the years, knowledge and technology have given a stable operation and a low energy consumption per tonne produced FeMn, on average varying between 2000 and 3000 kWh. The energy consumption is varying with charge mix and furnace operation (Olsen et al. 2007).

The energy developed in the furnace is used to melt and reduce oxides to metal. The chemical processes powered by the electrical energy added to the system can be divided into several zones (Olsen et al. 2007). These are indicated in Figure 1-2.

The raw materials are loaded at the top of the furnace. They enter the *preheating zone* where the materials are dried. The water content of the ore and coke is important for the energy consumption, as the evaporation process is endothermic. Hence, an increase of the water content will increase the energy usage (Olsen et al. 2007). In this zone there are also other low temperature

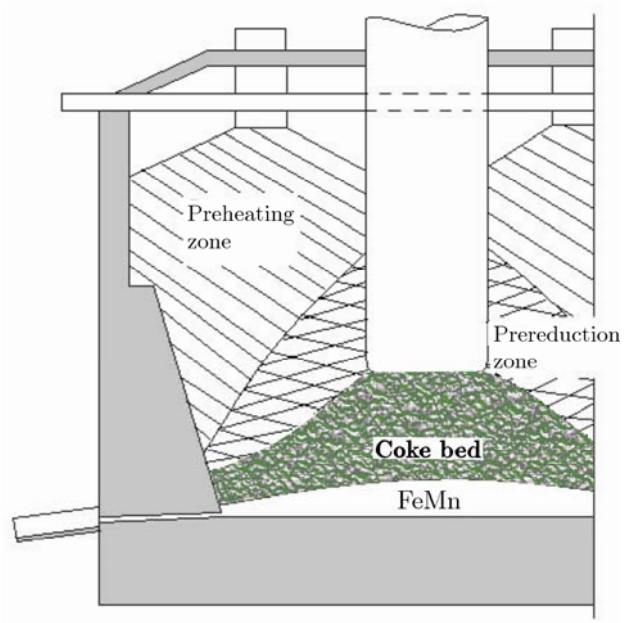

Figure 1-2: Sketch of a submerged arc furnace used for FeMn production. Based on figure in Olsen (1997).

reactions taking place. Some of the water that evaporates reacts with the CO present in the furnace gas and hydrogen is formed due to the shift reaction (1.1).

The magnesium carbonate ($MgCO_3$) in the dolomitic limestone decomposes in an endothermic reaction (1.2) and a low temperature reduction of MnO_2 takes place (1.3), which is an exothermic reaction. As a summary the following reactions occur in the preheating zone between 25°C and about 400°C. (Olsen et al. 2007)

$$H_2O(g)+CO(g)=H_2(g)+CO_2(g) \quad (1.1)$$

$$MgCO_3=MgO+CO_2(g) \quad (1.2)$$

$$2MnO_2+CO(g)=Mn_2O_3+CO_2(g) \quad (1.3)$$

Further down in the furnace, in what is often called the *prereduction zone*, the temperature rises to about 1200°C-1500°C. Further reduction of the manganese ore occurs in this area, see Equations (1.4) and (1.5). The iron in the ore may also be reduced (1.6) and the $CaCO_3$ in the dolomitic limestone decomposes, releasing CO_2 (1.7). In this zone the CO_2 both from the ore and from the

limestone starts to react with carbon in the Boudouard reaction (1.8) above 800°C. Both the decomposition of limestone and the Boudouard reaction are endothermic, and especially the Boudouard reaction is unwanted as it increases the energy use of the furnace. The reactions in the prereduction zone can be summarized by the following reactions:

$$3Mn_2O_3+CO(g)=2Mn_3O_4+CO_2(g) \quad (1.4)$$

$$Mn_3O_4+CO(g)=3MnO+CO_2(g) \quad (1.5)$$

$$Fe_3O_4+4CO(g)=3Fe+4CO_2(g) \quad (1.6)$$

$$CaCO_3=CaO+CO_2(g) \quad (1.7)$$

$$C+CO_2(g)=2CO(g) \quad (1.8)$$

The final reduction takes place in the *smelting zone* and in the coke bed. This is a high temperature zone situated below and around the electrode tip. The highly endothermic reduction of MnO (1.9) and SiO_2 (1.10) occurs in this region. Carbon is also dissolved in the metal up to carbon saturation (1.11) (Tangstad 1996).

The chemical reactions occurring in the smelting zone can be summarized as:

$$MnO(l)+C=Mn(l)+CO(g) \quad (1.9)$$

$$SiO_2+2C=Si+2CO \quad (1.10)$$

$$C=\underline{C} \quad (1.11)$$

In the three-phase SAF used in the production of FeMn a constant and high furnace load is wanted. To obtain a constant furnace load, a constant furnace resistance set point is used for the specific process. By regulating the electrode tip position up and down it is possible to maintain a constant resistance, giving a constant power output. If the resistivity of the coke bed decreases, the electrode tip position, i.e. the distance between the electrode tip and the metal bath, will increase to keep a constant furnace resistance. It is, however, not beneficial if the electrode tip is placed too high in the burden since the energy

concentration in the coke bed will decrease. A lower energy concentration will lead to a lower temperature, which again leads to a higher viscosity of the slag and metal. As a result of a higher viscosity the furnace will be difficult to tap. When producing SiMn, the composition of the tapped metal will also change due to the lower temperature when the electrode tip position is increased, increasing the carbon and decreasing the silicon content. If the electrical energy is available, an increase in the furnace load would be wanted by the producers. However, increasing the furnace load can not be done by solely increasing the electrode tip position. A possibility would be to start using carbon materials with a higher electrical resistivity. More energy can then be developed without increasing the electrode tip position.

1.3 Scope and outline of the thesis

Submerged arc furnaces are used by the Norwegian ferromanganese industry. The process is based on a coke bed where carbon is used both as a reductant and as an electrical conductor. As current flows through the coke bed, heat is generated through ohmic heating. Traditionally, metallurgical grade coke from a limited amount of suppliers has been used by the ferroalloy melting plants. With increasing coke prices and decreasing availability of good raw materials on the market, it can be an advantage not to be dependent on a small number of suppliers. To be able to change raw materials it is important to know the effect this may have on the furnace process. One question may be if the electrodes seeking down in the furnace due to the new coke having a higher bulk resistivity compared to the old one.

The main purpose of this thesis is to increase the knowledge and understanding of the parameters influencing the electrical resistivity of a coke bed, mainly by experimental work.

More specifically, the research involves development of a method for measuring the material resistivity and contact resistance of carbon materials at temperatures up to 1600°C. More measurements on bulk resistivity of carbon

materials will be done. Finally, a simple model explaining empirical observations should be developed, with special emphasis on the influence of particle size.

It is worth noting that there is a focus on industrial relevance in this thesis. The materials that will be tested in this work are industrial raw materials, with the challenges this poses to the experimental work.

The contents of the chapters of this thesis are as follows:
Chapter 2 gives a literature survey which includes: 1) Dig-outs of industrial furnaces, where the presence of a coke bed was confirmed, 2) The calculated resistivity of coke beds based on smelting resistivity experiments, 3) Measurements of the bulk resistivity of dry coke beds, i.e. with no slag, 4) Measurement of material resistivity and 5) Determination of contact resistance. The chapter also includes a section describing approaches for modeling the resistivity of a coke bed, and an introduction to contact resistance theory and electrical conduction in graphite.

Chapter 3 gives the results of the characterization of the carbon materials tested in this work. The tests include XRD, porosity, proximate analysis and analysis of the ash content.

Chapter 4 presents the apparatus developed for measuring the material resistivity and contact resistance at elevated temperatures. In this apparatus it was focused on replicating the raw material sizing used in the industrial processes. The results obtained are presented together with an evaluation of the method. Graphite has been included as a reference sample material.

Chapter 5 presents the bulk resistivity apparatus and the results from the bulk resistivity measurements. There have been two main goals for the bulk resistivity measurements:

- Determination of the bulk resistivity of on specific types of raw materials.
    a. Difference between the various groups of carbonaceous materials.
    b. Difference between the materials within the same group of material.
- Confirm the observations reported in the literature concerning particle size dependency.

Chapter 6 gives the results of three pilot scale experiments. To test the influence of the coke particle size on the bulk resistivity of the coke bed, only the coke particle size was changed between two of the three experiments, i.e. the charge mix was otherwise the same. In the third experiment SiMn was produced. The bulk resistivity of the coke bed was determined using a modeling approach.

Chapter 7 presents a simple mathematical model used to explain the electrical resistivity of a dry coke bed. The development of the model is a result of the obtained empirical data.

Chapter 2 Literature Study

As an introduction to the electrical resistivity of the coke bed, a brief presentation will be given of the basic terms used to describe the electrical conditions of a coke bed. A literature study of the experimental work will then be presented. This will include dig-outs of industrial furnaces, measurement of *bulk resistivity*, measurement of *material resistivity* and the measurement of *contact resistance*. A presentation will also be given of theoretical and modeling work that has been done; modeling of the coke bed as found in a submerged arc furnace, modeling of the dry coke bed and contact theory. Finally the production of metallurgical coke will be presented as well as a brief introduction to the conduction of electricity in graphene crystallites.

2.1 Introduction to terms describing the coke bed

Various terms have been used in the literature when describing the electrical relations in the coke bed. To avoid any misunderstanding, a brief presentation of the terms used in this thesis will be given.

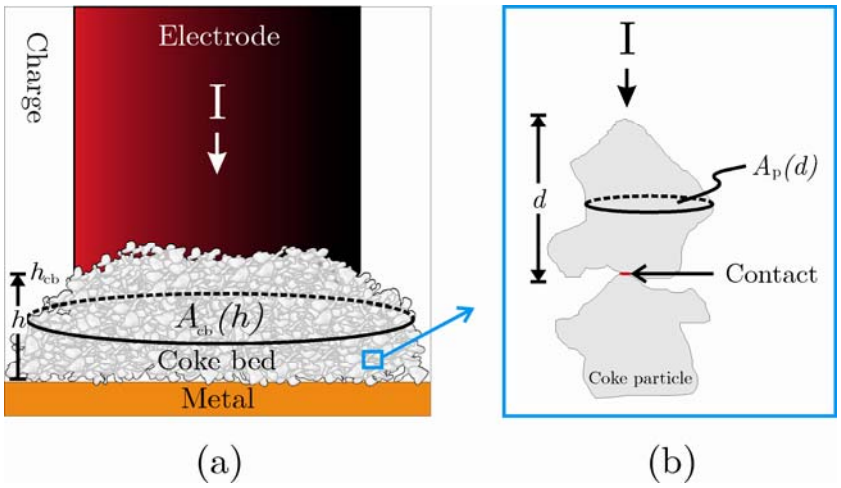

Figure 2-1: (a) The coke bed resistance is given by the *bulk resistivity* and the geometrical dimensions of the coke bed. (b) The resistance of two particles in contact is dependent on the geometry of the coke particles, the *material resistivity* and the *contact resistance.*

For an arbitrary shaped, inhomogeneous conductor, here illustrated by the coke bed in Figure 2-1 (a), the relation between the *resistance of the coke bed*, R_{cb} [Ω], and the *bulk resistivity*, ρ_{cb} [Ω·m] is:

$$R_{cb} = \int_0^{h_{\mathrm{cb}}} \frac{\rho_{\mathrm{cb}}(h)}{A_{\mathrm{cb}}(h)} dh \tag{2.1}$$

where h_{cb} is the electrode tip position, i.e. the height distance between the electrode tip and the metal, and A_{cb} is the cross section area of the coke bed normal to the current. This simplified formula assumes that the current is uniformly distributed over A_{cb}.

For simplicity the coke bed is, in this work, assumed to have a *constant resistivity*, called bulk resistivity. The *resistance* of the coke bed is then dependent on the *bulk resistivity* of the coke bed and the *geometry* of the coke bed. The *bulk resistivity* of a *dry* coke bed, i.e. a coke bed with no slag, is dependent on the geometrical shape of the coke particles, the *material resistivity* of the coke, and the particle-to-particle *contact resistance*. The latter will be presented more thoroughly in Section 2.7.3.

2.2 Dig-outs of industrial furnaces

In several submerged-arc-furnace processes, e.g. FeMn, SiMn and FeCr, a coke enriched volume of various geometrical shapes have been observed in dig-outs of the three processes mentioned above (Ando et al. 1974; Barcza et al. 1979; Yoneka et al. 1981; Ringdalen and Eilertsen 2001; Olsen and Tangstad 2004). The coke bed consists of varying amounts of coke, slag, metal droplets and gas. The coke content is varying, but in the following the term *coke bed* will be used for the coke enriched area between the electrode tip and the metal bath, where the oxides are liquid. The shape and size of the coke bed may vary from a cylinder of approximately the same diameter as the electrode, extending from the electrode tip to the metal (Ringdalen and Eilertsen 2001), to a wide coke bed stretching between the electrodes (Olsen and Tangstad 2004). The shape and size may be due to operating conditions as well as the process. In the following a selection of the excavations will be presented more thoroughly.

Barcza et al. (1979) excavated and analysed a 75 MVA *HC-FeMn* furnace. Prior to shutting down the furnace, it was not operating well. The problems were thought to be due to exchanging the original 48 MVA transformers with 75 MVA transformers without redesigning the furnace shell. After increasing the load, several burn-outs occurred. It was concluded that the current paths changed, from the original path from the electrode tip via the metal bath to the other electrodes, to a situation where the current would flow through the side walls of the furnace. During the weeks prior to the shut down of the furnace, the furnace load had to be reduced due to several electrode breaks and baking-in periods. An abnormal smelting zone was expected due to the problems experienced. The zones surrounding one of the electrodes are shown in the sketch of the furnace in Figure 2-2.

For electrode no. 1 in the 75 MVA HC-FeMn furnace the *electrode tip position*, i.e. the distance from the electrode tip to the metal bath, is 205 cm. Zone 1 is close to the electrode, and the materials in this zone descend rapidly into the coke bed zone, which is the active zone of the furnace. Zones 2 and 3 consist of

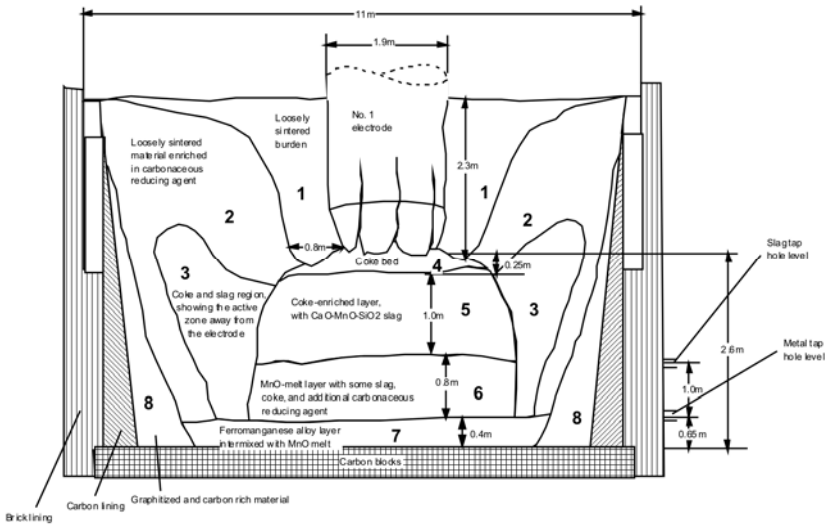

Figure 2-2: Sketch of one of the electrodes of the 75 MVA furnace excavated by Barcza et al. (1979). The zones surrounding the electrode are marked.

some slag, partly reacted raw materials and reducing agents. The material in these zones has a small velocity compared to zone 1. Zones 1 - 3 are what is previously called the preheating and prereduction zones. Zones 4, 5 and 6 are what is defined as the *coke bed* in this thesis. Zone 5 consists of slag and coke, while zone 6 consists of some slag and reducing agents and a layer of unreacted MnO, caused by the reduced furnace load. Zone 7 consists mostly of FeMn alloy, mixed with some MnO melt, slag and flakes of graphite. This dig-out shows a *bell shaped* coke bed.

The excavation of a 4 MVA, three phase, submerged arc furnace was reported by Yoneka et al. (1981). The *FeMn* furnace was operated for about one year with an average furnace load of approximately 2.5 MW. The operating conditions were good during the operating period. A furnace section is shown in Figure 2-3. The electrode tip position for all the electrodes is 130 cm. Zone A consists of Mn ore, lime and coke, and the height, H_1, is approximately 160 cm at the center of the furnace. This zone is what has been called the preheating and prereduction zone. Zones B, C and D are included in what is called the coke bed in this thesis. The height at H_2 is 75 cm. The size of the coke particles decrease down, from the top of zone B to zone D, which consists of pure slag. The metal bath is found at the bottom of the furnace, marked E. The shape of

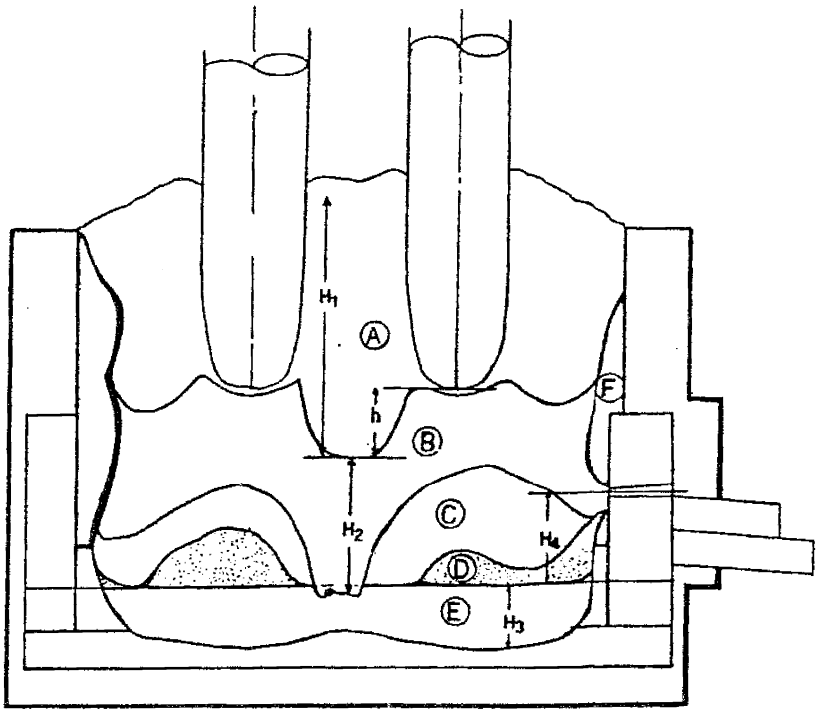

Figure 2-3: Sketch of a section of the furnace dig-out presented by Yoneka et al. (1981).

zone A, where there is a depression in the center of the furnace, is said to be due to the height and weight of the charge materials. The height of zone A is also thought to have an effect on the electrode tip position, where an increasing charge height gives an unwanted increase in the electrode tip position.

The furnace shown in Figure 2-4 is based on excavations of a three phase 16 MW furnace producing *SiMn*. The operating conditions were relatively good prior to shut down, with an operating time above 95 % and a furnace load above 15 MW. The power was turned off two thirds into a tapping cycle. The electrode tip position of the three electrodes was 60, 110 and 50 cm above the metal bath for electrode A, B and C respectively. Due to the good operating conditions it is assumed that an appropriate electrode tip position would be about 60 cm above the metal bath. It seems that an excess of coke in the furnace has lead to an accumulation of coke around electrode B, thereby increasing the electrode tip position. Zones consisting of almost only slag were found beneath the three electrodes. (Olsen and Tangstad 2004) These slag zones have

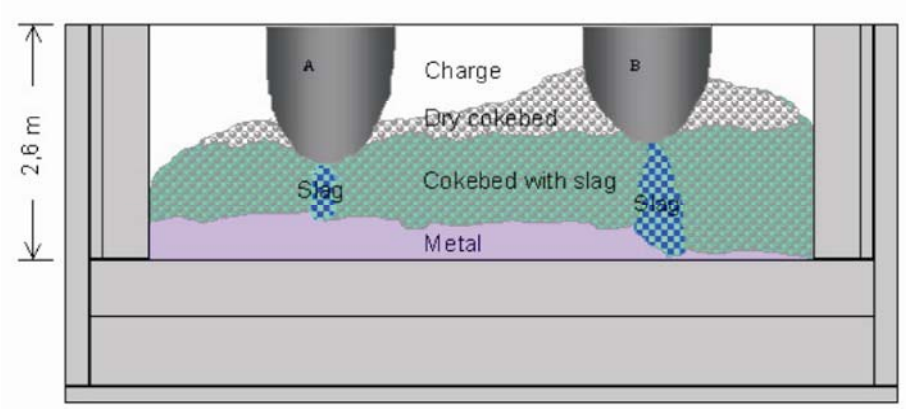

Figure 2-4: The dig-out of this 16 MW SiMn furnace revealed a wide coke bed (Olsen and Tangstad 2004).

been observed previously for FeMn production, both industrially and in pilot scale experiments (Tangstad 1996)

Some dig-outs have been done on FeCr furnaces as well. The FeCr process is, as mentioned, also a coke bed process with slag present. The observations done during the dig-out of a 54 MVA FeCr furnace at Elkem Rana (Ringdalen 1999), which are summarized in Figure 2-5, can therefore be of interest. During the time prior to shut down the furnace had very good operation, and the furnace was shut down fifteen minutes after the last tapping. The dig-out showed that the distance between the electrode tip and the metal bath, the electrode tip position, was between 50 and 80 cm, varying between the electrodes. A small cavity of approximately 5 to 10 cm was observed between the electrodes and the respective coke beds. Ringdalen (1999) does not speculate whether or not the cavity was present during operation. The coke bed had, as indicated in Figure 2-5, a cylindrical shape, with a diameter approximately the same as the electrode, i.e. 1.5 meters. The main composition of the coke bed was 50 to 70 volume % coke, mixed with slag, metal, partly reduced chromite and some lumps of quartz, but the approximately top 5 cm of the coke bed was dry coke. In between the coke beds and electrodes there were loose charge, i.e. the coke beds were not connected.

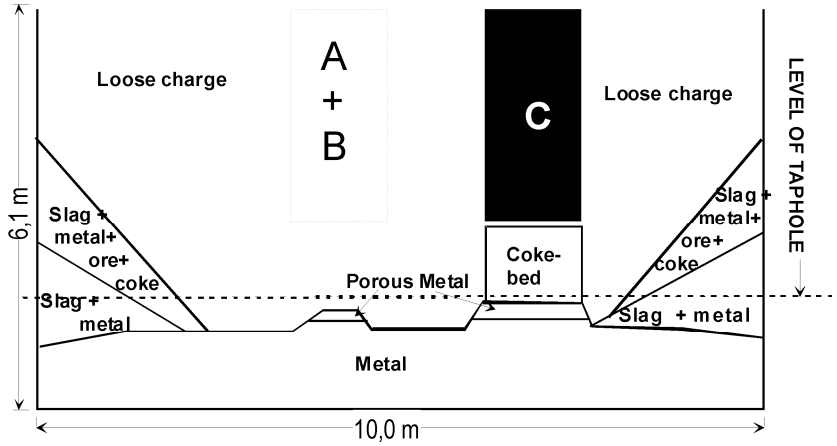

Figure 2-5: Idealized sketch based on the observations done during the dig-out of a 54 MVA FeCr furnace at Elkem Rana (Ringdalen 1999).

The geometrical shape of the coke beds observed in the four dig-outs presented in this section vary from a continuous coke bed connecting the three electrodes (Yoneka et al. 1981; Olsen and Tangstad 2004), via bell shaped (Barcza et al. 1979), to a cylindrical shaped coke bed (Ringdalen 1999). In both of the FeMn furnaces and in the SiMn furnace slag zones were observed in the coke bed. Barcza et al. (1979) comments that the MnO-melt layer observed in the 75 MVA furnace may be due to the poor operating conditions of the furnace prior to shut down. For the 16 MW SiMn furnace (Olsen and Tangstad 2004) and the 2.5 MW FeMn furnace (Yoneka et al. 1981) the slag zones are situated between the electrode tip and the metal bath. For the 16 MW SiMn furnace, which has the lowest coke bed of the two, the slag zone stretches from the electrode tip down to the metal. For the 2.5 MW FeMn furnace the slag zone makes a small cupola on top of the metal bath, right below the electrode tip. The slag zone may be caused by the pressure from the charge being lower below the electrode tips.

The variation in geometrical shape may have been influenced by several factors such as type of process, furnace size and operating conditions. The four dig-outs represent three different coke bed processes, FeMn, SiMn and FeCr. The temperature required is higher from the SiMn compared to the FeMn process,

and even higher for the FeCr, the latter being due to the high melting point of the ore. Due to the higher process temperature it may be assumed that the energy density has to be higher for FeCr compared to SiMn and for SiMn compared to FeMn. This can be achieved by keeping a low electrode tip position, i.e. a smaller volume through which the current flows. Prior to shut down the furnaces have had operating conditions varying from poor (Barcza et al. 1979) to very good (Ringdalen 1999). Barcza et al. (1979) comments that an enlarged coke bed zone was expected due to the poor operating conditions experienced prior to shut down. The three dig-outs representing furnaces that has had good operating conditions prior to shut down, do show a wide range of geometrical shapes and electrode tip positions. Olsen and Tangstad (2004) concludes that an ideal electrode tip position in that specific case would be 60 cm, and that a surplus of coke in the charge mix has given an elevated electrode tip position of electrode B in the 16 MW SiMn furnace. Ringdalen (1999) observed the coke bed that was smallest relative to the electrode size, and found a small cavity between the electrode tip and the coke bed. Ringdalen (1999) did not speculated whether or not the cavity was present during operation.

It is known that the amount of harmonics give an indication of the presence of an arc. The content of harmonics is, very simplified, the integral of the power spectrum above 130 Hz relative to the integral of the whole power spectrum. (Wasbø 1996) During normal operation of a FeMn or SiMn furnace, the amount of harmonics measured is far below the amount experienced during production of FeSi or Si, which are processes known to have an arc present (Ringdalen 2008). This is also supported by Wasbø (1996), who, based on the measurement of harmonics, found that some arcing occurs when the electrode tip position is raised from the coke bed. The content of harmonics registered varied, and it was speculated that this was due to the electrode tip position in relation to the top of the coke bed. Regulating the electrode tip position within the coke bed give less harmonics compared to raising the electrode tip above the coke bed. It was also observed that the amount of harmonics would decrease with time after the electrode was raised. This observation lead to the conclusion that the cavity

formed when the electrode was raised would be filled with new material, leading to a decrease of the observed harmonics to the normal level of 1 - 2 %.

Based on the presented dig-outs it is difficult, if not impossible, to conclude on the optimal coke bed shape or size. No cavity has been observed for any of the Mn-processes. This leads to the conclusion that there is no large arc involved in the process, despite the misleading name of the furnace.

As a summary of the main conclusions concerning the electrical relations in the coke bed the following points are worth noticing:

1. A coke bed was located in all dig-outs[1-5], and there are no signs indicating an arc in a gas filled cavity beneath the electrode such as is found in a SAF where Si is produced. (Ringdalen 2008).
2. The shape and size of the coke bed varies considerably depending on factors such as type of process, raw materials and operating conditions.
3. The authors that commented on the electrode tip position, agreed that it is not beneficial with a too high electrode tip position, as the concentration of energy goes down[2,3,5]. A surplus of coke in the furnace can cause a buildup of the coke beds, leading to an unwanted increase in the electrode tip position (Olsen and Tangstad 2004). An ideal position is determined by factors such as the type of process, raw materials and size of furnace.

2.3 Pilot scale experiments

A one electrode submerged arc furnace with a 150 kVA transformer has been used for several FeMn and SiMn experiments. After the experiments the furnace

---

[1] (Ando et al. 1974) [2] (Barcza et al. 1979) [3] (Olsen and Tangstad 2004) [4] (Ringdalen 1999) [5] (Yoneka et al. 1981) [6] (Tucker et al. 1907) [7] (Downing and Urban 1966) [8] (Lorenz and Marincek 1969) [9] (Rennie 1975) [10] (Willand 1975) [11] (Dijs et al. 1979) [12] (Bakken and Wærnes 1980) [13] (Dijs and Smith 1980) [14] (Bakken and Wærnes 1986) [15] (Miyauchi et al. 2001) [16] (Olsen 2003) [17] (Olsen and Eidem 2003) [18] (Miyauchi et al. 2004) [19] (Olsen 2004) [20] (Krogerus et al. 2006) [21] (Woollacott et al. 1975) [22] (Segers et al. 1983) [23] (Eric et al. 1991)

was cooled and cast in epoxy. A polished vertical cross section of the furnace has then been studied with respect to various aspects such as the degree of prereduction and coke bed shape. A further description of the furnace and method is given in Chapter 6. Only the results concerning the electrical conditions of the work by Tangstad (2001) and Røhmen (2002) will be presented here.

The reported experiments used an operating strategy where the electrode tip position and furnace load was kept constant. The latter was obtained by regulating the transformer voltage.

Both Tangstad (2001) and Røhmen (2002), studying SiMn and FeMn respectively, report an increase in resistance at the point of tapping, and a decrease in resistance towards the next tapping. The increase in resistance during tapping is explained by cold and consequently less conducting material entering the hot zone when slag is tapped out of the furnace. Wasbø (1996) speculates that similar observations for an industrial furnace can be due to the slag resistivity being lower compared to the coke resistivity, and thus the slag being the main conductor in the coke bed.

Based on the cross sections of the respective experiments Tangstad (2001) and Rhømen (2002) estimated the coke bed resistivity by dividing the coke bed into several horizontal slices. The coke bed was divided into two main parts with different resistivity; the upper part, consisting of mainly coke, and the lower part where slag and coke is mixed. The coke bed had an inconstant resistivity due to the division of the coke bed. The resistivity of the upper part of the coke bed, i.e. the part of the coke bed consisting of mainly coke, was assumed to be 2.5 mΩ·m. Tangstad (2001) estimated the resistivity of the lower part of the coke bed, where coke and slag is mixed, to be 7.5 mΩ·m for the SiMn process. Røhmen (2002), who studied FeMn, calculates the resistivity of the slag and coke mix to be between 1.20 mΩ·m and 3.40 mΩ·m, which is approximately the same resistivity as the top part of the coke bed consisting of mainly dry coke.

2.4 Bulk resistivity measurements

Several investigations have been done on the electrical resistivity of both *dry* coke beds[6-20], charge mixes[9-15,18,20] and of the Mn-related slags[7,21-23]. These investigations have been valuable in understanding how the *bulk resistivity* of the coke bed is affected by various factors such as temperature, type of carbonaceous material and particle size. In this thesis the main focus is, however, on the dry coke bed.

The main differences between the previously reported methods for measuring the *bulk resistivity* of the *dry coke beds* are the means of heating the coke sample and the particle sizes studied. The heating was either done indirectly[7,8,10-15,18,20] by means of an external heat source or by running a sufficiently high current to accomplish ohmic heating of the coke bed sample[6,9,16,17,19]. The particle sizes ranged from industrial sized materials with a particle diameter between 6 and 30 mm[9,10,12,14,16,17,19,20] and smaller sized, often crushed, material[6-8,11,13,15,18]. The experiments were all performed at elevated temperatures, with a maximum temperature between 1400°C and 1600°C. Extensive work has also been done at room temperature, see e.g. Dijs et al. (1979), Dijs and Smith (1980) and Willand (1975). The external mechanical pressure applied on top of the coke bed has also varied, from no added external force (Downing and Urban 1966), i.e., only the weight of the sample material, to about 250 kg added on to a 0.07 m^2 surface (Olsen 2003; Olsen 2004). Olsen (2004) varied the mechanical pressure on the coke bed from 2830 to 3540 kg/m^2 without being able to see any correlation between pressure and electrical resistivity. It may, however, be that the variation in pressure was not large enough to get any large variation in resistivity due to the pressure.

Many authors[7,9,11-20] have reported that as a general trend for different carbon materials that resistivity decreases with increasing temperature. Examples from three studies which illustrate this can be seen in Figure 2-6. In the matter of particle size dependency for packed beds containing solely coke, Bakken and Wærnes (1986) report an increasing resistivity with increasing particle size,

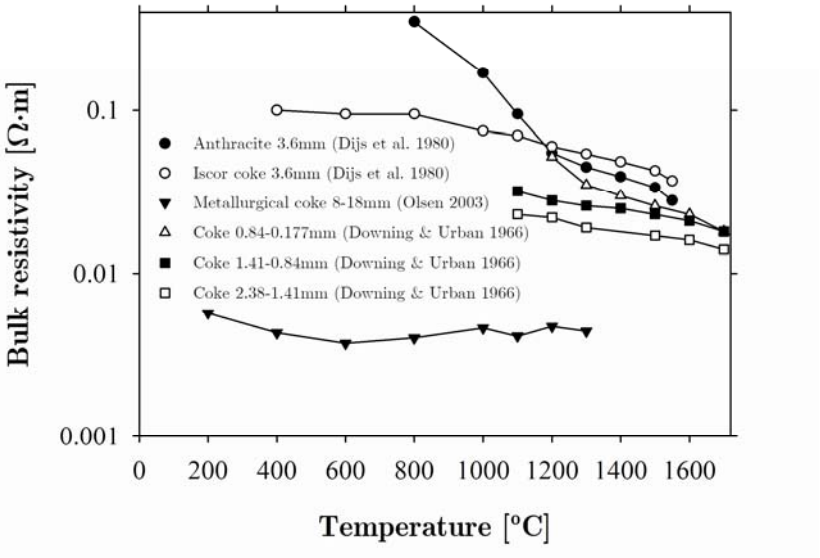

Figure 2-6: Examples of bulk resistivity measurements found in the literature.

while others[7,8,10,11,13,20] report the opposite. In Figure 2-6 the results from three particle sizes tested by Downing and Urban (1966) can be seen, showing a decreasing bulk resistivity with decreasing particle size at temperatures between 1100°C and 1700°C. Dijs et al. (1979) and Dijs and Smith (1980) report that increasing the amount of volatile matter increases the resistivity.

There are also standard ways of measuring the resistivity of the materials, such as the measurement of electrical resistivity of coke used in electrodes for aluminum production (ISO 10143 1995). In this standard test, the coke is crushed and sieved into a fraction of 0.5 to 1.0 mm. The coke is then washed, dried and placed in a cylindrical holder with electrical contacts at the top and bottom. A pressure of 3 MPa is applied. The compression and the voltage drop over the sample height are recorded. The measurement is done at room temperature.

2.5 Material resistivity

In a coke bed the single particle is the smallest unit. The coke particle is made up of a material, which influences the resistance of the coke particle. Typical values of some materials are given in Table 2-1. Some of the materials are not

Table 2-1: Resistivity of various materials at room temperature. (Speight 1994; Askeland 1998)

Material	Resistivity [Ω·m]
Ag*	$1.59 \cdot 10^{-8}$
Cu*	$1.67 \cdot 10^{-8}$
Au*	$2.35 \cdot 10^{-8}$
Al*	$2.65 \cdot 10^{-8}$
Fe*	$9.71 \cdot 10^{-8}$
Graphite*	$(0.8 - 1.0) \cdot 10^{-5}$
Graphite†	$4 \cdot 10^{-5}$
Anthracite, parallel to bedding†	70-900
Anthracite, perpendicular to bedding†	170-340
Bituminous coal, parallel to bedding†	$(0.004\text{-}360) \cdot 10^{6}$
Bituminous coal, perpendicular to bedding†	$(3.1\text{-}530) \cdot 10^{7}$
Brown coal, 20-25 % H_2O	10^{2}
Brown coal, dry	10^{8}-10^{11}

*(Askeland 1998, pp. 620) †(Speight 1994, pp. 229)

homogenous and have different resistivity depending on how it is measured in relation to the microstructure of the material.

In a standard material resistivity test, one piece of test material of a given geometrical shape is used. The resistivity measured includes the effect of pores and cracks that may be naturally present in the material. For materials that are delivered in large blocks of relatively homogeneous material, like metals and graphites, this is fairly trivial to do at room temperature using the principle of the *four point measurement*, see Appendix 4. For anode and cathode carbon material this is standardized, e.g. ASTM D 6120-97 (2007b).

Ukanakov et al. (1973) measured the *material* resistivity of metallurgical coke at room temperature. The four-point-measurement technique was used. The samples were prepared from coke particles 25-40 mm in diameter. The average material resistivity of the three metallurgical cokes tested, cokes from Kemerovo, Kuznetsk and West Siberia, were almost identical, with material resistivity of 0.125, 0.121 and 0.127 Ω·m, respectively. A considerable variation in the results

was, however, observed. The range of measured material resistivity of the coke would be typically in the range from 0.09 Ω·m to 0.29 Ω·m, with approximately 60 % to 80 % of the observations between 0.09 Ω·m and 0.16 Ω·m.

Sørlie and Gran (1992) demonstrated how the material resistivity of samples of cathode material for aluminum production could be measured up to 1000°C. The method used is a modified version of that described in ASTM D 6120-97 . Sørlie and Gran (1992) uses a sample diameter of 60 mm, and the ASTM standard calls for a 50 mm sample diameter. Three types of cathode blocks were tested, two that were based on electrocalcined anthracite and one that was graphitic. The material resistivity of the electrocalcined anthracite was measured to be 0.034 mΩ·m and 0.042 mΩ·m at 1000°C. One type of prebaked carbon block that was characterized as graphitic had a material resistivity measured as 9.0 μΩ·m, both at room temperature and at 1000°C.

Several graphite electrode manufacturers have published data on the electrical properties at high temperatures of their respective products. The methods used to do the measurements are, unfortunately, proprietary information.

2.6 Contact resistance

The contact resistance can be estimated by measuring the potential drop over two sample bodies. These should be in contact, and should be made from materials of known material resistivities. By subtracting the calculated contribution of the material resistance from the total measured resistance, the contact resistance is estimated. This method was used by Sørlie and Gran (1992) to determine the contact resistance between the collector bar and the cathode used in aluminum cells up to 1000°C. The carbon sample was mounted between two pieces of collector bar in a vertical tube furnace with an operating temperature up to 1000°C. The furnace and sample was then mounted in a universal testing machine so that the force on the sample could be varied. The temperature was recorded inside the carbon sample, which was 60 mm in diameter and 100 mm high, and the potential drop was measured by a two iron

wires mounted on to the steel collector bar samples at either side of the carbon sample. The iron wires were mounted at two levels of the carbon sample, 15 mm from the two steel-carbon contact interfaces. From the measurements, both the material resistivity and the contact resistance were calculated.

Sørlie and Gran (1992) report that the contact resistance measurements show a strong decrease in contact resistance with increasing temperature and contact pressure. The steel-to-carbon contact resistance at 975°C varies from 350 μΩ when 0.1 MPa is applied, to approximately 28 μΩ when 10 MPa is applied.

2.7 Modeling and theory

2.7.1 Modeling of current paths in the submerged arc furnace

The significance of the coke bed as the high energy zone in the furnace is largely dependent on the current flowing through the coke bed. This problem has previously been assessed by Dhainaut (2004) and Healy (1991). These two works will briefly be presented below.

The results from the simulations by Dhainaut (2004) are displayed in Figure 2-7. The computation is not time-dependent, but a "snapshot" at the instant of time where voltage at one electrode is +100 V and the voltage of the other two electrodes are -50 V. The resistivity for the 1500°C zone represents the coke bed, which is assumed to have the same resistivity as a dry coke bed, 6.7 mΩm. The electrical resistivity of the charge mix, relative to the resistivity of dry coke, at the respective temperatures indicated in Figure 2-7, have been taken from Miyauchi et al. (2001). The resistivity for the 1200°C, 800°C and 400°C zones are assumed to be 10 times, 100 times and 2000 times higher than the resistivity of the coke bed, respectively. The simulation looks at two situations where the electrode tip position, i.e. the distance between the electrode tip and the metal bath, is 1 m and 3 m. The coke bed height is adjusted accordingly. The simulation results shown in Figure 2-7 indicate that more than 95 % of the current flows through the coke bed zone, and just a minor part flow through the

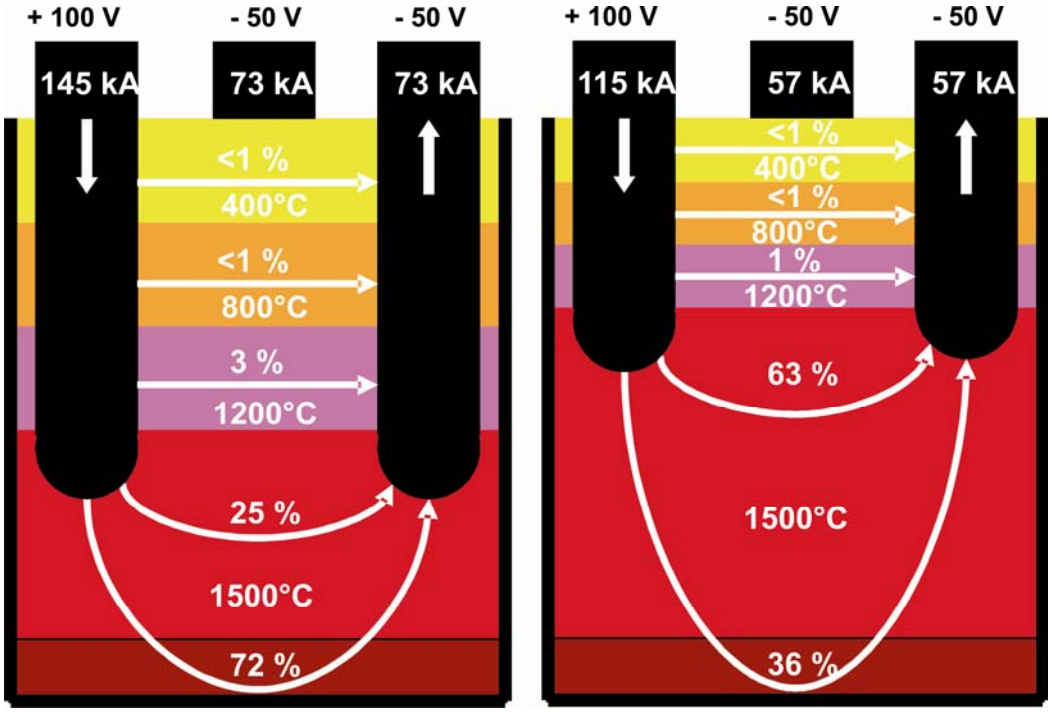

Figure 2-7: The simulations show that more than 90 % of the current flows through what is here defined as the coke bed area (Dhainaut 2004).

colder charge materials higher up in the furnace. According to Dhainaut (2004) the calculated total electrode resistance, 0.7 and 0.9 mΩ respectively, is within the order of magnitude observed for industrial submerged arc furnaces producing FeMn.

Healy (1991) studied the conduction through the charge materials in a SAF, from the electrode to the top of the coke bed. The current is assumed to flow through concentric hemispherical shells. The electrode runs through the center of the shells, from the top of the mix, down to the coke bed. Based on measurements by Dijs (1979) three bulk resistivities of the charge was used for the calculations, 0.05 Ω·m, 0.10 Ω·m and 0.20 Ω·m, of which the two first is the range observed by Dijs for a charge mix containing 50 volume % coke. The electrode to electrode voltage is set to 132 V, and the electrode to metal voltage drop is set to 66 V. The results of the calculations show that a charge resistivity of 0.05 Ω·m, 0.10 Ω·m and 0.20 Ω·m give a relative charge current of 20, 10 and 5 % of the total current, respectively.

The charge mix resistivity used by Healy (1991) is of the same order of magnitude as that used by Dhainaut (2002) for the 1200°C zone. The calculated relative amount of current flowing through the charge is higher according to Healy (1991), compared to the results obtained by Dhainaut (2002). This is probably partly due to the complexity of the calculations used, and partly due to the bulk resistivities used in the calculations, the latter being the most important. Results obtained by Healy (1991) show how a variation in the charge mix bulk resistivity significantly influences the calculated current paths. Both results does, however, show that the major part of the current flows through the coke bed zone.

2.7.2 Modeling of the coke bed zone

In the work concerning the modeling of the current paths in the submerged arc furnace the bulk resistivity of the charge mix and coke bed was set. No attention was paid to how the structure of the coke bed, i.e. packing and sizing of the raw materials, would influence the bulk resistivity, and thus the furnace resistance. In this section two models including structural parameters are presented. First, Wasbø (1996, pp. 141-158) models the coke bed by including factors such as the geometry of the coke bed, coke particle size and the resistivities of the coke, slag and gas. The second model presented, is the model by Dijs et al. (1979) and Dijs and Smith (1980), which describes the resistivity of a charge mix consisting of conduction and non-conducting particles. The model may also be used on dry coke beds.

As previously presented, the resistance R_{cb} of a coke bed of height equal to the electrode tip position h_{cb}, cross section A_{cb}, and resistivity ρ_{cb} can be expressed as shown in Equation (2.1). The current is assumed to be uniformly distributed over the cross section A_{cb}.

$$R_{cb} = \int_0^{h_{\mathrm{cb}}} \frac{\rho_{\mathrm{cb}}(h)}{A_{\mathrm{cb}}(h)} dh \tag{2.1}$$

Wasbø (1996) describes the electrode radius as a function of the coke bed height, as shown in Equation (2.2). The height is, however, increasing from the electrode down to the metal, i.e. the height at the electrode tip is 0 m, and at the metal bath h_{cb}. The radius of the coke bed at any coke bed height h is given by:

$$r = r_{el} + ah^{p} \tag{2.2}$$

where

r_{el} : Electrode radius

$a,\ p$: Coke bed shape parameters

Assuming a coke bed that is symmetrical around the z-axis, the area of any given slice of the coke bed will be:

$$A_{cb}(h) = \pi r(h)^2 \tag{2.3}$$

By combination of the equations above one gets:

$$R_{cb} = \int_{0}^{h_{cb}} \frac{\rho(h)}{\pi\left(r_{el} + ah^{p}\right)^2} dh \tag{2.4}$$

Some typical coke bed shapes were simulated by Wasbø (1996). The parameters determining the shape of the coke beds are given in Table 2-2. The geometrical shapes are plotted in Figure 2-8. Assuming a constant resistivity throughout the coke bed, the coke bed resistance will decrease with decreasing p and increasing a.

The *structure* of the coke bed, i.e. the arrangement of particles, slag and gas, is modeled in the following way; The coke bed consists of horizontal layers, i.e. perpendicular to the current flow, that consist of coke, slag and gas in a mix, see Figure 2-9. The resistances due to these components are parallel coupled within each layer. Between these layers consisting of coke, slag and gas, in the following named the *mixed layers*, there are layers consisting of only slag and gas. The resistance of the slag and the resistance of the gas is either parallel or

Table 2-2: Coke bed shapes obtained by varying the shape parameters (Wasbø 1996).

	Coke bed shape	*a*	*p*
I	Narrow cylinder	0	0
II	Wide cylinder	1	0
III	Wide top, bell-shaped	2	0.3
IV	Bell-shaped	2	0.5
V	Cone	2	1

series coupled, but Wasbø (1996) finds the parallel coupling more realistic due to a natural mixing of slag and gas in the coke bed. The resistance of the slag and gas layer $R_{i,slag+gas}$ is coupled in series with the resistance of the mixed layer $R_{i,coke+slag+gas}$. The resistance of each layer is calculated based on the volume fraction and resistivity of each element, as well as the geometrical dimensions of each layer, given by the previously presented equations. To test the influence of coke particle size on R_{cb}, the particle size was included as one of the factors influencing the height of the mixed layer, i.e. decreasing the coke particle size decreases the thickness of the layers and increases the number of layers in the coke bed.

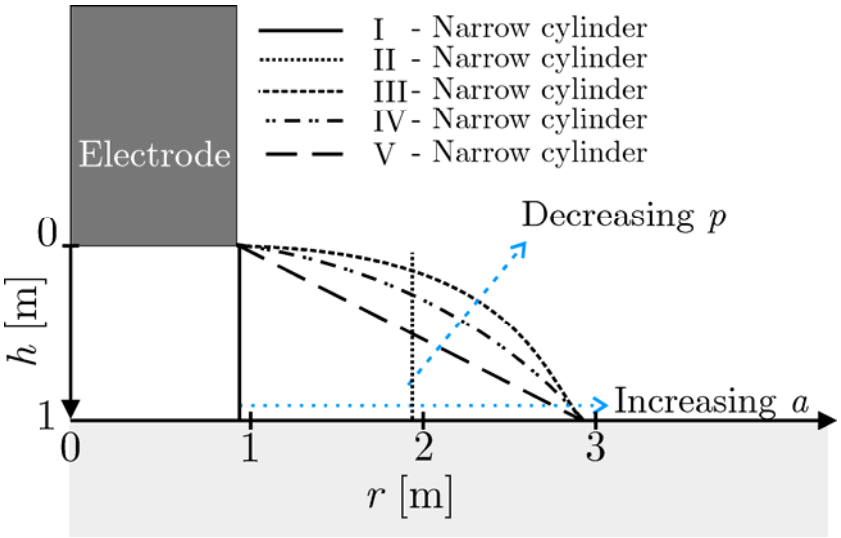

Figure 2-8: The coke bed shapes of Table 2-2 are illustrated. The blue arrows indicate how a variation in the shape factors will affect the coke bed shape.

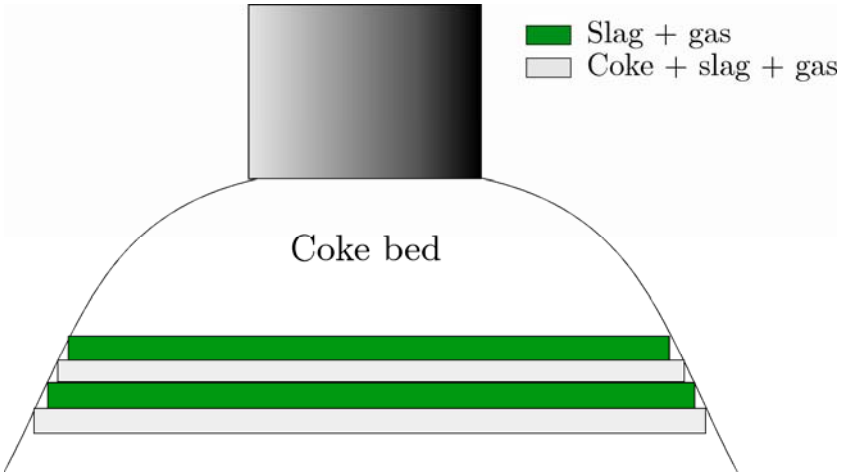

Figure 2-9: Between each layer containing coke, there is a layer containing only gas and slag. The layer thickness is dependent on the size of the coke particles.

The model showed that increasing the coke bed height, while keeping the other parameters constant, gave an increasing R_{cb}. Due to the slag and gas layer in between the mixed layers, increasing the resistance of the slag and the gas will increase the total resistance. The results of the simulations of a coke bed where the slag and gas is parallel coupled in the $R_{i,\ slag+gas}$ layer show that the particle size of the coke has little effect on the coke bed resistance R_{cb} when the resistivity of the coke and slag are approximately the same. However, as the coke resistivity is decreased below the resistivity of the slag, the particle size has an increasing effect on R_{cb}, where the coke bed resistance *increases* with *decreasing* particle size. This effect is stronger when the slag and gas between the mixed layers are series coupled, i.e. when the slag and gas are in separate layers between the layers containing coke.

Dijs et al. (1979) and Dijs and Smith (1980) explore a packed bed consisting of a mixture of conducting and non-conducting particles. The resistance of a continuous array of conducting particles R_{array}, see Figure 2-10 and the probability that such arrays will form are among the central points of the model. The number of continuous arrays of conducting particles in the mix, n_{array}, is determined by the probability that these arrays are formed. The resistance $R_{mixture}$ of a mixture is expressed as:

$$R_{mixture} = R_{array} \Big/ n_{array} \tag{2.5}$$

The *bulk resistivity* of a dry coke bed, i.e. only conducting particles, is expressed as

$$\rho_{bulk} = R'_{array} \Big/ n'_{particles} \tag{2.6}$$

where R'_{array} is the resistance of a continuous array of conducting particles per unit length of the array, and $n'_{particles}$ is the number of particles per unit area. $n'_{particles}$ is determined empirically. R'_{array} is a function of the resistance of the bulk material, i.e. the material resistivity and the array geometry, the number of particle-to-particle contacts $n_{contacts}$ and the contact resistance R_c. It is assumed that the number of particle-to-particle contact points $n_{contacts}$ is inversely proportional to the particle diameter d, $n_{contacts} \propto 1/d$. It is also assumed that the particle-to-particle contact resistance R_c is inversely proportional to the particle-to-particle contact area, and that the contact area in turn is inversely proportional to the particle diameter squared, $R_c \propto \frac{1}{contact\ area} \propto \frac{1}{d^2}$. R'_{array} is expressed as

$$R'_{array} = \frac{1}{d^2}\left(a_2 + \frac{b}{d}\right) \tag{2.7}$$

where a_2 is a parameter depending on the material resistivity of the coke, and b is a parameter depending on the particle-to-particle contact resistance. Both parameters are determined empirically through least squares fitting.

Dijs et al. (1979) also describe the conductivity of a mixture of a conducting solution and conducting particles using Equation (2.7). It is assumed that the number of continuous arrays of, in this case coke, is proportional to the inverse particle diameter squared, $n'_{array} \propto 1/d^2$. When the fraction of conducting

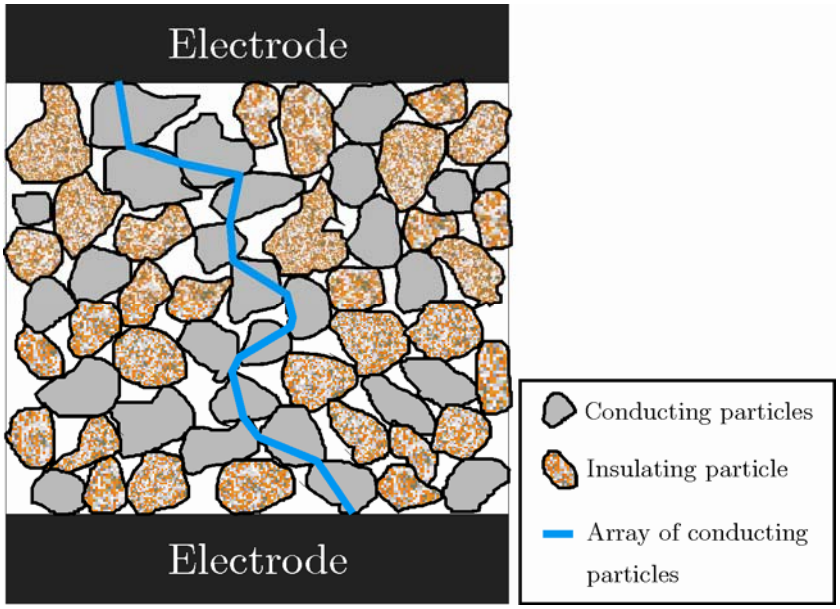

Figure 2-10: The current conduction in the charge is through arrays of conducting particles. Based on (Dijs et al. 1979).

particles is given as f, and the resistivity of the solution is given as $\rho_{solution}$, the resistivity of the mixture $\rho_{mixture}$ is given as

$$\frac{1}{\rho_{mixtrue}} = \frac{1-f}{\rho_{solution}} + \frac{1}{a_2 + b/d} \tag{2.8}$$

As Equation (2.8) reveals, the solution and conduction arrays of solid particles are thought to conduct current in parallel.

The main difference between the models presented by Wasbø (1996) and Dijs et al. (1979) and Dijs and Smith (1980) are that 1) Wasbø (1996) includes the *coke bed geometry*, 2) Wasbø (1996) describes the coke bed with slag and Dijs et al. (1979) and Dijs and Smith (1980) describe a charge mix, and 3) Dijs et al. (1979) and Dijs and Smith (1980) bases the model upon the assumption that conducting arrays of particles are formed as opposed to Wasbø (1996) who include horizontal layers in the coke bed that solely consists of slag and gas. The models proposed by Dijs et al. (1979) and Dijs and Smith (1980) can,

however, be introduced into a model describing the coke bed geometry, such as Equation (2.4).

2.7.3 Contact resistance theory

When two coke particles are in contact, as illustrated in Figure 2-1 (b) on page 10, the total resistance of the two particles can be divided into two components; 1) the *material resistivity* dependent part, which is a function of the geometry of the particle and the material resistivity, and 2) the *contact resistance*, which will be described more thoroughly below. Where not otherwise specified, the *metal* contact theory is based on Timsit (1999).

Unfortunately, the contact theory for coke or coke-like particles has not been explored. The contact resistance theory for metals is, however, well established. It is thus natural to present some fundamental principles that are assumed to be valid for the contact between two coke particles.

When two particles are in contact, as illustrated in Figure 2-11, only a fraction of the area that seems to be in contact is in electrical contact. The area that seems to be in contact is called the *apparent contact area* or *contact area*. The reason the whole area is not in *mechanical contact* is due to the uneven nature of the surface. The surface and shape of the metallurgical coke particles shown in Figure 2-12 leaves no doubt that this is the case also for metallurgical coke. Typically small peaks or asperities form the mechanical contact, as show in the illustration of the contact interface in Figure 2-11. Due to electrically insulating films only a fraction of the areas that are in *mechanical contact* is in *electrical contact*, the respective areas marked gray and black in Figure 2-11. In metallic interfaces, the area of the electrical contact spots may constitute only a small percentage of the apparent contact area (Holm 1967). In a coke particle-particle interfaces it is, however, expected that most of the mechanical contacts will be electrical contact spots since the carbon does not oxidize and create insulating films. However, as the carbon reacts with oxygen, ash residues such as Al_2O_3 may cause electrical contact spots to be degraded or fail.

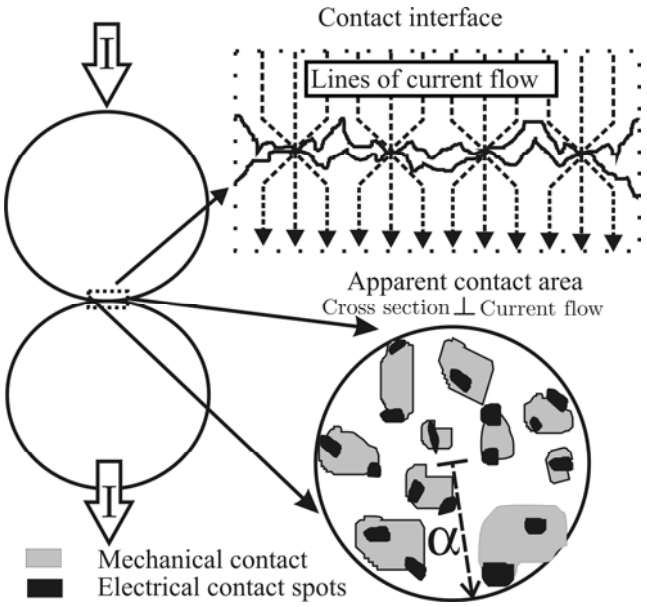

Figure 2-11: Only a fraction of the area that seems to be in contact is in electrical contact through the electrical contact spots.

Figure 2-12: Picture of Corus coke 15-20 mm. (Picture by M. Gall)

When flowing from particle one to another, the current must pass through the contact spots at the particle-particle interface. Since the contact spots area is only a fraction of the width of the conductor, the current density at the contact spots will increase, as indicated by the current flow lines in Figure 2-11. The resistance due to the current being forced though the contact spots is called *constructional resistance*. If the contact interface has a sufficiently large number of electrical contact spots evenly distributed throughout the contact area, the contact resistance can be approximated as

$$R_c = \rho_m / 2\alpha \tag{2.9}$$

where α is the radius of the area containing the electrical contact spots, usually referred to as the *Holm's radius*. Equation (2.9) describes an approximation of the contact resistance due to *constriction*. For metals, and thus most likely for coke, the Holm's radius is *not* equal, but smaller than the apparent contact area, i.e. not as idealized as in Figure 2-11. It is generally accepted that the Holm's radius is controlled by the hardness of the material and the force applied to the

contact, which will cause deformation of the asperities that are in mechanical contact. The relationship between the load F applied to the contact, the circular contact area $A_{contact}$ expressed by α, and the hardness of the material $H_{material}$ is

$$F = A_{contact} H_{material} = \eta\pi\alpha^2 H_{material} \tag{2.10}$$

where η is an empirical constant equal to one for clean surfaces. The physical interpretation of Equation (2.10) is that the contact area $A_{contact}$ is *not* dependent on the size of the *apparent contact area*, i.e. the physical dimensions of the two contacting elements, only on the applied force and the hardness of the material. This may seem a bit odd, but may be explained by the following example from Timsit (1999): Two interfaces, 1 cm^2 and 10 cm^2, of identical material and with identical surface treatment are subjected by the same force F. Due to the identical surface treatment, the density of asperities are the same on the two contacting interfaces. The number of asperities that are create contact are then 10 times higher for the 10 cm^2 compared to the 1 cm^2 interface. On average the mechanical load developed on each asperity is F/n and $F/10n$ for the 1 cm^2 and 10 cm^2 interface, respectively, n representing the number of asperities. Assuming a fully plastic deformation, the contact area at each asperity will be 10 times higher for the 1 cm^2 compared to the 10 cm^2 interface, but the total area in electrical contact is the same. The assumption for Equation (2.10) is full plastic deformation. For metallurgical coke, which is very brittle, a deformation will be in the form of crushing. The combination of Equations (2.9) and (2.10) give Equation (2.11), which has been shown to be consistent for a range of published data on *metal* contacts.

$$R_c = \sqrt{\rho_m^2 \eta\pi H_{material} / 4F} \tag{2.11}$$

Equation (2.11) shows us that the contact resistance R_c is independent of the size of the apparent contact area, and merely a function of the force applied on the contact and the hardness of the material.

If there are surface films present at the contact spots, additional terms should be added to represent the effect these have on the contact resistance. This will, however, not be treated in this thesis as it requires knowledge concerning the resistivity, the thickness and the hardness of the surface film present at the contact spot. These physical properties are important since an applied force will, when large enough, crack the surface film so that an electrical contact spot can be formed.

A mechanism of particle-to-particle conduction that is discussed from time to time is arcing. Urquhart et al. (1973) looked at the possibility of the current being conducted from one particle to another by the means of an electric arc. The experiments showed that arcs did indeed form in both packed beds of coal char, i.e. a low temperature coke, and in coal char and chromium ore mixes. Urquhart et al. (1973) speculated that as two carbon particles were in contact, the conduction would at first be ohmic. Then, as the carbon in the contact point between the two particles reacted with oxygen from e.g. the slag or the ore, CO would be formed, as well as a very small gap. Even at very small voltages the potential over the CO filled gap would exceed the required potential for arcing in CO, approximately 30 kV/cm. As more carbon would react, and thus the gap increase, the arc would soon be extinguished. The experiments showed that the critical voltage for arcing to take place increases with temperature. The conclusion is that arcing will sporadically take place in the upper regions of the furnace, while the conduction in the lower parts of the furnace will largely be ohmic.

2.8 Metallurgical coke

Metallurgical coke is, as mentioned, the main reduction material used in the production of FeMn in Norway. The low size fractions of the coke produced for the blast furnaces is the main source for metallurgical coke, since blast furnace production demand a good quality coke that is not too small. An introduction is given to the production of metallurgical coke, due to its importance for determining the properties of the metallurgical coke. An introduction to electrical conduction in graphite and coke will also be given.

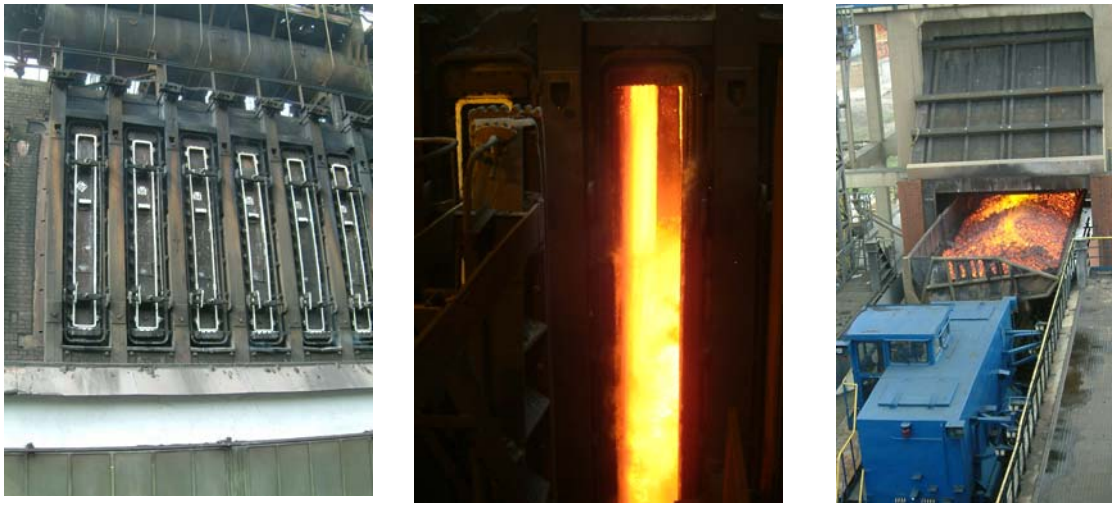

(a) (b) (c)

Figure 2-13: By-product Coke Oven Battery at the Zdzieszowice coking plant (a) seen from the side. (b) The pulverized and compacted coal is pushed into the slot oven. (c) When the coking is finished the slots are opened and the coke is pushed into cars and the coke is then quenched by water in the quenching tower.

The coke is produced by carbonization of a pulverized coal mix while heating to about 1100°C in an oxygen deficient atmosphere. The most common oven used today is the slot oven. The slot ovens, shown in Figure 2-13 (a), have typically inner dimensions of 400 mm to 600 mm wide, 4 m to 8 m high and 12 m to 18 m long. They are usually built side by side in so called coke oven batteries, the ovens are separated by combustion chambers which supply the heat needed for the coking. (Álvarez and Díaz-Estébanez 2000)

A coal mixture is either pushed into slots in the coke oven batteries, as shown in Figure 2-13 (a) and (b) or charged from the top of the furnace. The carbonization takes place in a reducing atmosphere. In this type of furnace the heat is transferred from the brick walls of the oven into the pulverized coal mix, as indicated in Figure 2-14. (American Iron and Steel Institute 2005) The oven wall temperature is kept at approximately 1300°C, heat supplied by external combustion of some of the off gasses from the process. As the coal is heated it softens and becomes plastic and becomes a coherent mass which swells and re-solidifies into what is known as coke. This process is known as *carbonization*.

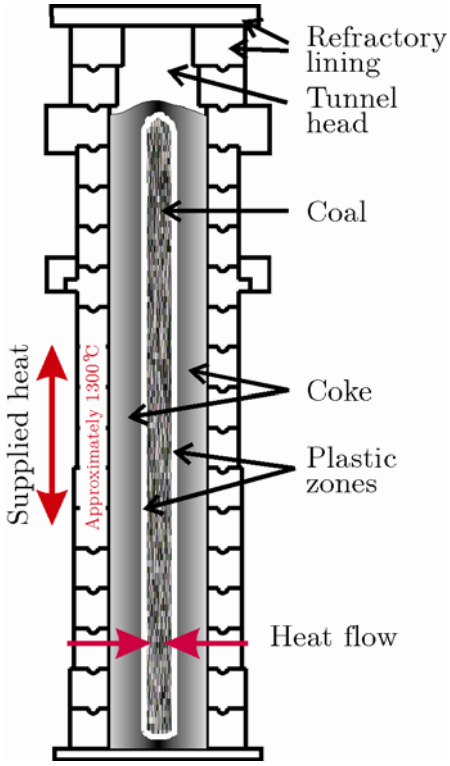

Figure 2-14: Cross section of a slot oven. The oven walls are approximately 1300C, heating the pulverized coal. Modified from original (American Iron and Steel Institute 2005)

The coal near the wall will heat quickly to form the plastic zone. The plastic zone moves towards the center of the coke oven as the coal reaches the temperature required to soften, see Figure 2-14. As the softened coal is heated further it solidifies into coke. When the center has reached the desired temperature, typically 900°C to 1000°C, a period of soaking follows as the finishing step of the process. The coking cycle depends on the dimensions of the oven, but is typically 12 to 18 hours for metallurgical coke. After the coking process is finished, the coke is pushed out of the slot oven into cars that take the coke for quenching. Figure 2-13 (c) shows a car filled with coke beeing pushed into the water quenching tower.

During the carbonization process in a coke oven, large amounts of coke oven gas and water vapor is produced. These large amounts of gas and liquid flows to the tunnel head, indicated in Figure 2-14, through cracks in the coke. The evolved

gases are also the reason for the porosity observed in the coke. (Álvarez and Díaz-Estébanez 2000)

A graphitizable carbon, such as pitch, will, as it is heated, go through the stages indicated in Figure 2-15. The four steps represent an increased order, and as the graph indicates, the transition from one stage to another is quite rapid. The first stage, the isometric coherent domain, is characterized by the coherent domains of the material that are randomly distributed and oriented. (Oberlin 1984) The coherent domains are below 1 nm in diameter and consists of only 2 or 3 graphene layers, as shown in Figure 2-16. The graphitizability of the carbon material is to a large extent determined by how ordered the coherent domains are and the number and type of defects present at this initial stage. The next stage is the columnar stage from about 800°C to 1500°C, as shown in Figure 2-15. At this stage the diameter of the layers are constant, but the number of graphene layers per stack increases from 2 to 3 up to about 10 and the neighboring columns tend to line up. This stage represents typical calcined cokes. The next stage starts at about 1500°C, where the layers start to coalesce, increasing the size of the graphene layers, stack height L_c and decreasing the

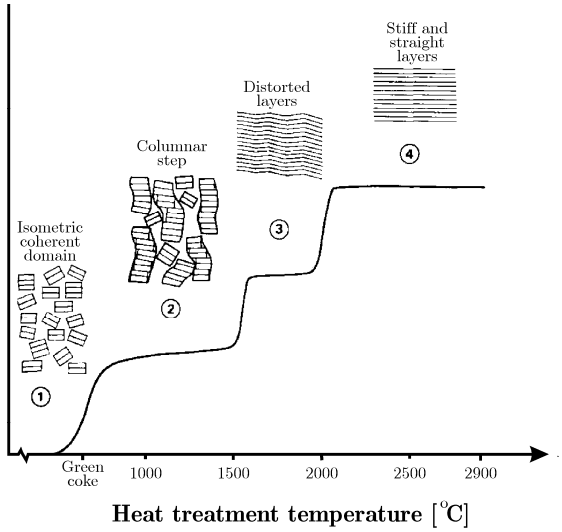

Figure 2-15: An increased ordering is achieved through higher heat treatment temperatures. (Oberlin 1984; Bourrat 2000)

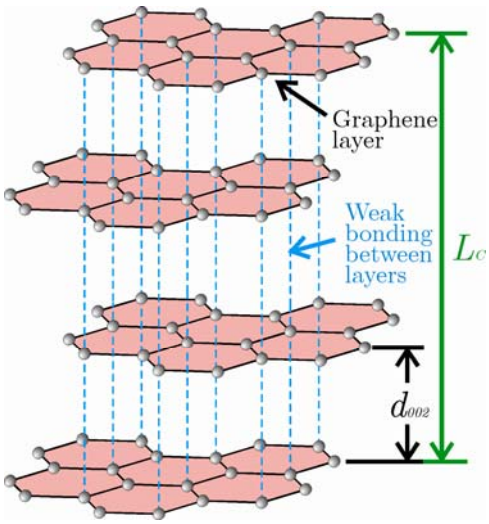

Figure 2-16: The poly aromatic rings form a strong layers, but the bonding between the layers are weak. (Zumdahl 1998)

distance d_{002} between the graphene layers. There is then a sharp change to the next stage, where the layers suddenly straighten. (Bourrat 2000)
Materials such as a coking coal, which has the ability to soften when heated, will partly go through the described graphitization process. The degree of graphitization that can be achieved is determined by the arrangement of the coherent domains in relation to each other, and the extent of cross-linking in the structure. Cross-linking being atoms linking the coherent domains together, preventing ordering of the coherent domains. (Oberlin 1984)

2.8.1 Conduction of electricity

Ultimately the conductivity of a material is decided by how easily the electrons are flowing through the material. Metals have a high conductivity of electricity. A common way of explaining this is that the regular structure of the metal cations is surrounded by a "sea" of valence electrons. The electrons are very mobile and can thus easily conduct electricity and heat. In the so-called band model the electrons in metals are excited from a filled electron band to an empty electron band. In metals the energy needed to excite an electron to the next band, also called the *energy gap*, is very small. (Zumdahl 1998, pp. 744)
Resistance is, very simplified, caused by the path of the electrons being obstructed, the electrons being slowed down. This effect is also called *scattering*. If the temperature is increased the resistivity will increase for metals (Heaney 2003). This is because the scattering will increase with increasing temperature.

Single graphite crystallite consists of structural units as shown in Figure 2-16. Each of the carbon atoms, grey in Figure 2-16, have four valence electrons available. Three of these valence electrons are used to form the rigid structure inside the graphene layers through forming σ-bonds with the three nearest neighboring carbon atom within the plane. These three electrons do not participate in the conduction of electricity. The fourth valence electron has an axis of symmetry that is perpendicular to the graphene layer. (Wallace 1947) These valence electrons form π orbitals, which are important both as the π bonds, which stabilize the graphite layers, and due to the delocalized electrons. The delocalized electrons in the closely spaced π orbitals are exactly analogous

to the conduction bands found in metals. (Zumdahl 1998) The energy gap is, as for metals, zero (Wallace 1947). This makes the electrons very mobile and the resistivity parallel to the graphene planes very low. However, the electrical resistivity perpendicular to the graphene planes much higher. The ratio between conduction in the two directions is more than 10^5 (Krishnan and Ganguli 1939). When heated, the material resistivity increases linearly with temperature. Single crystals of graphite have the same temperature dependence as metals, i.e. the resistivity increases with increasing temperature.

Polycrystalline graphite has a much higher resistivity compared to the single crystalline graphite. Whereas the single-crystalline graphite behaves as a metal, with an energy gap equal to zero, the polycrystalline graphite has a finite energy gap between the occupied valence band and the conduction band, similar to what is found for semiconductors. The degree of graphitization influences the size of the energy gap. Other factors that influence the material resistivity of polycrystalline graphite are listed below.

1) Due to the large ratio between the electrical conductivity parallel and normal to the graphene planes, the preferred direction of conduction is along the carbon crystals, i.e. parallel to the graphene planes.

2) Due to the preferred direction of conduction, the current path is increased due to the orientation of the crystals in relation to each other. The degree of graphitization or ordering of the graphene planes in relation to each other, and orientation of the graphene planes in relation to the axis of the current through the media will largely affect the material resistivity. An extruded graphite rod will have a higher conductivity parallel to the axis of the extrusion, compared to perpendicular to the axis of the extrusion. This is because the graphite crystallites will be oriented parallel to the extrusion axis.

3) The bonding between the crystallites is a barrier that will cause scattering of the electrons. The degree of scattering varies with degree of graphitization.

4) The distance between the graphene planes d_{002} varies, and it is known that d_{002} decreases with increasing crystallite size. A larger d_{002} means fewer graphene planes per unit volume.

5) Micro- and macro porosity, and micro cracks also causes an increased current path. These factors are mainly influenced by the raw materials and production method.

As mentioned in the preceding section, the heat treatment temperature of the carbon material greatly influences the ordering of the carbon material. The heat treatment of the carbon materials also has an impact on the electrical conductivity. Mrozowski (1952) reports that the variation in room temperature resistivity as a function of heat treatment temperature can be divided into three different stages:

$<$ 1000°C - The electrical resistivity decreases several orders of magnitude. This is largely due to the transition from a raw state to a baked carbon. Components such as hydrogen, nitrogen and oxygen are driven off in this region, causing a strong evolution of gasses as well as shrinking of the material. The foreign atoms are barriers for the conduction between crystallites. The concentration of free electrons also increases in this temperature region.

1000°C-2000°C - Only a very small change in the material resistivity is observed. An increased growth of the crystallites decreases the number of free electrons. These two effects are counteracting each other, thus causing a minimal change in the material resistivity. This region will stretch to higher temperatures for carbons that are not easily graphitizable.

$>$ 2000°C - A drop in the material resistivity is observed when the carbon sample is graphitized. As the heat treatment temperature is increased further,

the gap between the graphene planes decreases, causing a further decrease in the material resistivity.

The material resistivity of polycrystalline graphite is known to decrease when heated from room temperature as the number of activated electrons increase, i.e. the number of electrons that excited from the valence band to the conduction band. A minimum in the resistivity is then reached. Above this minimum, the material resistivity increases linearly with increasing temperature, as for the monocrystalline graphite. The temperature of the minimum resistivity varies with the degree of graphitization, decreasing with increasing degree of graphitization. (Mrozowski 1952)

Metallurgical coke is closer to polycrystalline graphite than to single crystalline graphite. The number of obstructions between the graphite crystallites will, however, be higher compared to the polycrystalline graphite. Thus the material resistivity of the metallurgical coke will be higher compared to the polycrystalline graphite. In the temperature range up to 1600°C, which has been the temperature range investigated in this thesis, a minimum in the material resistivity can not be expected to be observed. This is due to the low graphitizability of the coal used to produce metallurgical coke. A minimum in the material resistivity will probably be above 2000°C, which was the temperature of the material resistivity minimum of a baked carbon estimated by Mrozowski (1952).

Chapter 3 Material Characterization

An important part of this research is investigating differences within and between groups of carbon materials. To be able to do so, the materials have to be characterized in a variety of ways. Based on knowledge concerning how electrons are conducted in carbon materials one of the characterization methods is x-ray diffraction (XRD) analysis. From previous research such as Dijs et al. (1979) it is known that proximate analysis may influence the bulk resistivity. The ash composition is also investigated. This is due to a belief that surface films may be created at the particle-to-particle contact interface. Oxide films are, from metal contacts, known to increase the contact resistance. Finally, porosity is thought to influence the bulk resistivity. This may be due to porosity being an expression of how much carbon material is available for conduction of electrons. It may also be due to the mechanical strength of the coke particles decreasing due to decreasing strength with increasing porosity.

The characterization has also been done on various fractions of the carbon materials, where such have been available for the analyses.

For the materials tested in the bulk resistivity apparatus the bulk density and a particle size range was also determined. The respective methods and results are presented in Chapter 5, where the bulk resistivity is treated.

3.1 Porosity

The porosity of the cokes was determined by pycnometry and image analyses.

3.1.1 Pycnometry

The apparent density of the particle is determined using a GeoPyc 1360 Pycnometer, which uses fine sand to determine the volume of the particle. Dry sand with a very small particle size was used. The sand will encapsulate the particle but not penetrate it.

The absolute density was determined using an AccuPyc 1330 Helium Pycnometer. The helium is able to penetrate the particle and fill the pores.

The porosity is given by:

$$Porosity = \left(1 - \frac{apparent\,density}{absolute\,density}\right) \cdot 100\% \tag{3.1}$$

3.1.2 Image analyses

A selection of coke particles, typically 5 to 10 pieces, depending on the particle size, was cast in fluorescent epoxy under vacuum. The sample is then cut and polished. The finished sample then looks as in Figure 3-1.

By the use of ultraviolet light in an inverted reflected light microscope equipped with a motorized XY- stage and focus controller, a digital camera automatically acquires images of the sample. The images are automatically analysed by the use of image analysis software. The total area of the sample, the area of the open and the area of the closed pores, i.e. the pores not containing any fluorescent epoxy, is determined. Based on these area measurements the relative porosities are determined. The smallest pore size that can be detected by this method is 5 μm. See Rørvik et al. (2001) for further details on this method.

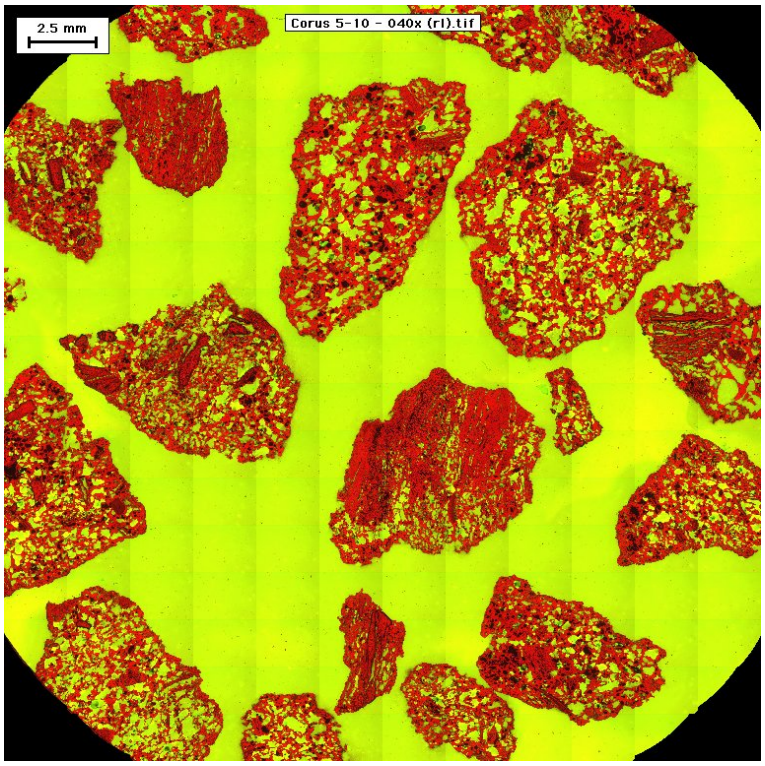

Figure 3-1: Coke particles embedded in fluorescent epoxy. Picture by S. Rørvik.

3.1.3 Results

The porosity measured by pycnometry is shown in Table 3-1. Four replicates were done for each particle size.

Table 3-1: Porosity determined by pycnometry. The standard deviation is given for the absolute and apparent density.

Sample	Absolute density (g/cm^3)	Apparent density (g/cm^3)	Porosity [%]
Corus 5-10mm	1.50 ± 7 %	1.05 ± 3 %	30
Corus 15-20mm	1.83 ± 8 %	1.08 ± 4 %	41
SSAB 3.3-6mm	1.01 ± 18 %	0.86 ± 24 %	15
SSAB 10-20mm	1.74 ± 12 %	0.98 ± 15 %	44

The results of the porosity measurements by image analyses are shown in Table 3-2.

Table 3-2: Porosity determined by image analyses. Both open and closed porosity, as well as total porosity is shown.

Sample	Porosity [%]		
	Open	Closed	Total
Corus 5-10mm	30.3	10.4	40.7
Corus 15-20mm	31.2	15.8	47.0
Corus 60-100mm	37.4	24.4	61.8
SSAB 1.68-3.3	19.4	8.2	27.6
SSAB 3.3-6mm	24.2	8.6	32.8
SSAB 6-10mm	28.3	23.7	52.0
SSAB 10-20mm	28.1	14.7	42.7
SSAB 60-100mm	9.9	47.6	57.6

3.1.4 Discussion

For both Corus coke and SSAB coke the porosity increases with increasing particle size, see Figure 3-2. A common contributor to the error of the estimates is the number of particles tested. In both tests only a few particles can be tested, especially for the larger particle sizes.

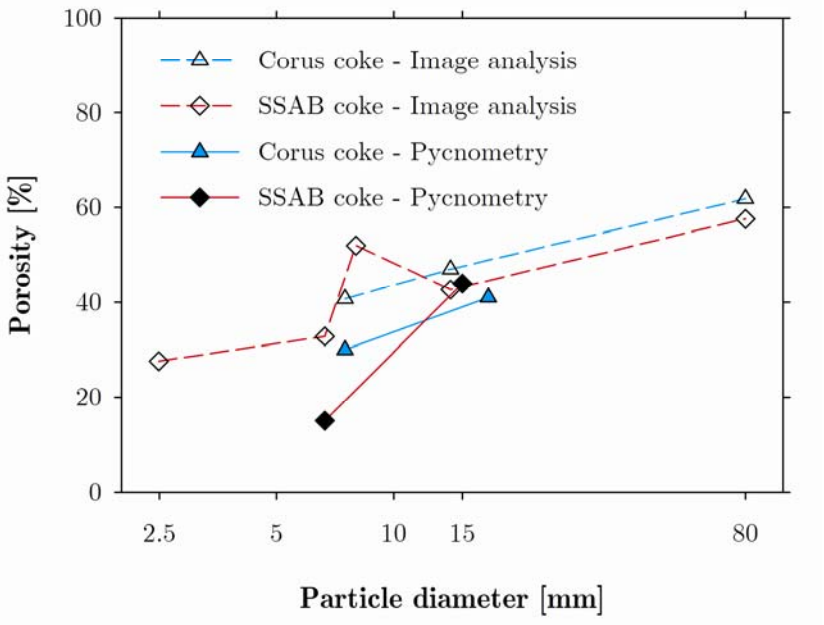

Figure 3-2: Porosity as a function of particle size for Corus and SSAB cokes.

In the pycnometry the particle has to be completely surrounded by the dry sand, or the apparent density measured will be wrong. From experience, the operator had to select particles that were as close to spherical as possible so that the packing would be correct. It is not known how or if this has affected the measured porosity.

The image analysis is dependent upon the epoxy penetrating the particle, if not, the measurement will be wrong. The lower particle size that can be detected of the microscope is, as mentioned, 5 μm, i.e. the micro porosity is neglected. Even though the image analyses test gives a pore size distribution, only the total porosity of the coke has been used in this work. This is because the electrical resistivity of the carbon material is much lower compared to the electrical resistivity of the gases, consequently the current flows through the carbon material. The porosity can be seen as a measure of how much carbon the coke particle consists of.

If the results from the pycnometry is compared to the results from the image analyses it can be seen that the results from the pycnometry is generally lower if compared to the total porosity found by the image analyses. This is probably due to the pycnometry only measuring open porosity. The pycnometry does, however, include the micro porosity, i.e. the pores below 5 μm. The real porosity of the cokes is expected to be higher compared to the porosity measured by the image analysis method.

3.2 Proximate analysis

The proximate analysis is determined by Eramet Norway AS. A brief presentation is given below of the proximate analysis, as described by ASTM D5142 (2004).

First the moisture content of the sample is determined by the weight loss measured when the sample is kept at a stable temperature between 104 and 110°C. The sample container is typically weighed every 3 minutes until two

successive weighings give the same result. The volatile matter is then determined by heating the sample to 950±20°C at a rate of 50°C/min in an inert atmosphere. The maximum temperature is to be kept for 7 minutes.

Table 3-3: Proximate analyses of the carbonaceous materials on dry basis.

Sample name	Material	Proximate analysis			
		H_2O [wt. %]	Ash [wt. %]	C-Fix [wt. %]	Volatile [wt. %]
Preussang Anthrazit	Anthracite	0.98±21.6%	7.54±90.1%	86.6±8.0%	5.86±9.5%
Siberian	Anthracite	5.55**	3.72±3.2%	93.75±1.3%	2.54±42.3%
Siberian, after exp.‡	Anthracite	1.57**	2.95**	95.78**	1.27**
Brazilian 4-35mm	Charcoal*	-	0.43**	81.3**	18.3**
Brazilian 4.7-13.4mm	Charcoal*	-	0.43**	81.3**	18.3**
Brazilian 13.4-35mm	Charcoal*	-	0.43**	81.3**	18.3**
Indonesian 4.7-13.4mm	Charcoal*	-	1.63**	77.5**	20.9**
Indonesian 13.4-26.9mm	Charcoal*	-	1.63**	77.5**	20.9**
Corus, 5-10 mm	Met. coke	0.16±8.8%	11.14±3.0%	87.91±0.5%	0.95±8.4%
Corus, 15-20 mm	Met. coke	0.29±9.8%	10.57±0.8%	88.52±0.1%	0.91±3.5%
Corus, 60-100 mm	Met. coke	0.96±85.0%	13.31±1.7%	85.55±0.2%	1.14±32.8%
Magnitogorsk	Met. coke§	-	14.0	84.28	1.42
Min Metals	Met. coke	0.5**	10.97±4.7%	87.8±0.5%	1.24±6.8%
Min Metals, after exp.‡	Met. coke	0.15**	10.82**	88.42**	0.76**
SSAB, -1.68 mm	Met. coke	0.47±7.6%	11.1±1.0%	87.79±0.1%	1.11±1.6%
SSAB, 1.68-3.3 mm	Met. coke	0.55±25.7%	12.68±0.7%	86.29±0.1%	1.04±7.7%
SSAB, 3.3-6 mm	Met. coke	0.63**	12.43±8.2%	86.44±1.1%	1.13±2.5%
SSAB, 6-10 mm	Met. coke	0.13±5.7%	10.83±0.9%	88.26±0.2%	0.91±11.4%
SSAB, 10-20 mm	Met. coke	0.66±11.9%	11.25±1.6%	87.49±0.3%	1.26±10.3%
SSAB, 60-100 mm	Met. coke	-	13.62**	85.43**	0.95**
Tian Jin	Met. coke	0.59**	10.84±0.5%	87.66±0.6%	1.51±36.5%
Tian Jin, after exp.‡	Met. coke	0.15**	10.82**	88.42**	0.76**
Zdzieszowice, 12-25 mm	Met. coke	0.27**	10.41±12.2%	88.35±1.8%	1.23±21.4%
Zdzieszowice, 60-100 mm	Met. coke	0.12**	8.97±11.5%	90.02±1.2%	1.02±4.9%
Chalmette	Pet. coke	0.45**	0.43±19.7%	88.29±0.2%	11.3±0.6%
Marietta shot	Pet. coke	0.39**	2.28±98.0%	86.38±2.8%	11.35±1.8%
Mar. shot, preh. 850°C	Pet. coke	0.66**	0.39**	88.83**	10.78**
Mar. shot, after exp.‡	Pet. coke	0.37**	0.4**	98.19**	1.41**
Marietta sponge	Pet. coke	0.38**	0.48±81.9%	86.54±1.9%	12.99±15.7%
Mar. sponge, preh. 850°C	Pet. coke	1.8**	0.22**	97.49**	2.29**
Mar. sponge, after exp.‡	Pet. coke	0.06**	0.22**	98.93**	0.85**

*From (Eidem 2004b) **Only one anaysis ‡After bulk resistivity experiment §From (Kaczorowski 2006)

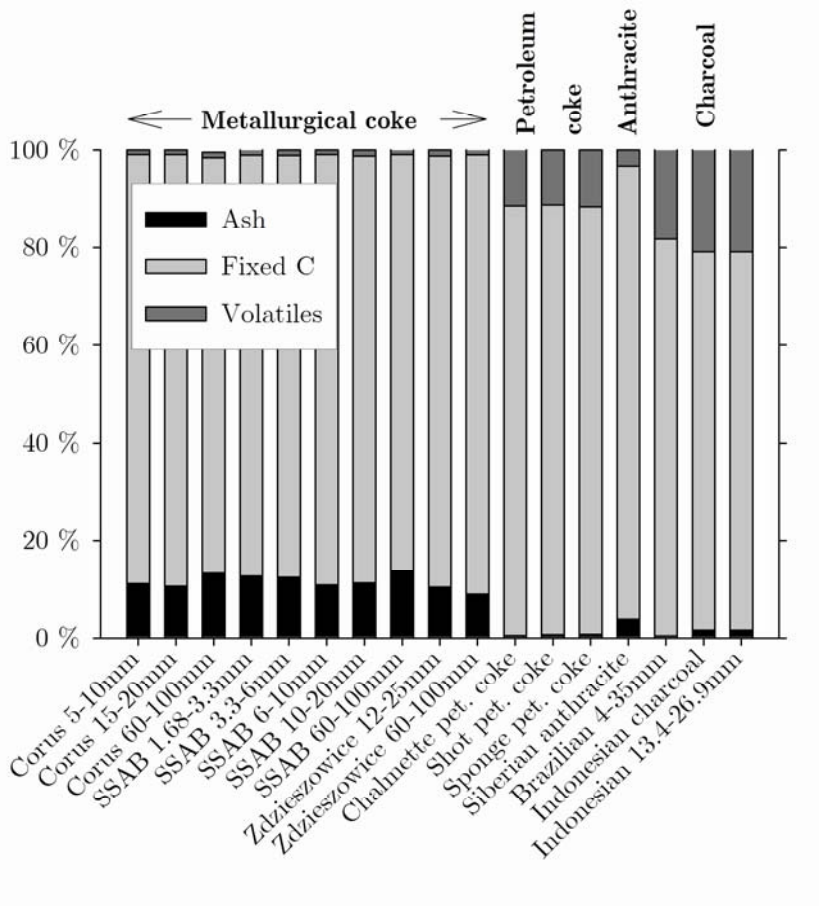

Figure 3-3: Graphical view of the proximate analyses of a selection of the carbon materials tested.

The weight loss is then used to determine the volatile content. The amount of ash is determined by heating the sample gradually from 600°C to 900-950°C in oxygen atmosphere and keep at 900-950°C until the weight has stabilized. The fixed carbon content is equal to the difference between the weight % of the ash, volatile matter, moisture and 100 %.

The proximate analyses of most of the carbon materials tested are shown in Table 3-3 and plotted in Figure 3-3. The metallurgical cokes have a much higher ash content compared to the charcoal, the petroleum coke and the anthracite. The ash in the metallurgical coke originates form the coals used to produce the coke. The very low ash content of the petroleum coke is due to the processing of the raw oil, where impurities are removed.

Of the metallurgical cokes, the coke from the Magnitogorsk steel mill, called Magnitogorsk coke in the following, has the highest ash content of the cokes with a content of 14 %. The content of fixed carbon, C-Fix, is also lower for this coke compared to the other cokes. The ash in the coke originates either from the coal or from the mining process of the coal, which is concentrated in the coke due to the coking process where volatiles from the coal are burned. This is also why the ash of the anthracites is lower compared to the metallurgical cokes. The anthracites are not heat treated.

The varying content of volatiles is also worth noticing. The metallurgical coke has a volatile content around 1 % due to the high temperature used in the coking process. In the production of petroleum coke the temperature is typically 500°C in the delayed coking process (Adams 1997), whereas in the production of metallurgical coke the temperature reaches typically 1000°C to 1300°C (Álvarez and Díaz-Estébanez 2000). The temperature for producing charcoal varies with the different production methods, but for the charcoal used in the bulk resistivity measurements the typical top temperature has been 450°C to 500°C (Monsen 2008).

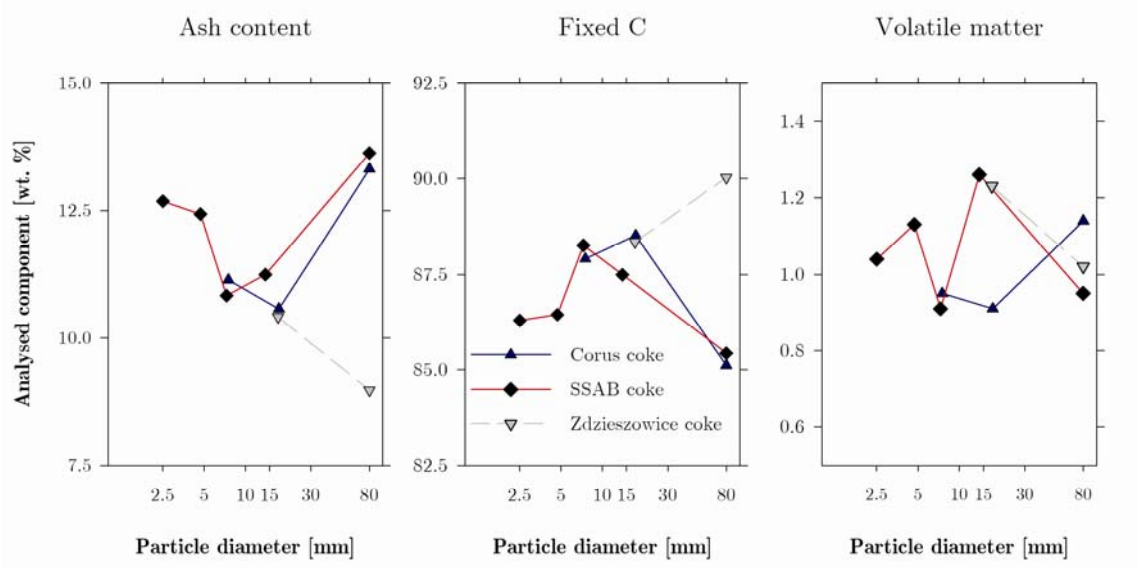

Figure 3-4: Proximate analyses of Corus, SSAB and Zdzieszowice cokes plotted as a function of the particle size.

To assess a possible difference in the proximate analyses due to particle size the Corus coke, the SSAB coke and the Zdzieszowice coke are graphed in Figure 3-4. No correlations can be seen when all particle size ranges are taken into consideration. This may be due to most of the coke size fractions being from different coke batches. Only the 1.68-3-3 mm and 3.3-6 mm SSAB size fractions and the Corus coke 5-10 mm and 15-20 mm are from the same batch of coke. If only the coke tested in the bulk resistivity test, i.e. below 30 mm, are compared, it can be seen that for both the SSAB coke and the Corus coke there is an indication that the ash content decreases with increasing particle size. For the fixed carbon the opposite can be seen. It is, however, important to remember that the amount of fixed carbon is calculated from the amount of ash.

3.3 Ash analysis

The ash residue of the proximate analysis in the coke, may originate either from minerals trapped in the coal or minerals that are present as a result of the mining of the coal. When the coke is heated and the coke is consumed in chemical reactions such as the Boudouard reaction in a dry coke bed, it is believed that the ash components can potentially be left as a film at the particle-to-particle contact interface. Some elements, such as iron, may be reduced and create a surface film that lowers the contact resistance, while other elements, such as Al_2O_3, potentially can create a low conducting surface film on the contact interface. The ash analyses are shown in Table 3-4.

The main difference that can be seen between the anthracites and the metallurgical cokes is that the amount of SiO_2, Al_2O_3 and Fe_2O_3 is much lower in the anthracites. This is a reflection of the lower ash content, seen in the proximate analyses in Table 3-3.

Within the metallurgical cokes, it can be seen that the Magnitogorsk coke has the highest content of SiO_2. This is probably due to an ash content that is higher compared to the other metallurgical cokes. The MnO content of the SSAB 60-100 mm is much higher compared to that of the other metallurgical

Table 3-4: Result of the ash analyses.

Sample name	Material	Ash				
		MnO [wt. %]	P_2O_5 [wt. %]	P [wt. %]	K_2O [wt. %]	MgO [wt. %]
Preussang Anthrazit	Anthracite	0.01±0.0%	0.13±95.5%	0.06±96.7%	0.13±159.9%	0.1±91.5%
Siberian	Anthracite	0.01**	0.04**	0.02**	0.05**	0.01**
Siberian, after exp.‡	Anthracite	0.01**	0.01**	0.01**	0.07**	0.01**
Corus, 5-10 mm	Met. coke	0.01±43.3%	0.08±0.7%	0.04±0.0%	0.11±5.1%	0.04±13.3%
Corus, 15-20 mm	Met. coke	0.01±43.3%	0.08±0.7%	0.04±1.6%	0.11±0.0%	0.05±0.0%
Corus, 60-100 mm	Met. coke	0.01±0.0%	0.12±2.0%	0.05±1.9%	0.15±4.0%	0.14±0.0%
Magnitogorsk	Met. coke§	0.35	0.15	-	0.26	0.14
Min Metals	Met. coke	0.01**	0.02**	0.01**	0.06**	0.01**
Min Metals, after exp.‡	Met. coke	0.01**	0.05**	0.02**	0.05**	0.04**
SSAB, -1.68 mm	Met. coke	0.01±0.0%	0.03±5.8%	0.01±5.1%	0.16±3.5%	0.05±0.0%
SSAB, 1.68-3.3 mm	Met. coke	0.01±86.6%	0.03±9.1%	0.01±5.1%	0.2±2.8%	0.07±8.7%
SSAB, 3.3-6 mm	Met. coke	0.01±141.4%	0.03±19.5%	0.01±17.0%	0.19±7.4%	0.06±23.6%
SSAB, 6-10 mm	Met. coke	0.01±0.0%	0.08±2.0%	0.03±1.7%	0.11±5.1%	0.05±0.0%
SSAB, 10-20 mm	Met. coke	0.01±0.0%	0.04±5.7%	0.02±6.3%	0.13±0.0%	0.04±0.0%
SSAB, 60-100 mm	Met. coke	1.93**	0.03**	0.01**	0.15**	0.04**
Tian Jin	Met. coke	0.01**	0.04**	0.01**	0.05**	0.06**
Tian Jin, after exp.‡	Met. coke	0.01**	0.05**	0.02**	0.05**	0.04**
Zdzieszowice, 12-25 mm	Met. coke	0.01**	0.13**	0.06**	0.2**	0.22**
Zdzieszowice, 60-100 mm	Met. coke	0.35±137.4%	0.1±7.2%	0.04±8.3%	0.18±7.9%	0.15±9.4%

*From (Eidem 2004b) **Only one anaysis ‡After bulk resistivity experiment §From (Kaczorowski 2006)

cokes. The reason for this is unknown, but it can be speculated that the sample has been polluted by FeMn slag or metal.

For both the Siberian anthracite and for the Tian Jin a small increase is seen in the Al_2O_3 content when the ash analyses before and after the bulk resistivity experiment is seen. However, when considering that the total ash content of the Siberian anthracite at the same time has decreased, see Table 3-3, it is evident that this is not a significant result.

The ash analyses of the charcoal were not available, and there was not sufficient ash after the proximate analyses of the petroleum cokes to perform the ash analyses.

content							
CaO [wt. %]	**SiO_2 [wt. %]**	**Al_2O_3 [wt. %]**	**Fe_2O_3 [wt. %]**	**Fe [wt. %]**	**ZnO [wt. %]**	**BaO [wt. %]**	**TiO_2 [wt. %]**
0.28±70.7%	3.05±98.5%	2.51±93.5%	0.3±52.8%	0.21±51.6%	0±69.3%	0.02±65.5%	0.09±115.6%
0.03**	1.98**	0.92**	0.28**	0.2**	0.001**	0.01**	0.04**
0.01**	1.36**	1.2**	0.06**	0.05**	0.001**	0.01**	0.04**
0.22±0.0%	5.85±6.7%	3.36±3.8%	0.61±10.9%	0.43±11.4%	0.003±0.0%	0.01±0.0%	0.17±10.2%
0.22±2.6%	5.49±0.5%	3.21±2.3%	0.58±7.5%	0.41±7.1%	0.003±17.3%	0.01±0.0%	0.16±6.3%
0.54±2.1%	6.47±2.5%	3.73±1.9%	0.71±4.9%	0.5±5.8%	0.004±0.0%	0.02±22.2%	0.2±0.0%
0.74	6.82	3.43	1.06	-	-	0.03	0.17
0.21**	5.6**	3.93**	0.47**	0.33**	0.003**	0.01**	0.16**
0.31**	5.28**	3.74**	0.41**	0.29**	0.002**	0.01**	0.16**
0.11±5.1%	6.24±3.6%	3.06±3.3%	0.63±0.9%	0.44±1.3%	0.004±15.7%	0.01±0.0%	0.16±3.5%
0.11±5.4%	7.35±2.6%	3.51±3.4%	0.6±2.6%	0.42±3.7%	0.004±0.0%	0.01±0.0%	0.17±0.0%
0.1±14.1%	7.19±4.3%	3.39±0.0%	0.78±43.5%	0.55±42.8%	0.005±15.7%	0.01±0.0%	0.17±0.0%
0.2±0.0%	5.58±2.4%	3.38±1.2%	0.61±3.8%	0.42±4.9%	0.003±0.0%	0.01±0.0%	0.17±0.0%
0.11±5.1%	6.38±1.7%	3.18±1.6%	0.61±9.7%	0.42±8.9%	0.003±0.0%	0.01±0.0%	0.17±3.5%
0.1**	6.8**	3.36**	0.71**	0.49**	0.005**	0.02**	0.18**
0.44**	5.03**	3.55**	0.48**	0.34**	0.003**	0.01**	0.15**
0.31**	5.28**	3.74**	0.41**	0.29**	0.002**	0.01**	0.16**
0.37**	3.81**	2.61**	0.87**	0.61**	0.003**	0.03**	0.11**
0.32±8.8%	3.8±11.5%	2.54±12.0%	0.71±11.0%	0.5±10.0%	0.003±0.0%	0.03±28.3%	0.12±11.8%

3.4 XRD analysis

The material was first ground and sieved to a particle size range of 20 µm to 50 µm. Approximately 10 wt. % ultra pure silicon (> 99.99999 wt. % Si) passing a 150 mesh sieve was mixed with the ground carbon sample using a mortar and pestle. The silicon is added so that the diffraction profiled could be appropriately adjusted to match the known position of the silicon peak. The mixed powder was transferred to a sample holder. The sample diameter was 25 mm and the depth was approximately 1 mm.

The diffraction profile was collected between 10 and 30 deg of 2θ with a step of 0.02 deg with a *Bruker AXS D8 Focus*. The goniometer radius was 217.5 mm, and the divergence slit width was 0.1°.

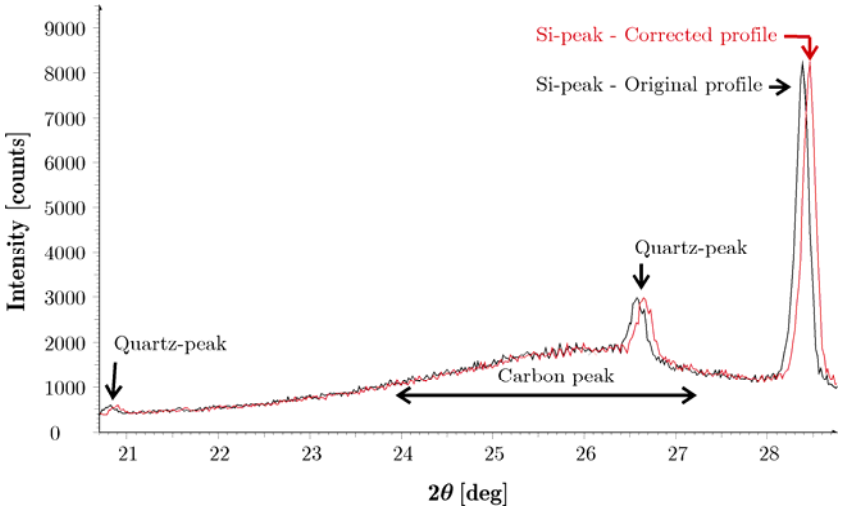

Figure 3-5: Shifting of the XRD profile was done. The carbon, silicon and quartz peaks are indicated. This is the profile for the -1.68 mm SSAB coke. Using Profile a mathematical function was fitted to the corrected profile.

Each diffraction profile was then corrected for Lorentz factor, polarization factor, absorption factor and atomic scattering factor of carbon, as described by Madshus (2005, pp. 47-49), who corrected the procedure described by Iwashita et al. (2004). These are all sample and instrument dependent factors.

Due to the low adsorption coefficient of the carbon materials for X-rays and preparation of the samples, the profile may be shifted and the peak may have been broadened. The added silicon was used to shift the profile and correct for broadening so that the silicon peak matched the silicon standard, according to (Iwashita et al. 2004). The computer program *EVA* was used for the shifting process. By using the *Profile* software, the profile was smoothed and the background was subtracted. A mathematical function was then fitted to the diffraction patterns using *Profile*. The *Pseudo-Voigt 2* function, one of the predefined functions in *Profile*, with split peaks, gave the best fit. The goodness of the fit was assessed using the *R*-factor, which is calculated by *Profile* according to the following equation:

$$R = \frac{\sum_{2\theta}\left|I\left(2\theta\right) - P_r\left(2\theta\right)\right|}{\sum_{2\theta} I\left(2\theta\right)} \cdot 100\% \tag{3.2}$$

where $P_r\,(2\theta)$ is the profile fitted and $I\,(2\theta)$ is the observed intensity. R should be as low as possible, preferably below 10 % (Iwashita et al. 2004). R was below 4 % for all the experiments.

The interplanar spacing, d_{002}, was calculated by *Profile* according to Bragg's law:

$$n\lambda = 2d\sin\theta \tag{3.3}$$

where $\lambda = 1.541838$ Å is the wave length used for the 2θ area in question and n is a constant here equal to 1. From the *full width at half maximum* (FWHM) the crystallite sizes is calculated according to the Sherrer equation:

$$L_c = \frac{K\lambda}{\beta\cos\theta} \tag{3.4}$$

where $K = 0.89$ (ASTM 2007a) and β is the $FWHM$ corrected for broadening:

$$\beta = \sqrt{B^2 - b^2} \tag{3.5}$$

where B is the $FWHM$ of the (002) carbon peak and b is the $FWHM$ of the (111) silicon reflection.

In Table 3-5 the structural parameters from the XRD analyses are given. Several particle size ranges were tested so that a possible correlation between particle size and structural parameters can be detected.

Of the metallurgical cokes that has not been through an experiment, the Magnitogorsk coke seems to have the lowest L_c combined with a high d_{002}, and SSAB coke 6-10 mm is the metallurgical coke with the highest L_c. This indicates that Magnitogorsk coke is the metallurgical coke with the least ordered carbon

Table 3-5: Structural parameters from XRD-analyses of metallurgical cokes. Results from Kaczorowski (2006) are included.

Sample name	Material	L_c [Å]	d_{002} [Å]	Sample name	Material	L_c [Å]	d_{002} [Å]
Preussang Anthrazit	Anthracite	-	-	SSAB, -1.68 mm	Met. coke	22.87	3.42
Siberian	Anthracite	-	-	SSAB, 1.68-3.3 mm	Met. coke	22.31	3.44
Siberian, after exp.‡	Anthracite	19.18	3.46	SSAB, 3.3-6 mm	Met. coke	23.42	3.43
Brazilian 4-35mm	Charcoal*	-	-	SSAB, 6-10 mm	Met. coke	27.92	3.43
Brazilian 4.7-13.4mm	Charcoal*	-	-	SSAB, 10-20 mm	Met. coke	27.04	3.43
Brazilian 13.4-35mm	Charcoal*	-	-	SSAB, 60-100 mm	Met. coke	24.34	3.43
Indonesian 4.7-13.4mm	Charcoal*	-	-	Zdzieszowice, 12-25 mm	Met. coke§	21.31	3.46
Indonesian 13.4-26.9mm	Charcoal*	-	-	Zdzieszowice, 60-100 mm	Met. coke	22.28	3.44
Corus, 5-10 mm	Met. coke	26.60	3.43	Chalmette	Pet. coke	-	-
Corus, 15-20 mm	Met. coke	25.27	3.42	Marietta shot	Pet. coke	-	-
Corus, 60-100 mm	Met. coke	22.87	3.45	Mar. shot, preh. one phase f.	Pet. coke	27.41	3.47
Magnitogorsk	Met. coke§	19.26	3.46	Mar. shot, after exp.‡	Pet. coke	57.84	3.42
Min Metals	Met. coke	-	-	Marietta sponge	Pet. coke	16.36	3.41
Min Metals, after exp.‡	Met. coke	33.65	3.42	Mar. sponge, preh. 850°C	Pet. coke	-	-
Tian Jin	Met. coke	19.66	3.44	Mar. sponge, after exp.‡	Pet. coke	27.42	3.45
Tian Jin, after exp.‡	Met. coke	27.17	3.42				

*From (Eidem 2004b) **Only one anaysis ‡After bulk resistivity experiment §From (Kaczorowski 2006)

structure and SSAB coke 6-10 mm is the metallurgical coke with the highest structural ordering. This may be due to different soaking time and temperature during production.

The sponge petroleum coke, which has been heated to only around 500°C, has a lower L_c compared to the metallurgical coke. The lower L_c is probably due to the lower heat treatment temperature.

When comparing results of Tian Jin metallurgical coke before and after the bulk resistivity experiment, where the coke is heated to approximately 1500°C, the L_c has increased from 19.66 Å to 27.17 Å. This indicates that the carbon structure will continue to develop during the experiment. This is also seen for the Marietta shot petroleum coke which has an increase in the L_c value from 27.41 Å to 57.84 Å. The big difference in increase of L_c between the metallurgical coke and the petroleum cokes is most likely due to the higher graphitizability of the petroleum coke compared to the metallurgical coke.

In Figure 3-6 the carbon crystallite parameters found by XRD analyses are plotted as a function of particle size. It is not possible to see any correlations valid for all cokes, but for Corus coke L_c decreases with increasing particle size. The same is seen in the same particle size range for the SSAB coke. However, for lower particle diameters of SSAB coke this trend is not seen.

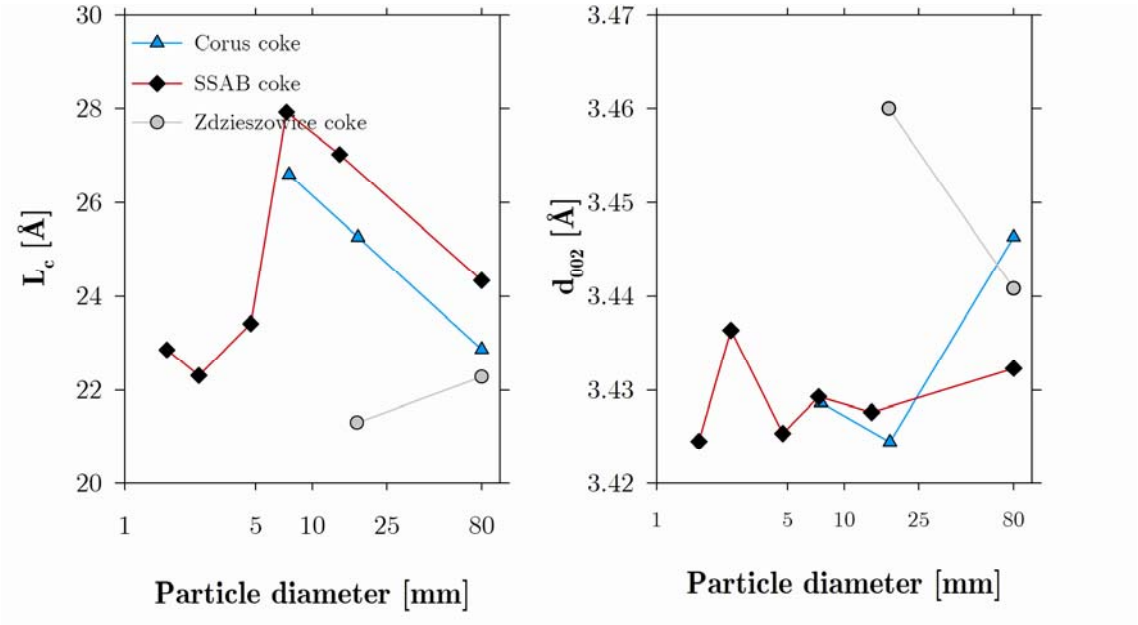

Figure 3-6: Carbon crystallite parameters plotted as a function of temperature for Corus coke, SSAB coke and Zdzieszowice coke.

Chapter 4 Material Resistivity and Contact Resistance

Environmental restrictions and increasing coal prices has lead to the shut down of many coke plants in Europe in the later years. Combined with the high demand for coke in China, the coke prices have increased and the availability has decreased after approximately year 2000. It has also been seen that blast furnace operators have started to use smaller particle sizes during the same period. As a result of this, the industry has been seeking more fundamental knowledge about the usage of various carbon materials.

Dig-outs have confirmed that there is a coke bed present in the FeMn, SiMn and FeCr processes. It is known that heat is developed in the coke bed as a result of ohmic heating, but little is known about the fundamental mechanisms controlling the resistivity of the coke bed.

In this chapter, two of these mechanisms are studied through experiments, namely the *material resistivity* and the *particle-to-particle contact resistance*. An apparatus was developed where the values could be measured at

temperatures up to 1600°C. The material resistivity of three metallurgical cokes and one anthracite has been measured. The contact resistance has also been measured for the three metallurgical cokes. Measurements on graphite are also included as a reference.

4.1 Apparatus and method

One of the goals of this thesis work was to develop an apparatus that would give reliable results that may be used for obtaining the material resistivity and contact resistance of carbon materials at elevated temperatures. In the following the measurement setup procedure of the experiments will be presented.

4.1.1 Measurement setup

The measurement circuit shown in Figure 4-1 is placed inside a graphite tube furnace capable of reaching the desired 1600°C, see Figure 4-2. The sample is placed between the graphite electrode and the graphite support. The measurement current is supplied to the graphite electrode via a molybdenum (Mo) wire as indicated in Figure 4-2. An alumina tube is placed around the wire for electrical insulation. The voltage drop measurements are done by two thin Mo wires that are wrapped around the sample in small grooves, approximately 3 mm from the top and bottom of the sample. The thin Mo wires are connected to thicker Mo wires, which again are connected to a data logger. An alumina tube is placed around the sample as a radiation shield and support for the top electrode. There is also an alumina tube placed around the graphite electrode, both to increase the weight of the electrode (461 g) and as electrical insulation. The applied force on the sample is 4.52 N. All graphite and alumina parts, as well as exposed Mo wires, are coated with Boron nitride (BN), and spacers made out of BN are mounted on the support. This is done to ensure that the measuring circuit is electrically insulated from the graphite tube heating element. Further detail on the four point measurement principle is shown in Appendix 4.

The measuring current going through the sample is supplied by a current controlled DC power source. The measuring current was kept at about 4.1 A

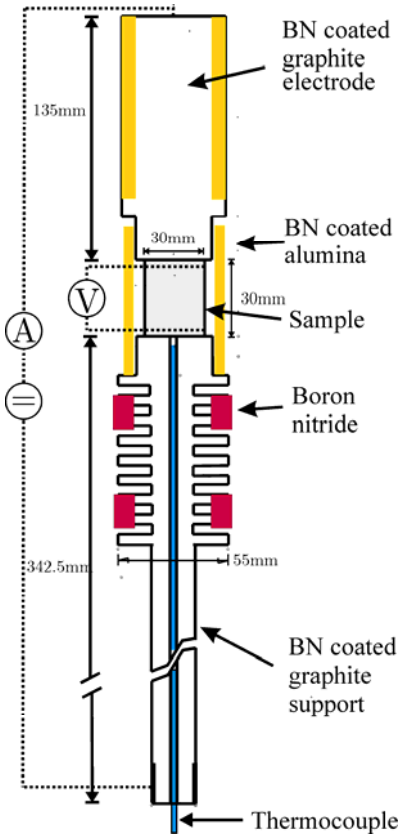

Figure 4-1: The measuring circuit for material resistivity and contact resistance.

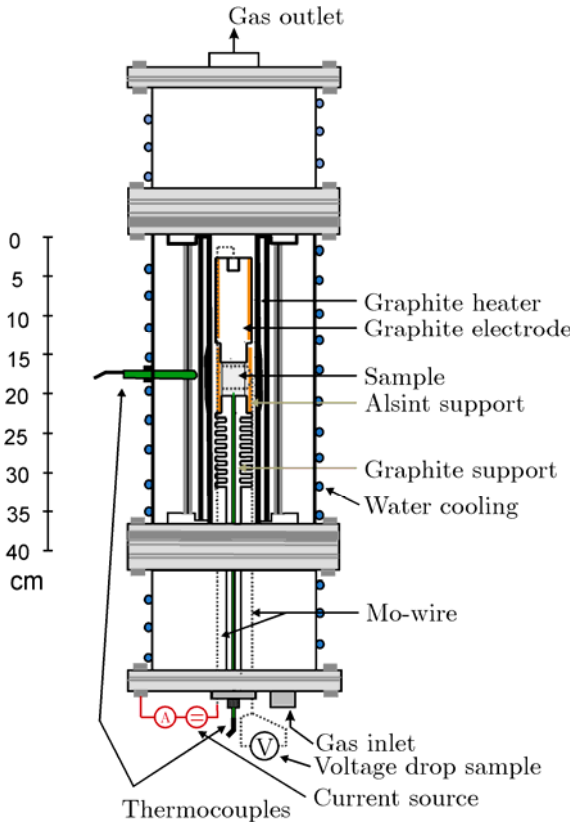

Figure 4-2: The measuring circuit is placed inside a graphite tube furnace so that measurements can be done at 1600°C.

during the experiments, which for the ϕ30/15 mm double cone sample corresponds to a current density of approximately 23 kA/m^2 at the 15 mm diameter neck. By comparison, in a 45 MVA furnace the current flowing through one of the electrodes, diameter 1.9 m, would typically be 100 kA, which corresponds to a current density of 35 kA/m^2 in the electrode. If the coke bed is bell shaped, as reported by Barcza et al. (1979), the current density will decrease as the radius of the coke bed increases. One experiment was done to check the influence of the current density on the measured resistance. The results will be presented in the results section. The calculation of the material resistivity and contact resistance will be presented in Section 4.3.

The temperature is measured below the sample, inside the graphite support, see Figure 4.1. A typical temperature development during an experiment is shown

as the solid black lined in Figure 4-3. The vertical temperature gradient over the carbon sample is about 10°C, as shown in Figure 4-4. The difference in temperature between the top of the sample and the position where the temperature is measured inside the graphite support, around 5 mm below the sample, is about 12°C. These differences in temperature are thought to be of little or no significance to the results.

The furnace is controlled by a separate thermocouple, indicated in Figure 4-2. The furnace thyristor regulator is programmed to follow the temperature path indicated by a broken line in Figure 4-3. From room temperature the furnace is programmed to increase the temperature to 500°C with a rate of 40°C/min. The furnace is held at 500°C for 5 minutes to avoid having large temperature gradients in the furnace. The furnace is then programmed to follow a 10.4°C heating rate to 1500°C. The temperature measurements below the sample do, however, show that the temperature measured by the control thermocouple is approximately 150°C lower compared to the temperature measured below the sample when the latter shows 1600°C. The reason for this difference is probably the heat shield separating the thermocouple from the heating element and the

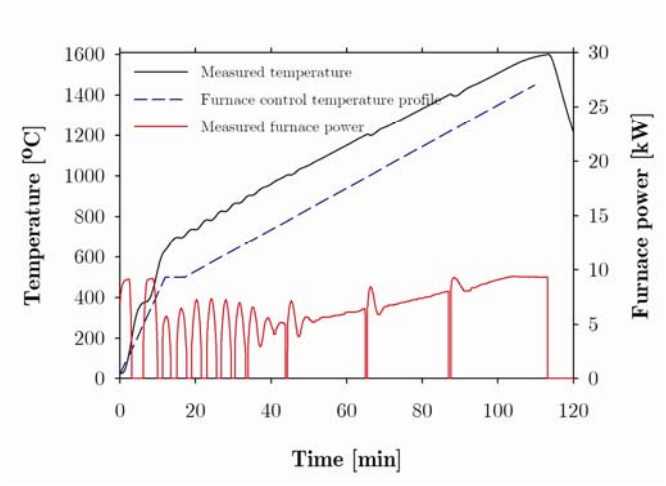

Figure 4-3: Temperature measurement, furnace power and furnace control temperature during experiment.

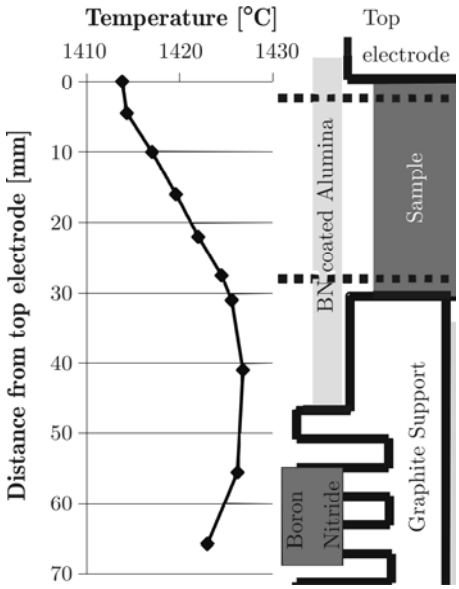

Figure 4-4: Vertical temperature profile in the measurement area.

relative closeness to the water cooling of the furnace. The measured temperature and furnace power shown in Figure 4-3 indicate that the furnace control is rather poor below 900°C. This can be seen as both the power and to some degree the measured temperature is fluctuating in this region. The previously mentioned difference in temperature measured by the two thermocouples is evident from around 500°C. The measured temperature below the sample reaches approximately 740°C before the heating continuous. The measured temperature during heating, i.e. not including the small decrease in temperature where the electrical measurements have been taken, follows the programmed slope. The reason for the decreasing difference between the furnace control temperature and the temperature measured below the sample is that the furnace control temperature plotted is the programmed temperatures. When the furnace is turned on after the electrical measurements have been done, the temperature has dropped a few degrees, and the furnace starts heating at the determined heating rate. Two examples of this temperature variation are shown in the next section.

The size of the apparatus is limited by the width of the graphite tube, 56 mm, and the height of the graphite tube. Radiation shields had to be mounted above the graphite electrode and be an integrated part of the graphite support. The graphite tube furnace also introduced potential problems concerning the measurements in the close vicinity of large currents. This was solved by turning off the power of the graphite tube furnace while taking the measurements at given temperatures.

4.1.2 Measurement procedure

Prior to and during the measurements, a checklist is followed so that the experimental conditions are as similar as possible. Below is a presentation of the procedure.

1) All the interfaces of the measuring circuit where current flows through are brushed lightly with sand paper. This is to remove any oxidation layers or misplaced boron nitrite. There is also a visual control that the boron nitrite

coating is covering all parts of the measuring circuit that are not supposed to get in electrical contact with the graphite tube.

2) Molybdenum (Mo) wires that are 0.127 mm in diameter are wrapped around the sample, 3 mm from the end surfaces of the sample, as will be shown in the next section where the sample shapes are more thoroughly presented. The Mo wire is placed in a very thin slit in the sample to prevent any movement of the wire during the measurement. The geometrical dimensions of the sample are measured and the distance between the Mo-wires are measured.

3) The sample is mounted in the apparatus, i.e. the Mo wires are connected to the HP 34970A Data Acquisition/ Switch unit and the heat shield and top electrode are mounted.

4) The furnace is closed and then evacuated and flushed with argon three times. A small amount of argon is allowed to flush through the furnace throughout the experiment. The flow rate of argon is measured with a flow meter not calibrated for argon, i.e. the exact amount is not known, but it is known to be the same for all experiments.

5) The water cooling is turned on, and the water pressure out of the furnace is noted (approximately 2 bar).

6) The resistance between the measuring circuit and the graphite heating element is measured to ensure that there is no electrical contact between the two.

7) The measurement current and the logger are turned on, the measurement current noted, and a measurement is made at room temperature before turning on the furnace power. The logging frequency is approximately every 3 seconds. Each channel is logged individually, and not simultaneously. This is done so that the measurements of one channel will not be affected by the other channels.

Consequently, the measurements are an integration over a period of time during the last three seconds. The integration time is controlled by the logging unit.

8) The second measurement is taken as the temperature passes through the maximum at the 5 minute holding temperature, i.e. the temperature first increases and then starts to decrease within this holding time. This is illustrated in Figure 4-5, where the recorded temperature and resistance of one of the Zdzieszowice coke experiments are shown. The period over which the measurement is done, approximately 3 seconds, is indicated in pink. The temperature is approximately 740°C. At this point the furnace control has turned the power off, see Figure 4-5.

9) Measurements are then taken at 1000°C, 1200°C, 1400°C and 1600°C. In Figure 4-5 the measurements done at 1000°C and 1400°C are shown as a typical example of the temperature recorded during the resistance measurements. Before the resistance is measured, the furnace power is turned off by the operator. The furnace power is turned on after 30 seconds. This is done to prevent the magnetic fields from the tyristor controlled furnace to influence the

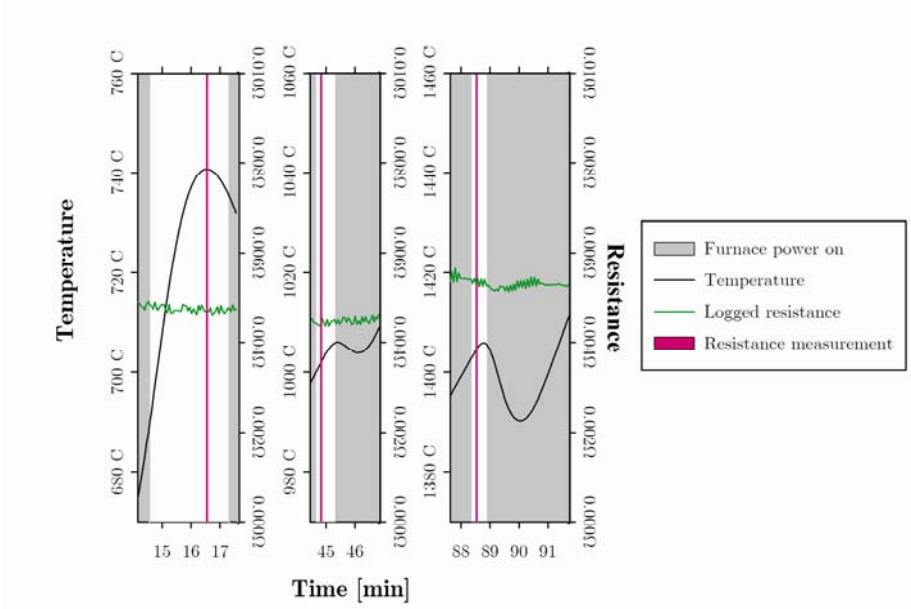

Figure 4-5: The furnace power is turned off while the measurement is taken to prevent any influence from the strong magnetic fields.

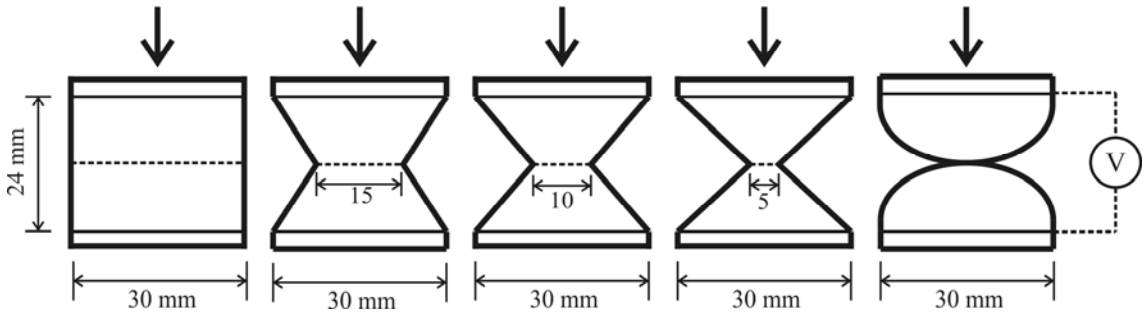

Figure 4-6: Samples shapes used for measuring contact resistance. The divided samples were divided at the dotted line.

measurements. The measurement used is the second measurement where the 3 second of logging period does not include the furnace being on, i.e. the 3 second measurement period can start from 3 to 6 seconds after the furnace power is turned off. It is expected that any radial temperature gradient that may be present in the sample is, to some extent, reduced within these 3 to 6 seconds. The measured temperature increases less than 1°C within the measurement time. Due to uncertainties of the appropriate time of measurement, the procedure of turning off the furnace for 30 seconds while doing measurements was chosen.

10) The furnace is turned off at 1600°C, and the logging is stopped. It was decided not to measure the electrical resistivity while cooling down the furnace since this is not relevant from an industrial perspective.

4.2 Samples

To measure the *material resistivity* 30 mm diameter cylinders were machined and core-drilled out of 60-100 mm coke and anthracite lumps. To determine how the *contact resistance* varied with contact area, samples with various contact area diameters were used. The sample shapes are shown in Figure 4-6.

The contact area diameters were 30, 15, 10 and 5 mm. The measurements were done first on a whole sample, and then at a different sample that was divided in two at the dotted lines in Figure 4-6. The contact resistance was estimated by

SSAB ϕ30/15 mm SSAB ϕ30/5 mm SSAB divided ϕ30/5 mm

Figure 4-7: Photos of machined samples of SSAB coke. The samples are representative in that they illustrate the challenge it has been to machine the sample shapes. Photos by M. Gall.

subtracting the resistance measured of the whole sample from the resistance measured on the divided sample. In the following the double cones will be denoted by the largest and smallest diameter of the sample: The notation "div. d.cone ϕ30/5 mm" represents a divided double cone sample that has a diameter of 30 mm at the voltage measuring point and a 5 mm diameter at the contact interface.

In Figure 4-7 photos of the machined samples of SSAB coke are shown, illustrating how porous the material is. Of the divided sample shapes, the double cone ϕ30/5 mm was the most challenging, both to machine and to line up when divided double cone was tested. Some of the samples had to be discarded due to defects, such as the left sample of the two divided double cone ϕ30/5 mm sample shapes in Figure 4-7.

Two half spheres were also tested, but not as a whole sample. This is the shape that is assumed to have a contact area most similar to that of particles in contact in a dry coke bed.

An overview of the experiments performed is shown in Table 4-1. Graphite is used as a reference material. To check if there are any drift in the apparatus,

Table 4-1: Overview of the number of experiments done for each of the sample shapes and parameters.

Type \ Shape	Cylinder ϕ30mm		D. cone ϕ30/15mm		D. cone ϕ30/10mm		D. cone ϕ30/5mm		Half spheres
	Whole	Divided	Whole	Divided	Whole	Divided	Whole	Divided	
Graphite	7	2	2	2	2	2	2†	2	2
Preussang Anthracite	1	-	-	-	-	-	-	-	-
Corus coke	4	1	1	-	1	1	-	-	2
SSAB coke	4‡	2	2	2	3*	2	1	1	2†
Zdzieszowice coke	5	2	2	2	3	3*	-	2†	1

†In addition experiments are repeated without taking the sample out

‡One sample ϕ15mm *One of the experiments not successful

graphite cylinders have been tested throughout the experimental series. Four replicate experiments[1] were also performed for the cylinder shapes of the three cokes to obtain a better estimate of the material resistivity of the metallurgical cokes. When possible, two parallels were performed of each of the other sample shapes, both whole and divided samples. However, metallurgical coke proved challenging to machine, something that is reflected in the number of samples produced for some of the cokes. One anthracite was also sent for machining, but no samples could be made due to the flaky structure of the material. Some additional experiments were done to investigate the effect of reheating the sample. For graphite this will indicate the operator influence on the experiments, and for metallurgical coke these experiments will indicate how the material has changed.

[1] In this thesis a replicate (or parallel) experiment (or run) is an experiment with a different sample of the same material and shape as the original sample, tested under the same conditions.

Most of the samples, except the half spheres, the whole 5 mm neck samples of the cokes, the Corus coke samples and the Preussang anthracite samples, had a 3 mm diameter hole through the centre of the sample. This is due to an unfortunate error in the machining. Due to lack of raw material, the samples could not be redone. This is compensated for in the calculations involving the cross section area of the samples, i.e. when calculating the material resistivity.

4.3 Calculation of material resistivity and contact resistance

The sample resistance R_{sample}, calculated from the measured current in the measurement circuit and the voltage drop indicated in Figure 4-6, is given by Equation (4.1). In Equation (4.1), which is Equation (2.1) rewritten, the material resistivity ρ_m is unknown, but assumed to be constant. The unknown material resistivity is calculated by putting in the expression describing cross section area of the sample A_{sample} at any height h of the sample, and solving for ρ_m.

$$R_{sample} = \int_0^{h_{sample}} \frac{\rho_m}{A_{sample}(h)} dh \tag{4.1}$$

where h_{sample} is the height between the two Mo-wires wrapped around the sample for measuring the potential drop. It is, as for Equation (2.1), assumed that the current is uniformly distributed over A_{sample}. Consequently, the potential lines are parallel to the end surfaces of the sample, i.e. where the current enters and exits the sample. If this assumption is valid for all the whole sample shapes shown in Figure 4-6, the number of experiments used for determining the average material resistivity would increase. For both SSAB and Zdzieszowice coke this would double the number of parallels, giving a better estimate of the material resistivity. As is shown in Appendix 1, this assumption does not hold for the double cones, and the resistivity values determined from the double cones are excluded from the material resistivity.

The *contact resistance* is calculated by subtracting the *resistance* of the whole sample from the resistance of the divided sample. Where parallel measurements of whole samples are done, as for most of the sample shapes, the average resistance of the parallel runs is used for the calculation.

4.4 Material resistivity

4.4.1 Results

In Figure 4-8 the material resistivity of the *graphite* cylinder, diameter 30 mm, and the material resistivity given by the graphite producer is plotted against temperature. The lowest recorded material resistivity is at about 740°C for the graphite. A deviation is seen when the producer's values and the measured values are compared. This is probably due to the producer's values being typical values for the given type of graphite, i.e. not the material resistivity for the specific batch of graphite used in these experiments (Tokai Carbon Europe Ltd. 2002).

The experimental data do, however, show the same profile as the producer's values, decreasing from room temperature to a minimum material resistivity at

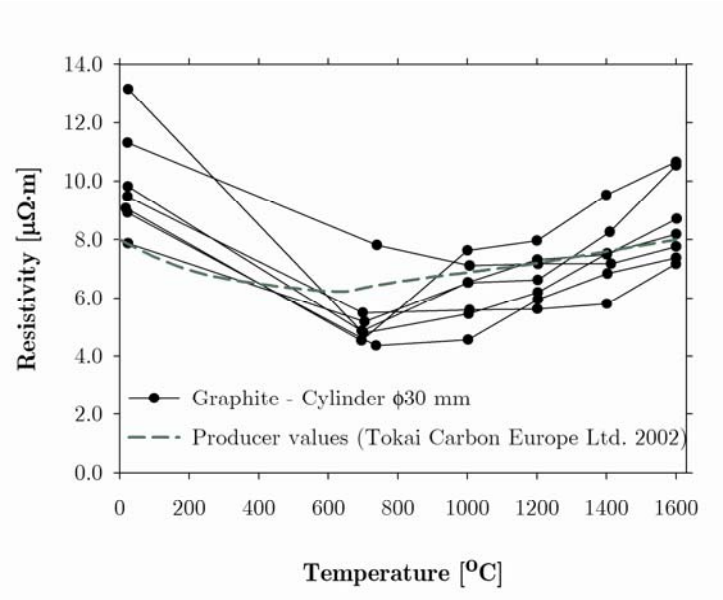

Figure 4-8: Measured resistivity of graphite cylinders and the typical value for the specific type of graphite, given by the producer (Tokai Carbon Europe Ltd. 2002).

a temperature below 1000°C. Above this temperature the resistivity yet again increases. Since the graphite cylinders ϕ30 mm were tested throughout the experimental period, a possible drift in the apparatus was assessed by adding a variable describing the run order. No drift was found. For further details, see Appendix 3.

The material resistivity results of the ϕ30 mm *metallurgical coke and anthracite* cylinders are plotted against temperature in Figure 4-9. It can be seen in Figure 4-9 that the material resistivity of the metallurgical cokes generally decreases, from room temperature to between 1200°C and 1400°C. For some of the experiments an increase in the material resistivity is then recorded when the temperature is further increased. This is also reflected in the average values shown in Table 4-2. For the Preussang anthracite the resistance was too high to get a good measurement below approximately 700°C. At 1600°C the material resistivity of the anthracite is approximately 4 times higher compared to the material resistivity of the metallurgical cokes. As expected, the material resistivity of the metallurgical cokes is more than one order of magnitude higher than that measured for graphite.

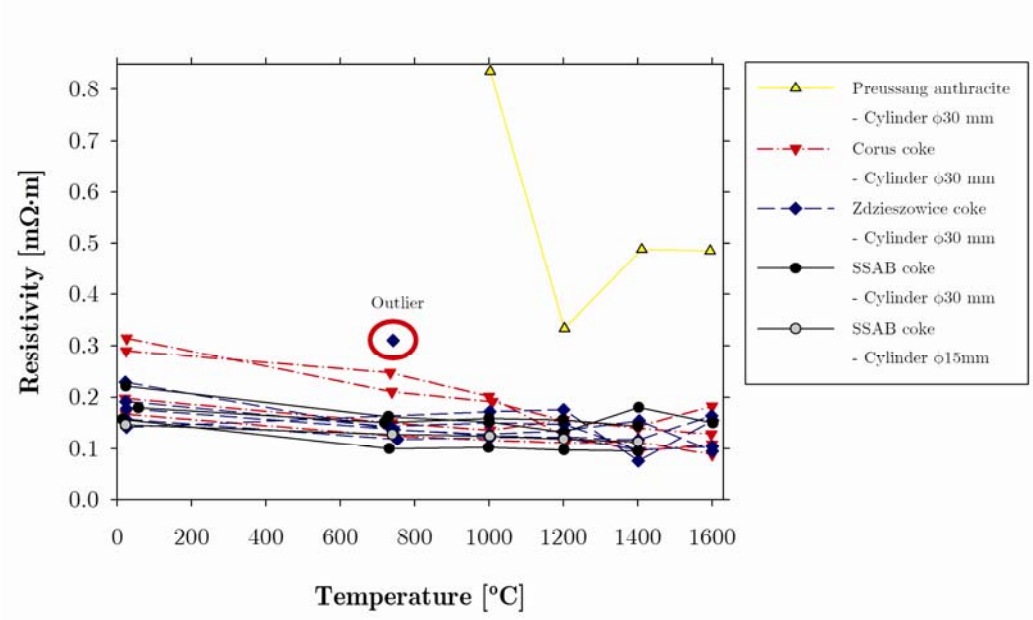

Figure 4-9: Measured material resistivity of Corus, SSAB and Zdzieszowice cokes and Preussang anthracite.

The material resistivity of the ϕ15 mm Zdzieszowice cylinder is within the material resistivity recorded for the other Zdzieszowice samples and will be included in the "Cylinder ϕ30 mm" when nothing else is specified.

Linear regression analysis has been done on the material resistivity data from 1000°C to 1600°C. This temperature region has been chosen since this is the temperature region of interest, and due to the furnace control being stable in this temperature span. The temperature was used as a variable in all the analyses as well as a variable describing a material property. The latter was introduced to be able to differentiate between the three cokes. The material properties used include the ash, fixed carbon and volatile content, and the graphene stack height, L_c. The d_{002} value was almost equal between the three cokes, and was thus not used. The regression results showed that there was no statistically significant difference between the material resistivity of the three cokes. This can also be seen from the standard deviations shown in Table 4-2, where the difference in the material resistivity between the metallurgical cokes is within the standard deviation. For further details, see Appendix 3.

An outlier in one of the experiments is shown in Figure 4-9. This point has been excluded from the statistical evaluation of the data. No correlation between the standard deviation and the temperature is observed.

Part of the variation in between the experiments is due to operator influence. The operator handles the sample, mounts the molybdenum measuring wires on

Table 4-2: Average material resistivity of the graphite and the metallurgical cokes. The standard deviation is given when two or more parallels have been done. Only the measurements were done on ϕ30 mm cylinders.

Temperature	25±9°C	728±18°C	1 002±3°C	1 202±2°C	1 403±4°C	1 600±1°C
Graphite	9.9 μΩ·m± 18%	5.3 μΩ·m± 22%	6.2 μΩ·m± 17%	6.7 μΩ·m± 12%	7.5 μΩ·m± 15%	8.6 μΩ·m± 17%
Corus coke	242 μΩ·m± 29%	183 μΩ·m± 30%	161 μΩ·m± 26%	137 μΩ·m± 16%	123 μΩ·m± 19%	127 μΩ·m± 32%
SSAB coke	177 μΩ·m± 19%	136 μΩ·m± 20%	135 μΩ·m± 20%	126 μΩ·m± 19%	133 μΩ·m± 28%	151 μΩ*
Zdzieszowice coke	180 μΩ·m± 21%	133 μΩ·m± 8%	140 μΩ·m± 17%	141 μΩ·m± 16%	109 μΩ·m± 31%	130 μΩ·m± 27%
Preussang anthr.	-	32 $\cdot 10^6$ μΩ*	840 μΩ*	330 μΩ*	490 μΩ*	480 μΩ*

*Only one experiment gave stable results

the sample, mounts the top electrode, closes and evacuates the furnace, regulates the argon gas flow and the cooling water flow, and so on. Although measures have been taken to minimize the variation, there will always be an influence by the operator. The influence of the operator has been investigated by doing repeated measurements on the same whole graphite double cone ϕ30/5mm, without taking the sample out of the furnace. Graphite is used since the material will not change due to the heat treatment. The operator dependent factors that may influence the measurements are then only adjustment of the cooling water and argon flow, which had to be switched off between the runs.

The results, shown in Figure 4-10, show no pattern between run number and the measured resistance. The standard deviation at the different temperature steps is below 6 %. The standard deviation of the measurements is highest at approximately 730°C, with 6 %.

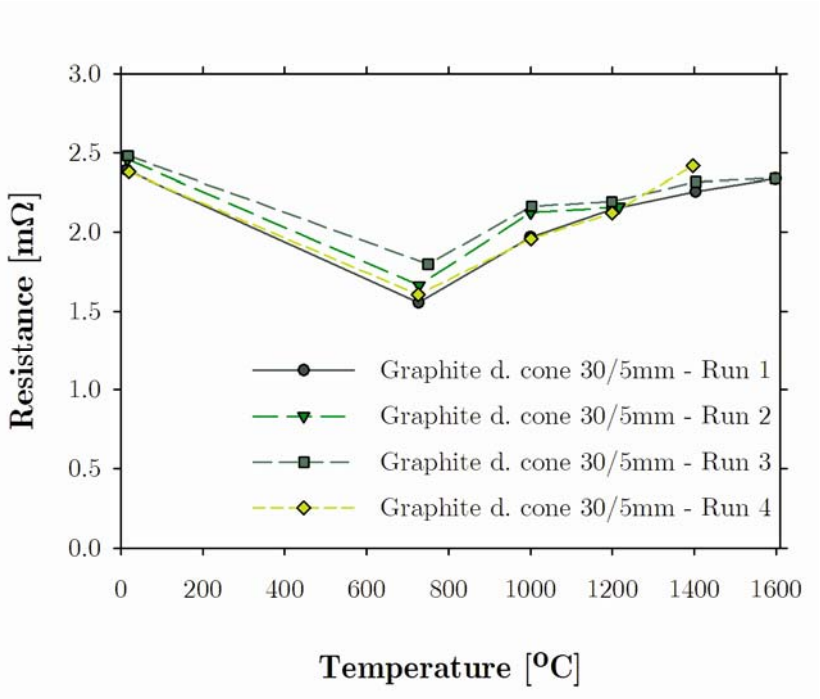

Figure 4-10: The variation due to operator influence is checked by reheating the sample without taking it out of the furnace.

In the various experiments the measurement current was the same, i.e. the current density varies with the neck diameter of the sample. One experiment was done to check the influence of the current density on the measured resistance of the sample. A graphite cylinder, 30 mm diameter with a 3 mm diameter hole through the middle, was used. The previously described procedure was followed to measure the resistivity of the sample up to 1600°C. The temperature was then adjusted to approximately 1400°C. To ensure stabilization of the system, 10 measurements were done over approximately 30 seconds 10 minutes after the last adjustment of the system parameters. The recorded measurements do, however, show that the system is stabilized a few seconds after the current adjustment. The furnace was *not* turned off during these measurements since this would influence the temperature of the furnace.

The results show that the measured resistance is slightly influenced by variations of the current, see Table 4-3. An increasing current density gives an increase in the measured resistance. However, most measurements are within two times the standard deviation of the average of the resistance measurements measured at 5920 A/m^2. The average resistance of all the samples is 214 μΩ ± 7 % .

The temperature during this part of the experiment is 1400°C ± 0.3°C.This is less than the thermocouple uncertainty, which is ± 2°C for this temperature region, see Appendix 2.

Table 4-3: Influence of current on the measured resistance of a graphite cylinder. The standard deviation is given for the measurements.

Current density [A/m^2]	Resistance [μΩ]	Temperature [°C]	Run order
2900 ± 0.1%	185 ± 1.2 %	1400	3
5840 ± 0.7%	215 ± 1.4 %	1400	6
5920 ± 0.7%	214 ± 1.7 %	1400	1
7160 ± 0.6%	220 ± 1.1 %	1400	4
8540 ± 0.6%	224 ± 0.7 %	1400	2
9950 ± 0.6%	227 ± 0.7 %	1400	5

4.4.2 Discussion

Graphite

The temperature dependency of the material resistivity shown in Figure 4-8 is typical for polycrystalline graphites. The material resistivity decreases from room temperature to between 700°C and 800°C. Beyond this temperature, the material resistivity increases. As explained by Mrozowski (1952) the decrease in material resistivity from room temperature to the temperature when the lowest resistivity is reached, is due to the increasing number of electrons excited to the conduction band. At one temperature the number of electrons in the conduction band is so large that when more electrons are excited, this does not cause a further decrease in material resistivity. So when the temperature is increased further, this causes increased thermal scattering of the electrons. The measured material resistivity is in agreement with the established empirical data and theory for polycrystalline graphite.

In Figure 4-8 the typical resistivity variation of the graphite with temperature reported by the producer, not specific for the graphite specimens used in these samples, is plotted (Tokai Carbon Europe Ltd. 2002). The average of the measured material resistivity of the graphite samples is lower compared to the producer values at all temperatures except room temperature and 1600°C, However, at room temperature, the producer values are within the standard deviation of the material resistivity measurements. Unfortunately no data is given by the producer on the accuracy of the test used, so it is difficult to evaluate the accuracy of the measurements obtained in this work compared to those done by the producer.

Metallurgical cokes

At room temperature the material resistivity of the metallurgical cokes is measured to be between 0.18 mΩ·m and 0.24 mΩ·m, and at 1000°C the material resistivity is measured to be between 0.14 mΩ·m and 0.16 mΩ·m. By comparison Ukanakov et al. (1973) measured the material resistivity of some metallurgical cokes at room temperature to be between 0.12-0.21 mΩ·m, i.e.

within the same range as measured in this work. Sørlie and Gran (1992), found the material resistivity of two types of prebaked carbon blocks based on electrocalcined anthracite to be 0.034 mΩ·m and 0.042 mΩ·m at 1000°C. One type of prebaked carbon block that was characterized as graphitic had a material resistivity measured as 9.0 μΩ·m, both at room temperature and at 1000°C. The graphitic carbon prebaked carbon block has a material resistivity similar to that measured for the graphite reference material in this work, which was measured as 6.2 μΩ·m at 1000°C. The two other carbon blocks are characterized as amorphous, probably due to the use of anthracite in the carbon blocks. However, it is not a material comparable to the Preussang anthracite measured in this work, since the Preussang anthracite is "pure" anthracite and the carbon blocks are a mixture of a binder phase and anthracite. The binder phase is most likely a highly graphitizable material such as coal-tar pitch, decreasing the material resistivity significantly compared to the anthracite and the metallurgical coke.

The results presented in Figure 4-9 indicate that the material resistivity of the metallurgical cokes decreases between room temperature and 1600°C, with a sharper decrease in material resistivity between room temperature and 740°C, compared to 740°C to 1600°C. The temperature dependency is, as discussed by Mrozowski (1952), probably due to a large energy gap between the valence band and the conductive band. As the temperature increases up to approximately 1000°C, which is the typical production temperature for metallurgical coke, the number of electrons in the conductive band increases. Above the production temperature it is expected, according to Mrozowski (1952), that there will be an increased crystallite growth. It has previously been shown empirically that there is a moderate crystallite growth in the temperature region 1000°C to 1600°C, with only a minor influence of the holding time at the heat treatment temperature (Tangstad 1994; Kawakami et al. 2006). Mrozowski (1952) concludes, as mentioned in Chapter 2, that this crystallite growth will reduce the number of mobile electrons available, reducing the material resistivity.

A reduction in material resistivity is also seen for the Preussang anthracite. Different from the metallurgical cokes, the anthracite will be greatly affected by the temperature, even low temperatures. Volatiles, which from previous works is known to increase the bulk resistivity, will be driven off as the material is heated. Some ordering of the carbon structure probably also occurs.

Looking closely at the data in Table 4-2 it can be seen that the average values of the SSAB and Zdzieszowice cokes increase slightly, SSAB from 1200°C to 1600°C, and Zdzieszowice from 1400°C to 1600°C. This is, although not as pronounced, the same as is observed for the bulk resistivity, where an increase in the bulk resistivity has occurred around 1200°C. Mrozowski (1952), concludes that the temperature at which the minimum material resistivity occurs is depending on the degree of graphitization of the material. An example is given of a carbon rod that has been baked to 1000°C. Based on material resistivity measurements up to approximately 1200°C, Mrozowski (1952) concludes that the minimum resistivity cannot be reached below 2000°C. However, these were petroleum coke rods, which probably are highly graphitizable. Consequently, the material will graphitize as the sample is heated, not reaching the minimum due to the further graphitization of the material. A metallurgical coke, on the other hand, may, since it is a non-graphitizable material, reach a minimum material resistivity at a lower temperature. This could, however, not be explored in the present apparatus due to its temperature limitation.

When comparing the material resistivity of the Corus coke, the SSAB coke and the Zdzieszowice coke, the large variance within the data makes it challenging to isolate a clear difference between the cokes, see Figure 4-9. Ukanakov et al. (1973) also observed that the electrical resistivity of metallurgical cokes were almost identical. Statistical analyses have been done in this work to find out if there is any significant difference in material resistivity between the types of metallurgical cokes. As mentioned, various parameters were used to describe the differences, including fixed carbon, volatile matter and L_c. None of the parameters gave any significant difference between the three metallurgical cokes.

It seems as though the variation between two pieces of coke within one type of metallurgical coke is larger than the difference between two metallurgical cokes. Both L_c and d_{002} are expected to influence the electrical resistivity of the cokes. The reason why this is not seen may be that the difference in these values between the three cokes is small. The d_{002} values are, as can be seen in Chapter 3, under XRD analyses, 3.45 Å, 3.43 Å and 3.44 Å for Corus, SSAB and Zdzieszowice cokes, respectively. And the L_c value is 22.87 Å, 24.34 Å and 22.28 Å for the Corus, SSAB and Zdzieszowice cokes, respectively. The d_{002} values are almost equal, and were thus not used as in the statistical analyses. The L_c does vary some more, but are well within what Kawakami et al. (2006) defines as a moderate change in crystal size. It is possible that the lack of difference in material resistivity is due to the fact that the cokes have similar material resistivity properties.

Compared to the material resistivity of the graphite reference materials, shown in Figure 4-8, the material resistivity of the metallurgical cokes is approximately one order of magnitude higher. This is as expected and is due to the very high degree of graphitization of the graphite. As shown by the XRD analyses of the materials, the L_c and d_{002} values of the metallurgical cokes are typically 23 Å and 3.4 Å, respectively. Safarian (2007, pp. 74) tested various graphites and found L_c values between 327 Å and 578 Å, and d_{002} values between 3.36 Å and 3.38 Å. The crystallite sizes, described by the L_c value, reveal a large difference between the graphites and the metallurgical coke, which explains the difference in material resistivity between the two types of materials. In addition other factors such as the much higher porosity of the metallurgical cokes, cracks in the material and the large difference in ash content, < 0.1 % vs. 10 % for the graphite and cokes, respectively, increase the material resistivity further.

Sources of error

Part of the scatter of the experimental results is due to the operator of the apparatus, even though precautions are taken to minimize these. By not taking out the sample between the experiments the combined variance due to the operator and material variation was evaluated. The standard deviation of the

resistances of the four runs is 6 % at approximately 730°C, and lower for the other temperatures. By comparison, the standard deviation of the graphite cylinder results is between 12 and 22 % the difference being due to variation in the material and the experimental operator.

As can be seen in Figure 4-10, the resistance is not dependent on the order the experiments were carried out. A statistical analysis of the resistivity results of the graphite cylinders tested throughout the experimental period reveal no correlation between material resistivity and time.

The results of the current density test show that a higher current density will give a slightly higher resistance. In the experiments the current density was varied from 2900 A/m^2 to 9950 A/m^2. The standard deviation of the measured resistance over the current density range is 7 pct, which again is lower compared to the standard deviation of the graphite cylinder results. A consequence of this is that the resistance will increase when the cross section area of the neck is reduced due to the increased current density. This will not affect the material resistivity results since cylinders were used exclusively.

4.5 Contact resistance

4.5.1 Results

As previously mentioned, the contact resistance is calculated by subtracting the average of the measured resistance of the whole samples from the measured resistance of the divided samples, i.e. the samples that consists of two sample bodies that when put together are of the same geometry as the whole samples, see Figure 4-6. By doing so, only the part of the measured resistance that is due to the samples being separated is included in the contact resistance.

Graphite

In Figure 4-11 the average values of the measured *resistance* of the divided and whole *graphite* samples and the calculated *contact resistance* are plotted against temperature.

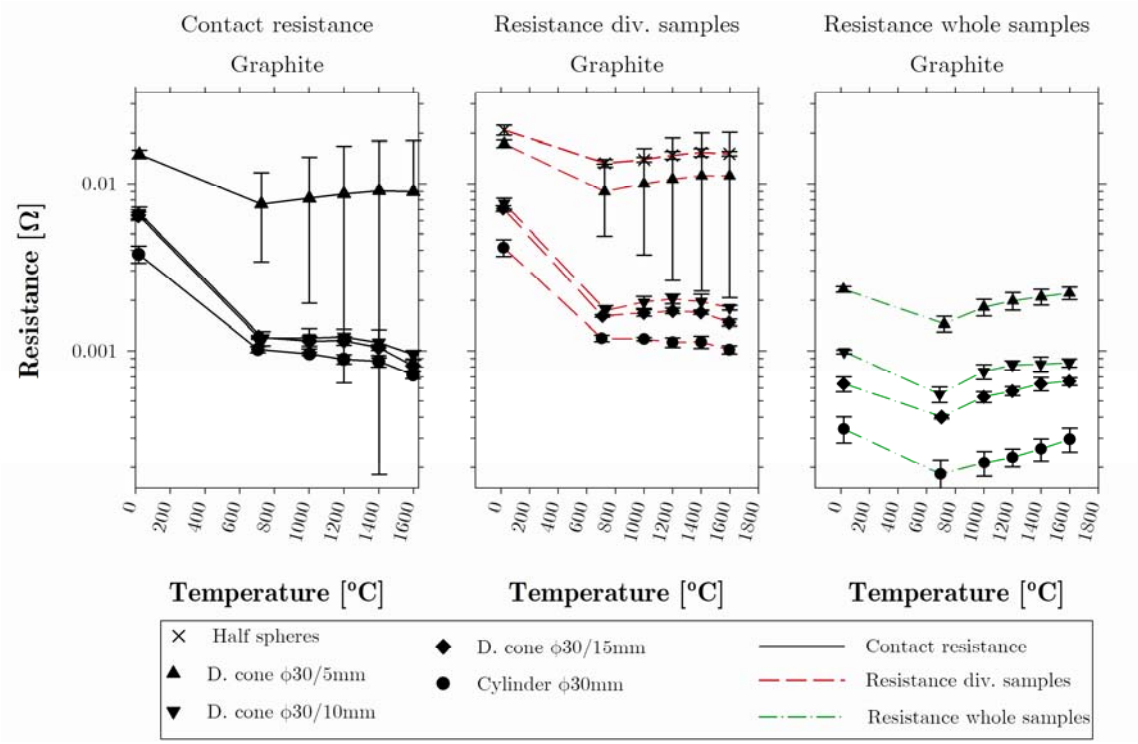

Figure 4-11: The calculated contact resistance, the resistance of the divided samples and the resistance of the whole graphite samples are shown. The standard deviation is indicated.

The resistance of the half spheres in contact and the contact resistance of the ϕ30/5 mm graphite double cone have a temperature dependency similar to that seen for the whole samples, i.e. a minimum is reached around 730°C. For the other sample shapes, the contact resistance decreases with increasing temperature from room temperature to approximately 730°C, then leveling out up to 1200°C and decreasing as the temperature is raised further. A similar trend can be seen for the divided samples, with the difference that the resistance increases from 730°C to 1200°C, before decreasing towards 1600°C.

It can be seen from Figure 4-11 that the contact resistance contributes significantly to the resistance when two sample bodies are in contact. The ratio R_c/R_{div} is between 0.87 and 0.92 at room temperature and between 0.53 and 0.80 at 1600°C, i.e. the contribution of the contact resistance decreases from 87 - 92 % at room temperature to 53 - 70 % at 1600°C. The R_c/R_{div} ratio generally decreases with increasing temperature and decreasing neck size. For

Table 4-4: Mean resistance [mΩ] ± std. dev. [%] of parallel runs of the graphite samples tested with pooled estimate of the standard deviation for each temperature.

Temperature	21±3°C	712±19°C	1001±2°C	1201±2°C	1401±4°C	1599±2°C
Cylinder ϕ30mm	0.34mΩ±18%	0.18mΩ ±22%	0.21mΩ ±17%	0.23mΩ ±12%	0.26mΩ ±15%	0.30mΩ ±17%
Div. cylinder ϕ30mm	4.14mΩ ±12%	1.19mΩ ±4%	1.18mΩ ±2%	1.12mΩ ±6%	1.13mΩ ±8%	1.02mΩ ±5%
Double cone ϕ30/15mm	0.64mΩ ±10%	0.40mΩ ±2%	0.53mΩ ±7%	0.57mΩ ±6%	0.64mΩ ±9%	0.66mΩ ±5%
Div. d. cone ϕ30/15mm	7.10mΩ ±4%	1.61mΩ ±2%	1.68mΩ ±5%	1.73mΩ ±4%	1.69mΩ ±3%	1.47mΩ ±4%
Double cone ϕ30/10mm	0.99mΩ ±3%	0.55mΩ ±11%	0.75mΩ ±10%	0.82mΩ ±6%	0.84mΩ ±10%	0.85mΩ ±6%
Div. d. cone ϕ30/10mm	7.63mΩ ±8%	1.74mΩ ±7%	1.94mΩ ±9%	2.04mΩ ±7%	1.96mΩ ±11%	1.80mΩ ±3%
Double cone ϕ30/5mm	2.32mΩ ±4%	1.45mΩ ±11%	1.82mΩ ±12%	1.98mΩ ±12%	2.09mΩ ±11%	2.20mΩ ±9%
Div. d. cone ϕ30/5mm*	17.4mΩ ±5%	8.99mΩ ±46%	10.0mΩ ±63%	10.7mΩ ±75%	11.2mΩ ±80%	11.2mΩ ±81%
Half spheres	20.9mΩ ±7%	13.3mΩ ±5%	14.0mΩ ±3%	14.8mΩ ±5%	15.4mΩ ±6%	15.1mΩ ±3%
Pooled std. deviation	15 %	18 %	15 %	12 %	15 %	13 %

Pooled estimate of the standard deviation of all the replicate runs: s = 14.7 pct.

*Excluded from pooled standard deviation

the divided cylinder and the ϕ30/15 mm and ϕ30/10 mm double cones the contact resistance decreases with increasing temperature, from room temperature to 1600°C. The contact resistance of the divided ϕ30/5 mm double cone and the resistance of the half spheres increases after a minimum contact resistance is reached at around 700°C.

In Table 4-4 the measured resistances of both the whole and the divided samples are given with the standard deviation. For the whole ϕ30 mm cylinder seven replicate runs were performed. For the other experiments two parallel runs were done. A pooled standard deviation is also calculated for each temperature level. This was done by calculating the mean squares of the pure error, which is an estimate of the error variance, according to Box et al. (2005, pp. 74).

From the data in Table 4-4 it is not possible to see any trend in the standard deviations suggesting that the variance, i.e. the squared standard deviation, is dependent upon temperature. The high standard deviation in the divided double cone ϕ30/5mm measurements is due to a shift in the positioning of the two samples in one of the experiments. The measurements are excluded from the pooled standard deviations. For the last six replicate runs of the ϕ30 mm

cylinder, graphite of another stock was used. This increased the standard deviation by a few per cent.

Metallurgical cokes

In Figure 4-12 the measured resistance of the divided samples, the calculated contact resistance and the resistance of the whole samples of the *Corus coke* samples are shown. Since the whole sample experiment of the ϕ30/10 mm double cone failed above 1200°C, the contact resistance at the 1400°C level was calculated as 86 % of the measured resistance of the divided samples, which is the same contribution that was found for the 1200°C level.

For the two divided samples and the half spheres, the measured resistance decreases with increasing temperature. This is, as expected, also the temperature dependency seen for the contact resistance of the divided ϕ30 mm cylinder and the whole samples. However, the contact resistance of the divided

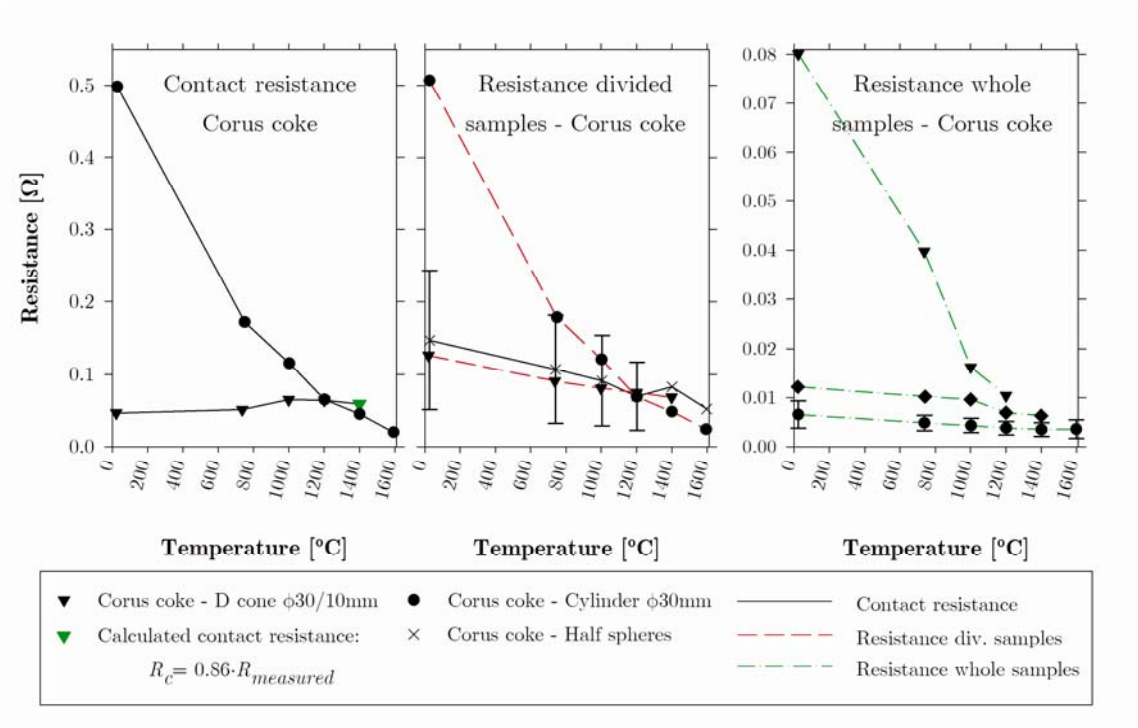

Figure 4-12: The resistance of the divided samples, the resistance of the whole samples and the calculated contact resistance for Corus coke is shown. The standard deviation is shown when two or more experiments have been carried out.

ϕ30/10 mm double cone *increases* from room temperature to 1000°C, and then level out up to 1400°C. This is due to the sharp decrease in the measured resistance of the whole ϕ30/10 mm sample in this temperature area, see Figure 4-12. For the whole temperature range of the whole samples, and above 1200°C for the divided samples and contact resistance, the resistance decreases with increasing neck diameter. Below 1200°C the resistance of the divided ϕ30 mm cylinder is more than twice compared to the measured resistance of the half spheres.

The graph show that the contact resistance contributes to a major part of the resistance when two sample bodies are in contact. For the ϕ30 mm cylinder the R_c/R_{div} ratio *decreases* from 0.99 at room temperature to 0.84 at 1600°C. For the ϕ30/10 mm divided double cone the R_c/R_{div} ratio *increases* from 0.37 at room temperature to 0.86 at 1200°C.

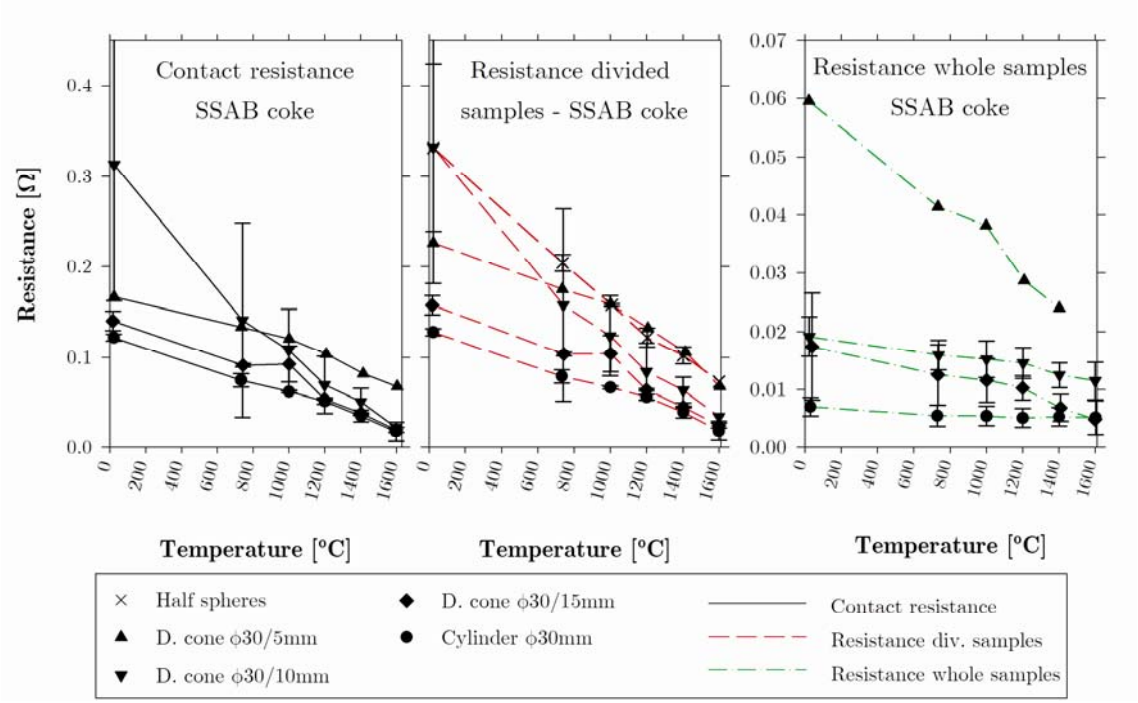

Figure 4-13: The calculated contact resistance, the measured resistance of the divided samples and the resistance of the whole samples of SSAB coke is shown. Standard deviation is indicated where two or more experiments have been carried out.

In Figure 4-13 the calculated contact resistance, the resistance of the divided samples and the resistance of the whole *SSAB coke* samples are shown. The standard deviation is shown when two experiments have been done.

For all the samples both the measured resistance of the divided and whole samples as well as the calculated contact resistance decreases from room temperature to 1600°C. For the divides and whole samples the measured resistance decreases with increasing neck diameter for all temperatures above room temperature. There is a large deviation between contact resistance results of the two parallel ϕ30/10 mm divided double experiments, one measurement being below the resistance of the ϕ30/5 mm double cone, and one experiment above. This is reflected by the indicated standard deviation and can also be seen in the calculated contact resistance. The ϕ30/10 mm divided double cone sample with the highest measured resistance had a very uneven contact area. This explains the higher resistance and thus the high standard deviation. At the temperature levels above 1000°C the contact resistance is also so that an increasing neck diameter decreases the contact resistance, with the half spheres as the highest resistance.

The R_c/R_{div} ratio is 0.95 - 0.90 for the divided cylinders, decreasing with temperature. The R_c/R_{div} ratio decreases with decreasing neck diameter to 0.74 - 0.78 for the ϕ30/5 mm double cone, increasing with increasing temperature. The R_c/R_{div} ratio is higher compared to the ratio found for graphite. Above 1000°C the contact resistance of SSAB is comparable to that of Corus coke. The resistance of the half spheres and the whole double cones are, however, higher for SSAB coke.

In Figure 4-14 the resistance of the whole and divided samples and the average contact resistance for *Zdzieszowice coke* are plotted as a function of temperature. In general, both the measured resistance of the divided samples, the whole samples and the contact resistance decrease from room temperature to 1600°C. However, it can be seen that the average of the divided cylinders increases

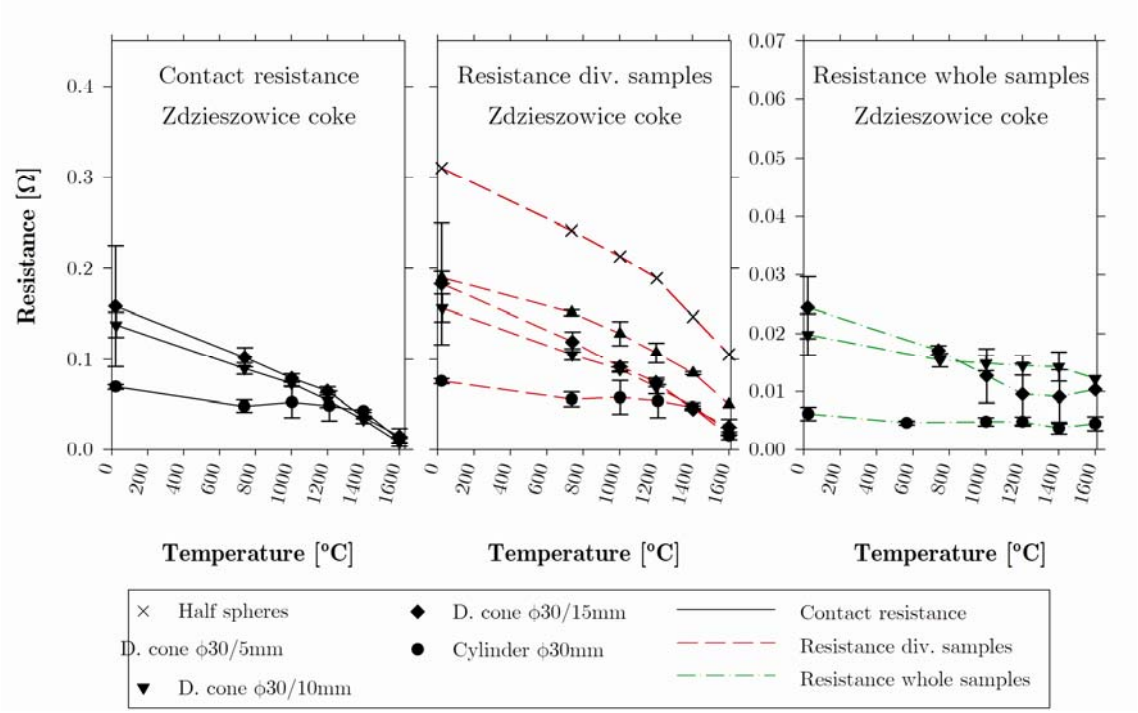

Figure 4-14: The calculated contact resistance, the resistance of the divided samples and the resistance of the whole Zdzieszowice coke samples are plotted as a function of temperature. Standard deviation is indicated where more than one experiment have been carried out.

slightly between approximately 740°C and 1000°C. This is also seen for the average of the whole ϕ30/15 mm double cone when comparing the resistance at 1400°C and at 1600°C.

It can be seen that the measured resistance of the divided Zdzieszowice coke samples decreases with increasing neck diameter, as seen for the graphite and the other cokes. The exception is, however, the ϕ30/10 mm and the ϕ30/15 mm divided double cones and the whole ϕ30/15 double cone. The divided ϕ30/15 mm double cone has a higher contact resistance compared to the divided ϕ30/10 mm double cone for all temperatures except 1600°C, and the whole ϕ30/15 mm double cone has a higher resistance compared to the whole ϕ30/10 mm double cone up to 1000°C. The values are, however, not very different in magnitude.

The R_c/R_{div} ratio of the ϕ30 mm cylinder is 0.92 at room temperature and 0.72 at 1600°C. The ratio does not decrease with increasing temperature, as seen for the SSAB coke, but drops from 0.92 to 0.72 between 1400°C and 1600°C. However, a decreasing ratio with increasing temperature is seen for the ϕ30/15 mm and the ϕ30/10 mm samples. The R_c/R_{div} ratio is between 0.70 and 0.88 for both samples, at all temperature levels up to 1400°C. At 1600°C the ratio has dropped to 0.59 and 0.39 for the ϕ30/15 mm and the ϕ30/10 mm samples, respectively.

A statistical analysis is performed on the contact resistance data. Since the temperature region between 1000°C and 1600°C is the most interesting region concerning the conditions in industrial furnaces, the lower temperatures were excluded from the analysis. Corus coke was also excluded from the analysis due to too few experiments having been performed. To get replicates so that the *pure error* could be calculated and thus the *Lack of Fit* test could be done, the temperature was rounded to the nearest 10°C, as in the statistical analysis of the material resistivity data. T^* is used as the modified temperature. The *Holm's radius* used in the metal contact theory states that the contact resistance is proportional to the inverse diameter of the apparent contact area if the contact spots are evenly distributed within this area and there is no thin film, thus $R_c \propto 1/2\alpha$ (Timsit 1999). The *Holm's radius*, α, is here assumed to be equal to the radius of the apparent contact area, $d_{neck}/2$. A dummy variable represented the type of coke, +1 representing SSAB coke and -1 representing Zdzieszowice coke.

The result of the standardized regression equation is shown in Equation (4.2), and the uncoded result is shown in Equation (4.3). All the predictors shown are significant and there is no significant lack of fit, see Appendix 3 for further details. It can be seen, from Equation (4.2), that the *type* of coke has less influence on the contact resistance than both the temperature and neck diameter, d_{neck}.

$$R_c = 61.2 \cdot 10^{-3} - 31.4 \cdot 10^{-3} \cdot \frac{T^* - 1300}{300} + 21.7 \cdot 10^{-3} \cdot \frac{1/d_{neck} - 117}{142} + 4.5 \cdot 10^{-3} \cdot type \quad (4.2)$$

$$R_c = 167 \cdot 10^{-3} - 105 \cdot 10^{-6} \cdot T^* + 260 \cdot 10^{-6} \cdot 1/d_{neck} + 4.50 \cdot 10^{-3} \cdot type \quad (4.3)$$

From the regression equation it can be seen that the Zdzieszowice coke has a lower contact resistance compared to the SSAB coke. The statistical analyses of the *material resistivity* data in section 4.4.1 did not show any statistical difference between SSAB coke and Zdzieszowice coke. This shows us that a difference between the *bulk resistivity* of metallurgical cokes may be determined by the *contact resistance* and that the *material resistivity* is of less importance.

For one of the SSAB coke half spheres experiments and one of the Zdzieszowice ϕ30/5 mm experiments the furnace was *not* dismantled after the experiment. The measurement procedure was redone a couple of days later. This was done to see if the contact had improved during the experiment. The measured resistance of each of the two runs of the two experiments is shown in Figure 4-15.

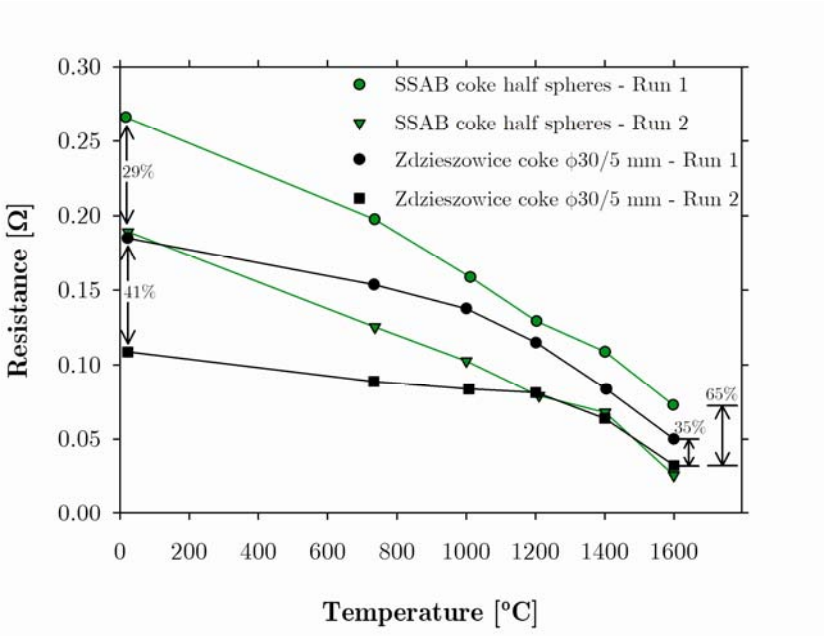

Figure 4-15: The same sample was reheated without dismantling the apparatus.

An improvement of the *material resistivity* due to the heating of the sample in the first run would, due to the R_c/R_{div} ratio being above 0.8 for most of the temperatures, only have a minimal influence on the resistance of the sample when the sample is reheated.

For both of the experiments the second run has a lower resistance compared to the first run. For the SSAB coke half spheres the difference between the resistivity of the two experiments increase from room temperature to 1600°C. At room temperature the resistance of the reheated sample is only 71 % of the resistivity recorded before the heating started in the first run. At 1600°C the resistance of the second run is only 35 % of the resistance measured at 1600°C for the first run of the half spheres SSAB coke sample. By comparison, the resistance of the second run of the Zdzieszowice ϕ30/5 mm sample is 59 % at room temperature and 65 % at 1600°C.

Microprobe analyses of the contact area

Element analyses of the contact surfaces of a Zdzieszowice coke divided cylinder ϕ30 mm sample were done by microprobe, before and after the experiment. This was done to see if any changes had occurred that could indicate areas where the contact resistance might have been changed due to changes in the chemical composition of the surface, e.g. areas where the iron oxide content has been reduced.

The surfaces prior to the experiments are given in Figure 4-17 and Figure 4-16, surfaces 1 and 2, respectively. Only the elements that gave the highest intensities are included. Aluminum (Al) and silicon (Si) are the most common constituents of the ash in metallurgical coke. They do, however, appear as oxides in the ash. Typically 50 % of the ash is SiO_2. From the Al and Si pictures in Figure 4-16 it can be seen that there are some ash particles spread fairly evenly in the sample. There is also an ash particle containing iron (Fe).

For surface 2 a large ash particle can be seen at approximately 11 o'clock in Figure 4-17. The ash particle has a high content of both Al and Si. It can also

be seen that there is iron almost all over the contact surface, most likely in the form of iron oxide.

The microprobe images of the surfaces after the experiments are shown in Figure 4-18 and Figure 4-19, surface 1 and 2 respectively. It seems as though both the Si and the Fe content on surface 1 has increased, see Figure 4-18. The large ash particle seen on surface 2 in Figure 4-17, is now placed between 6 and 7 o'clock in Figure 4-19. The level of Al and Si seem to have gone down. This may, however, be the color bar, which is different in the two images.

Based on the presented element analyses of the contact surfaces it is not possible to determine any electrical contact spots.

4.5.2 Discussion

Graphite

The contact resistance decreases from room temperature to the 730°C level. For the ϕ30/5mm and the half spheres samples the contact resistance then increases slightly. For the larger samples the temperature does not seem to have a large effect on the contact resistance from about 700 to 1400°C, but there is a small decrease in contact resistance form 1400 to 1600°C. This is different from what is seen for the whole samples, which have a minimum at approximately 730°C. The reason for this difference is probably the introduction of a contact, and that the contact does not follow the same relationship as described by Mrozowski (1952) and discussed in the section concerning the material resistivity.

When the contact resistance is compared to the measured resistance of the whole graphite samples, see Figure 4-11, it is evident that the contact resistance accounts for a large portion of the measured resistance when two particles are in contact. The relative amount of contact resistance, or the R_c/R_{div} ratio, is relatively stable for the various graphite sample sizes. It decreases from 87 - 92 % at room temperature to 53 - 64 % at 1600°C. One explanation is that the contact is improved with temperature, caused by material changes. Graphite is,

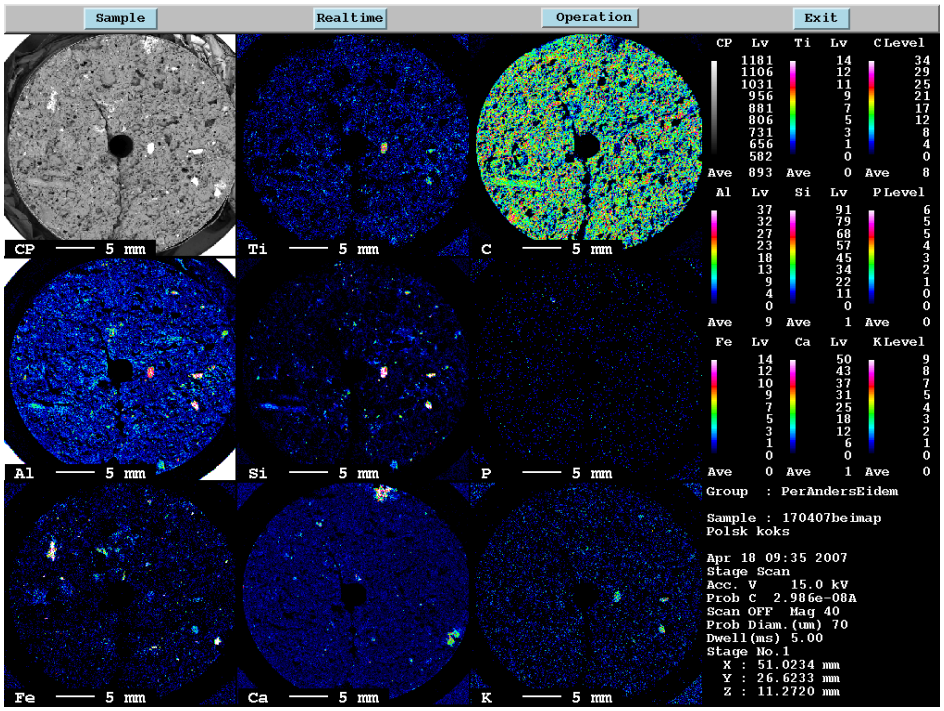

Figure 4-16: Element analyses of the contact surface prior to contact resistance experiment. The sample is a Zdzieszowice coke divided cylinder ϕ30mm, Surface 1.

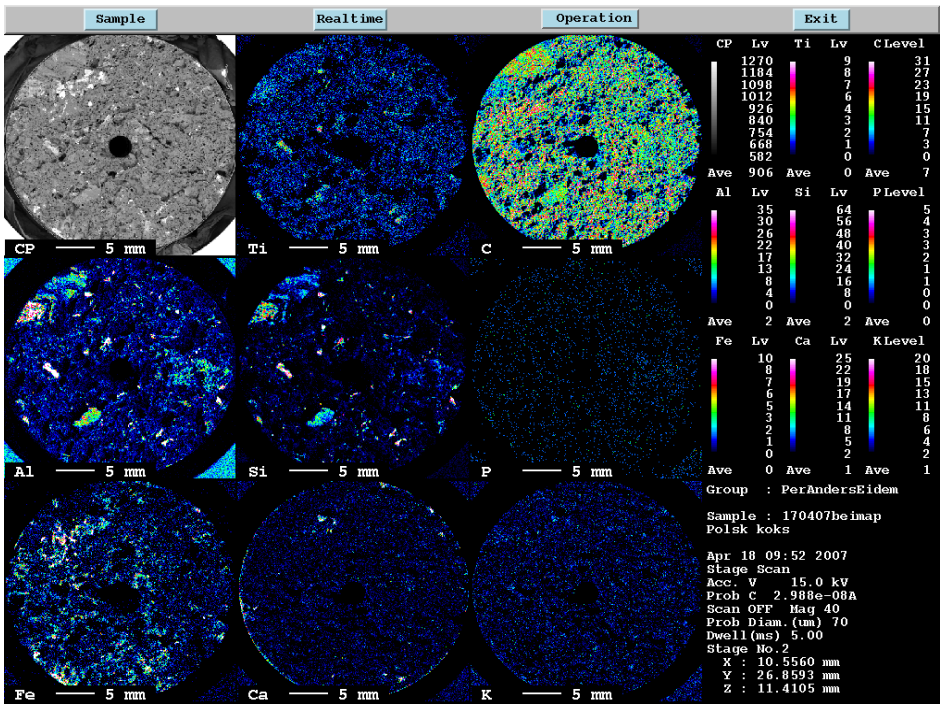

Figure 4-17: Element analyses of the contact surface prior to contact resistance experiment. The sample is a Zdzieszowice coke divided cylinder ϕ30mm, Surface 2.

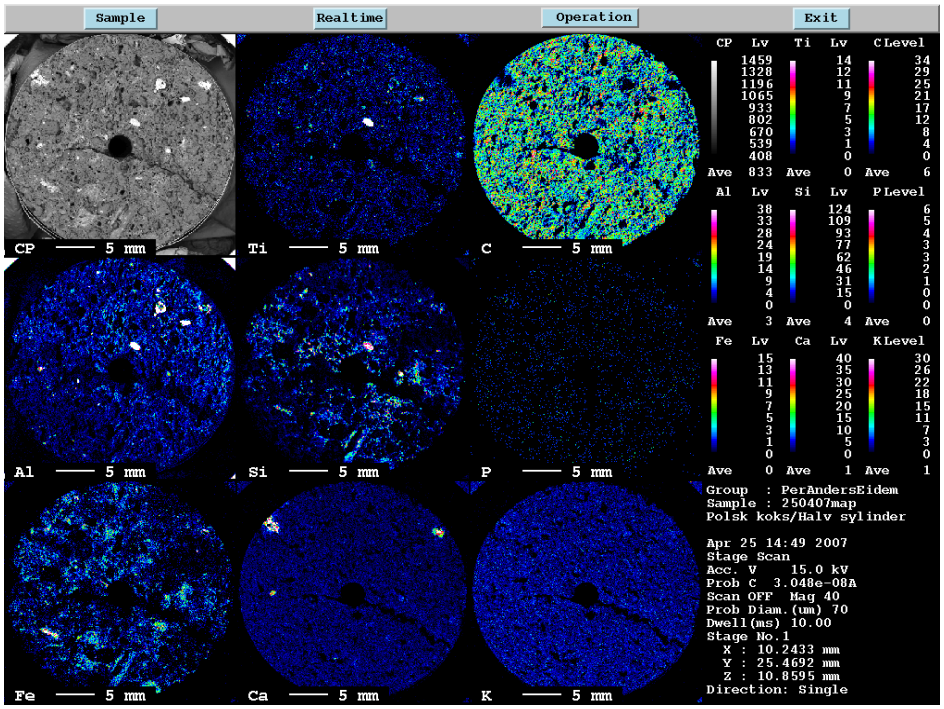

Figure 4-18: Element analyses of the contact surface after contact resistance experiment. The sample is a Zdzieszowice coke divided cylinder ϕ30mm, Surface 1.

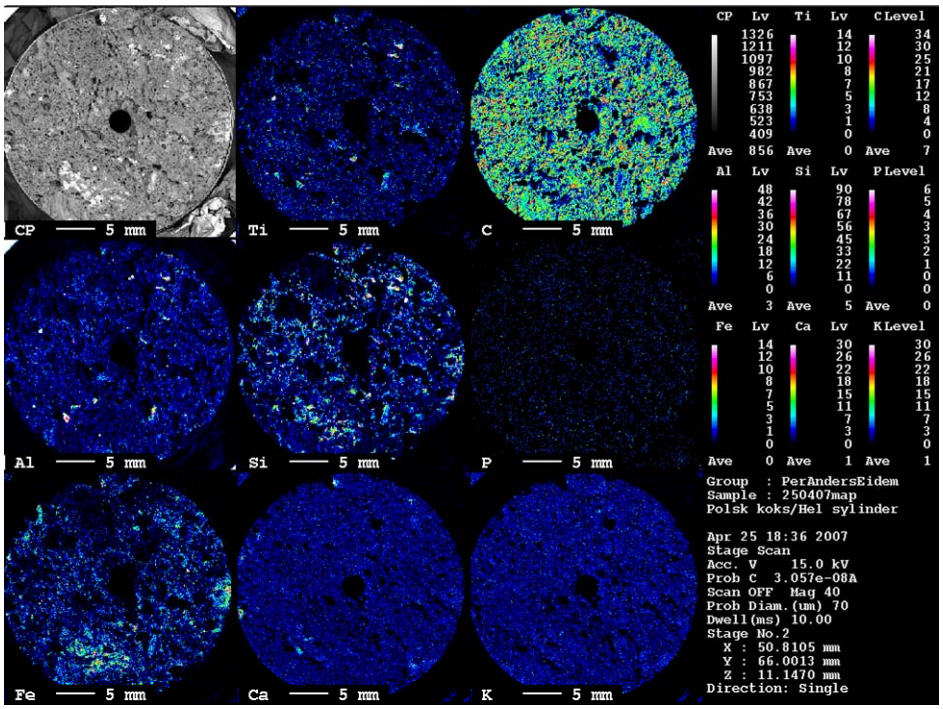

Figure 4-19: Element analyses of the contact surface after contact resistance experiment. The sample is a Zdzieszowice coke divided cylinder ϕ30mm, Surface 2.

however, a very stable material as shown with the repeated heating of a single sample. A change in the material is thus not a very likely explanation. Another possible explanation is that the contact may be looked upon as an added energy gap. As the contact is heated more energy is added to the electrons. The added energy compensates for the added energy gap. This argument is similar to the argument used by Mrozowski (1952) to explain part of the added resistance when comparing monocrystalline and polycrystalline graphite.

The contact resistance of the sample with the largest contact area is, as expected, the lowest contact resistance. Although the results at 1600°C show an increase in the contact resistance with decreasing contact area, there is not a very large difference between the three largest samples. The ϕ30/5mm divided double cone and the point contact does, however, show a significantly higher contact resistance compared to the other sample shapes.

Metallurgical coke

With a few exceptions, the general trend is that the contact resistance of metallurgical coke decreases with increasing temperature, from room temperature to 1600°C, see Figure 4-12, Figure 4-13 and Figure 4-14. In general, the R_c/R_{div} ratio also decreases with increasing temperature. The difference from graphite is that the metallurgical coke is *not* a stable material. This was illustrated by the repeated runs shown in Figure 4-15. In addition to the added energy to the electrons, a change in the material at the contact intersection, such as a further ordering of the carbon material or the formation of a conductive film, may have contributed to reducing the contact resistance. This may be iron oxide being reduced to iron, or volatiles coking at the surface. For a few of the experiments it was found that the two sample halves were sticking together after the experiment. The results of these experiments did, however, not deviate from the other experiments. These changes were not possible to detect in the microprobe mappings of the contact area, see Figure 4-16, Figure 4-17, Figure 4-18 and Figure 4-19.

In the two experiments where the sample was reheated without dismantling the furnace, the room temperature contact resistance decreased with 29 % for the SSAB coke half spheres and 41 % for the Zdzieszowice coke divided $\phi 30/5$ mm sample, after being heated to 1600°C in the first run. Since the R_c/R_{div} ratio is above 0.8 at the low temperature, it can be assumed that this is mainly due to a change of the contact, and not due to a change in the material resistivity.

One of the factors that are thought to have an effect on the contact resistance is formation of surface films at the contact spots. It is thought that, similar to metal contacts, one or more conducting spots is formed, and most of the current runs through these spots. Due to the constriction of the current when the current flows through the small contact spots, the temperature of a very small volume of the material surrounding the contact spot will be higher compared to the bulk temperature. Due to this increase in temperature, ash components may be either reduced out to form a film that decreases the contact resistance, e.g. iron, or form an oxide film that has a lower conductivity compared to carbon, e.g. Al_2O_3. From the presented surface mappings it is, as mentioned, not possible to locate any conducting spots. This is due to the size of these conducting spots, which is $<<$ 1 mm^2, and the roughness of the coke sample surface. It is, however, possible to see that the intensity of both the iron and the silicon has increased, see Figure 4-16, Figure 4-18, Figure 4-17 and Figure 4-19 for the surface mapping before and after the experiment for Surface 1 and 2 respectively. The silicon oxide present prior to the experiment has, at least partly, been converted to silicon carbide (Gill and Dubrawski 1984). The iron, iron oxide(s) and manganese oxide have probably been reduced to the respective metals. A surface film of metals will decrease the contact resistance due to the difference in resistivity between metal and carbon. The absolute content of Al_2O_3 and SiO_2 is higher in SSAB coke 60-100 mm particles compared to Zdzieszowice coke 60-100 mm particles. These components are thought to have a degrading effect on the particle-to-particle contacts. This is in line with the regression analysis of the contact resistance data, showing that the contact

resistance of the Zdzieszowice coke has a lower contact resistance compared to the SSAB coke.

It is evident from the regression results of the *contact resistance* data that increasing the diameter of the apparent contact area, d_{neck}, decreases the contact resistance. This can also be seen when the contact resistance of the metallurgical cokes measured at 1600°C is plotted against the sample shape, see Figure 4-20. Since the top electrode weight is constant the contact area pressure will increase when the apparent contact area, i.e. the intersection area between the two joining particles, is reduced. It is known from metal contacts that increasing the contact force will reduce the contact resistance, but that reducing the apparent contact area will increase the contact resistance. It is also known that an increased hardness of the metal will decrease the effect of increasing the applied contact force due to less deformation of the contact material (Timsit 1999). In the contact resistance experiments the contact areas of the divided double cones ϕ30/15mm, ϕ30/10mm and ϕ30/5mm with a 3 mm diameter hole

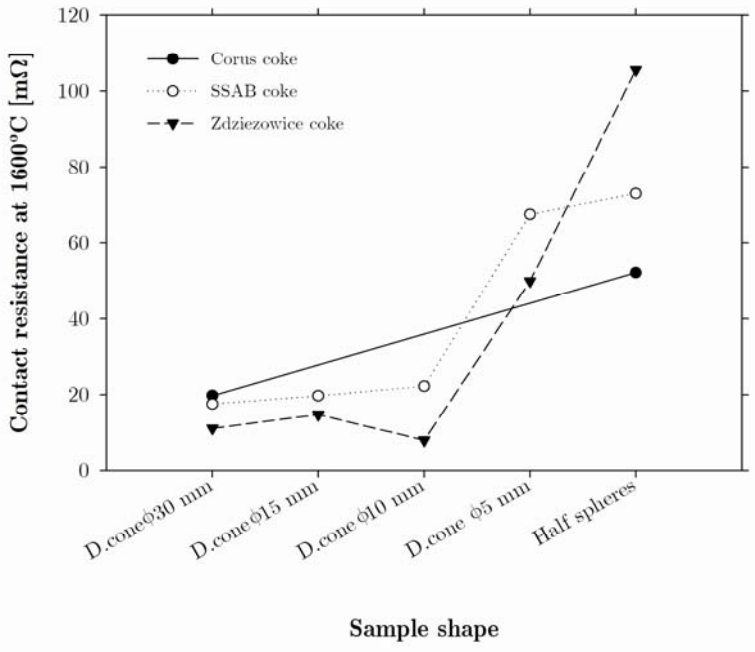

Figure 4-20: The contact resistance measured for the metallurgical cokes at 1600°C is plotted versus the sample shape.

through the centre has a reduction in the resistance of a factor 4.1, 9.8 and 55.7, respectively, from the divided cylinder ϕ30mm sample. Since the applied force on the sample is given by the weight of the top electrode, the contact pressure, i.e. the force per unit contact area, will increase with the respective factors. Up to 1200°C the contact resistance decreases with increasing apparent contact area, see Figure 4-13 and Figure 4-14. This shows us that the increased apparent contact area is more important than the increased contact pressure. The contact pressure is, in other words, too low to deform the asperities and thus increasing the contact area, which is what happens when the applied force is increased on metal contacts. Assuming that the contact areas have the same number of contact spots per unit area, a larger area gives a higher number of contact pots. Above 1200°C the differences are not that clear, but the point contact resistance is at all times higher compared to the other contact area sizes.

A decreasing neck diameter does, however, seem to decrease the relative contribution of the contact resistance to the total resistance of the divided samples, i.e. the R_c/R_{div} ratio. This is puzzling, since it was expected that a lower contact resistance would also lower the contribution of the contact resistance on the total resistance of the divided samples.

From the regression analysis of the contact resistance of the SSAB and Zdzieszowice cokes, it can be seen that the Zdzieszowice coke has a lower contact resistance compared to the SSAB coke. The statistical analyses of the *material resistivity* data did not show any statistical difference between SSAB coke and Zdzieszowice coke. This shows us that a difference between the *bulk resistivity* of metallurgical cokes may be determined by the *contact resistance* and that the *material resistivity* is of less importance.

4.6 Conclusions

An apparatus is developed that can be used to determine the material resistivity and contact resistance of various calcined carbonaceous materials at temperatures up to 1600°C. The material resistivity at 1600°C was measured as

8.6 μΩ·m for graphite, 130-150 μΩ·m for metallurgical coke and 480 μΩ·m for anthracite.

The material resistivity of the metallurgical coke decreases with increasing temperature, from room temperature to 1600°C. Above approximately 1000°C the decrease in material resistivity is moderate compared to below 1000°C. A possible explanation is that a growth of the graphite crystallites decreases the number of free electrons available for electrical conduction.

Statistical analysis of the material resistivity data revealed that there is no significant difference between the material resistivity of the Corus, SSAB and Zdzieszowice cokes.

The resistance of two half spheres in contact at 1600°C, which is the closest representation to the particle-to-particle contact resistance found in a coke bed, is measured as 15.1 mΩ for graphite, 52 mΩ for Corus coke, 73 mΩ for SSAB coke and 106 mΩ for Zdzieszowice coke.

The contact resistance generally decreases with increasing temperature, from room temperature to 1600°C. In this range the relative contribution of the contact resistance to the total resistance of the divided samples decreases. With the exception of a few single experiments, this was found for all materials and material shapes. A possible explanation is that the increased temperature compensates for the added energy gap that the contact represents. For the metallurgical cokes, there is most likely also a change in the material at the contact intersection.

A clear correlation was seen between the inverse neck diameter and the contact resistance. An increasing neck diameter decreases the contact resistance. These results show that the increased contact pressure due to the decrease in neck diameter of the metallurgical coke samples is not sufficient to increase the area

of the contact spots so that the contact resistance decreases with increasing pressure.

Chapter 5 Bulk Resistivity

With an increasing shortage of raw materials, the ferroalloy industry is forced to change the raw materials more often. A direct method of knowing the bulk resistivity of carious carbon agents is to measure the resistivity over larger quantities of carbonaceous agents.

In this section of the thesis the bulk resistivity measurements are presented. The term b*ulk* is, as previously mentioned, used due to a large number of particles being involved in the measurement. Current flowing through the cylindrical coke bed heats the carbon sample to 1600°C by ohmic heating. A voltage drop is measured over a given volume of sample material, and the *bulk resistivity* can be calculated.

Since the most important reduction material for the ferromanganese industry in Norway at present is metallurgical coke, the majority of the tested materials have been metallurgical cokes. However, also petroleum cokes, anthracites and charcoals have been tested. The particle size distribution and the bulk density of the tested carbon materials is given in this chapter, while the ash and proximate analyses are found in Chapter 3.

Part of the experimental work was a part of previous works by the author (Eidem 2004a; Eidem 2004b). The reports are not readily available and data has been insufficiently analyzed, so the data are included in these works.

5.1 Apparatus and method

5.1.1 Measurement setup

The apparatus shown in Figure 5-1 consists of a high-alumina refractory cylinder, built around an upper and a lower 304.8 mm standard graphite electrode. The layer of Kaowool (Thermal Ceramics LTD, England) fiber insulation, which can be seen in Figure 5-2, reduces the heat loss and reduces temperature gradients that are believed to be inside the coke sample. Water-cooled copper bus bars connect the power supply to the top and bottom graphite electrodes. Weights are added to the top electrode to increase the total pressure to 381 kg/m^2. This apparatus is a further improvement of the apparatus developed by Olsen and Eidem (2003).

Thermocouples inserted through the top electrode, measure the temperature at the positions of the electric potential measurements. The voltage drop over the

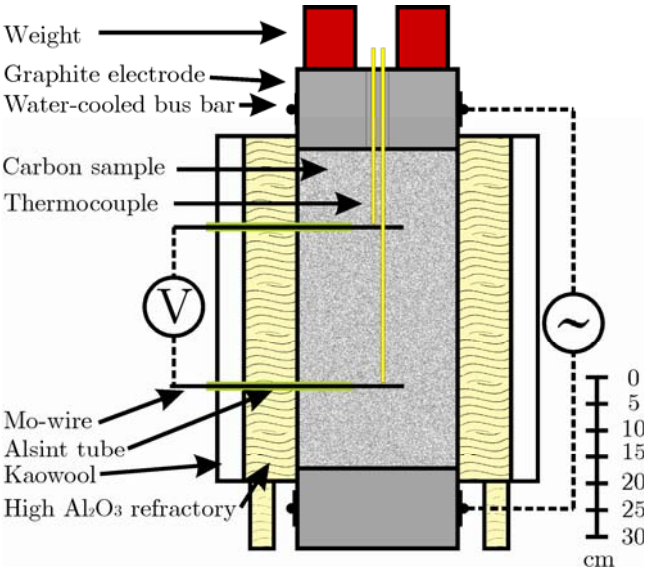

Figure 5-1: Apparatus used to measure bulk resistivity. The sample is heated by ohmic heating.

Figure 5-2: Photo of the apparatus. Photo by M. Gall.

central part of the coke bed is measured by molybdenum wires inserted through the wall at the positions indicated in Figure 5-1. This eliminates errors due to contact resistances between the coke bed and the upper and lower graphite electrodes. The *four point measurement principle* was used to eliminate measurement error due to the contact resistance between the molybdenum wires and the carbon sample material. Further details on the four point measurement principle are given in Appendix 4.

Heat is supplied by direct ohmic heating of the coke bed. The current used both for heating and as a measuring current is delivered by two series connected OTC Krumc-1500 AC arc welding transformers. These are able to deliver a constant current throughout the voltage range experienced during the bulk resistivity measurements. The maximum continuous current is 1600 A, and the open circuit voltage is 180 V. The current density is kept between 7.4 and 14.1 kA/m^2. For comparison, in a 45 MVA furnace, the current running through one of the electrodes with a 1.9 m diameter would typically be 100 kA, which corresponds to a current density of 35 kA/m^2 in the electrode. If the coke bed in the industrial furnace is bell shaped, as reported by Barcza et al. (1979), the current density will decrease as the radius of the coke bed increases. Wall effects are minimized by only exposing the molybdenum wire to the central part of the coke bed, and by keeping the particle size below 10 % of the diameter of the apparatus, i.e. below 30 mm. A uniform current distribution is assumed, and the following equation is used to calculate the bulk resistivity, ρ_{bulk}:

$$\rho_{bulk} = \frac{U \cdot A}{I \cdot h} \tag{5.1}$$

where U is the measured voltage drop; I, the measured current; A, the cross-sectional area of the coke bed sample; and h, the distance between the measuring points. Equation (5.1) is a version of Equation (2.1), modified to the cylinder case.

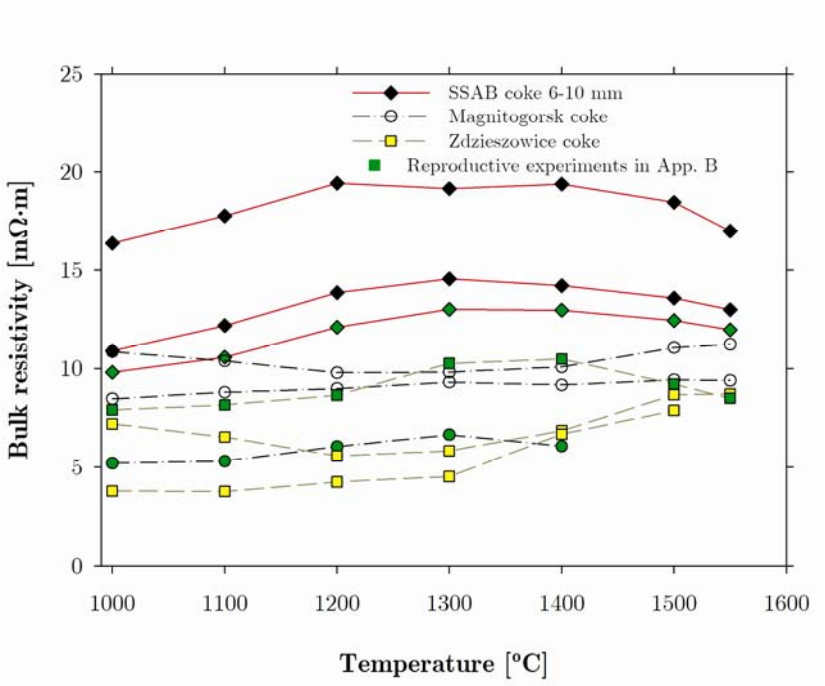

Figure 5-3: Experiments performed in both App. A and App B. The experiments done in App. B have green symbols.

Representative samples are split out from a larger bulk of material samples, both as a basis for the electrical measurement and for determining the size distribution. The coke is heated until one of the thermocouples read 1600°C. The heating rate is roughly 60°C/min up to 500°C. The heating rate from 500°C to 1600°C varies from roughly 12°C/min to 60°C/min depending on the current density used and the resistance of the carbon sample. Due to temperature gradients in the furnace, the mean temperature never reached 1600°C, which is the maximum operating temperature of the furnace lining.

At one point, a new apparatus had to be built, named "App. B" in the following description. The main differences between the two designs were as follows:

- The current density in Apparatus 1 ("App. A") was higher than the current densities used in App. B. In App. A the current density was between 8.5 kA/m^2 and 14.1 kA/m^2 and in App. B the current density was between 7.1 kA/m^2 and 9.9 kA/m^2.

- In App. A, the thermocouples were inserted through the wall, instead of through the top electrode
- The thickness of the thermal insulation was increased in App. B to decrease the thermal gradients inside the coke bed.

To determine if there was any variation between the two designs, one additional parallel was done for SSAB coke 6-10 mm, Magnitogorsk coke and Zdzieszowice coke. The results are shown in Figure 5-3. No apparent correlation between the apparatus and the measured resistivity can be found.

To assess the reproducibility, most of the measurements have been conducted as two parallel runs. The parallel runs were performed in a random manner to determine whether there was any significant drift in the apparatus.

Most of the raw materials were dried at 105°C for approximately 12 hours to lower the water content. The charcoal and one of the Marietta sponge petroleum coke samples was heated to 850°C, at a rate of approximately 2°C/min and kept at 850°C for one hour. The other petroleum cokes were heat treated in a 150 kVA, one-phase furnace where the temperature, unfortunately, could not be measured. The heat treatments were done to lower the volatile content of the charcoals and petroleum cokes. Preliminary tests revealed that the untreated charcoals and petroleum cokes had a resistivity that was too high to get any current flowing through the coke bed and, as a consequence, no heat could be evolved.

5.1.2 Measurement procedure

An overview of the number of experiments, and which of the two furnaces they were performed in, is shown in Table 5-1. A set procedure is followed for every experiment to minimize variation due to time. The points that were followed for every experiment were:

- The density of the coke was measured by using a 10 liter container and a scale. After the 10 liter container had been weighed, the carbon material was emptied into the coke oven.
- The molybdenum wires and the thermocouples were placed in at the correct measuring heights shown in Figure 5-1. 10 cm of the wires were revealed in the middle of the coke bed.
- When the apparatus was filled to approximately 1 cm from the top, the graphite top electrode was put in place, and additional weight was applied, making the total pressure on the top of the coke bed 381 kg/m^2.
- The current and the logger were turned on. The logging frequency was logging approximately one second.
- When one of the thermocouples shows 800°C, the furnace is turned off for 3 minutes. This is done to equalize the temperature gradients inside the measuring cell. The differences between the two thermocouples give the indication that the vertical temperature gradients decrease due to this stop.
- The experiment is terminated when one of the two thermocouples reach 1600°C. The other thermocouple is usually 100°C below this temperature.

For some of the cokes with the lowest bulk resistivity, the current had to be increased during the experiment. This was done to maintain the temperature profile achieved for the other metallurgical cokes.

5.2 Experimental results

5.2.1 Particle size distribution

A splitter was used to get a representative test sample, both as a basis for the electrical measurement and to calculate the size distribution. Sieves with the appropriate sizes were used. All sieves were based on square shaped holes.

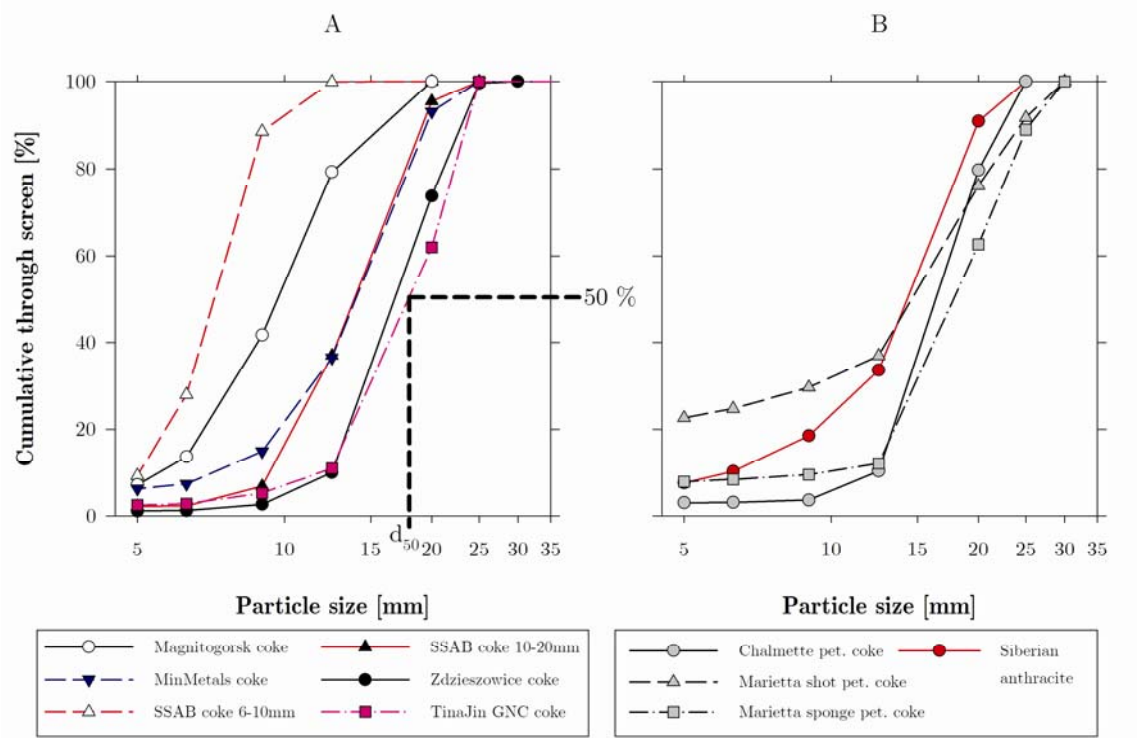

Figure 5-4: Particle size distribution of A) the metallurgical cokes B) the petroleum cokes and the Siberian anthracite. The median particle size of the bulk material is found based upon the size distribution curves.

In Figure 5-4 A the particle size distribution of the SSAB coke size fractions and the coke from the Magnitogorsk steel mill and the Zdzieszowice coking plant is shown. The particle size distribution of the petroleum cokes and the Siberian anthracite it shown in Figure 5-4 B. No particle size distribution was obtained for the Corus coke and the smaller fractions of SSAB coke, as they were sieved to obtain the respective fractions. There was not enough material available to obtain a sample of Vietnamese anthracite. It is also shown in Figure 5-4 A how the median particle size diameter, d_{50}, is found based on the particle size distribution curves. The median particle size diameter of all the cokes tested in the bulk resistivity apparatus is presented in Table 5-1.

The d_{50}, or the median of the particle size, of the industrial sized coke varies from around 10 mm to 18.5 mm. These are samples that have not been sieved prior to the test, i.e. not sieved after delivered from the coke producer. However, except from the Magnitogorsk coke, the other industrial sized material have a

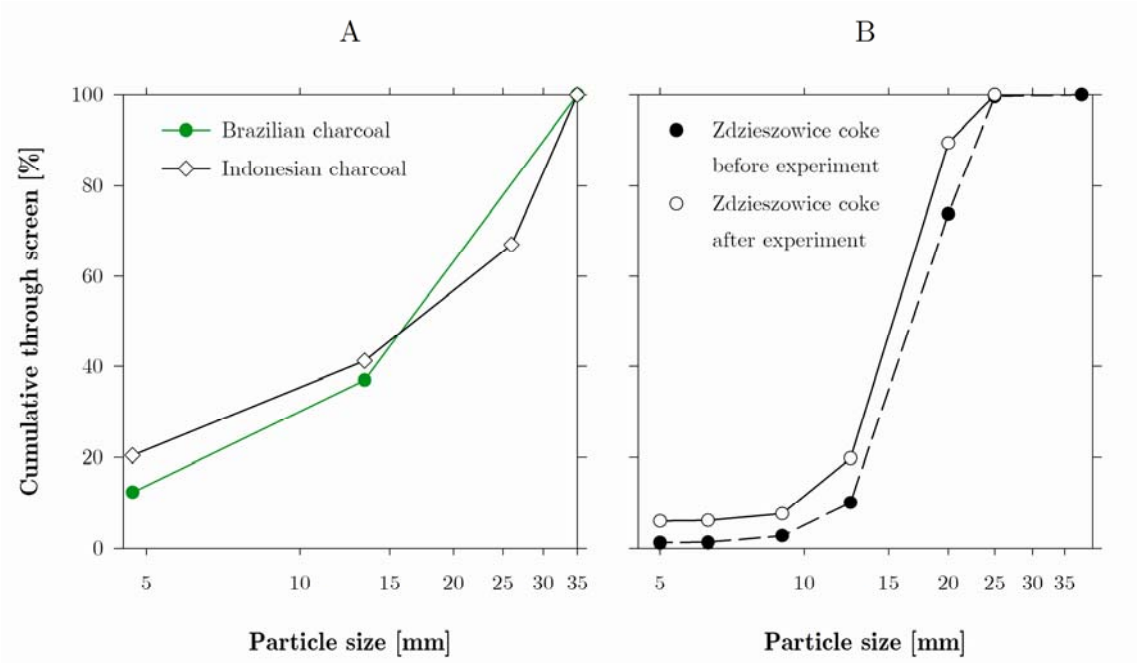

Figure 5-5: A) The particle size distribution of the charcoals. B) The particle size distribution of Zdzieszowice coke before and after the experiment.

d_{50} within 5 mm of each other, and the slope of the curve is almost equal. The latter indicates that the packing is similar. From the particle size distribution curve it is possible to see that the SSAB 6-10 mm coke, the Magnitogorsk coke and the MinMinerals coke fractions contain about 10 wt. % of fines, i.e. particles below 5 mm. Observations made when drying the raw materials showed that the fines content increased when the metallurgical coke was dried. On the moist coke, there were fines sticking to the moist surface. This may be the reason for the low fines content of the Zdzieszowice coke, which was not dried prior to the experiments.

It can be seen in Figure 5-4 B that the Marietta shot petroleum coke has a high amount of fines, i.e. particles below 5 mm, compared to the other raw materials. This variation in fines content may be due to the calcination in the one phase furnace, but there was also a lot of fines present prior to the calcination process.

In Figure 5-5 A the particle size distribution of the Brazilian and the Indonesian charcoal is shown. Both of the charcoals have a broader particle size

Table 5-1: Bulk density and d_{50} of the carbonaceous materials tested in the bulk resistivity apparatus. The number of parallel experiment and the furnace in which they were performed is also shown. The standard deviation is shown where available.

Name	Type	Bulk density [kg/m³]	d_{50} [mm]	Parallels Apparatus‡
Siberian	Anthracite	945	15	1 B
Vietnamese 6-25mm	Anthracite	905	15.51	1* B
Brazilian 4-35mm	Charcoal	315	19.5	2" B
Brazilian 4.7-13.4mm	Charcoal	310	9.1†	2" B
Brazilian 13.4-35mm	Charcoal	320	24.2	2" B
Indonesian 4.7-13.4mm	Charcoal	306	9.1†	2" B
Indonesian 13.4-26.9mm	Charcoal	309	20.2†	2" B
Corus 5-10mm	Met. coke	639** ± 17	7.5†	4§+2* A
Corus 15-20mm	Met. coke	574** ± 15	17.5†	4§+2* A
Magnitogorsk steel mill	Met. coke	641**± 70	9.7	2* A, 1* B
MinMetals	Met. coke	544	14	2 B
SSAB 1.68-3.3mm	Met. coke	529 ± 7	2.5†	1* B
SSAB 3.3-6mm	Met. coke	527 ± 24	4.7†	2* B
SSAB 6-10mm	Met. coke	637**± 27	7.3	2* A, 1 B
SSAB 10-20mm	Met. coke	507 ± 20	14	2* B
TianJin	Met. coke	553	18.5	2 B
Zdzieszowice 12-25mm	Met. coke	606**± 33	17.3	2* A, 1* B
Chalmette	Pet. coke	726	16.7	1* B
Marietta shot	Pet. coke	781	15	1*+1 B
Marietta sponge	Pet. coke	483	18.2	1*+1 B

*Eidem (2004a) " Eidem (2004b) **Not dried †Arithmetic mean
‡App.1 = A, App.2 = B §4 exp. from Olsen and Eidem (2004)

distribution compared to the other raw materials. The fines content is also quite high. In Figure 5-5 B the particle size distribution of the Zdzieszowice coke prior to and after the experiment is shown. The fines content has increased from about 1 to about 6 wt. %. This indicates a degradation of the coke during the experiment. One of the reasons may be that ash components such as SiO_2 will react with the carbon, weakening the carbon structure (Gill and Dubrawski 1984) in addition to handling of the material and thermal stresses that may occur during the bulk resistivity experiments.

5.2.2 Bulk density

In Table 5-1 the measured bulk densities of the various carbonaceous materials tested in the bulk resistivity apparatus and their respective median particle sizes

d_{50} is given. The table also includes information concerning which of the cokes were not dried prior to the experiments, the number of experiments and the apparatus they were tested in.

It can be seen that the bulk density of the anthracite, which is a very compact material, is much higher compared to the other materials, and that the charcoal has a bulk density that is lower than the other test materials. The very porous, as the name reveals, Marietta sponge petroleum coke has a bulk density that is lower compared to the metallurgical cokes, but higher compared to the charcoal. The two other petroleum cokes has a bulk density in between the metallurgical coke and the anthracite. Of the metallurgical cokes, it can be seen that the metallurgical cokes that have not been dried has a higher bulk density compared to the metallurgical cokes that has been dried. It is commonly known that the coke can hold a lot of moisture.

In Figure 5-6 the bulk density of the charcoals and the Corus and SSAB cokes are plotted against the respective particle sizes. As shown in Table 5-1, the Corus coke and the 6-10 mm fraction of the SSAB coke was not dried.

It can be seen that the bulk density of the metallurgical cokes decreases with increasing particle size. The reason for this may be that due to the size of the 10 liter container, the wall effect is significant. The wall effect would cause the packing to go down, i.e. more void space in the packed bed, when the particle size was increased. However, it can also be seen that the bulk density of the charcoal slightly *increases* with increasing particle size. This may be due to the difference in shape when comparing the metallurgical coke and the charcoal. The metallurgical coke is similar to a walnut in shape, and the charcoal is flakier due to the structure of the tree, from which it originates. Another possibility is that there is no wall effect.

The possible presence of a wall effect has been tested by measuring the bulk density of three SSAB size fractions using two containers. One is the small 10

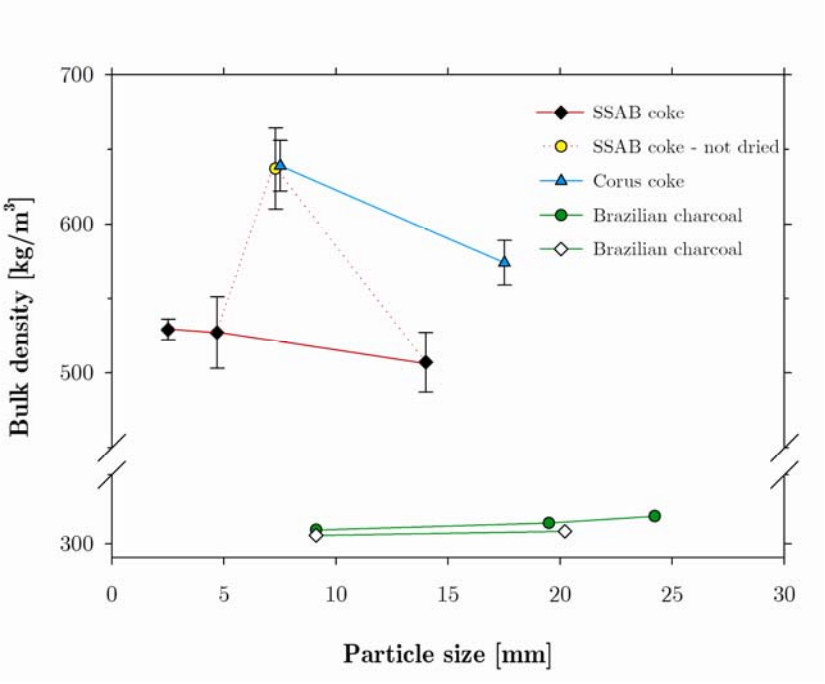

Figure 5-6: Bulk density plotted as a function of particle size for a selection of carbon materials. The Corus coke size fractions and the 6-10 mm SSAB coke were not dried. Standard deviations are indicated where available.

liter container used for the bulk density measurements shown in Table 5-1, the other is a large container with a volume of approximately 80 liters. The small 10 liter container has a diameter of 200 - 225 mm, the large container a diameter of 435 - 455 mm. A rule of thumb is that the wall effect is not significant if the particle size is below 10 % of the container diameter. To prevent the packing from being influenced by the particle size of the coke particles, the particle size increments within each fraction is approximately 100 %. The results of the bulk density measurements are shown in Table 5-2.

Table 5-2: Measured bulk density in small and large container.

Particle size fraction	Density 10 liter container [kg/m3]	Density large container [kg/m3]
SSAB coke 1.68-3.3mm	529 ± 7	520
SSAB coke 3.3-6mm	527 ± 24	506
SSAB coke 10-20mm	507 ± 20	514

The results show that the bulk density measured using the larger container does not show a statistically significant lower bulk density. The standard deviation of all the bulk density measurements for SSAB coke is below 5 %, and the variation in bulk density due to wall effect can thus be neglected.

5.2.3 Bulk resistivity

In Figure 5-7 four examples of the continuous bulk resistivity vs. temperature curve is shown. Other bulk resistivity measurements are shown in Appendix 6 as a reference for future work. The complete temperature range is not included for all the materials as the temperature region of main interest is between 1000°C and 1600°C. However, all materials, without exception, had bulk resistivity trends, with respect to temperature, as shown in Figure 5-7, where the bulk resistivity decreases from room temperature to 1600°C. For the metallurgical cokes the bulk resistivity decreases by a factor 5 to 10 between room temperature and approximately 500°C. The bulk resistivity levels out with yet increasing temperature.

In Figure 5-8, the electrical resistivities of the various metallurgical cokes are shown for the temperatures ranging from 1000°C to 1550°C. The bulk resistivity

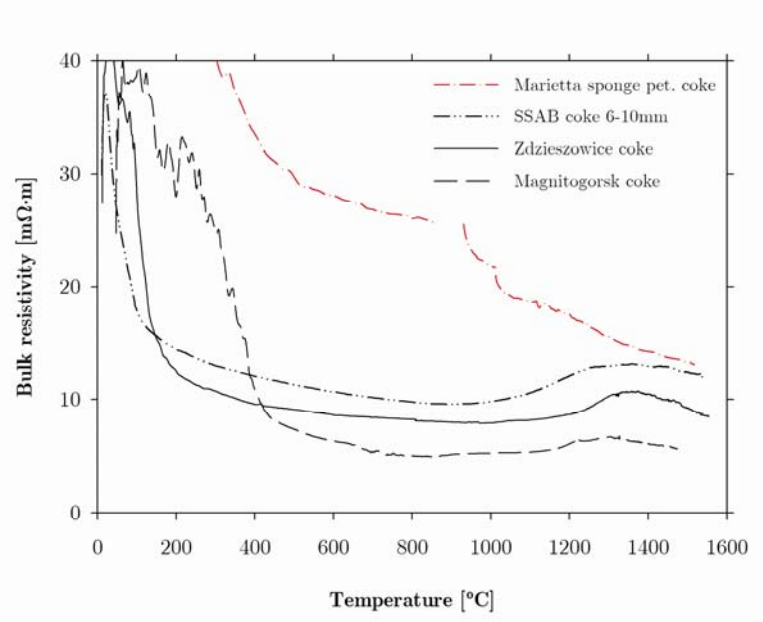

Figure 5-7: Measured bulk resistivity of Marietta sponge petroleum coke and Magnitogorsk, SSAB and Zdzieszowice metallurgical coke from room temperature to 1600°C.

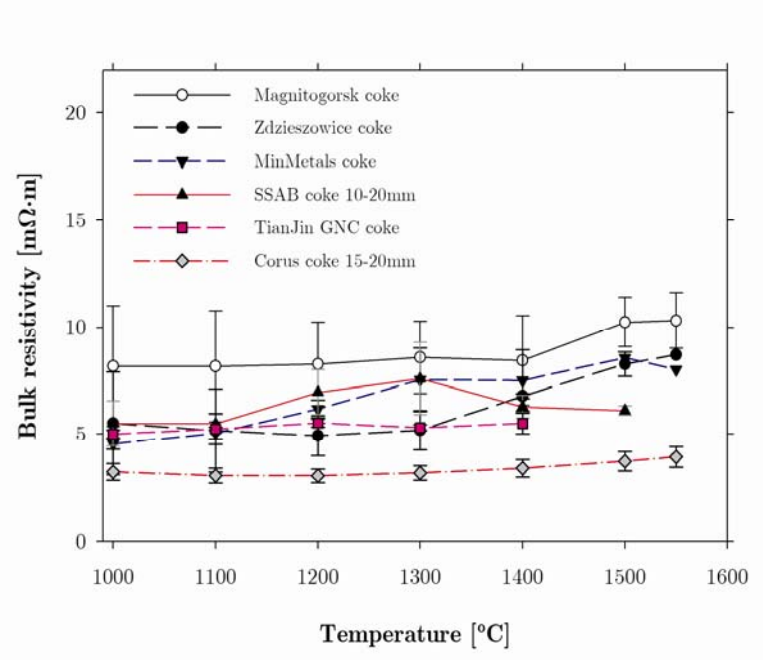

Figure 5-8: Bulk resistivity of metallurgical cokes from 1000 to 1550°C. The standard deviation is indicated where two or more parallels have been performed.

measurements at the temperatures indicated by the symbols in the graph were used to estimate the average bulk resistivity plotted in Figure 5-8. The standard deviation of the experiments is indicated for the experiments with two or more parallel experiments. The average values and standard deviations are given in Table 5-3.

Table 5-3: Average bulk resistivity and the standard deviation of the metallurgical cokes where parallel experiments were done.

	1000°C	1100°C	1200°C	1300°C	1400°C	1500°C	1550°C
	[mΩ·m±%]	[mΩ·m±%]	[mΩ·m±%]	[mΩ·m±%]	[mΩ·m±%]	[mΩ·m±%]	[mΩ·m±%]
Corus 5-10mm	4.23±25%	4.07±26%	4.00±25%	4.03±21%	4.13±17%	4.26±12%	4.23±10%
Corus 15-20mm	3.63±26%	3.50±29%	3.50±29%	3.58±27%	3.68±23%	3.83±16%	3.91±13%
Magnitogorsk	8.18±35%	8.17±32%	8.28±24%	8.59±20%	8.45±25%	10.25±11%	10.32±13%
MinMetals	4.52±5%	5.03±6%	6.17±7%	7.54±20%	7.50±19%	8.57*	8.02*
SSAB 3.3-6mm	11.10±29%	12.29±34%	13.72±30%	14.89±17%	15.21±6%	14.55±1%	14.11*
SSAB 6-10mm	12.37±29%	13.53±28%	15.13±25%	15.60±21%	15.53±22%	14.83±22%	14.00±19%
SSAB 10-20mm	5.49±19%	5.47±8%	6.95±15%	7.59±22%	6.27±8%	6.09±3%	-
TianJin GNC	4.99±4%	5.23±14%	5.51±4%	5.29±3%	5.49±9%	-	-
Zdzieszowice	6.30±35%	6.15±36%	6.16±37%	6.87±44%	8.01±27%	8.59±8%	8.61±2%

*No parallel measurement

It is worth noticing that for all the metallurgical cokes an increase in the bulk resistivity was registered from around 1200°C, see Figure 5-8 and Figure 5-7. This will be called the *hump* in the following. Since the mean value has been plotted in Figure 5-8 this *hump* is not as significant as in Figure 5-7. Below the temperature where the hump starts, the bulk resistivity seems to be almost independent of the temperature. This can also be seen for the metallurgical cokes plotted in Figure 5-7. This increase in resistivity around 1200°C is not seen for the Siberian anthracite, the petroleum cokes or the charcoals, see Figure 5-9 and Figure 5-10 A.

The resistivity for the petroleum cokes and anthracites are presented in Figure 5-9. The petroleum cokes and the Siberian anthracite have an almost linear decrease in bulk from approximately 1000°C to 1600°C, i.e. no hump was registered. For the Vietnamese anthracite, there is an increase in the bulk resistivity from 1100°C. One sample of the Marietta sponge petroleum coke was calcined at 850°C for one hour, as previously described. The other petroleum cokes were heat treated in the one phase furnace. Due to problems during one of the two Marietta shot petroleum coke experiments, the bulk resistivity was only measured in the region 1100°C to 1300°C.

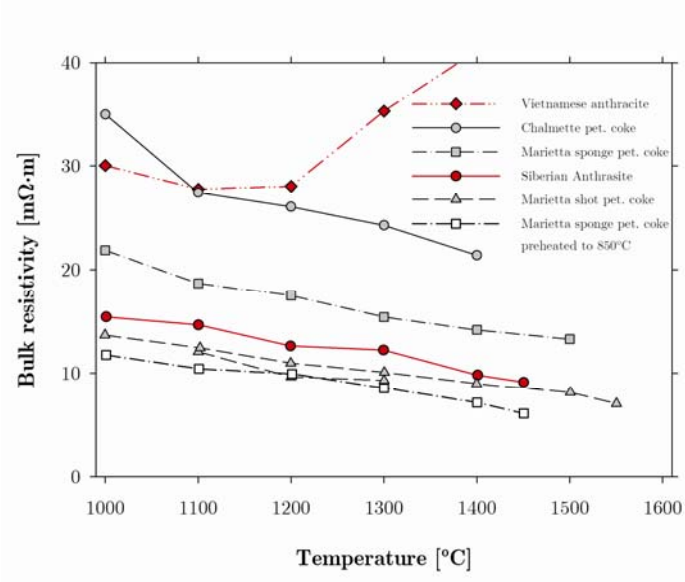

Figure 5-9: Bulk resistivity of petroleum cokes and anthracites.

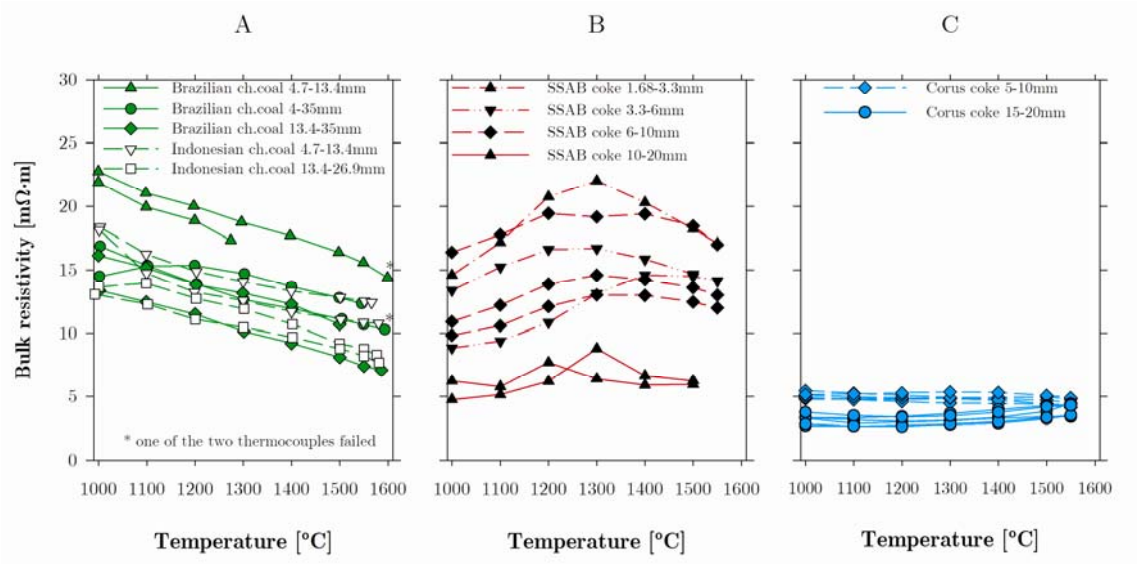

Figure 5-10: The influence of particle size is illustrated in these graphs where varying particle size ranges of A) the charcoals (Eidem 2004b), B) the SSAB coke (Eidem 2004a) and C) the Corus coke (Olsen and Eidem 2003; Eidem 2004a) is plotted as a function of temperature.

When comparing the bulk resistivity of the petroleum cokes to the bulk resistivity of the metallurgical cokes, it is seen that at 1000°C the bulk resistivity of most of the metallurgical cokes are approximately half of the bulk resistivity of the Marietta sponge and shot petroleum cokes. As the temperature increases, the difference decreases. The same is true for the Siberian anthracite.

The bulk resistivity of the two charcoals is presented in Figure 5-10 A. It can be seen that the bulk resistivity is in the same range as the petroleum cokes and the Siberian anthracite. The smaller fractions of the SSAB coke, presented in Figure 5-10 B, has a bulk resistivity equal or higher compared to the bulk resistivity of the Marietta shot and sponge petroleum cokes, the Siberian anthracite and the charcoals at the presented temperatures. The bulk resistivity of the two fractions of Corus coke, see Figure 5-10 C, is, at 1600°C, lower compared to all the other tested materials.

One interesting aspects is the influence that particle size has on the bulk resistivity. Varying particle sizes of charcoal, SSAB coke and Corus coke have

been tested. The results are plotted in Figure 5-10 A, B, and C, respectively. Due to a possible influence of packing on the result, it was decided to sieve the SSAB coke into size fractions of approximately 100 % increments. The packing of the particles will then be the same for all the particle sizes.

It is worth noticing that for both the two charcoal and the metallurgical cokes, the bulk resistivity decreases with increasing particle size. For the Brazilian charcoal, where the 4-35 mm size fraction was sieved into two fractions, the mixed fraction has a bulk resistivity that is between the two other size fractions.

The hump is observed for both the Corus coke 15-20 mm and for all of the SSAB coke size fractions. The hump cannot be seen for the 5-10 mm Corus coke, and only a slight increase in the bulk resistivity is seen for the 15-20 mm size fraction. For the SSAB coke it seems as though the amplitude of the hump decreases with increasing particle size. The hump is, as mentioned, not seen for the charcoals, which decreases almost linearly in resistivity from 1000°C to 1600°C.

The particle size influence on the bulk resistivity is summarized in Figure 5-11 A, where the bulk resistivity of the SSAB and Corus cokes and the Brazilian and Indonesian charcoals are plotted as a function of temperature. 1500°C is chosen since there are more results at 1500°C compared to 1600°C. Linear regression trend lines have been added to ease the reading of the graph. The slopes of the curves are quite different. The reason for this may be due to packing of the particles. This is influenced both by the particle size ranges, the shape of the particles. The difference in particle shape is quite significant when comparing the shape of the charcoal and the metallurgical coke. A difference in packing would, however, influence the bulk density, given that the shape of the particles is the same.

The bulk density does not have such a clear influence on the bulk resistivity as the particle size, see Figure 5-11 B. It can be seen that the difference in bulk

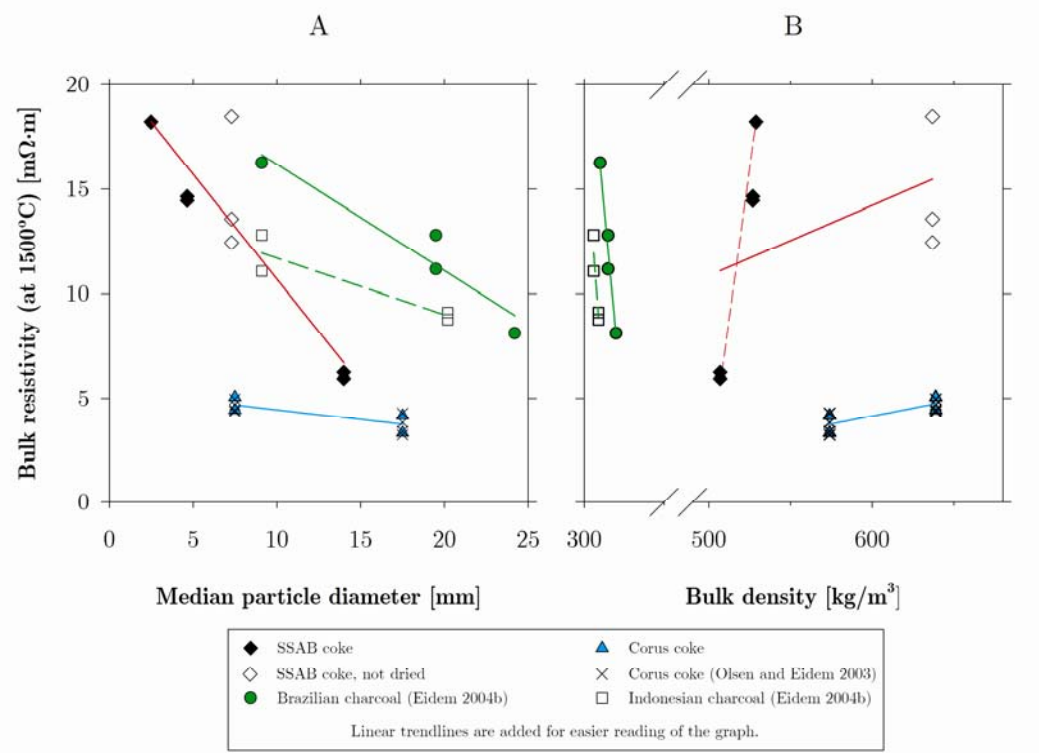

Figure 5-11: Bulk resistivity at 1500°C plotted against A) the particle size and B) the bulk density of metallurgical cokes and charcoals. The SSAB coke 6-10 mm size fraction was not dried prior to the experiment. Linear trend lines are added for easier reading.

density is very small for the material that has been dried, i.e. the charcoal with a bulk density of 306-320 kg/m^3 and the SSAB coke fractions that has a bulk density of 507-529 kg/m^3. For the charcoals it can be seen that for both the Indonesian charcoal and the Brazilian charcoal the bulk resistivity decreases with increasing bulk resistivity. For the SSAB coke the bulk resistivity, excluding the 6-10 mm size fraction that has not been dried, and the Corus coke the bulk resistivity increase with increasing *average* bulk resistivity. It is, however, important to keep in mind that the standard deviation of the bulk density of the SSAB cokes of the 1.68-3.3 mm, 3.3-6 mm and the 10-20 mm fractions is large compared to the difference between the three.

Other variables that are known to influence the electrical conduction of carbon materials is the graphene layer stack height, L_c, and the distance between the graphene layers, d_{002}. The bulk resistivity of the Corus coke 15-20 mm, Magnitogorsk coke, SSAB coke 10-20 mm and the Zdzieszowice coke at 1500°C

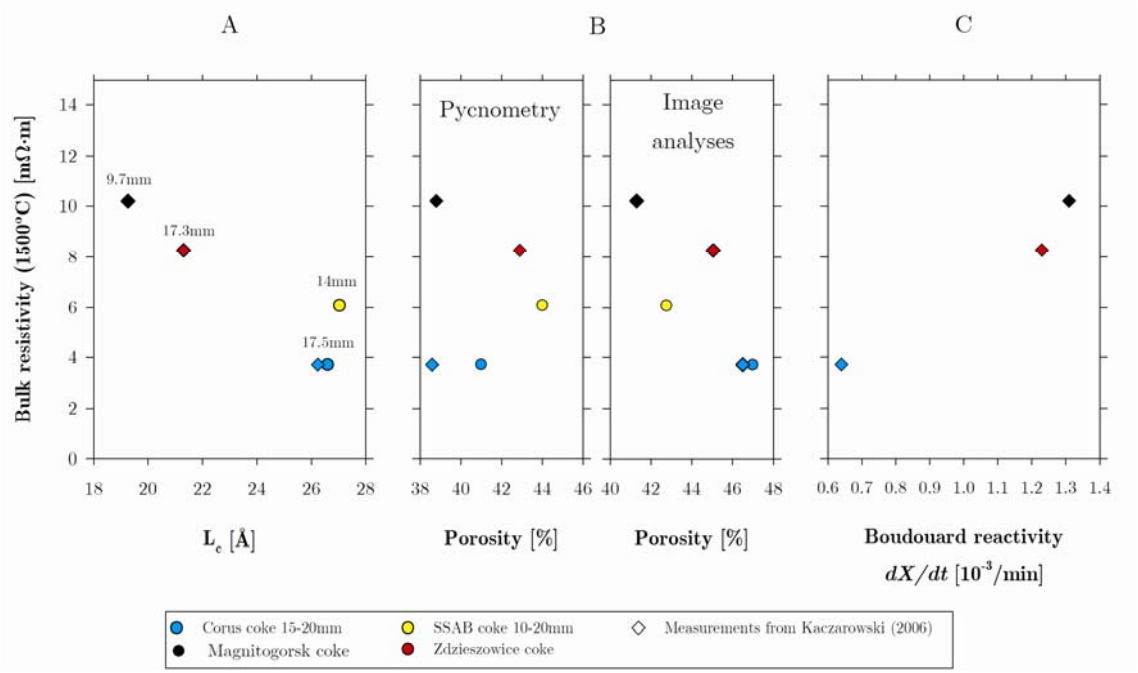

Figure 5-12: The bulk resistivity of metallurgical cokes with a median diameter above 9 mm is plotted against A) L_c, B) the porosity and C) the Boudouard reactivity. Measurements from (Kaczorowski 2006) has been included.

is plotted as a function of L_c in Figure 5-12 A. Measurements from Kaczorowski (2006) that were made on Magnitogorsk coke, Zdzieszowice coke and Corus coke are included. The size range tested by Kaczorowski (2006) is unknown. From the graph it can be seen that there is a decrease in bulk resistivity with increasing L_c. The difference in interplanar distance between the cokes were insignificant, and was not plotted.

However, when the bulk resistivity of the various size fractions of SSAB and Corus cokes are plotted as a function of L_c and d_{002}, respectively, it can be seen that neither can characterize the resistivity of the materials alone, see Figure 5-13. As mentioned in Chapter 3, concerning material characterization, a correlation can be seen between the particle size and the L_c, d_{002} and porosity, within each type of material.

In Figure 5-12 B the porosity measured both by pycnometry and by image analysis is included. As mentioned in the material characterization chapter, the

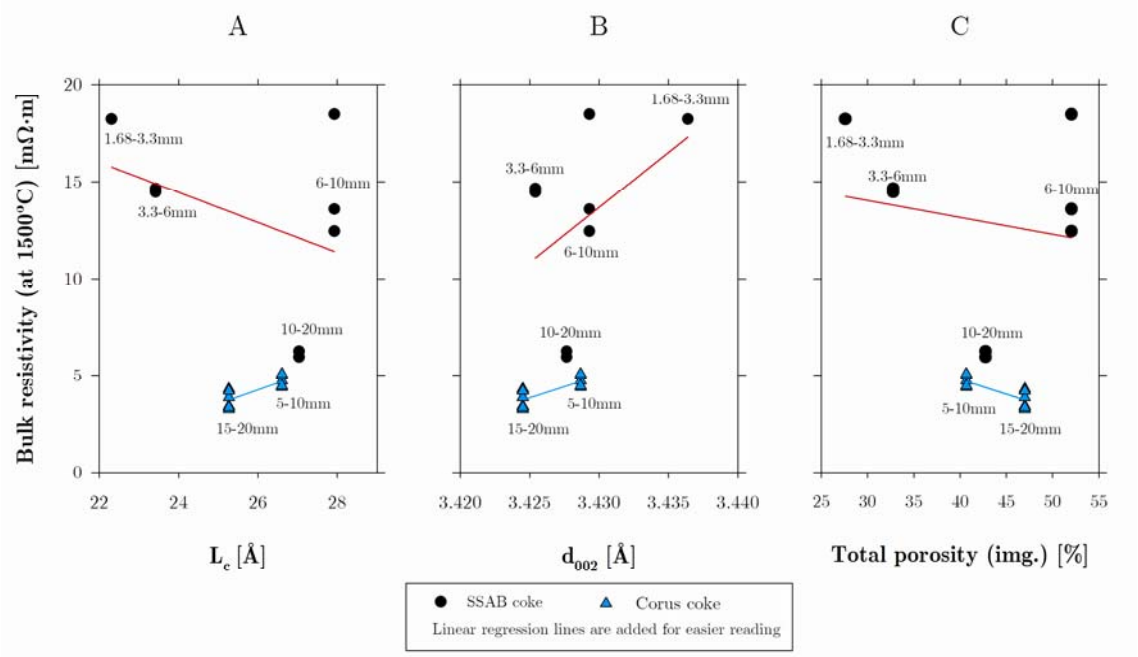

Figure 5-13: The A) L_c, B) d_{002} and C) total porosity (by image analysis) are plotted as a function of the bulk resistivity at 1500°C. Particle size ranges are indicated.

image analyses give a higher porosity compared to the pycnometry. For the pycnometry it is seen that if the Corus coke 15-20 mm is not taken into account, there is a decrease in bulk resistivity with increasing porosity. For the image analysis the same correlation is seen.

Kaczorowski (2006) studied the Boudouard reactivity of metallurgical cokes. Included in the study are three cokes also studied in this work. The Boudouard, or CO_2, reactivity, as determined by a thermobalance scales, was determined for the Corus coke, the Magnitogorsk coke and the Zdzieszowice coke. The bulk resistivity of these cokes at 1500°C is plotted as a function of the results, see Figure 5-12 C. It can be seen that an increasing Boudouard reactivity correlates with a lower bulk resistivity.

From the literature (Dijs and Smith 1980) it is known that the volatile content may also have an influence on the bulk resistivity. The results of the proximate analysis of the cokes that has a median particle size above 9 mm is plotted against the bulk resistivity at 1500°C for the respective cokes in Figure 5-14.

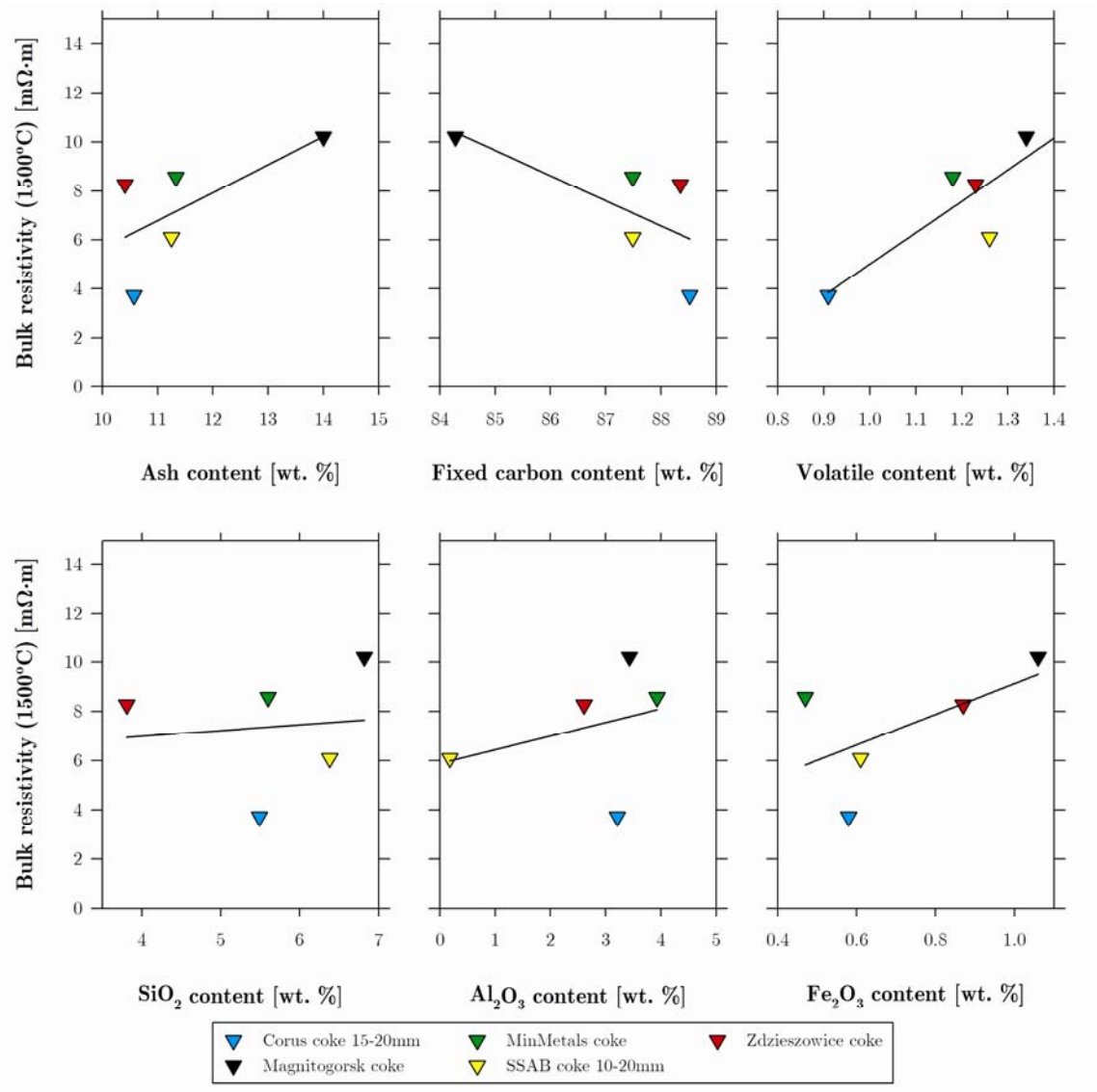

Figure 5-14: The bulk resistivity at 1500°C of various cokes are plotted as a function of the ash, fixed carbon and volatile content, as well as some common ash components.

The analysis is of the green materials, i.e. prior to the experiments. The results from 1500°C is, as previously mentioned, used since this is the temperature closest to what is believed to be the temperature of the coke bed with more results compared to 1550°C. The bulk resistivity at 1500°C seems to be influenced by both the ash and the fixed carbon content. It is, however,

important to remember that the sum of the fixed carbon, ash and volatile is equal to 100 wt. pct, see Chapter 3 for further details on the proximate analysis. It also seems as though these conclusions are dependent upon the Magnitogorsk points, and if these points are excluded, there will be no correlations present.

For the volatile content the correlation is clearer, and it can be seen that the bulk resistivity increases with increasing volatile content.

In the chapter concerning material resistivity and contact resistance the influence of ash components on the contact resistance was discussed. In Figure 5-14 the bulk resistivity at 1500°C is plotted against the most common ash components in these cokes, SiO_2, Al_2O_3 and Fe_2O_3. Again, the data are very spread out, making it difficult to see any clear trends. For the Al_2O_3 content, the Corus coke is, again, the odd result deviating from the trend. There does, however, seem to be a trend that an increasing Fe_2O_3 content increases the bulk resistivity at 1500°C.

5.3 Discussion

5.3.1 Effect of temperature on bulk resistivity

In general; for all the presented bulk resistivity experiments, the bulk resistivity decreases from room temperature to around 1550°C. This is in accordance with trends reported in previous publications[1-11]. There are two reasons for this: 1) A further graphitization of the carbon material due to the temperature exceeding the previous heat treating temperature, and 2) The increased temperature causes more electrons to enter the conductive bands of the graphite crystallites present in the coke (Mrozowski 1950).

[1] (Downing and Urban 1966) [2] (Rennie 1975) [3] (Dijs et al. 1979) [4] (Dijs and Smith 1980) [5] (Bakken and Wærnes 1986) [6] (Miyauchi et al. 2001) [7] (Olsen 2003) [8] (Olsen and Eidem 2003) [9] (Miyauchi et al. 2004) [10] (Olsen 2004) [11] (Krogerus et al. 2006)

At about 1100°C to 1400°C the bulk resistivity of SSAB, Magnitogorsk, and Zdzieszowice metallurgical cokes starts to increase with an increase in temperature before it yet again decreases with an increase in temperature. For the other carbonaceous materials, shown in Figure 5-9 and Figure 5-10A, this phenomenon is only seen for the Vietnamese anthracite, for which the decrease in resistivity was not recorded. How pronounced this ''hump'' is varies considerably with the type of coke and particle size. The hump has previously been reported for both dry coke beds and charge mixes[2-11]. Rennie (1975) suggests that the hump is a result of volatiles evaporating and poisoning the conduction surfaces. Further heating will make the volatiles evaporate, decreasing the resistance. Bakken and Wærnes (1986) suggest that the resistivity hump is due to shrinking of the coke particles due to evaporation of moisture and volatiles. However, in the results reported by Olsen (2004), the hump is observed even after keeping the coke at temperatures of 1400°C to 1600°C for longer periods, followed by cooling to room temperature and reheating to elevated temperatures again. These observations make the explanation based on volatiles and moisture very unlikely since the observed phenomenon is reversible. The hump has not been observed in the material resistivity and contact resistance experiments presented in Chapter 4. This indicates that the hump is related to a packed bed situation, where many particles are packed together. A possible explanation is a thermal expansion as the temperature increases. This would not be observed in the material resistivity and contact resistance experiments. As the temperature rises and the coke expands there may be a reordering of the particles. Reordering the particles will cause contact points between particles to break and new contact points to be established, and during this process the bulk resistivity increases. If there is a contact film that has lowered the *contact resistance*, e.g. Fe, breaking the contact point will cause the resistivity to increase. If, on the other hand, an insulating film is formed on the contact area, breaking the contact point will cause the resistivity to decrease.

In some of the cases the reported maximum temperatures are significantly lower than 1600°C. This is due to high vertical temperature differences in the coke bed. As mentioned before, measures were taken to minimize this error, but it is still present. However, in most cases the differences in bulk resistivity between two temperatures, such as 1500°C and 1600°C, are lower than the differences in bulk resistivity between two types of carbon materials. In one of the SSAB experiments shown in Figure 5-10 B and two of the charcoal experiments shown in Figure 5-10A, one of the thermocouples failed. This possibly caused a shift of the data toward a higher temperature.

At rising temperatures the variance decreases, and at 1500°C and 1550°C, there is a significant difference between the metallurgical cokes, see Figure 5-8. At 1550°C, SSAB coke 6-10 mm has the highest variance of the metallurgical cokes with a variation of approximately 19 % about the mean.

5.3.2 Effect of carbon material types on the bulk resistivity

The lowest bulk resistivity recorded at 1550°C is for Corus coke with 3.9 mΩ·m, followed by the TianJin GNC, SSAB, MinMetals and Zdziesowice cokes. The Magnitogorsk coke, measured as 10.3 mΩ·m, shows the highest bulk resistivity of the metallurgical cokes, and also has the smallest particle size, d50, see Table 5-1. By comparison, Downing and Urban (1966) measured the bulk resistivity of 1.41-2.38 mm granular coke to be 16 mΩ·m at 1600°C, and Dijs et al. (1979) measured the bulk resistivity of anthracite as 28 mΩ·m and Isocor coke as 37 mΩ·m at 1550°C. The size fractions tested by Dijs et al. (1979) had a median particle size of approximately 3.35 mm. The tested particle size fraction is smaller than the size fractions used in the bulk resistivity experiments, and the results are therefore expected to be higher. Downing and Urban (1966) and Dijs et al. (1979) did not apply any force to the charge. This would probably also affect the bulk resistivity. Olsen (2003) measured the bulk resistivity of an 8-18 mm metallurgical coke, with an applied force on the coke bed. The bulk resistivity was measured as 4.4 mΩ·m, i.e. within the range measured in this work.

At room temperature the bulk resistivity of the petroleum cokes and the anthracites, presented in Figure 5-9, is higher than that of the metallurgical cokes, but as the temperature rises the difference in bulk resistivity decreases. This was also observed by Dijs et al. (1979). There are, however, exceptions. The Vietnamese anthracite has a significant increase in bulk resistivity from 1200°C. At 1550°C, the bulk resistivity of the Marietta shot petroleum coke is 7.05 mΩ·m, which is a lower resistivity than measured for the Magnitogorsk, MinMetals and Zdzieszowice metallurgical cokes.

The Marietta sponge petroleum coke that was calcined at 850°C for one hour has the lowest bulk resistivity of the petroleum cokes, with a 6.1 mΩ·m at 1450°C. The reason for the difference in bulk resistivity between the two Marietta sponge petroleum coke samples is probably due to the calcination procedure. The holding time at the maximum temperature was longer for the sample heated to 850°C compared to the holding time of the sample heat treated in the one-phase furnace. The exact holding time and temperature for the sample heat treated in the one-phase furnace is, however, not known. The longer holding temperature would probably give further carbonization of the material and consequently a lower bulk resistivity. From Figure 5-9 it can be seen that the bulk resistivity of the Marietta sponge petroleum coke that has been heat treated to 850°C is, indeed, lower compared to the petroleum coke sample that was heat treated in the one phase furnace.

In Figure 5-12 A the bulk resistivity at 1500°C of the metallurgical cokes with a median particle size diameter above 9 mm is plotted as a function of the carbon crystallite stack height, L_c. Generally it seems as though an increasing stack height, as expected, decreases the bulk resistivity. This is in agreement with what is known from graphites (Mrozowski 1952). As described previously, an increased graphitization decreases the energy gaps between the valence bands and the conduction bands, decreasing the resistivity. However, if the bulk resistivity at 1500°C is plotted as a function of the XRD results of the various

particle size ranges of the Corus and SSAB cokes, no correlation can be seen between the bulk resistivity and the L_c or the d_{002}.

Based upon the proximate analyses shown in Table 3.3, the major differences between the type of carbon material lay in the amount of volatiles in the *green* materials, which is significantly higher for the petroleum cokes and the charcoals compared to the metallurgical cokes. By heat treatment, the content of volatiles will be reduced dramatically and it is evident, from the fact that these materials are practically non-conducting in the green state, that the volatile content has considerable influence on the bulk resistivity, at least at lower temperatures. In Figure 5-14 it can be seen that at 1500°C that an increasing volatile content increases the bulk resistivity of the metallurgical cokes. This is in accordance with the findings of Dijs et al. (1979) and Dijs and Smith (1980). However, within the three cokes with a volatile content between 1.18 and 1.26 this trend is not followed. This is also seen for the SSAB coke size fractions, where no correlation is found between the volatile content and the bulk resistivity.

The other obvious difference between the different carbon materials is the ash content, where the metallurgical cokes far exceed the other materials, see Table 3.3. As mentioned in Chapter 3, the ash content is confounded with the amount of volatile and the amount of fixed carbon. Some of the ash components will react with carbon. Above 1400°C, SiO_2 in the ash, typically 50 wt. % of the ash components, reacts at a considerable rate to SiC (Gill and Dubrawski 1984). It is, however, hard to determine the dominating effect, as the type and amount of SiC formed is not known. The amount of Fe_2O_3 and FeO in the ash may also influence the bulk resistivity. The iron oxides are reduced prior to the SiO_2, and the reduction product is Fe, which will decrease the contact resistance if deposited at the contact interface between two coke particles. In Figure 5-14 the bulk resistivity at 1500°C is plotted as a function of the relative amount of SiO_2, Al_2O_3 and Fe_2O_3 in the respective material, i.e. *not* the relative amount in the ash. It can be seen that there is little correlation between the bulk resistivity

and the SiO_2 and the Al_2O_3, but that an increasing amount of Fe_2O_3 seem to *increase* the bulk resistivity. If iron is deposited in the particle-to-particle intersection, the reduced contact resistance is counteracted by other factors such as L_c or the volatile content.

Porosity may influence the bulk resistivity in two ways; 1) a higher porosity means less carbon material for the current to flow through and consequently a higher resistance, and 2) a higher porosity is known to decrease the strength of the coke (British Coke Research Association 1969; Pitt and Rumsey 1980). A decreased coke strength is thought to cause a crushing of the asperities of the coke particle. As a result, the area of the particle-to-particle contact interface increases, decreasing the bulk resistivity. The results presented in Figure 5-12 B indicate a possible correlation between the porosity and the bulk resistivity at 1500°C. Then the bulk resistivity decreases with increasing porosity, i.e. contradictory to the assumption that a lower porosity would give more carbon material through which the current can flow. However, as the porosity increases with increasing particle size the mechanical strength of the coke decreases. This decreased mechanical strength will lead to further crushing and as a result enlargement of the particle-to-particle contact points. This effect is further enhanced by the increased contact pressure due to fewer particles in the cross section of the coke bed as the particle size increases.

The points plotted in Figure 5-12 C indicate that some of the same factors may influence both the Boudouard reactivity and the bulk resistivity. Kaczorowski (2006) concludes that the Magnitogorsk coke has the highest Boudouard reactivity due to three main factors: 1) the highest content of a catalyst in the ash component, 2) the lowest anisotropy compared to the other cokes, and 3) the highest surface area of the three cokes. The Corus coke, which has the lowest reactivity of the three cokes, has the lowest content of the catalyst, the highest anisotropy and the lowest surface area of the three cokes. Of the three factors influencing the reactivity, the anisotropy is the factor, besides the Boudouard reactivity itself, that may influence the bulk resistivity. L_c is

determined from the *Full Width Half Maximum*, which is found through the XRD analysis. The broader the width of the carbon peak, the lower the anisotropy, the less ordered the material is. As previously mentioned, the bulk resistivity at 1500°C also decreases with increased ordering of the carbon structure, i.e. a higher anisotropy, see Figure 5-12 A. Another effect of the difference in the CO_2 reactivity is that the carbon at the particle-to-particle contact interfaces will react faster, leaving ash residue that increases the contact resistance. The two are, however, confounded and cannot be told apart.

The shapes of the particles are also quite different for the four materials. The metallurgical coke has a relatively spherical shape, but with pointed edges. The anthracite is similar in shape, but has a more stone-like surface. The Marietta shot petroleum coke particles are spherically shaped with a smooth surface, whereas the charcoal has a more flaky shape. The shape of the particles certainly influences the packing, and therefore the number of contact points involved in the coke bed. A smooth, round shape, such as the Marietta shot petroleum coke, will probably give fewer contact points compared to the flaky charcoal. The orientation of the flaky charcoal, in relation to the current direction, will also influence the bulk resistivity. More contact points in the direction of the current will increase the bulk resistivity, whereas more contact points perpendicular to the current path will decrease the bulk resistivity of the coke bed. The difference in the particle shape of the metallurgical cokes, the anthracites and the petroleum cokes is small, and is consequently assumed to have a negligible effect on the bulk resistivity.

Other factors that will influence the bulk resistivity are the material resistivity and the contact resistance. As concluded in Section 4.4, there is no statistically significant difference between the *material resistivity* of the SSAB coke, Zdzieszowice coke and Corus coke, but a significant difference in the *contact resistance* between the three metallurgical cokes. The Zdzieszowice coke had the lowest *contact resistance* compared to the SSAB coke, Corus coke was not included in the statistical analyses due to few experiments. When the bulk

resistivity is compared, Zdzieszowice coke has the highest bulk resistivity compared to the SSAB coke 10 - 20 mm, and the bulk resistivity of the 15-20 mm Corus coke is lower compared to the SSAB coke, see Figure 5-8. The bulk resistivity results and the contact resistance results are, in other words, contradictory. Data are, however, available for all three metallurgical cokes on half spheres, see Section 4.5. The half spheres is the shape where the particle-to-particle contact is closest to the particle-to-particle contact found in a coke bed. The results show that the resistance of two half spheres is 83 mΩ for the Corus coke, 102 mΩ for the SSAB coke and 147 mΩ for the Zdzieszowice coke. This is comparable with the bulk resistivity results. Based on these results it can be concluded that the particle-to-particle contact is a main variable in the bulk resistivity of a coke bed.

Comparing the bulk resistivity presented in this work with the results found in the literature, the results are within the variation found. Dijs et al. (1979) found that the bulk resistivity of 3.6 mm anthracite and 3.6 mm Iscor coke at 1500°C is approximately 34 mΩ·m and 43 mΩ·m, respectively. It is slightly higher compared to the bulk resistivity of the 1.68-3-3 mm size fraction of SSAB coke, which is measured as 18.2 mΩ·m at this temperature. A comparable size range was also tested by Downing and Urban (1966), who found that the bulk resistivity of a 1.41-2.38 mm Buckwheat coke was approximately 1.7 mΩ·m, which is lower compared to the bulk resistivity of any of the materials tested in this work. Olsen (2004) used an apparatus of approximately the same dimensions as the bulk resistivity apparatus presented in this work. He reports a bulk resistivity of an unknown coke with an 8-18 mm particle size fraction as 4.4 mΩ·m at 1300°C. By comparison the bulk resistivity of Corus coke 5-10 mm is typically around 4.9 mΩ·m at this temperature.

The reason for the difference in the measured bulk resistivity is due to the design of the apparatus used to test the materials. As mentioned in the literature review, the method of measuring varies quite a bit. The differences between the mentioned measurements are that Olsen (2004) uses a high alumina

refractory cylinder, diameter 310 mm, with a top and bottom electrode. The heat is supplied through ohmic heating of the coke bed, and the potential drop is measured by a probe inserted into the coke bed. The applied pressure on the coke bed was approximately 3600 kg/m^3. Dijs et al. (1979) uses indirect heating of a graphite crucible 200 mm diameter, determining the resistivity based on the potential drop from a probe placed in the center of the graphite crucible, and the crucible wall. No pressure was applied on the coke bed. Downing and Urban (1966) use a tungsten crucible, 50.8 mm in diameter, heated in a graphite tube furnace. The potential drop was measured by two tungsten electrodes inserted into the granular bed. No weight is applied on the coke bed. Downing and Urban (1966) comment that the data are not as good as desired, and that the measurements were influenced by the electrodes that were forced into the coke bed, compacting the coke and thus lowering the measure bulk resistivity. Based on these comparisons it can be concluded that bulk resistivity performed in different apparatus will vary due to the different conditions under which the materials are tested. If a company wishes to compare the bulk resistivity of two cokes with two different apparatus, a standard material should be tested in both apparatus to determine any difference.

5.3.3 Particle size dependency

The effect of particle size on bulk resistivity is summarized in Figure 5-11 A. It is evident that all the materials show a decreasing bulk resistivity with increasing particle size, in agreement with the previously reported results[2].

The difference in the slopes of the trend lines may be either an effect caused by the different particle size distributions tested, or by material dependent factors. A study of the carbon crystallite stack height, L_c, and the interplanar distance of the graphene planes, d_{002}, of the various fraction of Corus coke and SSAB coke, reveal that the L_c and d_{002} varies with the particle size, see Figure 5-13 A and B respectively. If the SSAB 6-10mm fraction is excluded, the L_c increases

[2] (Downing and Urban 1966; Lorenz and Marincek 1969; Willand 1975; Dijs et al. 1979; Dijs and Smith 1980; Krogerus et al. 2006)

with increasing particle size. For the Corus coke the opposite is seen, i.e. Corus coke 15-20 mm has a lower L_c compared to the 5-10 mm Corus coke size fraction. A difference in bulk resistivity due to a change in particle size will be enhanced by the L_c increasing with increasing particle size, and opposite. The difference in material properties between the SSAB cokes is, as mentioned in Chapter 3, probably due to the size fractions originating from various batches of coke.

The packing of the SSAB coke is close to constant for all the particle size fractions. For the Corus coke the packing is decreased when the particle size is increased. This is due to the increment within each particle size fraction not being constant. For the SSAB coke there is an increase in the particle size of approximately 100 % within each fraction, whereas the increase in particle size is 100 % for the 5-10 mm Corus coke fraction and 33 % for the 15-20 mm Corus coke fraction. A decrease in the packing does, however, give less material for the current to flow through, consequently decreasing the bulk resistivity compared to if the packing was kept constant. This will, in other words, not explain the difference in slope between the materials.

The Al_2O_3 content of the SSAB coke and the Corus coke is quite similar. The Fe_2O_3 and MnO content are higher for the Corus coke compared to the SSAB coke. The two latter components are thought to be ash components that may be reduced, decreasing the particle-to-particle contact resistance. This may explain the difference in the magnitude of the bulk resistivity between the two metallurgical cokes.

The choice of particle size ranges for the SSAB cokes gives an almost constant packing between the particle size ranges. This is reflected in the standard deviation of the bulk density measurements. When all SSAB bulk density measurements made with the 10 liter container are included, both the dried samples and the samples that are not dried, the standard deviation of the bulk density is approximately 11 %. It is, however, evident that the bulk density of

the SSAB coke that has not been dried is significantly higher compared to the SSAB coke that has been dried. When only the dried coke is included the standard deviation of the bulk density of the SSAB coke is reduced to 4 pct, indicating that the goal of constant packing has been achieved and the wall effect can be neglected.

5.3.4 Measurement uncertainty and error

The standard deviations shown in Table 5-3 give an indication of the accuracy of the method. At 1400°C the standard deviation varies between 6 % and 27 %, at 1500°C between 1 % and 22 %, and at 1550°C the standard deviation varies between 2 % and 19 %.

Looking at the data in Figure 5-8 it can be seen that the difference between the bulk resistivity of the metallurgical cokes above 1400°C is larger than the standard deviations indicated. This means that it is possible, despite of the standard deviation being above 20 %, to differentiate between the bulk resistivity of the metallurgical cokes.

During the measurements there will be rather large temperature gradients in the furnace. This was partly compensated for by turning off the current if the difference in temperature at the two measuring points was too large. Some measurements were done in the high alumina refractory, close to the inner wall of the cylinder. The temperature there never reached above approximately 500°C, indicating that the radial temperature gradients are significant. The radial temperature gradients were, however, not investigated further. The effect of the temperature gradients on the results is that if the average temperature is not representative of the mean temperature in the coke bed, the measurement point will be shifted to a higher or lower temperature. If the radial temperature gradients are large enough, the bulk resistivity measurements show that the colder parts of the coke bed will have a higher resistivity compared to the warmer parts. As a result, less current will flow through the colder parts and more through the warmer parts. The assumption of Equation (5.1) is then not

fulfilled. The "real" bulk resistivity will then be lower compared to what is calculated from Equation (5.1).

Variation in current density may have affected the measurement result. When comparing measurements that were done using App. A, using current densities in the upper region of the current density region, with results from App. B, where the current density used was in the lower part of the current density region, no difference was seen.

During the experiments currents of between 0.5 kA and 1 kA was used. Measures were taken to minimize the electromagnetic fields so that the induced voltages in the measurement circuit would be minimized. These measures included twisting the two cables supplying the current to the apparatus and also twisting the cables of the voltage measurement. The open area was also minimized. Due to the measurement current being the current source used for the measurements, it was not possible to turn this current off during the measurements, as was done for the material resistivity and contact resistance measurements. Neither was it possible to turn off the current to assess the possible impact of the electromagnetic field on the measurement circuit. It is, however, thought that the induced voltage is negligible.

Variation in the raw materials is one of the sources of error. The samples were, mostly, delivered in big bags, from which the samples were extracted. Although not possible to detect by the naked eye, there was possible segregation of the raw materials within the big bag. The larger particles would then appear in the first experiments, decreasing as samples were extracted from further down in the big bag. It has, however, not been possible to see any correlation with time of the Corus coke samples, which all were extracted as described.

5.4 Conclusions

The results obtained confirm that the bulk resistivity of carbon materials decreases with increasing temperature from room temperature to 1600°C. An increase in resistivity at 1000°C to 1200°C is, however, observed for all the

metallurgical cokes. The resistivity decreases yet again when heated further. Observations show that this is a reversible effect, suggesting this is a result of thermal expansion and contraction.

According to the bulk resistivity measurements, metallurgical coke generally has a lower electrical bulk resistivity than anthracite, petroleum coke, and charcoal at lower temperatures. Difference in texture and volatile matter can explain the differences; petroleum and charcoal having a much higher content of volatile matter compared to metallurgical coke.

The lowest bulk resistivity recorded at 1500°C is for Corus coke, measured as 3.9 mΩ·m, followed by the SSAB coke, as 6.02 mΩ·m, and Zdziesowice coke, as 8.59 mΩ·m. Magnitogorsk coke has the highest electrical resistivity of the metallurgical cokes, measured as 10.2 mΩ·m. The two petroleum cokes that reached 1500°C were Marietta shot petroleum coke, measured as 8.13 mΩ·m, which is in the metallurgical coke area, and Marietta sponge petroleum coke, measured as 13.3 mΩ·m, which is higher. Brazilian and Indonesian charcoal sorts in between petroleum coke and metallurgical coke with measured bulk resistivities of 8.11 mΩ·m and 9.17 mΩ·m, respectively. Anthracites seem to have a bulk resistivity that ranges from approximately the lowest of the petroleum cokes to a resistivity far higher than the highest resistivity of any of the other materials tested. This should, however, be confirmed by more experiments. No single parameter, like porosity, L_c, d_{002} or volatile content, can explain the difference in bulk resistivity between the various carbon materials.

The one single parameter that will affect the resistivity the most is the particle size. Within each material the bulk resistivity will decrease with increasing particle size. The results indicate that there may be a correlation between the porosity and the particle size within each material, where the porosity increases with increasing particle size. Results from the literature show that the mechanical strength of the particles decreases with increasing porosity, i.e. within each type of material the mechanical strength decreases with increasing

particle size. A decreasing mechanical strength leads to crushing of the particle-to-particle contacts which again increase the area of the electrical contacts, decreasing the particle-to-particle contact resistance.

It is seen that for the metallurgical coke an increasing volatile content, an increasing CO_2 reactivity and a decreasing L_c indicate a higher bulk resistivity. No correlation has been found between the bulk resistivity of the carbon crystallite stack height, L_c, the distance between the graphene planes, d_{002}, or the bulk density that can explain the difference in bulk resistivity between different metallurgical cokes if the various size fractions of Corus and SSAB metallurgical cokes are included. The results presented in Chapter 4 also showed that there is no significant difference in material resistivity between the Corus, SSAB and Zdzieszowice cokes. It is, however, seen that the resistance measured on two half spheres of the Corus, SSAB and Zdzieszowice cokes indeed give an indication of how the bulk resistivity of the metallurgical cokes are in comparison to each other.

Chapter 6 Pilot Scale Furnace Experiments

As the availability of premium raw materials for the production of ferroalloys has gone down in the later years, there has been an increasing focus on increasing the knowledge of the processes. The main goal of this thesis has been to increase the fundamental knowledge concerning the electrical resistivity of dry coke beds. In this chapter three experiments are presented where ferroalloys were produced in a pilot scale oven. The goals of these experiments have been to verify the influence of coke particle size on the coke bed resistivity and to assess the influence of slag on the resistivity of the coke bed.

After the experiment the furnace was cast in epoxy, cut in half and polished. From the cross section of the furnaces the geometrical dimensions of the coke bed was determined. The electrical resistivity of the coke bed could then be determined based on the obtained geometrical dimensions and the furnace resistance prior to shutting down the furnace.

The influence of the coke particle size was tested by varying the particle size of coke between two FeMn experiments. One SiMn experiment was also done to study the effect of high resistance slag on the total resistance.

6.1 Apparatus and method

6.1.1 The pilot scale furnace

Figure 6-1 shows a picture of the pilot furnace, and a schematic drawing with dimensions is shown in Figure 6-2. The pilot furnace is a one phase 150 kVA furnace, using a 152 mm graphite electrode as the top electrode. The top electrode is centered in the circular furnace and the height may be adjusted mechanically. The bottom of the furnace is electrically conductive and functions as the bottom electrode. The top electrode holder and the bottom electrode are water cooled.

The furnace transformer is controlled by adjusting the voltage in steps within three major voltage areas. The current is limited within the voltage areas as shown in Table 6-1, and is determined by the voltage and the furnace resistance.

Figure 6-1: Picture of the 150 kVA one phase furnace (Slizovskiy et al. 2007).

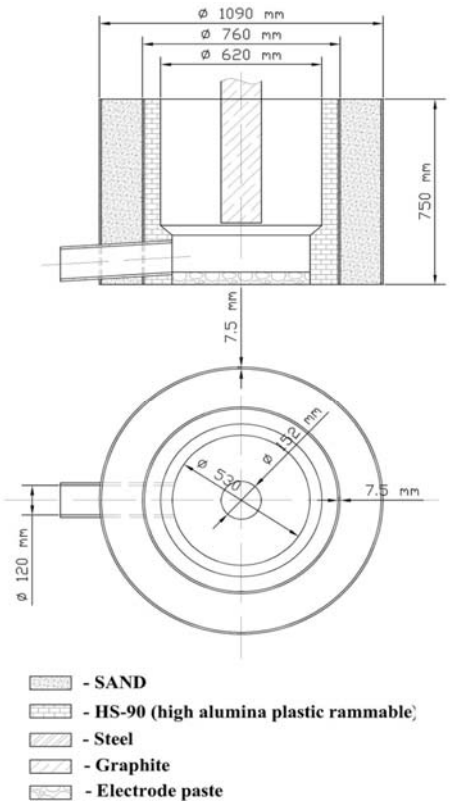

Figure 6-2: Schematic drawing of the pilot furnace (Slizovskiy et al. 2007).

Table 6-1: Voltage-ampere characteristics of the transformer.

U [V]	Imax [A]
10 - 20	6000
20 - 40	6000 - 3750
40 - 80	3750 - 1875

6.1.2 Furnace operation

All the experiments were operated with a constant electrode tip position of 20 cm above the bottom electrode and a constant power of about 150 kW. The charge level was at all times kept at the height of the casing.

At the initial stage of the experiments 5 kg of Corus coke, which was the coke of choice in all three pilot scale experiments, was charged to the empty furnace, and the electrode was lowered to create contact. For the SiMn experiment the furnace was preheated for 100 kWh over approximately one hour before adding the charge materials. For the two FeMn experiments the furnace was preheated for 19.5 kWh before adding the first charge.

The furnace was tapped approximately every 80 kWh for the SiMn experiment and every 60 kWh for the two FeMn experiments. The first tapping was done after 180 kWh for the SiMn experiment, and after 160 kWh for the two FeMn experiments. The tapping time, from opening to closing of the furnace tap hole, was typically 2 minutes.

During the experiment the voltage and current is continuously logged by a data logger. A power meter is used to determine the electric power consumption used between taps. No correction for reactive power and voltage was found necessary as the power factor, cos φ, is close to one (Sævarsdóttir 2002, pp. 217).

Table 6-2: Charge content mix in FeMn experiments.

Material	Weight [kg]
Asman 46%	11.4
Comilog MMA	6.5
Comilog sinter	14.0
FeMn fines	0.7
Dolomite	1.1
Corus coke	7.3

Table 6-3: Charge mix used in the SiMn experiment.

	Charge 1 and 2 [kg]	Charge 3 [kg]	Charge 4 [kg]	Cahrge 5 to 9 [kg]
CVRD sinter	22.5	22.5	22.5	22.5
Asman ore	27.5	27.5	27.5	27.5
Quartz	0	7	11	14
Dolomite	2	1	1	1
Corus coke 5-20mm	12	14	15	16

6.1.3 Charge mix

The charge component mix for the two FeMn experiments is given in Table 6-2. The particle size ranges of Corus coke were different in the two experiments, 5-10 mm and 15-20 mm, respectively. The coke is from the same batch of coke as the coke tested in the bulk resistivity apparatus. The proximate and ash analyses of the Corus coke is given in Chapter 3, and the analyses of the other charge components are given in Appendix 5.

In Table 6-3 the charge mix used in the SiMn experiment is shown. A 5-20 mm Corus coke fraction was used. The analyses of the raw materials are given in Appendix 5. The charge mix changes from the production of FeMn to SiMn, and hence the charge composition changes throughout the first 5 batch mixes, see Table 6-3.

6.1.4 Post experimental work

39 kWh after the last tapping the furnace is shut off. Due to the highly endothermic reactions occurring in the coke bed area, the chemical reactions will stop within minutes of shutting off the power (Tangstad 1996). The furnace is then cooled for approximately 72 hours before epoxy is poured into the furnace. After another 48 hours the epoxy has hardened and the furnace can be cut in half and polished. The shape of the coke bed can then be evaluated.

The tapped slag and metal is separated and weighed, and representative samples of slag and metal from each tap is taken. Raw materials that are mixed with the slag and metal can make the separation difficult.

6.1.5 Determination of the coke bed resistivity

During production of FeMn and SiMn the ore and sinter particles are reduced to slag at the edge of the coke bed. In the coke bed there is no ore or sinter particles present, only coke and slag. The method used to determine the outer edges of the coke bed is to outline the ore and sinter particles on the polished cross section of the furnace. In the SiMn experiment the melted ore and sinter particles were outlined, giving the same result. Based on the outlined ore and sinter particles the geometry of the coke bed was determined.

A multi physics modeling software, COMSOL Multiphysics 3.3, was then used to estimate the resistivity of the coke bed. A 2D axial symmetric geometry is made based on the furnace cross sections. Since the skin depth at 50 Hz is assumed to be large compared to the radial dimensions of the furnace, i.e. negligible current displacement, the Conductive Media DC module in COMSOL Multiphysics 3.3 is used. The module solves the current continuity equation:

$$\nabla \cdot \mathbf{J} = -\nabla \cdot \left(\frac{1}{\rho} \nabla V \right) = 0 \tag{6.1}$$

where $\nabla \cdot \mathbf{J} = 0$, since the total amount of current entering the furnace must also exit the furnace. ρ is the electrical resistivity and V the electric potential.

Only the coke bed area, the metal and the electrodes, all part of the geometry which is determined based on the furnace cross sections, are included in the model. This is due to the assumption that the charge mix has a resistivity of more than one order of magnitude higher compared to the coke bed area when the temperature drops below about 1200°C (Miyauchi et al. 2001). As a result only an insignificant current is assumed to flow through the parts of the furnace

above the coke bed area. As mentioned in the introduction, previous modeling of an industrial furnace has shown that more than 95 % of the current flows through the coke bed area (Dhainaut 2004).

The material and electrical properties used in the estimation of the electrical resistivity of the coke beds are shown in Table 6-4. All the electrical properties were measured seconds prior to shutting down the furnace and should thus be representative of the electrical properties of the furnace defined by the cross section. The metal height is fixed to 10 cm over the full width of the coke bed, with an electrical resistivity of $8.93 \cdot 10^{-8}$ Ω·m, the electrical conductivity of iron at room temperature in the COMSOL material library. The graphite electrode height is 1.0 m in all the simulations, with an electrical resistivity of $1.00 \cdot 10^{-5}$ Ω·m, as measured by the material resistivity test, reported in Chapter 4.

It is assumed that all three sub domains, i.e. the electrode, the metal and the coke bed area, have a uniform electrical resistivity independent of temperature. This assumption is based on the measurement of the electrical resistivity of metallurgical coke, which shows a relatively stable electrical resistivity between 1000°C and 1600°C. The voltage and current used for the estimation of the

Table 6-4: Electrical parameters used in the model to estimate the electrical resistivity of the coke bed.

	Symbol	Value	
Electrical properties*			
FeMn, Corus coke 5-10mm	U	28	V
	I	5227	A
FeMn, Corus coke 15-20mm	U	24	V
	I	6688	A
SiMn, Corus coke 5-20mm	U	34	V
	I	4510	A
Material properties			
Resistivity of graphite	$\rho_{graphite}$	$1.00 \cdot 10^{-5}$	Ω·m†
Resistivity of metal	ρ_{metal}	$8.93 \cdot 10^{-8}$	Ω·m‡

*Average of last 20 sec. †As measured in Chapter 4

‡Resistivity of iron at room temp from COMSOL

electrical resistivity of the coke bed is the average of the last 20 seconds of the respective measurements.

To assess the uncertainty of the calculations due to the geometrical dimension of the furnace, the calculations are done for several geometrical shapes.

6.2 Results

6.2.1 FeMn experiments

The tapped slag and metal and their respective analysis will be presented. The electrical conditions will then be presented.

Tapped slag and metal, and energy consumption

After the experiments, the tapped slag and metal were separated and weighed. During the tappings, raw materials will sometimes follow the slag and metal out of the furnace tap hole. Unfortunately, part of the slag and metal was mixed with the tapped raw materials and could not be separated. This can be seen as the metal/slag/raw material mix in Table 6-5 and Table 6-6, where the metal and slag weight for the Corus coke 5-10 mm and 15-20 mm experiments are given, respectively.

Table 6-5: Weight of tapped materials and the energy consumption for the Corus coke 5-10 mm experiment.

Tap	Metal [kg]	Slag [kg]	Slag+ metal+ raw materials [kg]		Energy consumt. [kWh/ton]	Slag/metal ratio
1	25	15	7		5573	0.59
2	16	8	7		3752	0.52
3	7		34			
4	12	12	7		4812	0.97
5	12	3	17		5046	0.22
6	15	15	3		3886	0.98
7	20	16	2		3000	0.82
8	19	11	13		3085	0.56
Sum:	127	80	89	**Avg*:**	3966	0.71

*Average of tap 4-8

Table 6-6: Weight of tapped materials and the energy consumption for the Corus coke 15-20 mm experiment.

Tap	Metal [kg]	Slag [kg]	Slag+ metal+ raw materials [kg]		Energy consumt. [kWh/ton]	Slag/metal ratio
1	26	25	4		5299	0.93
2	11	11	2		5682	1.06
3	17	10	2		3438	0.59
4	11	12	5		5315	1.12
5	16	8	3		4038	0.48
6	12	8	3		3529	0.70
7	17	12	1		3842	0.66
8	15	11	2		4622	0.76
Sum:	125	97	21	**Avg*:**	4269	0.74

*Average of tap 4-8

Based on the weight of the metal, it seems as though the total production of metal is about the same in the two experiments. The calculated energy consumption per 1000 kg metal is based on the amount of tapped metal. Due to the high amount of slag/metal/raw material mix, particularly in the Corus coke 5-10 mm experiment. The calculated energy consumption is therefore uncertain. The energy consumption per tonne tapped metal is shown in Table 6-5 and Table 6-6. As expected, the energy consumption decreases, if the average of the first four and last four tappings are compared.

Slag and metal analyses

The analyses of the tapped metal and slag for the Corus coke 5-10 mm experiment is shown in Table 6-9 and Table 6-10 and in Table 6-7 and Table 6-8 for the Corus coke 15-20 mm experiment. R is the ratio of the main basic and acid oxides in the slag and should be constant if the analyses are correct. These oxides are not reduced in the furnace, and since R is constant in the charge mix, it should be constant in the slag. According to the charge mix calculations R should be 1.81, which is close to the measured values.

The metal analyses are about the same for the two experiments, with a manganese content of 80 wt. %, an iron content between 11 wt. % and 14 wt. % and a carbon content of approximately 7 wt. %. The silicon content of the 15-20 mm Corus coke experiment is a little higher compared to the 5-10 mm Corus coke experiment, which may indicate a higher temperature.

Since the metal analyses are assumed to be correct, more accurate analyses of the slags can be calculated based on the metal analyses and the raw material analyses. The calculated analyses are given in Table 6-11 and Table 6-12 for the Corus coke 5-10 mm and 15-20 mm experiment, respectively. R is now stable at 1.81 for the Corus coke 5-10 mm experiment and 1.83 for the Corus coke 15-20 mm experiment. KB2, which also includes SiO_2, is slightly higher in the 15-20 mm experiment, compared to the 5-10 mm experiment. Losses of Mn in the off gas, or inaccurate analyses of the raw materials give a lower MnO content in the slag than the theoretical assumptions.

Table 6-9: Metal analyses, Corus coke 5-10 mm experiment.

	Tap 1 [wt.%]	Tap 2 [wt.%]	Tap 3 [wt.%]	Tap 4 [wt.%]	Tap 5 [wt.%]	Tap 6 [wt.%]	Tap 7 [wt.%]	Tap 8 [wt.%]
Mn	79.8	79.7	79.9	79.8	79.9	80.0	80.7	80.8
Fe	12.4	12.6	12.3	12.5	12.4	12.3	11.8	11.8
Si	0.08	0.33	0.13	0.10	0.15	0.28	0.47	0.72
P	0.18	0.18	0.17	0.17	0.17	0.16	0.15	0.15
Ti	0.01	0.02	0.02	0.01	0.02	0.04	0.06	0.07
C	7.1	6.9	7.0	7.1	7.0	6.9	6.8	6.7
Total	99.5	99.8	99.6	99.6	99.7	99.7	100.0	100.2

Table 6-10: Slag analyses, Corus coke 5-10 mm experiment.

	Tap 1 [wt.%]	Tap 2 [wt.%]	Tap 3 [wt.%]	Tap 4 [wt.%]	Tap 5 [wt.%]	Tap 6 [wt.%]	Tap 7 [wt.%]	Tap 8 [wt.%]
MnO	42.5	41.0	47.2	39.0	37.0	34.7	34.4	31.4
SiO_2	21.0	21.5	20.9	22.3	24.7	24.4	25.9	25.5
CaO	14.1	15.8	14.9	16.7	17.8	18.7	19.4	20.7
MgO	4.0	4.2	3.8	4.6	4.9	5.1	5.5	5.5
Al_2O_3	15.2	14.8	14.4	14.1	13.8	14.2	15.3	15.5
K_2O	0.25	0.08	0.42	0.38	0.39	0.37	0.32	0.49
BaO	1.1	1.1	1.1	1.2	1.2	1.3	1.3	1.4
Total	98.1	98.6	102.7	98.2	99.8	98.6	102.0	100.6
$R*$	1.2	1.3	1.3	1.5	1.6	1.7	1.6	1.7

*$(CaO+MgO)/Al_2O_3$

Table 6-7: Metal analyses, Corus coke 15-20 mm experiment.

	Tap 1 [wt.%]	Tap 2 [wt.%]	Tap 3 [wt.%]	Tap 4 [wt.%]	Tap 5 [wt.%]	Tap 6 [wt.%]	Tap 7 [wt.%]	Tap 8 [wt.%]
Mn	77.9	78.1	78.0	79.2	79.8	79.9	80.2	80.4
Fe	14.2	14.3	12.6	12.6	12.3	11.7	11.0	10.9
Si	0.4	0.2	1.1	0.4	0.5	0.9	1.1	1.2
P	0.2	0.2	0.2	0.2	0.2	0.2	0.2	0.2
Ti	0.01	0.01	0.03	0.03	0.03	0.05	0.07	0.08
C	7.1	7.1	7.0	7.2	7.1	7.0	6.8	6.9
Total	99.8	99.9	98.9	99.7	99.9	99.6	99.4	99.6

Table 6-8: Slag analyses, Corus coke 15-20 mm experiment.

	Tap 1 [wt.%]	Tap 2 [wt.%]	Tap 3 [wt.%]	Tap 4 [wt.%]	Tap 5 [wt.%]	Tap 6 [wt.%]	Tap 7 [wt.%]	Tap 8 [wt.%]
MnO	46.7	50.5	39.9	40.1	39.7	34.9	31.9	27.9
SiO_2	20.5	19.6	22.8	22.6	23.5	23.5	23.7	24.5
CaO	14.9	14.1	17.2	17.1	16.5	18.4	19.2	21.0
MgO	4.2	3.9	5.0	4.9	5.0	5.2	5.8	7.1
Al_2O_3	12.4	11.9	12.0	11.8	12.0	13.5	14.9	16.1
K_2O	0.2	0.1	0.3	0.3	0.3	0.3	0.4	0.3
BaO	1.0	1.0	1.1	1.1	1.1	1.2	1.3	1.4
Total	100.0	101.1	98.3	97.8	98.0	97.1	97.2	98.3
$R*$	1.5	1.5	1.9	1.9	1.8	1.7	1.7	1.7

*$(CaO+MgO)/Al_2O_3$

Table 6-11: Slag analyses calculated based on the metal analyses of the Corus coke 5-10 mm experiment.

Tap	MnO [wt. %]	SiO_2 [wt. %]	Al_2O_3 [wt. %]	CaO [wt. %]	MgO [wt. %]	KB2*	R*
1	54.5 %	15.9 %	9.8 %	14.0 %	3.8 %	0.69	1.81
2	55.9 %	15.1 %	9.7 %	13.5 %	3.7 %	0.69	1.78
3	54.0 %	16.0 %	9.9 %	14.2 %	3.8 %	0.69	1.81
4	55.0 %	15.7 %	9.7 %	13.9 %	3.7 %	0.69	1.81
5	54.5 %	15.8 %	9.8 %	14.0 %	3.8 %	0.69	1.81
6	54.2 %	15.7 %	10.0 %	14.2 %	3.8 %	0.70	1.81
7	51.4 %	16.3 %	10.8 %	15.2 %	4.1 %	0.71	1.79
8	52.1 %	15.8 %	10.9 %	14.8 %	4.2 %	0.71	1.74

* KB2 = $(MgO+CaO)/(Al_2O_3+SiO_2)$, R = $(MgO+CaO)/Al_2O_3$

Table 6-12: Slag analyses calculated based on the metal analyses of the Corus coke 15-20 mm experiment.

Tap	MnO [wt. %]	SiO_2 [wt. %]	Al_2O_3 [wt. %]	CaO [wt. %]	MgO [wt. %]	KB2*	R*
1	61.9 %	13.0 %	8.3 %	11.9 %	3.2 %	0.71	1.83
2	61.8 %	13.3 %	8.2 %	11.8 %	3.2 %	0.70	1.82
3	58.8 %	13.4 %	9.1 %	13.1 %	3.6 %	0.74	1.83
4	56.2 %	14.9 %	9.5 %	13.7 %	3.7 %	0.71	1.83
5	54.8 %	15.1 %	9.9 %	14.2 %	3.9 %	0.72	1.83
6	51.9 %	15.4 %	10.8 %	15.5 %	4.2 %	0.75	1.83
7	47.3 %	16.0 %	12.1 %	17.4 %	4.7 %	0.79	1.83
8	46.7 %	16.1 %	12.3 %	17.7 %	4.8 %	0.79	1.83

* KB2 = $(MgO+CaO)/(Al_2O_3+SiO_2)$, R = $(MgO+CaO)/Al_2O_3$

Furnace resistance during operation

The furnace resistance during operation is shown in Figure 6-3 and Figure 6-4. The initial stages of both experiments are very unstable due to the electrode tip position being increased at this stage. As the electrode height is increased, the furnace resistance increases. This effect is more significant in the 15-20 mm Corus coke experiment due to a more rapid increase in the electrode tip position. For both experiments, the furnace resistance stabilizes over time. It can also be seen that the furnace resistance increases as the furnace is tapped. Similar observations were also made for the SiMn experiment.

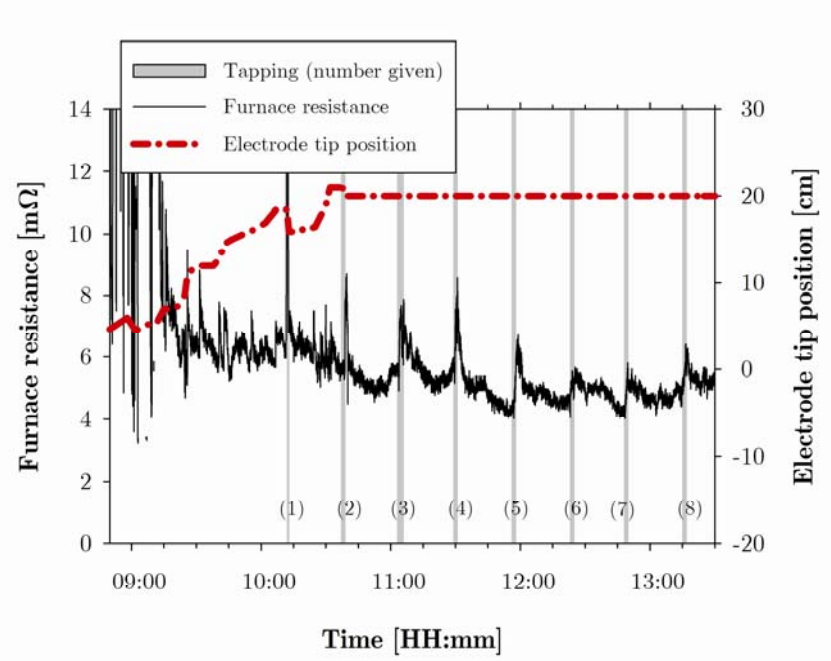

Figure 6-3: Furnace resistance and electrode tip position of the Corus coke 5-10 mm experiment where FeMn was produced. Taps are indicated in gray.

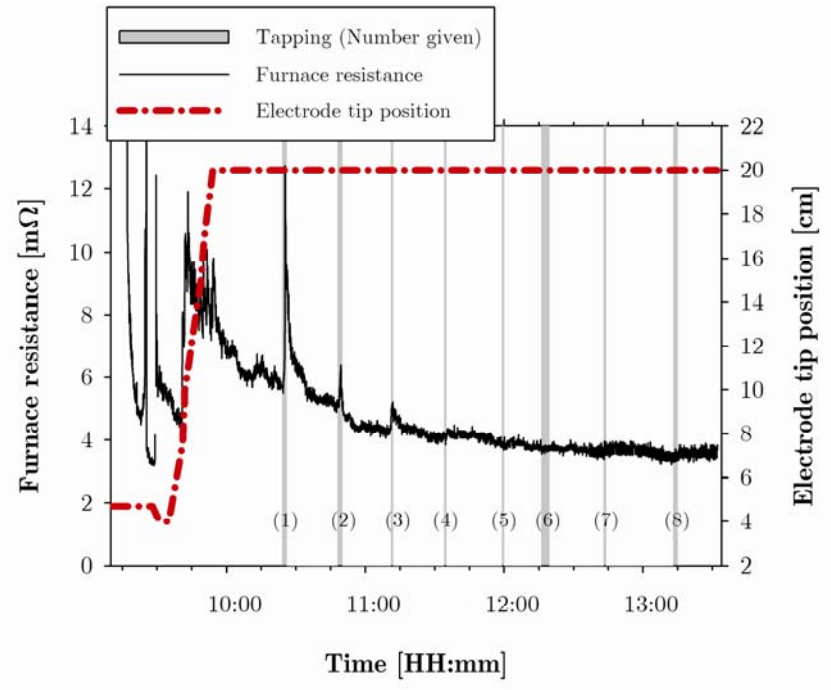

Figure 6-4: Furnace resistance and electrode tip position of the Corus coke 15-20 mm experiment where FeMn was produced. Taps are indicated in gray.

In both of the experiments the furnace resistance decreases from the first to the last experiment, see Figure 6-3. The furnace resistance of the 15-20 mm Corus coke experiment is lower compared to the furnace resistance observed for the 5-10 mm Corus coke experiment. The higher furnace resistance may be due to the increased coke particle size used. It may also be due to a buildup of the coke bed. For the three first tappings of the 15-20 mm Corus coke experiment and throughout the Corus coke 5-10 mm experiment, the furnace resistance increases for a short period of time as the furnace is tapped.

Furnace cross sections; coke bed geometry

The coke bed shape and size is, as mentioned, determined by outlining the lowest ore and sinter particles, see Figure 6-5 and Figure 6-7. Based on these pictures a simplified geometry of the coke bed was determined for each case, as shown in Figure 6-6 and Figure 6-8.

In all the experiments, the electrode had a diameter of approximately 153 mm prior to the experiments. In the SiMn experiment the electrode shape after the experiment was pointed, see Figure 6-10. In the two FeMn experiments

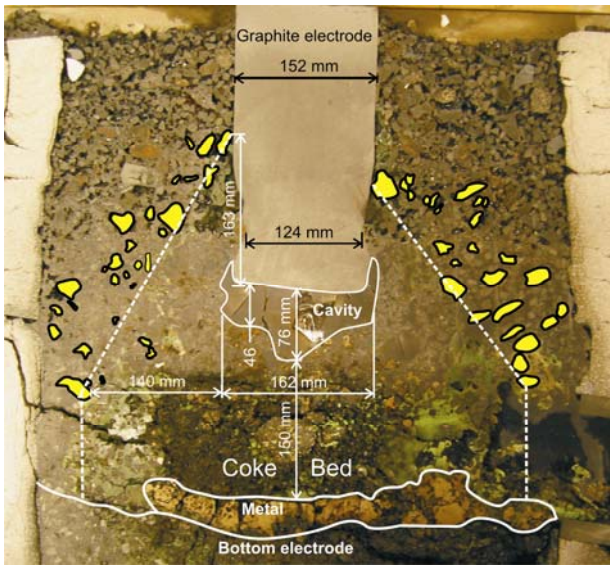

Figure 6-5: Furnace cross section of the 5-10 mm Corus coke experiment. The lower solid Mn-containing particles outlining the coke bed have been outlined.

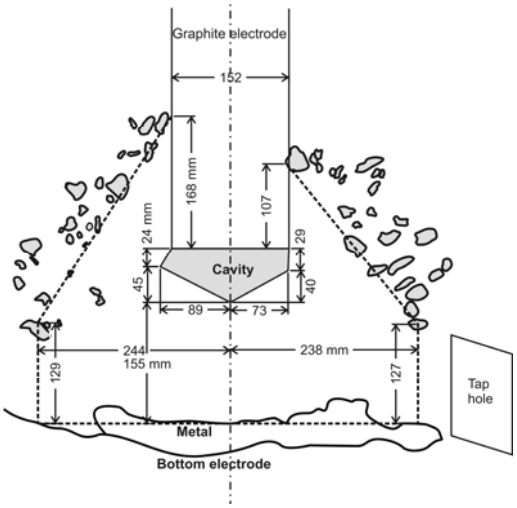

Figure 6-6: Furnace model used for determining the coke bed resistivity of the Corus coke 5-10 mm experiment.

presented in this section a neck has developed on the bottom part of the electrode, see Figure 6-5 and Figure 6-7.

The cross sections of both the FeMn experiments show an asymmetric coke bed. For both the experiments the coke bed height is lower on the tap hole side, the right side for the Corus coke 5-10 mm experiment and the left side for the Corus coke 15-20 mm experiment. Observations during the experiment indicate that the vertical velocity of the raw materials has higher on the tap hole side compared to the non-tap hole side, in the following called the *opposite side*.

Estimation of the coke bed resistivity

After the experiments, the furnaces were, as previously described, cast in epoxy, cut in half and polished. The coke bed geometry was then determined by outlining the ore and sinter particles. Together with the voltage and current logged prior to shutting down the furnace, the coke bed resistivity was estimated using *Comsol Multiphysics 3.4* modeling software.

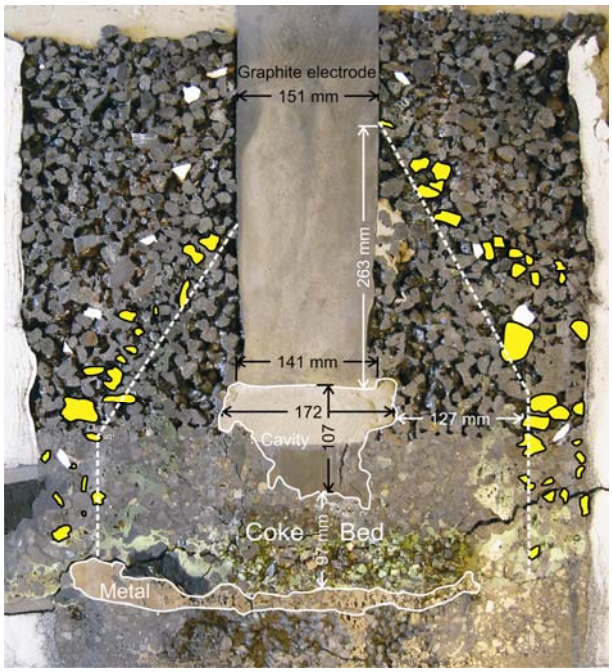

Figure 6-7: Furnace cross section of the Corus coke 15-20 mm experiment. The lower solid Mn-particles outlining the coke bed have been outlined.

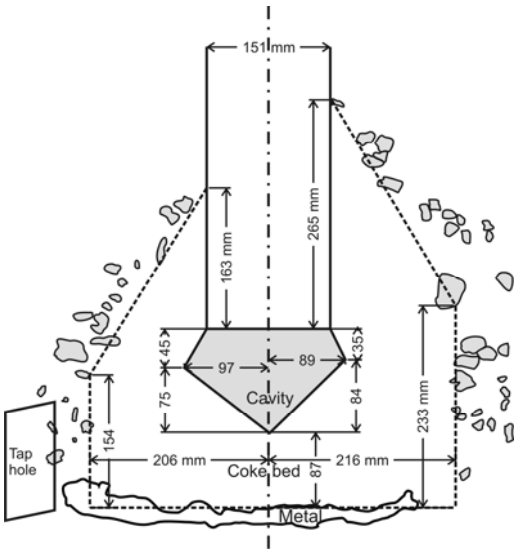

Figure 6-8: Furnace model used for calculating the coke bed resistivity of the Corus coke 15-20 mm experiment.

Table 6-13: The estimated coke bed resistivities of both the experiments have been based on either the tap hole half of the furnace or the opposite half of the furnace. All the calculations have been based on axial symmetry.

Condition	Corus coke 5-10mm	Corus coke 15-20mm
Tap hole side	2.0 mΩm	1.11 mΩm
Opposite side	1.94 mΩm	1.41 mΩm
-10% coke bed radius, tap hole side	1.80 mΩm	0.95 mΩm
+10% coke bed radius, tap hole side	2.2 mΩm	1.26 mΩm
-10% coke bed radius, opposite side	1.71 mΩm	1.21 mΩm
+10% coke bed radius, opposite side	2.2 mΩm	1.62 mΩm
-10% electrode tip position, tap hole side	2.2 mΩm	1.24 mΩm
+10% electrode tip position, tap hole side	1.71 mΩm	0.99 mΩm
-10% electrode tip position, opposite side	2.2 mΩm	1.54 mΩm
+10% electrode tip position, opposite side	1.72 mΩm	1.31 mΩm

The estimated electrical resistivities of the coke bed of the FeMn experiments are shown in Table 6-13. The coke bed resistivity was found to be between 1.71 mΩ·m and 2.2 mΩ·m for the Corus coke 5-10 mm experiment and between 0.95 mΩ·m and 1.62 mΩ·m for the Corus coke 15-20 mm experiment, depending on the coke bed size. From this it seems as though an increased coke particle size gives a lower electrical resistivity of the coke bed, which is also what is found for dry coke beds, see Chapter 5.

The uncertainty of the calculation is assessed through estimating the resistivity of the coke bed both for the tap hole side and the opposite side. In addition single parameters such as the electrode tip position and the width of the coke bed and the cavity shape have been varied to assess the sensitivity due to these factors. The coke bed width and the electrode tip position were found to have the largest influence on the resistivity and the only variables included in the results. The calculations show that, as expected, if the electrode tip position is higher the calculated coke bed resistivity is lower.

Comparing the charge height of the experiments, see Figure 6-5 and Figure 6-7, it is possible to see that the charge height of the Corus coke 5-10 mm experiment is approximately 10 cm lower compared to the charge height of the

Corus coke 15-20 mm experiment. A possible effect of this is that the height of the coke bed is lower. A lower coke bed height will *increase* the *furnace resistance* due to the decreasing volume conducting current, see Equation (2.1). Since the voltage and current of the estimation is given by the measurements made prior to shut down of the pilot furnace, a *decrease* in the height of the coke bed gives a *decrease* in the *coke bed resistivity*. A higher charge will also increase the force on the coke bed, which probably will decrease the coke bed resistivity.

6.2.2 SiMn experiment

Tapped slag and metal and energy consumption

In Table 6-14 the weight of the tapped metal and slag is shown. The slag/metal ratio decreases from the first three taps, 1.43, to the last three taps, 0.57. This is due to the change in charge mix, from FeMn to SiMn.

The average energy consumption of the three first taps, where FeMn is produced, is 4600 kWh/tonne, and for the three last taps, where SiMn is produced, it is 4430 kWh/tonne.

Table 6-14: The weight of the tapped slag and metal, the slag/metal ratio and the energy consumption for the SiMn experiment.

Tap	Metal [kg]	Slag [kg]	Energy consumpt. [kWh/ton]	Slag/metal ratio
1	16	30	4990	1.90
2	22	21	3684	1.00
3	15	21	5427	1.40
4	19	16	4275	0.80
5	17	11	4819	0.60
6	16	11	4947	0.70
7	23	8	3525	0.40

Table 6-15: Analyses of the metal tapped during the SiMn experiment.

	Tap 1 [wt. %]	Tap 2 [wt. %]	Tap 3 [wt. %]	Tap 4 [wt. %]	Tap 5 [wt. %]	Tap 6 [wt. %]	Tap 7 [wt. %]
Mn	68.7	71.6	69	67.6	67.6	66.6	66.7
Fe	24.4	20	18.8	17	15.5	15.2	14.4
Si	1.6	3	8	11.3	13.3	14.6	16.4
P	0.2	0.2	0.2	0.1	0.1	0.1	0.1
Ti	0.1	0.1	0.2	0.2	0.2	0.2	0.2
C	6.6	5.5	3.6	2.6	2.2	2	1.7
Total	101.5	100.4	99.7	98.9	98.9	98.7	99.5

Slag and metal analyses

The analyses of the tapped metal and slag are shown in Table 6-15 and Table 6-16, respectively. It is, however, believed that there is a low accuracy in the slag analyses as done for the FeMn experiments. The metal analyses show that FeMn was produced in the first three tappings and SiMn in the three last, which is according to the raw materials added to the furnace. The slag analyses show an R value that is almost constant between 1.2 and 1.3.

Table 6-16: Analyses of the slag tapped during the SiMn experiment.

	Tap 1	**Tap 2**	**Tap 3**	**Tap 4**	**Tap 5**	**Tap 6**	**Tap 7**
	[wt. %]	**[wt. %]**	**[wt. %]**	**[wt. %]**	**[wt. %]**	**[wt. %]**	**[wt. %]**
MnO	57.6	45.4	44.2	41.2	39.8	45.7	35.6
SiO_2	19.4	28.0	29.4	31.1	32.3	24.8	35.0
CaO	9.7	10.6	10.2	11.8	12.4	10.9	12.5
MgO	2.3	3.1	3.0	3.4	3.6	2.9	3.8
Al_2O_3	11.0	10.8	11.1	12.0	12.0	10.6	14.2
K_2O	0.4	1.0	1.0	1.0	1.0	1.0	1.2
BaO	1.2	1.1	1.1	1.2	1.2	1.1	1.2
Total	101.6	100.0	100.0	101.6	102.3	97.0	103.5
R^*	1.1	1.3	1.2	1.3	1.3	1.3	1.2

*$(CaO+MgO)/Al_2O_3$

Furnace resistance during operation

In Figure 6-9 the furnace resistance and electrode tip position of the SiMn experiment is shown. The duration of the tappings are marked as gray areas with tap number indicated.

The furnace resistance stabilizes over time. This is also the trend previously reported by Røhmen (2002). It may also be seen that there is a slight decrease in resistance over time if the average resistance between tappings one to three (approximately 8-9 mΩ) and five to seven (approximately 7 mΩ) are compared. These tapping represent the FeMn and SiMn parts of the experiment, respectively, but the change in furnace resistance may also be due to a more stable temperature profile in the furnace as seen in the FeMn experiments.

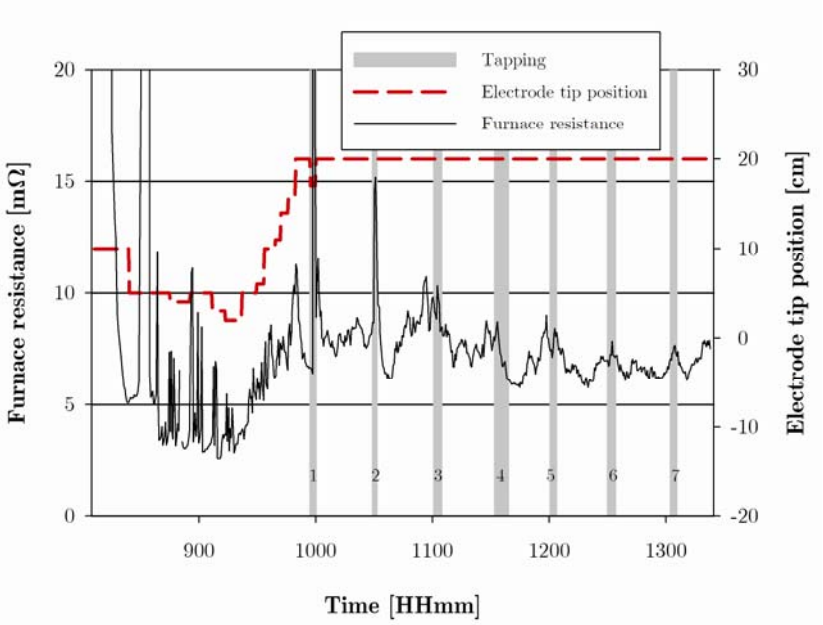

Figure 6-9: Furnace resistance and electrode tip position during the SiMn experiment. The tappings are marked with gray.

The decrease in resistance after each tapping, shown in Figure 6-9, indicates that a dry coke bed has a lower resistivity than a coke bed filled with slag. At most the total resistance dropped more than 20 %. This is also supported by previous investigations (Tangstad 2001; Røhmen 2002). After tappings 2 to 7, the furnace resistance increases as the furnace is being filled with slag, i.e. as time lapses from one tapping to another. As the production, according to plan, changes from FeMn to SiMn, this effect does, however, seem to decrease. This may be due to the lower production of slag and metal, and thus a lower filling of the coke bed. It may also be due to the lower slag/metal ratio in the later taps, as shown in Table 6-14. For FeMn, Røhmen (2002) reports an increase in resistance at the point of tapping, and a decrease in resistance towards the next tapping. The increase in resistance during tapping is explained by cold and thus less conducting material entering the hot zone when slag is tapped out of the furnace. This is, as mentioned, also observed in this experiment, and can be seen in Figure 6-9, especially for tappings 1 and 2.

A slight decrease in resistance seems to happen if the average resistance between tappings 1-3 and tappings 5-7 are compared. If a constant coke bed size

is assumed, the opposite would be the expected, since FeMn slag has a lower resistivity than SiMn slag (Downing and Urban 1966; Røhmen 2002). Still assuming a constant coke bed size, a solution may be that the resistance of the slag has only a small influence on the total resistance of the coke bed. This is supported by the fact that there is a decreasing variation in resistance due to slag being tapped from the furnace as the experiment moves from FeMn to SiMn, and that the resistivity of SiMn slag is approximately 5 times higher than the resistivity of a dry coke bed. SiMn slag has a resistivity of about 25mΩ·m at 1600°C (Downing and Urban 1966; Segers et al. 1983), while the resistivity of a dry coke bed of Corus coke is 5 mΩ·m at the same temperature, see Chapter 5. The estimated resistivity of the coke bed is also very close to the measured resistivity of Corus coke, which is the coke used in this experiment. Simultaneously with the decrease in amount tapped slag, the slag/metal ratio decreases. The electrical resistivity of the slag/metal mix will most likely decrease as result of the increasing amount of metal in the mix, but this has, to the author's knowledge, not been studied. It is, however, not possible to establish the dominating mechanism.

The basis for these speculations has been a constant coke bed size. At the start of the experiment 5 kg of metallurgical coke was placed at the bottom of the empty furnace, and the electrode was lowered on to the coke bed. The initial height was only a couple of cm higher than the initial electrode tip position indicated in Figure 6-9. During the experiment, the electrode was first lowered further into the coke bed. As the furnace was heated and filled with charge, the electrode was heightened to the desired level. Since the coke bed at the end of the experiment is larger than the initial coke bed, the coke bed has increased in size at some point of the experiment. This probably happens as a continuous increase in coke bed size since it is also observed for the FeMn experiments. Assuming that the increase has been continuous through the experiment, the increasing coke bed size will give a higher volume of material with a low electrical resistivity in the coke bed and, as a consequence, the resistivity of the coke bed decreases. This, combined with the lesser filling of slag and the

relatively higher content of metal in the slag/metal mix, gives a decreasing resistivity of the coke bed as the experiment goes from production of FeMn to SiMn.

Furnace cross section; coke bed geometry

After the experiment the furnace was cooled and cast in epoxy. After hardening the furnace was cut and polished. A photo of the cross section is shown in Figure 6-10. Softened particles have been marked in the picture so that the coke bed size could be determined. The softened particle mark the upper part of the coke bed. Based on this a simplified coke bed geometry was made, shown in Figure 6-11.

For the electrical resistivity, the important zones of the furnace are the electrode (labeled II), the furnace lining (IV), the coke bed (III, VI and VII), the metal (VIII) and the bottom electrode (X). The coke bed is divided into three different parts, where area III is an almost dry coke bed, area VI is a mixture of coke, metal and slag, and, finally, area VII is, as area VI, a mixture of coke, slag and metal, but the fraction of metal is higher here.

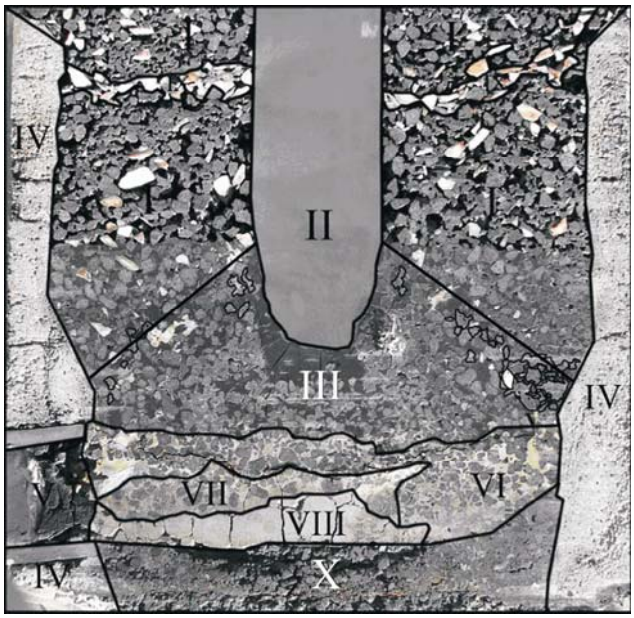

Figure 6-10: Cross section of the furnace from the SiMn experiment.

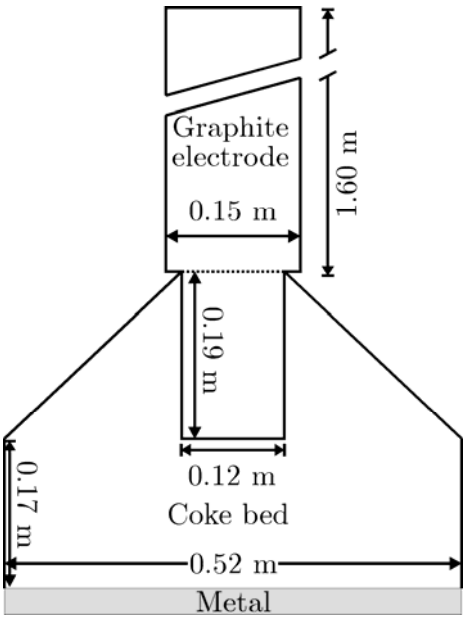

Figure 6-11: Geometry used for determining the coke bed resistivity of the SiMn experiment.

There is also a cavity or void below the electrode tip. The cavity is smaller compared to the cavities found in the FeMn experiments. The cavity is included in one of the calculations. The furnace lining, area IV, is not electrically conductive.

Estimation of the coke bed resistivity

In the model shown in Figure 6-11 the area around the electrode and the electrode is slightly different to the real geometry. Two other geometries will therefore also be tested. One has a 2 cm thick non-conducting cylinder right below the electrode and one has a pointed electrode.

The boundary conditions of all external boundaries, except the top of the electrode and the bottom of the metal, were given as *electric insulation*, i.e. no current flows across the boundary. During the experiment the current and potential drop was measured. To estimate the resistivity of the coke bed, the boundary condition of the top surface of the electrode was defined as *inward current flow* of 248.5 kA/m^2, which is equivalent to the measured total current of 4.511 kA flowing through the electrode. The bottom surface of the metal was defined as ground, i.e. V = 0 V. In Figure 6-12 the electric potential of the cylindrical electrode model used is shown.

The estimated resistivity of the coke bed is 4.0 mΩ·m. When increasing or decreasing the geometrical measurements of the height of the electrode in the coke bed, the height of the coke bed and the coke bed radius with 5 % the

Table 6-17: Estimated coke bed resistivity of the SiMn experiment.

Case	Resistivity [mΩ·m]
1) As defined in Figure 6-11	4.0
2) Geom. -5%	3.9
3) Geom. +5%	4.1
Pointed electrode	3.5
Cylindrical with cavity	3.6

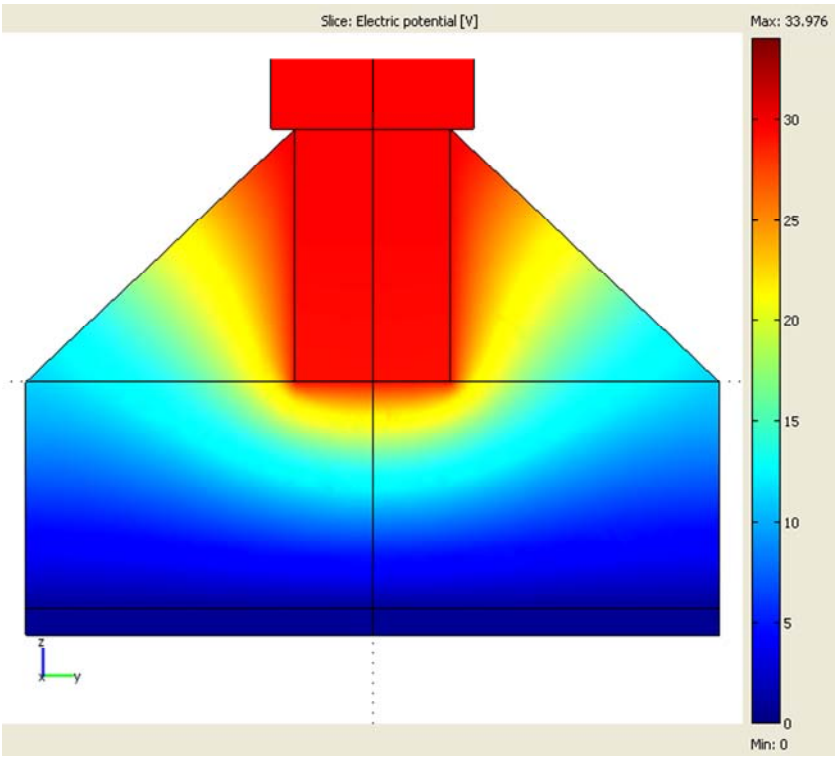

Figure 6-12: Electric potential in the model used for determining the coke bed resistivity of the SiMn experiment.

results, shown in Table 6-17, vary only by about 2.5 % from the original measurements.

In the previous calculation a cylindrical electrode is assumed, see Figure 6-12. If it is assumed that the electrode is pointed, the resistivity *decreases* to 3.5 mΩ·m. This geometrical shape is closer to what is observed in the cross section of the furnace. The cross section also reveals a small cavity below the electrode tip. It is believed that this cavity is *not* present during the experiment, but is due to the charge settling after the experiment. It is still interesting to see the effect of such a cavity and how much it influences the estimated coke resistivity. To test this, a cylinder, height 2 cm and radius equal to the electrode radius, is added below the electrode. The resistivity is then estimated to 3.6 mΩ·m. To sum up, it is believed that the calculated resistivity of the coke bed of the SiMn experiment is between 3.5 mΩ·m and 4.1 mΩ·m.

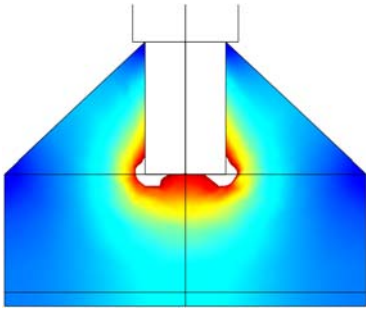

Figure 6-13: Current density plot. The highest current density is at the bottom edges of the electrode.

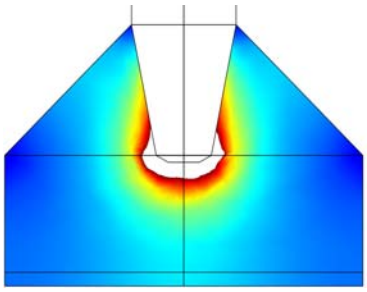

Figure 6-14: Current density when the electrode is pointed.

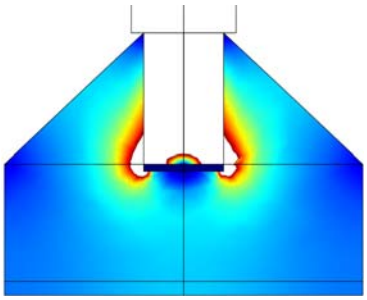

Figure 6-15: Current density when there is a cavity present in the SiMn experiment.

Current density and resistive heating in the coke bed

In Figure 6-13 the current density is plotted. The white areas are areas where the current density is higher than the area included in the scale. The area with the highest current density is around the bottom edge of the electrode. From the plot it seems as though the current density is slightly higher towards the center of the coke bed than at the edges. In Figure 6-14 the electrode is pointed, and the color scale is the same as in Figure 6-13. The current density below the electrode tip as well as the current density higher up in the coke bed has increased.

In Figure 6-15 there is a non conducting cavity right below the electrode tip. There is, naturally, no current flowing through this area. The only way for current flowing through this area would be through an arc. Due to the relatively high conductivity of the coke bed, and the need for the high voltage potential required to sustain an arc of 1 cm length, this is not viewed as a possibility. The area with the highest current density is still at the lower edge of the electrode.

Figure 6-16 shows the resistive heating in the furnace. At the initial state of the experiment, the electrode was cylinder shaped. The model shows that most of the resistive heating occurs where the current density is the highest, around the edges of the electrode. This explains why the electrode after the experiment is pointed, as the consumption of electrode material will be highest in this area.

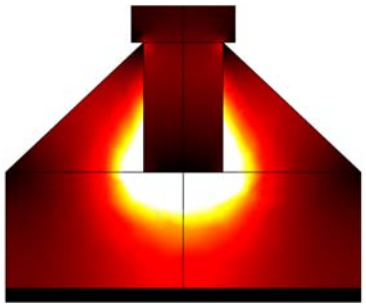

Figure 6-16: Resistive heating in the SiMn experiment when the electrode is cylindrical. (Uniform temperature assumed)

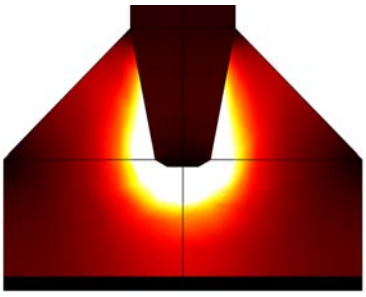

Figure 6-17: Resistive heating when the electrode is pointed in the SiMn experiment. (Uniform temperature assumed)

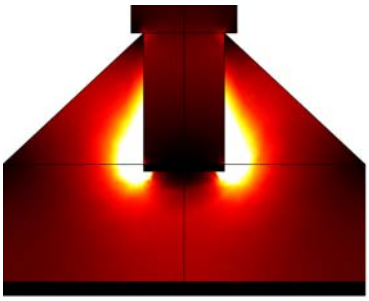

Figure 6-18: Resistive heating in the SiMn experiment when there is a cavity present. (Uniform temperature assumed)

As seen in Figure 6-14, the current density will be higher right below the electrode for a pointed electrode. As can be seen in Figure 6-17, the highest concentration of resistive heating will, as a result of the high current, occur in this area. There is a non-conducting cylinder below the electrode in Figure 6-18, representing the cavity observed under the electrode, as seen in Figure 6-10. The heating is now concentrated around the lower edges of the electrode.

Calculations show that 27 % of the total current flows through the bottom of the electrode when the electrode is cylindrical. This area is only 5 % of the area of the cross section of the coke bed. Figure 6-13 show that the current density is particularly high around the lower edge of the electrode. As a result, the energy dissipation by ohmic heating is highest in this area. Since the model is based on the assumption that the resistivity of the coke bed is constant, the current seeks to spread out in the lower part of the coke bed to minimize the resistance.

If the electrode is pointed, the bottom part of the electrode will represent a larger resistance compared to a cylindrical electrode. The simulations show that a larger part of the current will enter the coke bed higher up on the electrode, and only 17.5 % of the current will exit through the bottom of the electrode.

Figure 6-14 indicates a more concentrated current density around the electrode tip. This also leads to a more concentrated energy development in this area.

When there is a cavity present below the electrode, the current density will be high at the lower edge of the electrode, see Figure 6-15. As a result, the ohmic heating will be highest in this area, see Figure 6-18. As the electrode becomes more pointed throughout the experiment and the cavity decreases with it, the energy development will be more concentrated in the area around the cavity.

6.3 Discussion

6.3.1 Tapped slag and metal

The chemical analyses of the tapped slag for the FeMn are shown in Table 6-9 and Table 6-7, for the Corus coke 5-10mm and 15-20 mm experiments, respectively. The chemical analyses of the tapped slag from the SiMn experiment are presented in Table 6-16. R is the ratio of the main basic and acid oxides in the slag and should be constant if the analyses are correct. R varies between 1.2-1.7 for the Corus coke 5-10 mm experiment and 1.5-1.9 for the Corus coke 15-20 mm experiment, and for the SiMn experiment R is between 1.1 and 1.3. This indicates that the slag analyses are inaccurate.

The metal analyses are about the same for the two FeMn experiments, with a manganese content of 80 wt. %, an iron content between 11 and 14 wt. % and a carbon content of approximately 7 wt. %. The silicon content of the 15-20 mm Corus coke experiment is a little higher compared to the 5-10 mm Corus coke experiment, which may indicate a higher temperature. This can be due to the lower coke bed resistivity of the Corus coke 15-20 mm experiment. A lower coke bed resistivity will give a higher current density in the central parts of the coke bed, thus increasing the temperature. The metal tap analyses of the SiMn experiment show an increasing content of Si as the process is changed from producing FeMn to producing SiMn, reaching 16.4 weight % Si at tap 7, see Table 6-15.

6.3.2 Energy consumption

The energy consumption is calculated based on the measured kWh between each tap and the amount of tapped metal. At the initial stages of the experiments the energy consumption is high due to heating of the furnace. The average energy consumption of taps 4-8 is approximately 4000 and 4300 kWh/tonne tapped metal for the 5-10 mm and the 15-20 mm Corus coke experiments, respectively. The figures are inaccurate due to the high amount of unseparable mix of metal/slag/raw material. For the SiMn experiment, the energy consumption is 4600 kWh/tonne for the first three taps and 4430 kWh/tonne for the three last taps, where FeMn and SiMn was produced, respectively. The furnace lining will not reach a stable temperature within the time frame of the experiment, and will continue to increase for some hours after the experiment. This is, however, not believed to have any significant influence on the experiment, since the metal analyses will tell us if the temperature in the reaction zone has reached the desired temperature or not. By experience it is assumed that the temperature in the coke bed zone stabilizes after two to three hours.

6.3.3 Furnace resistance during operation

The furnace resistance during operation, calculated from the measured current and voltage, stabilizes over time, both for the FeMn and SiMn experiments, see Figure 6-3 and Figure 6-4. The furnace resistance is very unstable at the initial stages of all three experiments. This is due to the electrode tip position being increased at this stage. As the electrode height is increased, the furnace resistance increases. This effect is more significant in the 15-20 mm Corus coke experiment due to a more rapid increase in the electrode tip position. Common for all three experiments is that the furnace resistance stabilizes over time. For the first three tappings of the 15-20 mm Corus coke experiment and throughout the SiMn and the Corus coke 5-10 mm experiments the furnace resistance increases for a short period of time as the furnace is tapped. The effect is more pronounced for the SiMn experiment compared to the Corus coke 5-10 mm FeMn experiment. The increase in furnace resistance was also observed in the

SiMn experiment and has been reported previously (Røhmen 2002) and can be explained by cold material entering the hot zone of the furnace as the furnace is emptied of slag and metal.

In both FeMn experiments and in the SiMn experiment the furnace resistance decreases from the first to the last experiment. The furnace resistance of the Corus coke 15 - 20 mm experiment is lower compared to the furnace resistance of the Corus coke 5 - 10 mm experiment. FeMn is, as mentioned, produced in both experiments. For the Corus coke 5-10 mm experiment the furnace resistance is approximately 5 mΩ after the last tapping, and for the Corus coke 15-20 mm experiment the furnace resistance is approximately 4 mΩ after the last tapping. The difference in furnace resistance between the two FeMn experiments is probably influenced both by the change in particle size, as known from the bulk resistivity of dry coke beds, see Chapter 5, and a buildup of the coke bed, see Figure 6-5 and Figure 6-7. The build-up of the coke bed will increase the amount of coke, which is a rather good electrical conductor compared to other charge components such as ore. This decreases the resistance of the current path, from the top to the bottom electrode. An increased amount of coke will also widen the coke bed, which increases the cross section area and thus decreases the resistance of the current path according to Equation (2.1). In Equation (2.1) ρ_{cb} is the resistivity of the conductor, h_{cb} is the height of the coke bed and A_{cb} is the cross section area of the coke bed perpendicular to the current direction at position h. The geometry of the coke bed has to be established before the *resistivity* of the coke bed, and thus the influence of factors such as the coke particle size, can be assessed, as shown in Equation (2.1).

$$R_{\mathrm{cb}} = \int_0^{h_{\mathrm{cb}}} \frac{\rho_{\mathrm{cb}}(h)}{A_{\mathrm{cb}}(h)} dh \qquad (2.1)$$

The furnace resistance of the SiMn experiment is higher compared to the two FeMn experiments, with a furnace resistance measured as approximately 7 mΩ. The higher furnace resistance seen in the SiMn experiment may be due to the

increased electrical resistivity of the slag. According to Segers et al. (1983) the slag compositions indicate an electrical resistivity of the FeMn slag as 6-7 mΩ·m and of the SiMn as 25 mΩ·m.

6.3.4 Coke bed geometry

A coke bed was found in all three experiments, consisting of a coke and slag mix, with an increasing amount of slag from the electrode tip to the metal bath. No separate slag layer was found.

The cross sections show that in all the experiments a cavity is present under the electrode. This is probably due to a combination of two factors; 1) settling of the charge after the furnace has been turned off and 2) low radial mass flow below the electrode tip. As mentioned, for both the FeMn experiments it is possible to see that there has been erosion on the lower part of the electrode so that a neck has been formed, see Figure 6-5 and Figure 6-7. A cavity has probably been formed as the electrode tip position has been increased. As a result of this the current has been flowing through the sides of the electrode, creating a high temperature region where the neck is situated. As the coke bed has not yet reached the height of this area, the slag and ore has reacted with the graphite electrode. The cavity is, as shown in Figure 6-6 and Figure 6-8, included in the simulations. The pointed tip of the SiMn experiment indicates that the cavity seen in Figure 6-10 has probably not been present throughout the experiment.

For both the FeMn experiments the coke bed height is lower on the tap hole side, the right side for the Corus coke 5-10 mm experiment and the left side for the Corus coke 15-20 mm experiment. The reason for this is that some of the raw materials came out with the slag and metal while tapping the furnace. The vertical velocity of the raw materials has thus been higher on the tap hole side compared to the non-tap hole side. This asymmetry is not seen for the SiMn experiment. This is probably because the amount of raw materials tapped out of the furnace was smaller.

Table 6-18: Overview of estimated coke bed resistivities from the pilot scale experiments. Included are also the electrical resistivity of the slags from the FeMn and SiMn experiments, the bulk resistivity of the Corus coke size fractions and the material resistivity of Corus coke.

	Resistivity [mΩ·m]
Coke bed - pilot, FeMn, Corus 5-10mm	1.71-2.2
Coke bed - pilot, FeMn, Corus 15-20mm	0.95-1.62
Coke bed - pilot, SiMn, Corus 5-20mm	3.5-4.1
Dry coke bed, Corus 5-10mm, 1500°C (Ch. 5)	4.26±0.51
Dry coke bed, Corus 15-20mm 1500°C (Ch. 5)	3.83±0.61
Material resistivity, Corus coke, 1600°C (Ch. 4)	0.127±0.041
FeMn slag - pilot, 1500°C, Segers et al. (1983)	6 - 7
SiMn slag - pilot, 1500°C, Segers et al. (1983)	25

6.3.5 Electrical resistivity of the coke beds

The coke bed resistivity for the FeMn experiments was found to be between 1.71 mΩ·m and 2.2 mΩ·m for the Corus coke 5-10 mm experiment and between 0.95 mΩ·m and 1.62 mΩ·m for the Corus coke 15-20 mm experiment, see Table 6-18. By comparison, the bulk resistivity of Corus coke at 1500°C is measured to 4.26 ± 0.51 mΩ·m and 3.83 ± 0.61 mΩ·m for the 5-10 mm and 15-20 mm fraction, respectively, from Chapter 5. From the estimated coke bed resistivity it seems as though an increased coke particle size gives a lower electrical resistivity of the coke bed. Although this correlation is only based on two experiments, the result that the coke bed resistivity increases with decreasing particle size is supported by investigations of the dry coke bed, i.e. the results presented in Chapter 5.

The coke bed resistivity of the SiMn experiment is calculated to be between 3.5 mΩ·m and 4.1 mΩ·m. This is almost two times higher compared to the coke bed resistivity of the Corus coke 5-10 mm FeMn experiment, and around three times higher than the coke bed resistivity calculated for the Corus coke 15-20 mm experiment, see Table 6-18. However, the coke bed resistivity of the SiMn experiment is approximately the same as the measured *bulk resistivity* of Corus coke. This show that the influence of the slag is also dependent on the

resistivity of the slag, i.e. a decreasing electrical resistivity of the slag decreases the influence of the slag on the coke bed resistivity.

By comparison, Tangstad (2001) estimates the resistivity of the area of the coke bed consisting of mixed slag and coke to be 7.5 mΩ·m for the SiMn process, and Røhmen (2002), who studied FeMn, estimates the resistivity of this area to be between 1.20 mΩ·m and 2.5 mΩ·m. Both divide the coke bed vertically into two parts, the upper consisting of dry coke with a bulk resistivity of 2.5 mΩ·m, and a lower part consisting of mixed slag and coke. The resistivity was calculated in both instances for the lower part of the coke bed. Compared to the coke bed resistivities calculated from the three experiments presented in this thesis, the resistivity calculated by Tangstad (2001) is almost twice that calculated here. The resistivity calculated by Røhmen (2002) is within the upper range of the resistivity for the two FeMn experiments. The reason why Tangstad's estimate is higher compared to the coke bed resistivity calculated in this work may be the assumption of the low resistivity of the dry coke bed. Increasing the assumed resistivity of the dry coke bed would probably decrease the calculated value of the wet coke bed, decreasing the influence of slag resistivity on the resistivity of the coke bed.

If the original slag analyses are assumed to be correct, the electrical resistivity of the slag of taps 6-8 in both the FeMn experiments are between 6 and 7 mΩ·m and the resistivity of the slag of the last tap in the SiMn experiment is approximately 25 mΩ·m according to Segers et al. (1983). The resistivities are at 1500°C. By comparison the *material resistivity* of the Corus coke is approximately 0.127 mΩ·m at 1600°C, see Table 6-18. It is worth noticing that the measurements by Segers et al. (1983) are on synthetic slags, and that the exact composition of the slags from the experiments could not be matched. It is, however, assumed to be a good approximation of the electrical resistivity of the slag.

The effect of slag on the coke bed resistivity is difficult to estimate. For the Corus coke 5-10 mm experiment and the SiMn experiment the slag seems to have an effect on the furnace resistance, since there is an increase in the furnace resistance during tapping. The same is, as previously mentioned, observed in the 15-20 mm Corus coke experiment. However, since tappings does *not* seem to have an effect on the furnace resistance during the last 5 taps of the latter experiment, it may be that the changes seen in the Corus coke 5-10 mm experiment and the SiMn experiment is due to geometrical changes of the coke bed. Before tapping the coke bed there are slag present between the coke particles. Due to the difference in electrical resistivity when the electrical resistivity of slag is compared with the material resistivity of Corus coke, the current will probably "prefer" to flow through the coke particles. However, since the slag fills the voids between the coke particles the current will thus not be forced to flow though the contact points between the particles, which are accountable for the major part of the resistance when two particles are in contact, see Chapter 4. When the coke bed is tapped of slag, there will probably be slag left at the interface between two particles. This layer of slag may uphold the effect the slag has on the contact between two particles; and thus no effect of the tapping is seen in the 15-20 mm Corus coke experiment.

A model has been made in COMSOL Multiphysics 3.4, so that the amount of current flowing through the coke particles in a coke slag mix can be calculated. The simple model consists of four spheres arranged as seen in Figure 6-19.

The radius of the particles is 10 mm, and the centre of the particles are 20 mm apart. As a result, the point of contact is infinitely small. The particles are suspended in a slag bath, and the material resistivity is as measured for Corus coke in Chapter 4, 0.127 mΩ·m. The resistivity of the slag is 25 mΩ·m and 6.5 mΩ·m to represent the electrical resistivity of the slag tapped in the SiMn and FeMn pilot scale experiments, respectively. A current is entering and exiting at the short ends of the slag volume, all other sides of the slag cuboid is electrically

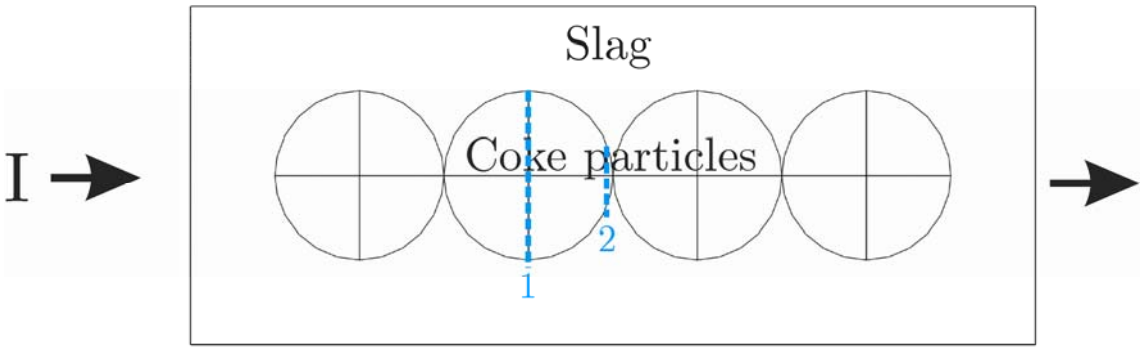

Figure 6-19: COMSOL model illustrating the importance of the coke particles in a slag/coke mix.

insulating. Direct current is used, and the current density is 10 kA/m^2, i.e. within the range used in the bulk resistivity apparatus described in Chapter 5. There is no surface resistance between the slag and the coke.

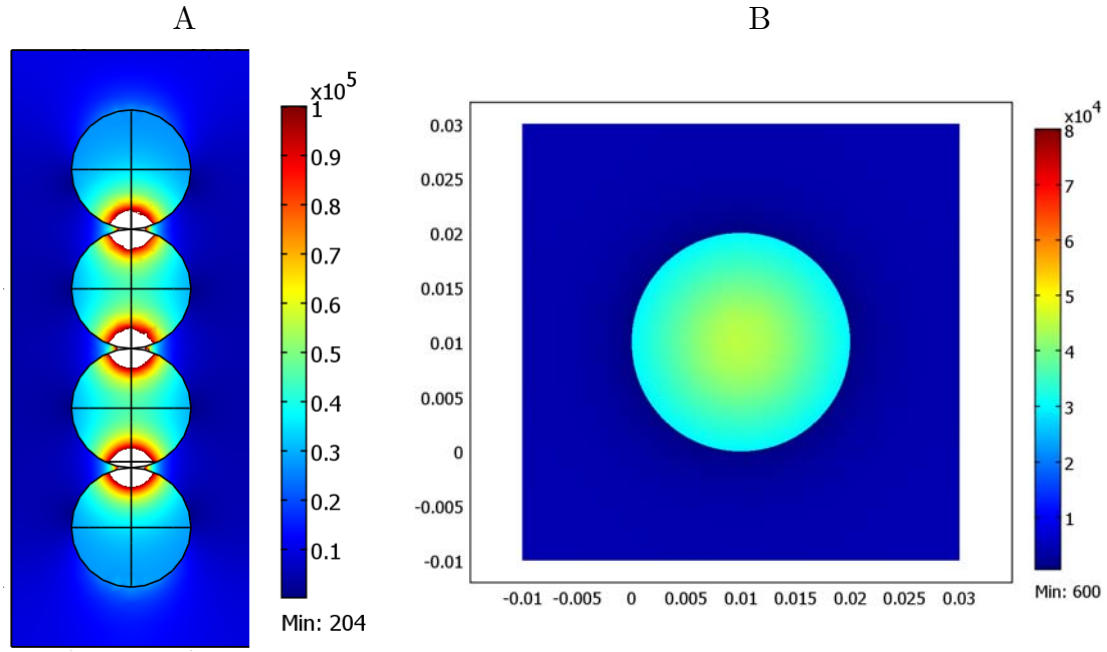

Figure 6-20: Cross section through the center of the particles showing the current density variation when A) the current is flowing from top to bottom, and B) when the current is flowing perpendicular to the page surface. The slag has a resistivity of 6.5 mΩ·m, representing the FeMn slag composition found in the pilot scale experiments. Geometrical dimensions are indicated.

A cross section parallel and perpendicular to the current direction is shown in Figure 6-20 A and B, respectively. The parallel cross section is the same cross section as shown in Figure 6-19, and the cross section perpendicular to the current direction cuts through the coke particle as indicated by the blue line 1 in Figure 6-19.

From Figure 6-20 A it can be seen that the current density is highest where the coke particles meet, even though the spheres are not in contact other than in one point that is infinitely small. The current flows through the slag in this area, from one coke sphere to another. It can also be seen that the current density in the slag is lower compared to that in the coke spheres. This is also seen in the cross section perpendicular to the current direction, see Figure 6-20 B.

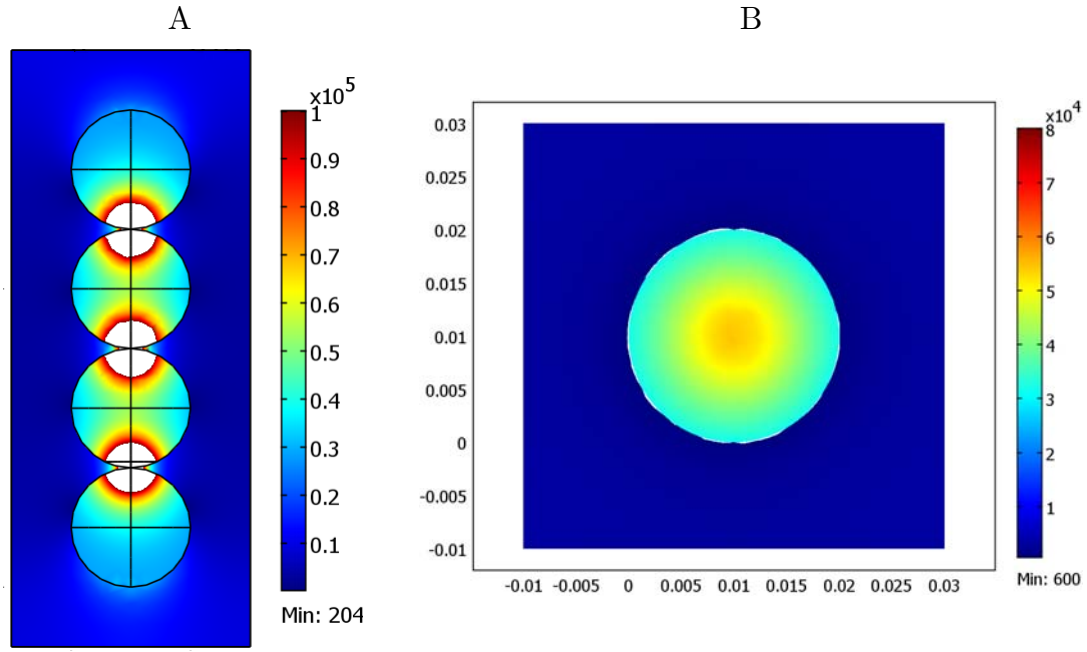

Figure 6-21: Cross section through the center of the particles showing the current density variation when A) the current is flowing from top to bottom, and B) when the current is flowing perpendicular to the page surface. The slag has a resistivity of 25 mΩ·m, representing the SiMn slag composition found in the pilot scale experiments. Geometrical dimensions are indicated.

Figure 6-21 shows the same cross sections as given in Figure 6-20, but the slag now has the electrical resistivity representing that of the SiMn slag tapped in the pilot scale experiments. The color scale is the same in Figure 6-20 and Figure 6-21 so that they may be more easily compared. It can be seen that the current density in the particles are higher when the resistivity of the slag is increased to represent the SiMn slag.

To find the amount of current flowing through the coke particle relative to the slag, an integration is done over the cross section area of the particle at the two levels of the coke particle indicated with broken lines in Figure 6-19. Cross section 1 is though the equator of the coke spheres, and cross section 2 is through the coke spheres 1 mm from the particle surface. The results are shown in Table 6-19. It can be seen that the current prefers to flow through the coke particles due to their low material resistivity compared to that of the slag. It is also seen that as the particle diameter decreases, an increasing amount of current flows through the slag.

Table 6-19: Relative amount of current flowing through the coke particles.

	Integration point	Current [A]	Relative amount
Total current		16.0	100 %
FeMn slag			
	1	11.3	71 %
	2	6.5	41 %
SiMn slag			
	1	12.6	79 %
	2	8.4	53 %

6.3.6 Uncertainties of the calculations

The uncertainty of the calculation of the bulk resistivity of the coke bed is assessed through estimating the resistivity of the coke bed both for the tap hole side and the opposite side. In addition single parameters such as the electrode tip position and the width of the coke bed and the cavity shape have been

varied to assess the sensitivity due to these factors. The coke bed width and the electrode tip position was found to have the largest influence on the resistivity and is thus the only variable included in the results. This is also expected due to the relations described in Equation (2.1):

$$R_{\mathrm{cb}} = \int_0^{h_{\mathrm{cb}}} \frac{\rho_{\mathrm{cb}}(h)}{A_{\mathrm{cb}}(h)}\, dh \tag{2.1}$$

The three estimates of the coke bed resistivity is based on two main assumptions: 1) The resistivity and temperature is the same throughout the coke bed and 2) the skin effect is insignificant, and thus DC is a good estimation of the AC. This will be discussed in the following.

The resistivity of a dry coke bed of the coke used in the FeMn experiments does *not* vary considerably with temperature within the region 1200 to 1600°C, see Chapter 5. There have been some studies on the resistivity dependency on temperature for ferrochromium charges[1], and they have all found that the resistivity of the charge mix is strongly affected in the temperature region 1200 to 1500°C. Willand (1975) concluded that the amount and type of reducing agent has the most pronounced influence on the resistivity of the charge mix. Downing and Urban (1966) and Segers et al. (1983) measured the resistivity of SiMn slag to be approximately 25 mΩ·m at 1600°C, which is approximately two orders of magnitude higher than the *material resistivity* of metallurgical coke, i.e. the resistivity measured on a single coke particle, see Chapter 4. Downing and Urban (1966) do, however, report a strong temperature dependency in the range 1300 to 1600°C. In the coke bed there is only melted ore present, and the high temperature dependency of the charge mixes previously mentioned, will thus not have a great influence on the resistivity of the coke bed. The observed variation in furnace resistance during tappings indicate, as previously discussed, that the slag only has a minor influence on the furnace resistance. From this it

[1] (Willand 1975; Dijs et al. 1979; Dijs and Smith 1980; Krogerus et al. 2006)

may be concluded that the temperature gradients of the coke bed zone, and through this a variation in the coke bed resistivity, has a minor influence on the result of the estimations. Incorporating temperature gradients in the model will thus only change the result to a minor degree, but simultaneously introduce assumptions and uncertainties concerning the thermal properties of the system.

In direct current (DC) systems the current will be evenly distributed throughout the cross section of a homogenous, well conducting conductor, i.e. copper. However, with alternating current (AC) the current density near the surface of the conductor is greater than at the core of the conductor due to the changing electromagnetic fields. The skin depth δ is dependent on the resistivity ρ of the material, the relative permeability of the material, μ_r, and the frequency, f, of the current, see Equation (6.2).

$$\delta = \frac{1}{\sqrt{\pi \mu_0}} \sqrt{\frac{\rho}{\mu_r f}} \tag{6.2}$$

μ_0 is the permeability in free space, equal to $4\pi \cdot 10^{-7}$ H/m. For most materials the relative permeability, i.e. $\mu_{material}/\mu_0$, is equal to unity, but for iron it is usually higher due to its magnetic properties. Here a value of 4000 is used, taken from the material library of COMSOL Mulitiphysics 3.3. For the coke bed and the graphite electrode unity is assumed. The skin depths are then calculated to be approximately 2 - 4 meters for the coke bed, 0.2 meters for the graphite and 2 mm for the iron, see Table 6-20. The radius of both the graphite electrode and the coke bed is below the skin depth, i.e. the current will penetrate the whole cross section. When the current flows through the iron, it will concentrate in the outer edges. This will, however, not have any significant effect on the result.

Table 6-20: Calculated skin depths of the pilot scale furnace.

Material	Skin depth [m]
Coke bed	2.1-4.5
Graphite	$225 \cdot 10^{-3}$
Iron	$2.1 \cdot 10^{-3}$

6.4 Conclusions

Three pilot scale experiments have been done, two where FeMn was produced and one experiment where SiMn was produced. The objective was to see how a change in the coke particle size influenced the coke bed resistivity and to assess the influence of slag on the resistivity of the coke bed. The two FeMn experiments had the same charge composition, but different coke particle sizing. After the experiments, the furnaces were cast in epoxy and cut so that the geometry of the coke bed could be determined. By using the Comsol modeling software the coke bed resistivity could be determined based on the geometry of the coke bed and the electrical parameters obtained prior to shutting down the furnace.

It was found that the coke bed resistivity decreases with increasing particle size, as seen for the bulk resistivity of dry coke beds. The coke bed resistivity of the FeMn experiments where Corus coke 5-10 mm is estimated to be between 1.71 mΩ·m and 2.2 mΩ·m, and the coke bed resistivity of the Corus coke 15-20 mm experiment was estimated to be between 0.95 mΩ·m and 1.62 mΩ·m.

The coke bed resistivity calculated from a coke bed in a SiMn experiment is estimated to be between 3.5 mΩ·m and 4.1 mΩ·m, i.e. twice the resistivity of coke bed estimated for the FeMn experiments and approximately equal to the bulk resistivity of dry Corus coke.

The coke bed resistivity is approximately one third of the electrical resistivity of the tapped slag from the respective experiments. For the FeMn experiments, the coke bed resistivity is approximately half of the bulk resistivity of Corus coke of

the respective particle sizes. The lower coke bed resistivity is probably due to the slag decreasing the particle-to-particle contact resistance.

The difference in coke bed resistivity between the FeMn and SiMn experiments may also be explained by an increasing particle-to-particle contact resistance due to the difference between the electrical resistivity of the FeMn and SiMn slag. As the electrical resistivity of slag increases, the influence of the slag on the coke bed resistivity decreases. The results show that when the electrical resistivity of slag is high enough, the coke bed resistivity approaches the bulk resistivity of a dry coke bed.

Chapter 7 Modeling of the Coke Bed

When producing FeMn in submerged arc furnaces, the operation of the furnace is mostly based on knowledge on how to react when an incident or a certain pattern is observed. During the last quarter of the 20th century the knowledge concerning the structure of the reaction zones, the reactions and the electrical conditions of the submerged arc furnace increased.

Part of this work involved modeling of the submerged arc furnace. However, finding a model that describes the electrical conditions of the coke bed has proved challenging.

A mechanistic model of the coke bed can help us to understand what factors influence and determine the bulk resistivity. However, due to the simplicity of the mechanistic models, the results may not be entirely accurate. With the help of *discrete element method* (DEM) modeling, parameters such as packing of the particles and contact area between the particles can be integrated into the models. Both methods of modeling have been used in this thesis to develop a model that can explain the observed relationship between the particle size and the bulk resistivity.

The DEM modeling included in this works was performed by Z. Y. Zhou and A. B. Yu at Centre for Simulations and Modeling for Particulate Systems, School of Materials Science and Engineering at the University of New South Wales, Australia, as part of a collaboration with NTNU.

7.1 Mechanistic models

Several mechanistic models are proposed in the following. Each try to include possible mechanisms that can cause the bulk resistivity to vary with varying particle size. The purposes of the developments of the models have been to explore the range of possible explanations for the observed correlation between particle size and bulk resistivity.

7.1.1 Model development

A simplified model of a dry coke bed is presented as a possible explanation of the particle size dependency shown in the experiments. In the model a uniform current distribution is assumed over the cross section of the coke bed of the dimensions $A \cdot B \cdot H$, as shown in Figure 7-1 (a). The particles are cubically packed and the particles are, for simplicity, modeled as cylinders, height equal to diameter d, see Figure 7-1 (b). The coke bed may then be viewed as N_p parallel conductors, each consisting of n particles in series, as shown in Figure 7-1 (c). The resulting resistance of each conductor is the sum of the particle-to-particle contact resistance, R_c, and the material resistance, R_m, of one particle. The total bulk resistance, R_{tot}, may then be expressed as shown in Equation (7.1) as the sum of the material dependent resistance, $R_{material}$, and the contact dependent resistance, $R_{contact}$.

$$R_{tot} = R_{material} + R_{contact} \tag{7.1}$$

where

$$R_{material} = \frac{R_m n}{N_p} = \frac{\frac{4\rho_m}{\pi d}\frac{H}{d}}{AB / d^2} = \rho_m \frac{4H}{\pi AB} \tag{7.2}$$

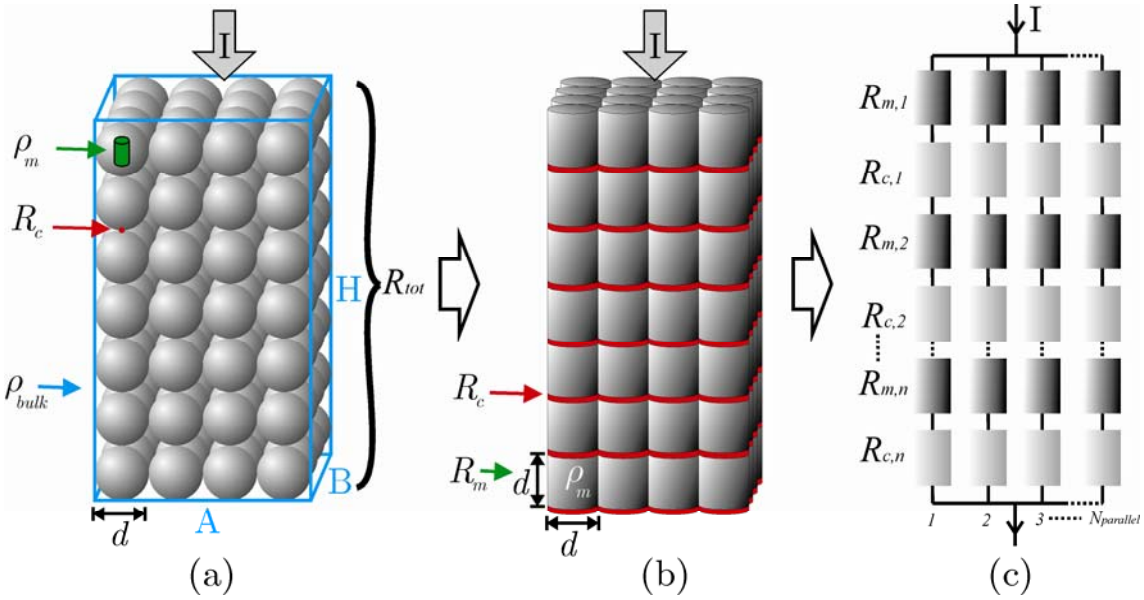

Figure 7-1: (a) Illustration of a cubically packed coke bed with the dimensions indicated and (b) the circuit diagram used in the calculations.

and

$$R_{contact} = \frac{R_c n}{N_p} = \frac{R_c H / d}{AB / d^2} = \frac{R_c H}{AB} d \tag{7.3}$$

The bulk resistivity will vary as

$$\rho_{bulk} = \frac{AB}{H} R_{tot} = \frac{4}{\pi} \rho_m + R_c d \tag{7.4}$$

The variable $R_{material}$ is independent of the particle size and varies as a result of the change in the material resistivity, ρ_m, the geometrical shape of the coke bed and the shape of the particles. The material resistivity may vary due to parameters such as the temperature, microstructure of the material, and chemical composition of the ash. The variable $R_{contact}$ varies as a result of the geometrical shape of the coke bed and the particle size, d. This is the same correlation as observed empirically by Bakken and Wærnes (1986).

The calculation is based on the assumptions that 1) the current is evenly distributed throughout the cross section of the coke bed and 2) the contact resistance, R_c, is constant. The results found in Chapter 5, concerning the particle size dependency of bulk resistivity contradict the results obtained by Bakken and Wærnes (1986). This may be due to the temperature gradients inside the test apparatus used in this thesis. In the apparatus used by Bakken and Wærnes (1986) the heat was supplied by an external heat source and the measurement current was pulsed to prevent heating due to the resistance of the coke.

If the radial temperature gradient in the bulk resistivity apparatus used in this thesis is in the order of several hundred degrees, the resistivity of the carbon material close to the lining is higher compared to the carbon material at the center of the bulk resistivity apparatus. Then the assumption that the current is evenly distributed throughout the cross section of the furnace may not be valid. It is more likely that the current density will be higher in the areas where the temperature is highest, given that the temperature gradient is sufficient to cause a radial difference in the bulk resistivity. Due to a larger current flowing through these areas the temperature will increase, causing the main part of the current to flow through hot channels. This will reduce the number of contact points in the cross section of the coke bed that conducts the current, N_p. This effect may be introduced to the model by reducing the cross section by multiplying $A{\cdot}B$ with a factor, $0 < q \leqslant 1$. As shown in Equation (7.5), this will not change the particle size dependency, but will only increase the resistivity.

$$\rho_{bulk} = \frac{1}{q}\left(\frac{4}{\pi}\rho_m + R_c d\right) \tag{7.5}$$

Another possibility of incorporating a hot channel in the model is keeping the number of contact points in the cross section of the coke bed that conducts the current constant (Wasbø 2006). This is done by keeping N_p, in Equation (7.3), constant. The resistivity will now be strongly dependent on the particle

diameter, as shown in Equation (7.6), but the particle size dependency is now as found in the experiments.

$$\rho_{bulk} = \frac{1}{\mu}\left(\frac{4}{\pi}\frac{1}{d^2}\rho_m + \frac{R_c}{d}\right) \tag{7.6}$$

where $\mu = N_p/(A \cdot B)$ is the number of contact points per unit area. From this it follows that the cross section area of the current path is: $A_{cnducting} = N_p \cdot d^2$. This implies that $A_{cnducting}$ will increase by a factor 36 if the N_p is constant and the particle diameter is increased from 2.5 mm to 15 mm. It is very unlikely that the difference in conducting cross section area will be that large.

The observed correlation between d and R_{tot} may also be explained by the contact pressure between two particles. The theory for contact between metals is, as mentioned in the introduction, well established (Holm 1967). To the author's knowledge, studies of contacts between coke particles have not been published. For metals a general rule is that the current carrying contact spot area is only a fraction of the apparent contact area. The contact resistance decreases with increasing pressure on the contact area. Surface films of non-conducting materials are very damaging for the contact conductance. This is counteracted by a rough surface which increases the pressure in the contact points and potentially cracks the surface film. For a contact between two coke particles the surface is very rough. This will initially give very small contact points. When the pressure is increased sufficiently the protruding contacts will eventually crack, leading to a larger contact area. If a surface film is present at the contact interface, this may break so that a better contact can be established. In the bulk resistivity apparatus the coke bed is subject to an applied pressure. A change in the particle diameter will change the number of contact points in the cross section, $A \cdot B$, and thus the pressure in each particle-to-particle contact point. The force on one contact point, f_c, depends on the number of contact points in the cross section, N_p, and on the mechanical force, F, applied to the top of the coke bed according to Equation (7.7).

$$f_c = \frac{F}{N_p} = F\frac{d^2}{AB} \tag{7.7}$$

The contact resistance, R_c, is proportional to the reciprocal force on one contact point, and therefore the bulk pressure, p_{bulk}.

$$R_c = \frac{C_2}{f_c} = \frac{C_2}{F}\frac{AB}{d^2} = \frac{C_2}{p_{bulk}}\frac{1}{d^2} \tag{7.8}$$

where C_2 is a constant dependent on the physical properties of the material. In addition a constant C is included, giving the contact resistance when the particle diameter is very large.

$$R_c = C + \frac{C_2}{f_c} = C + \frac{C_2}{p_{bulk}}\frac{1}{d^2} \tag{7.9}$$

When combining Equation (7.9) with Equations (7.1) to (7.3) the total bulk resistivity is defined as:

$$\rho_{bulk} = d\left(R_m + R_c\right) = \frac{4}{\pi}\rho_m + \left(\frac{C_2}{p_{bulk}}\frac{1}{d} + C \cdot d\right) \tag{7.10}$$

The correlation between the bulk resistivity and the particle diameter is not clear from Equation (7.10). It can, however, be seen that the material dependent contribution is not affected by the particle size, but on the particle packing, the material resistivity and the shape of the particles. Consequently more voids give a higher bulk resistivity. The contact resistance contribution depends on the diameter, the bulk pressure and the contact resistance between two particles when the contact area is very large. An increasing bulk pressure gives a lower bulk resistivity. The bulk pressure is increased either by increasing force applied on the coke bed or by decreasing cross section area on which it is applied. A change in C_2 may be the result of variation in one or more of several

factors. The two most important factors are 1) the material resistivity at higher temperatures and 2) the hardness of the material. Due to current constriction the small volume of material in the contact points is heated to temperatures higher than the bulk temperature. Consequently, the material resistivity at elevated temperatures is important. The hardness of the material affects the deformation of the contact point when pressure is applied. A softer material will deform more easily than a hard material when pressure is applied. An increase in material resistivity and an increasing hardness of the material will consequently give an increase in C_2.

7.1.2 Model evaluation

To evaluate the models described in the previous section, a set of parameters has to be entered into the models. When the parameters such as the height and cross section area of the coke bed are measurable, these are used. The parameters used in the simulations are reported in Table 7-1. The unknown parameters were calculated based on the measured bulk resistivity of 3.3-6 mm SSAB coke at 1550°C. The average bulk resistivity at this particular diameter is measured as 14.6 mΩ·m, see Chapter 5.

In Figure 7-2 the measured values of SSAB coke at 1550°C are compared to the four models. In the first and the second model, defined by Equations (7.1) to (7.3) and Equation (7.5) respectively, the unknown is the contact resistance R_c. The equations are both on the general form $y = a + b \cdot d$. From Figure 7-2 it is

Table 7-1: Parameter values for the models plotted in Figure 7-2.

Parameter	Value
A, B and H	0.305 m
ρ_m (SSAB coke, 1600°C, Chapter 4)	$151 \cdot 10^{-6}$ Ω·m
R_c (For Equation (7.4) - calculated)	3.09 Ω
N_p (For Equation (7.6) - calculated)	400
R_c (For Equation (7.6) - calculated)	0.250 Ω
C (SSAB coke - div. cyl. 30mm, Chapter 4)	17.5 mΩ
C_2 (Material dependent parameter - calculated)	25.3 mΩ·kg
p_{bulk} (From bulk resistivity apparatus, Chapter 5)	381 kg/m^2

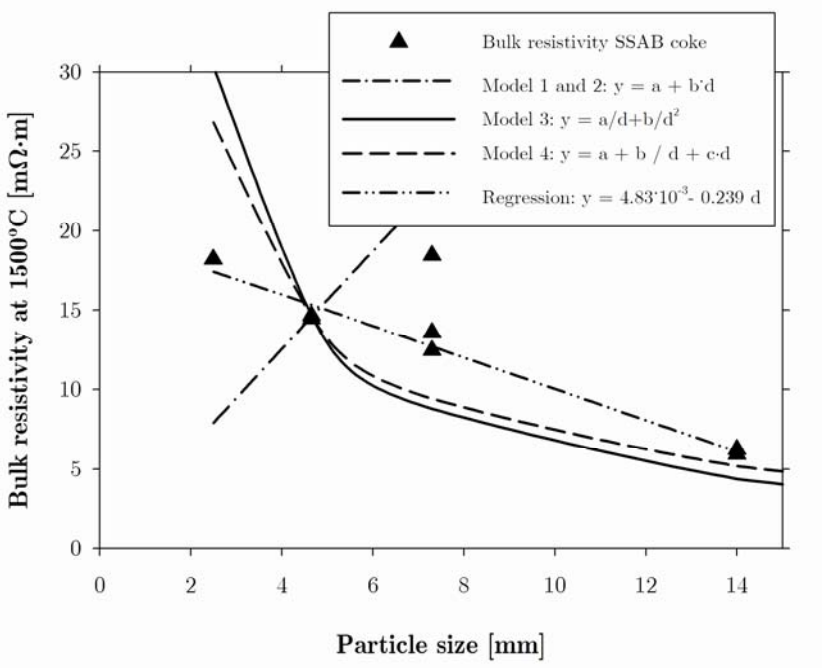

Figure 7-2: Plot of the measured bulk resistivity, the mechanistic models and the linear regression model of the bulk resistivity results of SSAB coke at 1500°C

seen that this does not, as previously commented, give a sensible model. The result is the opposite of the measured values, i.e. an increasing resistivity with increasing particle size.

The third model, expressed by Equation (7.6), has a constant number of particles per unit cross section area. Since the packing is cubically oriented there is only one contact point per particle. The number of contact points, N_p, is restricted by the cross section area. N_p was chosen so that the area of the particles in the cross section does not exceed the dimensions of the coke bed. Based on this a new estimation of R_c is calculated. The general form of the model is $y \quad a/d \quad b/d^2$. The second power reciprocal diameter dependency strongly influences the result, and makes the result very particle size dependent.

It is evident that the slope of the curve does not match that of the measured values, particularly at the lowest particle size. The third model shares the tendency of decreasing resistance with increasing particle size with the measured

values, but the particle size dependency of the model is too strong. The result is that the total resistance at the smallest particle size is far higher than the measured value, and the resistivity at 14 mm particle size is much smaller than the measured value. If the number of particles in the cross section had been higher, the idea of physical meaningfulness of the model would be breached since the area of the particles in the cross section would exceed the cross section of the coke bed. This would, however, give a less declining slope, as opposed to lowering the number of coke particles in the cross section.

In the fourth model, given by Equation (7.10), two parameters were undetermined. A constant, C, that give the contact resistance when the particle diameter is very large, and a material dependent parameter, C_2. The general term representing this equation is $y \quad a \quad b/d \quad c \quad d$. The constant C can be evaluated from the previously presented contact resistance measurements of large contact areas of SSAB coke, see Chapter 4. The contact area between two spherical particles will only be a fraction of this area, and the measured R_c value is used as an estimate of the contact resistance C of a large contact. Figure 7-2 show that this is the best of the four models presented, but not much better than the third model. All the models have parameters that has to be fitted. The calculated R_c values, or particle-to-particle contact resistance values, given in Table 7-1, differ with approximately a factor 10. These values are, however, supposed to represent the particle-to-particle contact resistance, which is comparable to the half spheres in contact, measured in Chapter 4. The measured resistance when two SSAB coke half spheres is in contact is 73 mΩ at 1600°C. The difference is due to the calculated values containing other factors that are not accounted for in the respective models.

Figure 7-2 shows that none of the mechanistic models are sufficient to explain the measured values.

7.2 Modeling using input from the discrete element method

DEM modeling is widely used to simulate complex particulate systems, such as heat transfer in packed beds. In the following the work performed by Z. Y. Zhou and A. B. Yu at Centre for Simulations and Modelling for Particulate Systems, School of Materials Science and Engineering at the University of New South Wales, Australia, as part of this project will be described. By modeling the bulk resistivity apparatus, estimations of non-measurable parameters such as the average particle-to-particle contact can be made. The mechanical strength of the particles and the particle size is varied in the calculations.

7.2.1 Generation of packing structure

The DEM model used here is the soft sphere model originally proposed by Cundall and Strack (Cundall and Strack 1979). The Young's modulus of the particle influences the deformation of the particle, as shown in Figure 7-3. A larger Young's modulus gives a sphere that is not as easily deformed. The packing structures used in the DEM simulations are randomly generated by gravity for the different particle sizes. This is done by random generation of non-overlapping spheres in a defined space. The spheres are then allowed to settle under gravity. For further details, refer to previous work (Xu and Yu 1997; Zhou et al. 1999; Zhu and Yu 2003).

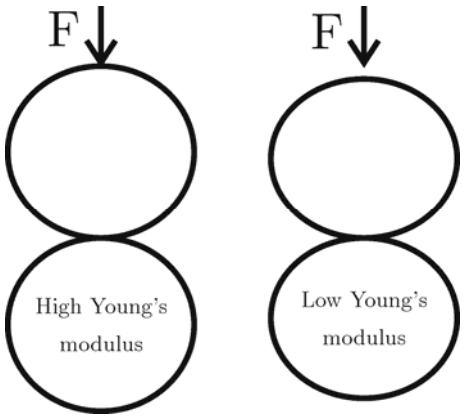

Figure 7-3: A lower Young's modulus gives a higher deformation of the particle and thus a larger particle-to-particle contact area.

Table 7-2: Simulation conditions for DEM simulation of packing of particles in the bulk resistivity apparatus.

Container geometry	
Diameter	300 mm
Height	600 mm
Particle properties	
Bulk density	541 kg/m^3
Particle sizes	7.5 mm, 10 mm, 15 mm and 20 mm
Young's modulus	0.1 GPa, 0.5 GPa and 1.0 GPa

The simulation conditions, shown in Table 7-2, were chosen so that the simulation would represent the conditions found in the bulk resistivity apparatus as closely as possible. The Young's modulus was chosen so that the time to generate the packing structure would not be too long. It was, however, discovered that the chosen Young's modulus were lower than the reported values. The range of Young's modulus measured by Isobe et al. (1981) is between approximately 1 and 15 GPa, and the British Coke Research Association report a Young's modulus of industrial coke of between 4.8 and 10.2 GPa. The packing structures used in the DEM simulations are randomly generated by gravity for the different particle sizes. Mono sized spherical particles were used in the simulation. No load is applied to the packing structure.

7.2.2 Results

The DEM generated packing structures for four different particle sizes are shown in Figure 7-4. The difference in filling of the cylinders is due to the number of particles not being a fixed input parameter, and the height of the bed is determined by the number of particles. The difference in height does not affect the packing structure or the contact area significantly.

In Figure 7-5 the results from the DEM simulation showing the variation in the radius of the average particle-to-particle contact areas with varying particle size is presented. The results show an increasing average particle-to-particle contact radius with increasing particle size. The contact radius is approximately

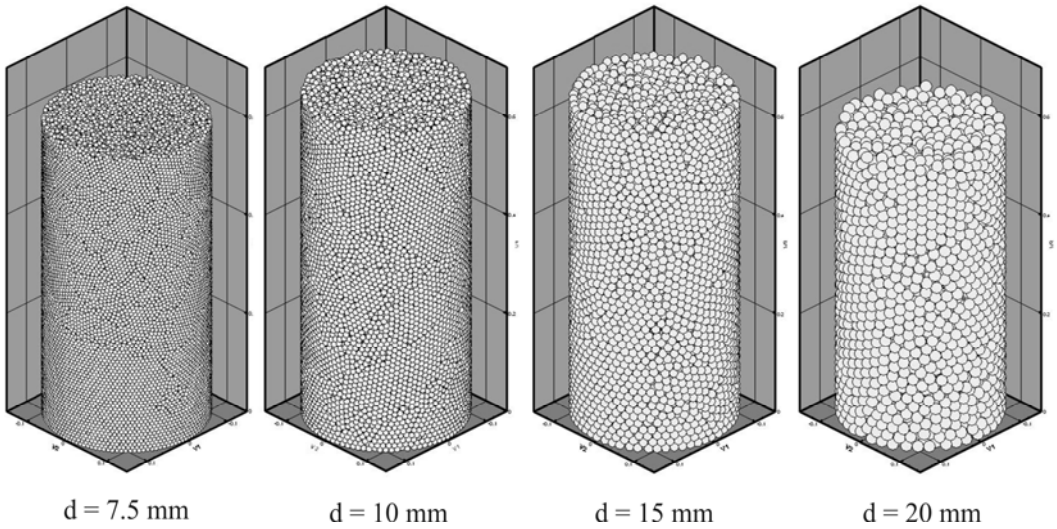

Figure 7-4: Packing structure of the bulk resistivity apparatus, generated by DEM. Figure by Zhou and Yu.

proportional to the particle diameter and not to the diameter squared, as assumed by Dijs et al. (1979). Although the coke particles are different from the soft spheres, the results give an indication of the size of the contact area. The

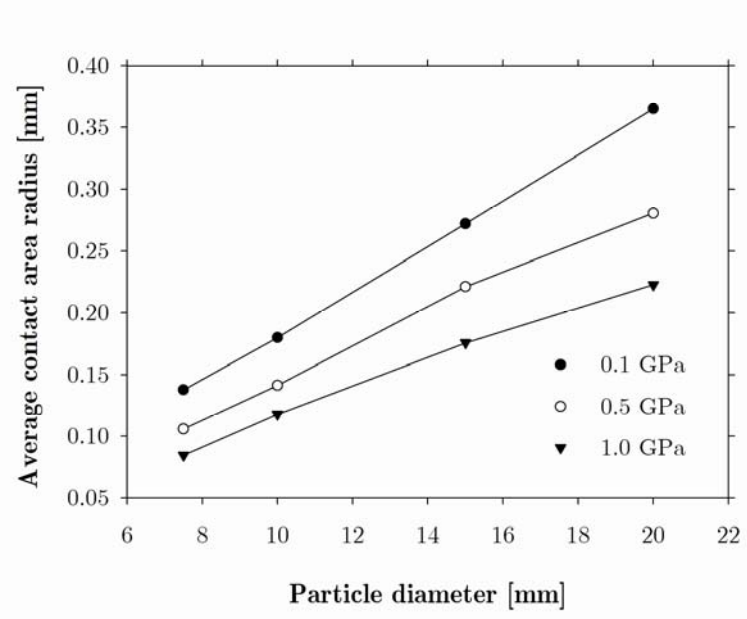

Figure 7-5: Variation of the radius of the average particle-particle contact area with varying particle size. Data by Zhou and Yu.

results show that by increasing the Young's modulus, i.e. hardening the particle, the average contact area decreases. This is expected to be valid also for increasing Young's modulus beyond 15 GPa.

As expected, the apparent contact areas of the sample shapes used in the previously presented contact resistance experiments reported in Chapter 4, are about two orders of magnitude higher than the modeled contact area radius, except for the half spheres contacts. The measured resistance of the half spheres should therefore be of the same order of magnitude as a contact resistance calculated based on the modeled average contact area.

7.2.3 Modified bulk resistivity model

In the first bulk resistivity model presented in section 7.1, Equations (7.1) to (7.3) the contact resistance R_c is assumed *constant* and hence, does *not* vary with particle size. According to the DEM model the contact area does indeed vary with particle size, see Figure 7-5. Due to the soft sphere model being used and the Young's modulus being lower compared to the actual Young's modulus of the metallurgical coke, the particle-to-particle contact area is probably smaller than the calculated area. It is, however, assumed that the principle of the Holm's radius applies, and the contact resistance can be expressed as in Equation (7.11). A combination of Equations (7.3) and (7.11) yield a contact resistance contribution dependent upon the contact area shown in Equation (7.12).

$$R_c = \rho_m \big/ 2\alpha \tag{7.11}$$

$$R_{contact} = \frac{\rho_m}{2\alpha}\frac{H}{AB}d \tag{7.12}$$

where α is the Holm's radius as introduced in Section 2.7.3. Figure 7-6 shows the bulk resistivity, $\rho_{bulk} = R_{tot}\, A \cdot B \big/ H$, as a function of the particle size according to Equations (7.1), (7.2) and (7.12). The average material resistivity ρ_m of SSAB coke at 1600°C, 102 μΩ·m, and the Holm's radius α, calculated from the average contact area found in the DEM modeling, was used in the

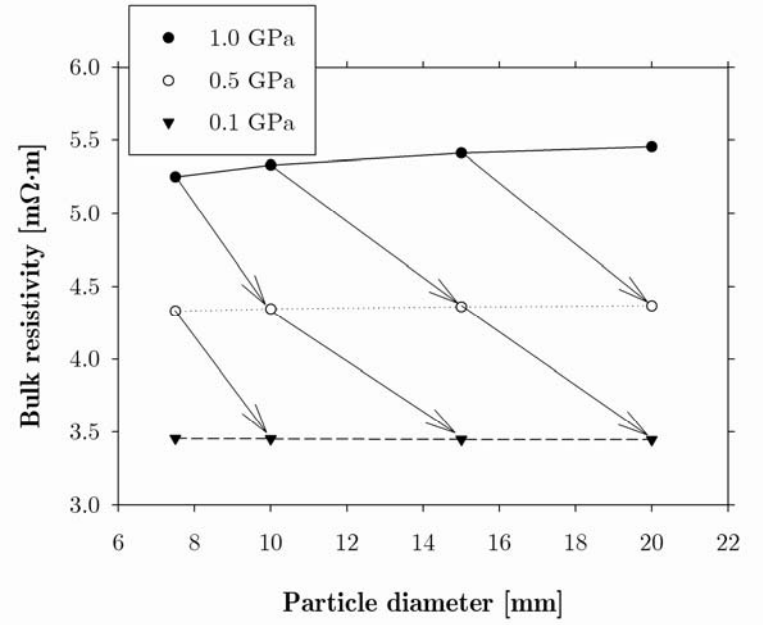

Figure 7-6: Results from modified model where contact area varies with particle size. Material resistivity data for SSAB coke is used in the model. The arrows indicate the effect of decreasing Young's modulus with increasing particle size.

model. Figure 7-6 shows that the bulk resistivity is independent of the particle size if Young's modulus is constant, but that it decreases with increasing particle size if the strength of the particles decreases with increasing particle size.

The results presented in Figure 7-6 show a bulk resistivity between 3.5 mΩ·m and 5.5 mΩ·m. By comparison the measured bulk resistivity of SSAB coke at 1500°C is approximately 6-17 mΩ·m, decreasing with increasing particle size, i.e. higher compared to the data obtained for the model. The bulk resistivity of Corus coke is, however, similar, measured as between 3.8 mΩ·m and 4.3 mΩ·m at 1500°C, for Corus coke 15-20 mm and 5-10 mm, respectively.

7.3 Discussion

It can be seen from Figure 7-2 that none of the mechanistic models are sufficient to explain that the bulk resistivity of SSAB coke decreases with increasing particle size. This may be due to the simplicity of the logical relations used in the models. However, Dijs et al. (1979) suggests a very similar model which give a bulk resistivity that is inversely proportional to the particle diameter. The

difference between the two models is that Dijs et al. (1979) assumes the *contact resistance* to be inversely proportional to the contact area, and that the contact area is proportional to the particle diameter squared, as shown in Equation (7.13). They do not, however, explain why this relationship is assumed.

$$R_c \propto \frac{1}{contact\,area} \propto \frac{1}{d^2} \tag{7.13}$$

From the experiments in Chapter 4 where the contact resistance was determined, it is known that the contact resistance accounts for approximately 80 % of the resistance when two particles are in contact at temperatures up to 1400°C and approximately 50 % at 1600°C. The experiments in Chapter 4 also show that there is *no statistically significant difference* between the measured material resistivity of the metallurgical cokes. Based on this, it is likely that the particle-to-particle contact is important, both as a contributor to the absolute value of the bulk resistivity and also as an explanation to the difference in bulk resistivity between metallurgical cokes. In the last of the purely mechanistic models presented a contact resistance varying with the particle size was introduced, see Equation (7.10). However, it is evident from Figure 7-2 that the trend is far from linear, which is the observed empirical trend for the SSAB coke.

The last approach uses the particle-to-particle contact area of a packed bed of spherical particles in a container similar to that of the bulk resistivity apparatus presented in Chapter 5. The particle-to-particle contact area can not be determined experimentally, as shown in Chapter 4. The calculated bulk resistivity is almost independent of the particle size when the Young's modulus is constant, see Figure 7-6. This is because the contact area radius is close to linearly dependent upon the particle diameter. The number of particles that one single particle is in contact with is not influenced by the particle size, assuming that the particles are monosized and that there is no wall effect. The total number of particle-to-particle contact points in a given cross section will, however, increase with decreasing particle size. As the number of particle-to-

particle contacts in the cross section of the coke bed increase, the mechanical pressure in each contact will decrease. If the strength of the coke, represented by Young's modulus in the DEM model, is assumed to be independent of the particle size, the average contact area should increase with increasing particle size.

Moreover, it has been shown that porosity has a negative influence on the strength of coke (Pitt and Rumsey 1980; Isobe et al. 1981), and both the image analyses and the pychnometry show that the larger particles have a higher total porosity compared to the small particles, see Chapter 3. This implies that the larger particles are mechanically less strong compared to the smaller particles. Both an increased hardness of the particle and a lower force on the electrical contact spot when the particles are smaller give less deforming of the electrical contact spots. As a result the contact resistance is higher for the small particles compared to the larger particles. When this is introduced to the model the bulk resistivity decreases with increasing particle size, as the arrows in Figure 7-6 indicate. The results in Chapter 5 support this theory. For both the SSAB coke and the Corus coke the results indicate that the total porosity of the coke increases with increasing particle size, see Figure 5.12 B.

Compared to the empirical data obtained for the SSAB coke, the calculated values for the *bulk resistivity* are lower and the particle size dependency is not as strong. The results of the calculations are, however, similar to those measured for Corus coke, both in magnitude and in particle size dependency. The measured average bulk resistivity for the Corus coke is 3.71 $\pm$ 0.45 mΩ·m for the 15 - 20 mm fraction and 4.67 $\pm$ 0.30 mΩ·m for the 5 - 10 mm fraction.

The calculated *contact resistance* between two 20 mm SSAB coke particles are 165 mΩ, 211 mΩ and 265 mΩ for the 0.1 GPa, 0.5 GPa and 1.0 GPa Young's modulus cases, respectively. The average measured resistance of two half spheres in contact for SSAB coke is 102 mΩ at 1400°C and 73 mΩ at 1600°C. By comparison, the measured resistance of two half spheres is 83 mΩ at 1400°C

and 52 mΩ at 1600°C for Corus coke. The difference between calculated contact resistance of SSAB coke and the resistance of two half spheres is not only due to the lack of material-specific data on Young's modulus. A decrease in Young's modulus would, as shown in Figure 7-5, increase the contact area and, as a consequence, lower the contact resistance. However, the Young's modulus of the metallurgical coke is, according to the studies done (Pitt and Rumsey 1980; Isobe et al. 1981) higher compared to the values used in the simulations.

Material related factors that may affect the material resistivity such as the chemical composition of the ash and the porosity of the material are included into the model through the measured material resistivity, ρ_m. These measurements do, however, not reveal any significant statistical difference in material resistivity between the Corus coke and the SSAB coke, see Chapter 4. A statistically significant difference has, however, been seen when the contact resistance of the SSAB coke and Zdzieszowice coke has been compared.[1] This indicates that there are material dependent parameters that affect the contact resistance which has not been taken into account since only the *material resistivity* is an input parameter into the model.

Other factors, such as uneven current and temperature distribution in the coke bed, may affect the result. These factors have not been taken into account in the presented model, as the level of complexity would then increase significantly.

As discussed in Chapter 6, where the pilot scale experiments were presented, adding slag will affect the resistivity of a coke bed. The results presented in Chapter 6 indicate that the slag will lower the coke bed resistivity, probably by reducing the contact resistance. The focus of this modeling has, however, been to try to explain the results obtained in the bulk resistivity apparatus. Wasbø (1996) included slag in the models of the coke bed. Within each coke layer the coke is coupled in parallel with the resistance due to the slag and the gas.

[1] There were not sufficient experiments of Corus coke to include Corus coke in the statistical evaluation. See Chapter 4 for further details.

However, by adding a layer consisting of only slag and gas between the layers containing coke, the coke bed resistance increases due to the slag. This is the opposite of what is seen when comparing the measured bulk resistivity of a dry coke bed from Chapter 5 with the estimated coke bed resistivity in Chapter 6.

7.4 Conclusions

It has been shown that using mechanistic models is useful for seeing how various factors influence the bulk resistivity, but that the proposed mechanistic models are insufficient in explaining the linear relationship between the bulk resistivity and the particle size of SSAB coke.

Through the use of DEM modeling, it is shown that the bulk resistivity decreases with increasing particle size, given that the mechanical strength of the particles decrease with increasing particle size. From literature it is known that an increasing porosity decrease the mechanical strength of coke, and measurements presented in Chapter 3 show that the porosity increase with increasing particle size.

The model lacks the ability to predict the difference seen between various types of coke. This may be due to the missing Young's modulus data. However, from Chapter 5, where the bulk resistivity results are presented, it is known that variables such as the crystallite size of the coke have to be included in order to describe the difference between cokes properly. Consequently, the model has to be fitted to data to be able to describe the variation between cokes.

Chapter 8 Conclusions

Dig-outs of industrial furnaces producing FeMn, SiMn and FeCr show that there is a coke bed present around and below the electrode tip. The coke bed is a coke enriched zone consisting of coke, slag, gas and metal. In the coke bed the metallurgical coke is a reducing agent and an electrical conductor. During production, the major portion of the current flows through the coke bed, supplying heat to the reduction process through ohmic heating.

In the last few years the availability of metallurgical coke has decreased, and the price has increased dramatically. As a result of this, the ferroalloy industry started to use a wider selection of carbon materials, and more knowledge was needed. This included knowledge about various properties of the material and the ability to predict the effect a change of raw material will have on the melting process. An important parameter, when it comes to metallurgical coke, has been the electrical characteristics, which has been the main topic of this thesis.

Most of the carbon materials tested were characterized by proximate analyses, ash analyses and XRD analyses. In addition the bulk density and the particle

size range were determined for the materials tested in the bulk resistivity apparatus.

The fundamental *material resistivity* and the *particle-to-particle contact resistance* were studied in an apparatus developed during this thesis work. It was found that *the material resistivity of the three metallurgical cokes tested decrease with increasing temperature, from room temperature to 1600°C.* However, above 1000°C there is only a moderate decrease in the material resistivity. Statistical analyses show that there is no significant difference between the material resistivity of Corus coke, SSAB coke and Zdzieszowice coke. The material resistivity of the metallurgical cokes at 1600°C is approximately 130-150 μΩ·m. By comparison the material resistivity of graphite is measured as 8.6 μΩ·m. The material resistivity of anthracite also decreases up to approximately 1200°C, with little change above this temperature. At 1600°C the measured material resistivity of Preussang Anthracite is 485 μΩ·m.

The contact resistance generally decreases with increasing temperature, from room temperature to 1600°C. This is seen for all the three metallurgical cokes tested here. When comparing the contact resistance to the total resistance when two samples are in contact, the data show that the contact resistance accounts for approximately 70-95 % of the total resistance, but at 1600°C this has decreased to approximately 50 %. This shows that the contact resistance is a major component in determining the bulk resistivity, but that relative contribution of the contact resistance to the total resistance decreases with increasing temperature. This was found for almost all materials and material shapes. A possible explanation is that the increased temperature compensates for the added energy gap that the contacts represent for the electrons. For the metallurgical cokes, there is most likely also a change in the material at the contact intersection. The measured resistance of two half spheres in contact at 1600°C is measured as 52 mΩ for Corus coke, 73 mΩ for SSAB coke and 106 mΩ for Zdzieszowice coke.

The results also show that an increasing contact area gives a decreasing contact resistance. This is probably due to an increasing number of electrical contact spots as the surface area increases.

For the bulk resistivity measurements the same particle sizes as in the ferroalloy industry were used, i.e. 10-30 mm. The measurements of dry coke beds confirm that *the bulk resistivity of carbon materials decreases with increasing temperature from room temperature to 1600°C.* This was seen for the six metallurgical cokes, two charcoals, two anthracites and three petroleum cokes included in the investigation. The bulk resistivity measurements also show that the metallurgical coke generally has a lower resistivity than anthracite, petroleum coke, and charcoal at lower temperatures. Variations in texture and volatile matter can explain the differences, as petroleum and charcoal have a much higher content of volatile matter compared to metallurgical coke. The bulk resistivity of the metallurgical cokes are typically between 4 mΩ·m and 14 mΩ·m at 1500°C. By comparison, the bulk resistivity of the petroleum cokes at the same temperature is between 8 mΩ·m and 20 mΩ·m. The bulk resistivity of Siberian anthracite was measured as 9 mΩ·m at 1450°C, and the bulk resistivity of Vietnamese anthracite as 41 mΩ·m at 1400°C.

In addition, various particle size ranges of two metallurgical cokes and two charcoals were included to study the effect of particle size on bulk resistivity. Within each type of coke the particle size will have a strong effect on the bulk resistivity. For both the Corus coke and the SSAB coke it is seen that *bulk resistivity decreases with increasing particle size.* This is also seen for charcoal. The analyses show that the porosity of the coke increases with increasing particle size, decreasing the mechanical strength of the larger particles. A decreasing mechanical strength leads to crushing of the particle-to-particle contacts which again increase the area of the electrical contacts, decreasing the particle-to-particle contact resistance.

It is seen that for the metallurgical cokes an increasing volatile content, an increasing CO_2 reactivity and a decreasing L_c indicate a higher bulk resistivity. It is also seen that the resistance measured on two half spheres of the Corus, SSAB and Zdzieszowice cokes, i.e. an indicator of the contact resistance, does indeed give an indication of how the bulk resistivity of the metallurgical cokes are in comparison to each other.

Three pilot scale experiments in a 150 kVA single phase furnace were done, two where FeMn was produced and one experiment where SiMn was produced. Different particle size ranges of metallurgical coke were used in the two FeMn experiments. The coke bed geometry was determined based on the cross section of the furnace of the respective experiments. Together with the electrical measurements made seconds before the furnace was turned off, the coke bed resistivity was estimated.

The results show that the coke bed resistivity decreases with increasing particle size, as seen for the dry coke beds, when the results from the two FeMn pilot scale experiments are compared. It is also seen that the estimated *coke bed resistivity* is lower compared to the measured *bulk resistivity*. The coke bed resistivity was estimated to be between 1.71 mΩ·m and 2.2 mΩ·m for the Corus coke 5-10 mm experiment and between 0.95 mΩ·m and 1.62 mΩ·m for the Corus coke 15-20 mm experiment. By comparison, the measured bulk resistivity of a dry coke bed is 4.23 mΩ·m for the Corus coke 5-10 mm and 3.91 mΩ·m for the Corus coke 15-20 mm.

Simulations indicate that due to the significantly lower material resistivity of the metallurgical coke compared to the electrical resistivity of the slag, the current will prefer to flow through the coke particles. However, the slag lowers the particle-to-particle contact resistance, which is a major contributor to the bulk resistivity of a dry coke bed, explaining the lower resistivity of the coke bed containing slag.

The estimated coke bed resistivity of the SiMn experiment is approximately twice that of the FeMn experiments. This can be explained by the increased electrical resistivity of the slag.

Chapter 9 Further Work and Recommendations

The research presented in this thesis, together with the previous work by other authors, represent a foundation for the future work within this field. It is a recommendation that measurement of the bulk resistivity of coke should be part of the standard characterization methods. For the operators of the furnace this would give valuable input to understanding changes in the furnace. Building a knowledge database of the properties of reduction material would also provide a good foundation for further studies of how material properties are influencing the bulk resistivity of coke. Testing materials before buying or using the materials would give information on how changing the coke will influence the furnace operation. A change in bulk resistivity may also be seen between ship loads of coke or even within a shipload.

The industry should continue to do bulk resistivity measurements. This will both give an indication of the effect a new raw material will have on the electrical operations of the furnace, and increase the knowledge of the raw materials in general.

It would also be of interest to develop a bulk resistivity apparatus that could include slag. Such measurements would be even closer to the conditions of the industrial coke bed. However, the results will only be comparable if the slag composition is kept the same. There would be challenges concerning the refractory material due to erosion from slag on the refractory.

In the industrial furnace coke bed there will be slag present. The furnace resistance measurements made during the pilot scale experiments indicate that the slag will affect the coke bed resistivity. It is seen that the coke bed resistivity of the SiMn experiment is higher compared to the coke bed resistivity of the FeMn experiments. In the simulations in Chapter 6, 70 - 80 % of the current flows through the center cross section of the particle, but close to the particle-to-particle contact this is reduced to approximately 40 - 50 %. This indicates that the slag reduces the significance of the particle-to-particle contact resistance in the coke bed. The effect of slag on the particle-to-particle contact resistance can be studied in the already established material resistivity and contact resistance apparatus. The sample shape does, however, have to be changed to contain the slag. This can be done as shown in Figure 9-1.

Another aspect of the particle-to-particle contact resistance which should be studied is the influence of force on the contact resistance. This was not done in this investigation, but from metal contacts it is known that increasing the force on a contact will decrease the contact resistance. Increasing the force applied on the divided samples used in Chapter 4 could reveal if the same correlation is seen for metallurgical coke. If so, this may indicate that there is a crushing of the asperities on the contact interface, as speculated in Chapter 4 and Chapter 7. The influence of mechanical forces could be studied by modifying the present apparatus so that the force on the top electrode would be pneumatically controlled.

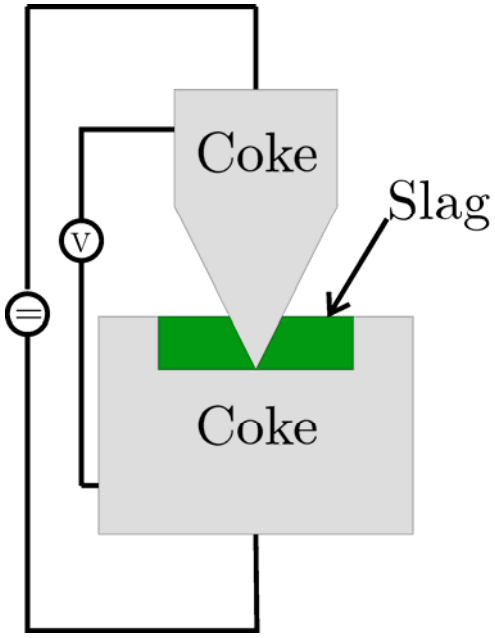

Figure 9-1: By modifying the sample shape the influence of slag on the contact resistance can be studied.

Related to the effect of force on the particle-to-particle contact resistance is the mechanical strength of the coke. The mechanical strength of coke can be tested either by making a test sample out of single particles or by testing the material as bulk.

Finally, further work should also be done on the development of a model describing the electrical relation in the coke bed. Two types of models are interesting, one being a mechanistic model that is intuitive enough, so that the effect of the variables on the bulk resistivity is relatively easy to grasp. The other model should be a model such as the discrete element method (DEM) model used by Zhou and Yu to calculate the contact area presented in this work. This type of model is used to describe heat transfer in blast furnaces, and the models are adapted to calculate the resistivity of both a dry coke bed and a coke bed with slag.

References

Adams, H. A., *Delayed Coking: Practice and Theory* in *Introduction to Carbon Technologies*, ed. Marsh, H., E. A. Heintz and F. Rodríguez-Reinoso. Alicante, Spain, University of Alicante, pp. 491-517, 1997.

Álvarez, R. and M.-A. D. Díaz-Estébanez, *Chemistry of Production of Metallurgical Coke* in *Sciences of Carbon Materials*, ed. Marsh, H. and F. Rodríguez-Reinoso. Alicante, Spain, University of Alicante, pp. 595-635, 2000.

American Iron and Steel Institute, L. C., Retrieved from http://www.steel.org/learning/howmade/coke_production.htm, 11. November 2005.

Ando, R., K. Yamagishi, T. Fukushima and K. Kawasaki, *A Study on the Silicomanganese Process*. 32nd Electric Furnace Conference, Pittsburg, USA, pp. 107-118, 1974.

Askeland, D. R., *The Science and Engineering of Materials*. Cheltenham, UK, Stanley Thornes (Publishers) Ltd, 1998.

ASTM, Standard Test Methods for Proximate Anlysis of the Analysis Sample of Coal and Coke by Instrumental Procedures, *D 5142 - 04*, 2004.

ASTM, Standard Test Method for Determination of Crystallite Size (L_c) of Calcined Peteroleum Coke by X-Ray Diffraction, *D 5187 - 91*, 2007a.

ASTM, Standard Test Method for Electrical Resistivity of Anode and Cathode Carbon Material at Room Temperature, *D 6120 - 97*, 2007b.

Bakken, J. A. and A. N. Wærnes, *Segregering i Råjerncharge, Delrapport 3: Elektrisk ledningsevne, Rapport for Norsk Jernverk A/S*, Report no.: 340942/JAB/tk STF34 A80036, SINTEF, Trondheim, Norway, 28.04.1980, 1980.

Bakken, J. A. and A. N. Wærnes, *Elektrisk ledningsevne i chargematerialer*, Report no.: 341173.10/ANW/11b, SINTEF, Trondheim, Norway, 19.03.1986, 1986.

Barcza, N. A., A. Koursaris, J. B. See and W. A. Gericke, *The 'Dig Out' of a 75 MV.A High-Carbon Ferromanganese Electric Smelting Furnace*. 37th Electric Furnace Conference, Detroit, USA, AIME, pp. 19-33, 1979.

Bourrat, X., *Structure in Carbons and Carbon Artifacts* in *Sciences of Carbon Materials*, ed. Marsh, H. and F. Rodríguez-Reinoso. Alicante, Spain, Universidad de Alicante, pp. 1-97, 2000.

Box, G. E. P., J. S. Hunter and W. G. Hunter, *Statistics for Experimenters*. New Jersey, USA, John Wiley & Sons, Inc., 2005.

Cundall, P. A. and O. D. L. Strack, *Discrete Numerical-Model for Granular Assemblies* Geotechnique 29(1), pp. 47-65, 1979.

Dhainaut, M., *Simulation of the electric field in a coke-bed*, Report no.: STF24 F03506, SINTEF, Trondheim, Norway, 17.01.2003, 2002.

Dhainaut, M., *Simulation of the electric field in a submerged arc furnace*. Tenth International Ferroalloy Congress; INFACON X, Cape Town, South Africa, pp. 605-613, 2004.

Dijs, H. M., *A laboratory investigation of reducing agents for use in the electric furnace industry*, Report no.: 1977, National Institute of Metallurgy, Randburg, South Africa, 20th of March, 1979.

Dijs, H. M. and D. J. Smith, *Factors affecting the resistivity and reactivity of carbonaceous reducing agents for the electric-smelting industry* J S Afr Inst Min Metall, pp. 286-296, 1980.

Dijs, H. M., J. F. Taylor, A. F. S. Schoukens, J. L. Farrel, R. G. Fagan and V. Newey, *A Laboratory Investigation of Reducing Agents for Use in the Electric-Smelting Industry*, Report no.: 1997, National Institute for

Metallurgy, Process development division, Randburg, South Aftrica, 20.03.1979, 1979.

DIN 51911, *Prüfung von Kohlenstoffmaterialen, Bestimmung des spezifischen Widerstandes nach dem Strom-Spannungsverfahren*, 1984.

Downing, J. H. and L. Urban, *Electrical Conduction in Submerged Arc Furnaces* JOM, pp. 337-342, 1966.

Eidem, P. A., *Determination of Specific Resistance of Coke*, Master thesis, Department of Materials Technology, NTNU, Norwegian University of Science and Technology, Trondheim, Norway, 2004a.

Eidem, P. A., *Electrical resistance measurements of charcoal compared to coke*, Report no.: STF80 F04012, SINTEF Materials Technology, Trondheim, Norway, 2004-10-19, 2004b.

Eric, R. H., A. A. Hejja and W. Stange, *Liquidus Temperature and Electrical Conductivities of Synthetic Ferromanganese Slag* Miner Eng 4(12), pp. 1315-1332, 1991.

Gill, W. W. and J. V. Dubrawski, *Silicon carbide in heat-treated cokes* Ironmaking Steelmaking 11(4), pp. 181-185, 1984.

Healy, G. W., *How Ferromanganese Mix Resistivity Affects Manganese Gas, Carbon Balance, and kWh per Metric Ton.* Electric Furnace Conference, pp. 251-258, 1991.

Heaney, M. B., *Electrical conductivity and resistivity* in *Electrical Measurement, Signal Processing and Displays*, ed. Webster, J. G. Boca Raton, FL, CRC Press, 2003.

Holm, R., *Electric Contacts, Theory and Application.* Berlin/Heidelberg/New York, Springer-Verlag, 1967.

ISO 10143, *Methods of sampling and test for Carbonaceous materials used in aluminium manufacture - Part 2: Electrode coke*
Section 2.10 Determination of electrical resistivity of calcined coke granules, 1995.

Isobe, M., K. Suzuki, M. Tate and H. Kitagawa, *Mechanical Behavior of Coke as a Material with Randomly Distributed Pores* ISIJ Int. 21(8), pp. 568-576, 1981.

Iwashita, N., C. R. Park, H. Fujimoto, M. Shiraishi and M. Inagaki, *Specification for a standard procedure of X-ray diffraction measurements on carbon materials* Carbon 42(4), pp. 701-714, 2004.

Kaczorowski, J., *The Boudouard Reaction in Manganese Production*, PhD thesis, Department of Materials Science and Engineering, NTNU, Trondheim, Norway, 2006.

Kawakami, M., H. Kanba, K. Sato, T. Takenaka, S. Gupta, R. Chandratilleke and V. Sahajwalla, *Characterization of thermal annealing effects on the evolution of coke carbon structure using Raman spectroscopy and X-ray diffraction* ISIJ Int. 46(8), pp. 1165-1170, 2006.

Krishnan, K. S. and N. Ganguli, *Large Anisotropy of the Electrical Conductivity of Graphite* Nature 144, pp. 667, 1939.

Krogerus, H., T. Lintumaa and P. Jokinen, *Laboratory Investigations of the Electrical Resistivity of Cokes and Smelting Charge for Optimizing Operation in Large Ferrochrome Furnaces*. Southern African Pyrometallurgy 2006 Intl. Conference, Johannesburg, The South African Institute of Mining and Metallurgy, pp. 309-328, 2006.

Lorenz, V. M. and B. Marincek, *Der elektrische Widerstand der Möllerstoffe im Elektro-Verhüttungsofen* Schweizer Archiv 35, pp. 91-103, 1969.

Madshus, S., *Thermal reactity and structure of carbonized binder pitches / Stian Madshus*, PhD thesis, Department of Material Science and Engineering, NTNU, Trondheim, 2005.

Miyauchi, Y., M. Mochida and Y. Fuchi, *High Thermal Electrical Property of Manganese Ore in Production of High Carbon Ferromanganese.* INFACON 9, pp. 236-243, 2001.

Miyauchi, Y., T. Nishi, K. Saito and Y. Kizu, *Improvement of High-Temperature Electric Characteristics of Manganese Ores.* INFACON X, Cape Town, South Africa, pp. 155-162, 2004.

Monsen, B., *Temperature for producing charcoal*, SINTEF Materials Technology, Trondheim, Norway, Personal communication, 2008

Mrozowski, S., *Electric Resistivity of Polycrystalline Graphite and Carbons* Physical Review 77(6), pp. 838, 1950.

Mrozowski, S., *Semiconductivity and Diamagnetism of Polycrystalline Graphite and Condensed Ring Systems* Physical Review 85(4), pp. 609, 1952.

Oberlin, A., *Carbonization and graphitization* Carbon 22(6), pp. 521-541, 1984.

Olsen, S., *Student Report: Elektrisk ledningsevne i koksmaterialer*, Department of Materials Science and Engineering, NTNU, Trondheim, Norway, 2003.

Olsen, S., *Måling av spesifikk motstand i koksmaterialer*, Master thesis, Department of Materials Science and Engineeringq, NTNU, Trondheim, Norway, 2004.

Olsen, S. and P. A. Eidem, *Specific resistance in coke beds*, Eramet Norway AS, Trondheim, Norway, 2003.

Olsen, S. E., *Ferroalloy Production Theory and Practice*, Institute of Metallurgy, NTH, Trondheim, Norway, 1997.

Olsen, S. E. and M. Tangstad, *Silicomanganese Production - Process Understanding*. Tenth International Congress on Ferroalloys; INFACON X, Cape Town, pp. 231-238, 2004.

Olsen, S. E., M. Tangstad and T. Lindstad, *Production of Manganese Ferroalloys*. Trondheim, Norway, Tapir Academic Press, 2007.

Pitt, G. J. and J. C. V. Rumsey, *Some features of the structure of metallurgical cokes and their effects on strength* J. Phys. D: Appl. Phys. 13, pp. 969-81, 1980.

Rennie, M. S., *The Electrical-Resistance Characteristics of the Charge in the Electrical Reduction Furnace*, Report no.: 1606, National Institute for Metallurgy, Johannesburg, South Africa, October, 1975.

Resource-Net, *Coke Market Survey - Annual Report*, Brussels, Belgium, 2007.

Ringdalen, E., *The High Carbon Ferrochromium Process, Reduction Mechanisms*, PhD thesis, Department of Metallurgy, NTNU, Trondheim, Norway, 1999.

Ringdalen, E., *Observation on level of harmonics*, SINTEF Materials Technology, Trondheim, Norway, Personal communication, 2008

Ringdalen, E. and J. Eilertsen, *Excavation of a 54 MVA HC-ferrochromium furnace*. Ninth International Congress on Ferroalloys; INFACON 9, Quebec City, pp. 166-173, 2001.

Røhmen, C. M., *FeMn Pilot Scale Experiments*, Report no.: 2002/33, Eramet Norway AS, 2002.

Rørvik, S., H. A. Øye and M. Sørlie, *Characterization of porosity in cokes by image analysis*. Warrendale, Pa., USA, Minerals, Metals & Materials Society, pp. 603-609, 2001.

Safarian, J., *Kinetics and Mechanisms of Reduction of MnO-Containing Silicate Slags by Selected Forms of Carbonaceous Materials*, PhD thesis, Department of Materials Science and Engineering, NTNU, Trondheim, Norway, 2007.

Segers, L., A. Fontana and R. Winand, *Electrical Conductivity of Molten Slags of the System SiO_2-Al_2O_3-MnO-CaO-MgO* Can. Metall. Q. 22(4), pp. 429-435, 1983.

Slizovskiy, D., D. Leroy, D. Vaganov and P. Drzystek, *Pilot Scale Experimental Report*, Norwegian University of Science and Technology, NTNU, Department of Materials Science and Engineering, Trondheim, Norway, 2007.

Speight, J. G., *The chemistry and technology of coal / James G. Speight*. New York, Marcel Dekker, 1994.

Sævarsdóttir, G. A., *High current AC arcs in silicon and ferrosilicon furnaces*, PhD thesis, Department of Materials Technology and Electrochemistry, NTNU, Trondheim, Norway, 2002.

Sørlie, M. and H. Gran, *Cathode Collector Bar-to-Carbon Contact Resistance*. Light Metals, San Diego, USA., The Minerals, Metals & Materials Society, pp. 779-787, 1992.

Tangstad, M., *Calcination of Metallurgical Coke*, SINTEF Materials Technology, Trondheim, Norway, May, 1994.

Tangstad, M., *The High Carbon Ferromanganese Process - Coke Bed Relations*, PhD thesis, Department of Metallurgy, The Norwegian Institute of Technology, Trondheim, Norway, 1996.

Tangstad, M., *Cokebed Resistance and Energy Development*, Report no.: 2001/16, Eramet Norway AS, 2001.

The British Coke Research Association, *Studies of Fissure Formation in Coke: The Tensile Strength of Industrial Cokes*, Report no.: 53, Derbyshire, U.K., October, 1969.

Timsit, R. S., *Electrical Contact Resistance: Fundamental Principles* in *Electrical Contacts, Principles and Applications*, ed. Slade, P. G. New York, Marcel Dekker Inc., pp. 1-83, 1999.

Tokai Carbon Europe Ltd., *Tokai's Extruded Graphite Data Sheet, FE,EE250*, 2002.

Tucker, S. A., A. Doty and R. W. Cauchois, *Granular Carbon Resistors* Transactions of the American Electrochemical Society 12, pp. 171-186, 1907.

Ukanakov, P. M., V. G. Mizin and G. V. Serov, *Electrical Resistivity of Different Forms of Carbonaceous Reudcing Agent* Coke & chemistry U.S.S.R. 1, pp. 29-33, 1973.

Urquhart, R. C., P. R. Jochens and D. D. Howat, *The Dissipation of Electrical Power in the Burden of a Submerged Arc Furnace*. Electric Furnace Conference, Cincinnati, USA, pp. 73-78, 1973.

Wallace, P. R., *The Band Theory of Graphite* Physical Review 71(9), pp. 622, 1947.

Wasbø, S. O., *Ferromanganese Furnace Modelling Using Object-Oriented Principles*, Dr. Ing. thesis, Department of Engineering Cybernetics, NTNU, Trondheim, Norway, 1996.

Wasbø, S. O., *Hot channel model*, Personal communication, Eramet Norway AS, Trondheim, Norway, Personal communication, 2006

Willand, K., *Measurement of the Electrical Resistance of Ferrochromium Furnace Charges*, National Institute for Metallurgy, Johannesburg, South Africa, 1975.

Woollacott, L. C., D. D. Howat and P. R. Jochens, *The Viscosities and Electrical Conductivities of Slags Associated with the Production of High-carbon Ferromanganese Alloys*. INFACON 74, Johannesburg, South Africa, pp. 227-232, 1975.

Xu, B. H. and A. B. Yu, *Numerical simulation of the gas-solid flow in a fluidized bed by combining discrete particle method with computational fluid dynamics* Chem. Eng. Sci. 52(16), pp. 2785-2809, 1997.

Yoneka, S., K. Harada, K. Kojima and K. Nakagawa, *Consideration of electric furnace dimension & dynamic operation based on research* Journal francais de l'électrothermie(1), pp. 29-34, 1981.

Zhou, Y. C., B. D. Wright, R. Y. Yang, B. H. Xu and A. B. Yu, *Rolling friction in the dynamic simulation of sandpile formation* Physica A 269, pp. 536-553, 1999.

Zhu, H. P. and A. B. Yu, *The effects of wall and rolling resistance on the couple stress of granular materials in vertical flow* Physica A 325, pp. 347-360, 2003.

Zumdahl, S. S., *Chemical Principles*. Boston, MA, USA, Houghton Mifflin Company, 1998.

Appendix 1: Sample Shapes for Determination of Material Resistivity

When determining the material resistivity it is beneficial to be able to use as many experiments as possible. In the following it will be shown that the double cone sample shapes in Chapter 4 could not be included in the material resistivity measurements.

The sample resistance R_{sample}, calculated from the measured current in the measurement circuit and the voltage drop is given by Equation (4.1). In Equation (4.1), which is Equation (2.1) rewritten, the material resistivity ρ_m is unknown, but assumed to be constant. The unknown material resistivity is calculated by putting in the expression describing cross section area of the sample A_{sample} at any height h of the sample, and solving for ρ_m. It is given from Equation (4.1) that the material resistivity is *independent* of the shape of the sample. The resistance of an arbitrary shaped particle can thus be expressed as:

$$R_{sample} = \int_0^{h_{sample}} \frac{\rho_m}{A_{sample}(h)} dh \tag{4.1}$$

where h_{sample} is the height between the two Mo-wires wrapped around the sample for measuring the potential drop.

In Figure A1-1 the material resistivity is given for the graphite double cones as well as the graphite ϕ30 mm cylinder. The material resistivity is calculated according to Equation (4.1). It can be seen that the material resistivity decreases with increasing neck diameter, i.e. indicating that the ϕ30 mm cylinder has a lower material resistivity compared to the ϕ30/5 mm double cone. This can also be seen if a linear regression analysis is done for the region 1000°C to 1600°C of the data displayed in Figure A1-1. The variables are the cross section area A_{neck} at the neck of the sample and the temperature rounded to the

nearest 10°C, T^*. The latter is done to get replicates and thus be able to asses the goodness of the fit through a *Lack of fit test*. The regression equation is shown in Equations (A1.1) and (A1.2). The variables in Equation (A1.1) have been standardized[1] so that the impact of the variables on ρ_m can be compared. The table of coefficients and analysis of variance table (ANOVA) is given in Appendix 3.

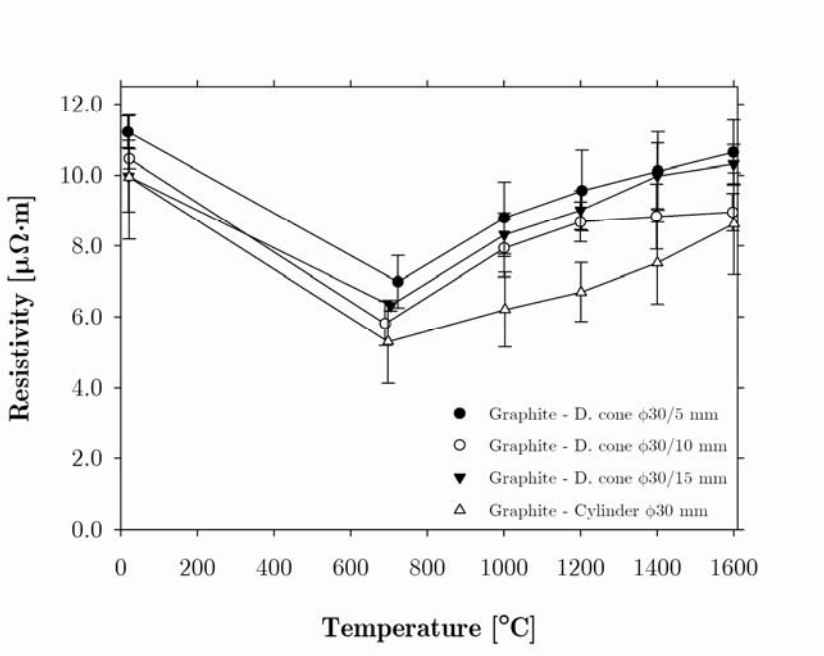

Figure A1-1 Resistivity of the cylinder and double cone shaped samples. The resistivity is calculated from Equation (4.1). There is a clear correlation between neck size and resistivity. The standard deviation is indicated.

The results show that both variables are significant, and that there is no significant lack of fit, i.e. the sample shape *does* indeed influence the material resistivity and the assumption that the potential surfaces are parallel to the end

[1] In this case the standardized variables both vary in the range -1 to 1, representing the whole range of data of the variable. The coefficients will then tell us which variable that has the most impact on the response. It is calculated the following way: $\text{Stand.var.} = \left(\text{Variable} - \textit{Midrange}\right) / \left(0.5 \cdot \textit{Range}\right)$, where *Midrange* is the center of the region, e.g. 1300°C in the region 1000 -1600°C, and *Range* is 600°C for the region 1000-1600°C

surfaces does not hold. From the regression equation (A1.1) it can be seen that the variables have almost equal impact on the resistivity. From Equation (A1.2) it can be seen that an increasing temperature increases material resistivity within the temperature region 1000°C to 1600°C, and that an increasing neck diameter reduces the material resistivity. This is as observed in the graph.

$$\rho_m = 8.38 \cdot 10^{-6} - 1.03 \cdot 10^{-6} \cdot \underbrace{\frac{T^* - 1300}{300}}_{\text{Standardized variable}} - 1.11 \cdot 10^{-6} \cdot \underbrace{\frac{A_{neck} - 356 \cdot 10^{-6}}{344 \cdot 10^{-6}}}_{\text{Standardized variable}} \quad \text{(A1.1)}$$

$$\rho_m = 5.05 \cdot 10^{-6} + 3.44 \cdot 10^{-9} \cdot T^* - 3.22 \cdot 10^{-3} \cdot A_{neck} \quad \text{(A1.2)}$$

In Figure A1-2 the material resistivities of all the whole sample shapes of the SSAB and Zdzieszowice cokes are shown with standard deviations indicated. Due to the large standard deviation of the measurement data, only temperatures above 1000°C are included. The ϕ30 mm cylinder shape gives the lowest average resistivity of the tested sample shapes within each type of coke. The others are more difficult to differentiate between.

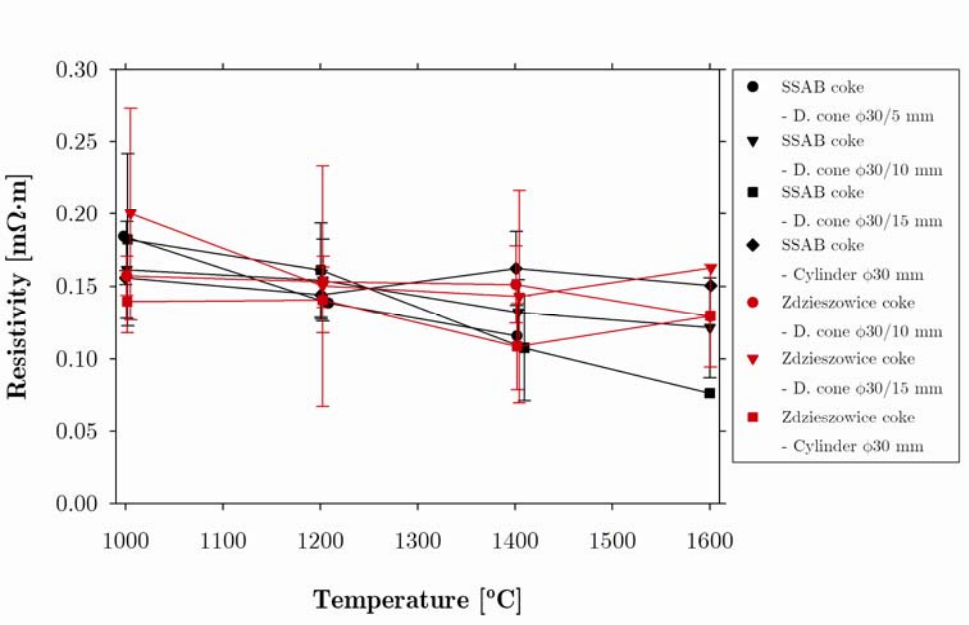

Figure A1-2: Calculated resistivity of all the whole SSAB and Zdzieszowice coke samples, calculated using Equation (4.1).

A linear regression analysis of the data displayed in Figure A1-2, treated as described for the graphite, i.e. with the variables T^* and A_{neck}, was done. A dummy variable[2], *type*, was added that could describe the *type* of material. In the analysis *type* was not a significant, and was thus excluded from the further treatment of the data. In the final regression result is shown in Equations (A1.3) and (A1.4), both the temperature T^* and the cross section area at the sample neck, A_{neck}, are significant. From Equation (A1.3), where the variables have been standardized for the analysis, it can be seen that temperature T^* has a larger impact on the neck cross section area, A_{neck}. This is different from the results obtained for the graphite, where the two variables had almost equal impact on the response, ρ_m. Another difference between the graphite and metallurgical cokes is that and increasing temperature decreases the material resistivity for the metallurgical cokes, whereas for the graphite opposite was seen. For further details on the statistical analysis, see Appendix 3.

$$\rho_m = 138.3 \cdot 10^{-6} - 20.2 \cdot 10^{-6} \cdot \frac{T^* - 1300}{300} - 3.22 \cdot 10^{-3} \cdot \frac{A_{neck} - 360 \cdot 10^{-6}}{340 \cdot 10^{-6}} \quad \text{(A1.3)}$$

$$\rho_m = 237 \cdot 10^{-6} - 67.3 \cdot 10^{-9} \cdot T^* - 30.4 \cdot 10^{-3} \cdot A_{neck} \quad \text{(A1.4)}$$

The plots and the statistical analyses show that when the resistivity was calculated according to Equation (4.1) the calculated resistivity was influenced by the sample shape. However, the material resistivity is *not* influenced by the shape of the sample. The assumption for Equation (4.1) is that the equipotential lines at all times will be parallel to the end surfaces of the sample. However, the results show that when the sample shape deviates from the cylindrical shape, the equipotential lines are not parallel to the end surfaces of the sample. As an illustration the equipotential lines for the ϕ30 mm cylinder and the ϕ30/10 mm double cone has been calculated using Comsol Multiphysics. The results are shown in Figure A1-3, and it is quite clear that the equipotential lines deviate

[2] A dummy variable is a variable does not have a continuous scale, but it typically -1 or 1, representing, in this case, two materials.

from what was assumed for Equation (4.1). Only the cylinder shapes could thus be used for the material resistivity calculations of the graphite. This effect will increase as the ratio between the minimum and maximum diameter decreases. If this is not compensated for, the resistivity calculated from the measured resistance will be higher than the true value, as can be seen in Figure A1-3. In standard material resistivity tests, e.g. DIN 51911 (1984), cylindrical samples are exclusively used to avoid this problem. The equipotential lines are then parallel to the surface throughout the sample, as shown in Figure A1-3 (a).

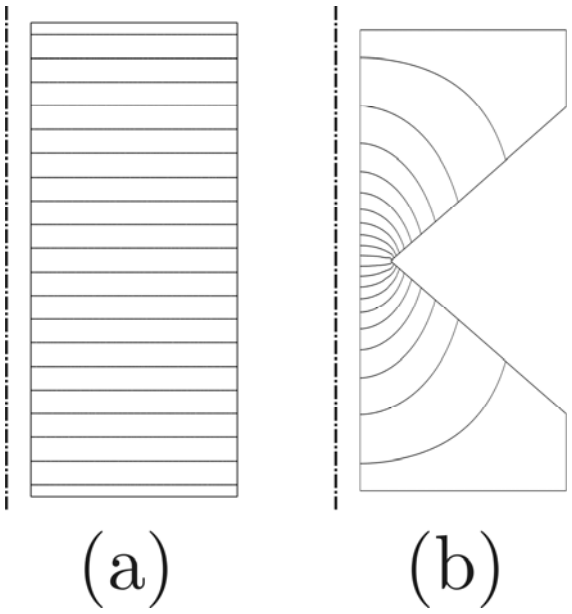

Figure A1-3: Equipotential lines for two sample shapes used in the experiments: Cylinder ϕ30 mm and double cone ϕ30/10 mm. Both samples have a 3 mm hole through the middle of the sample.

Appendix 1

Appendix 2: Calibration Certificates for Thermocouples

The following S-type thermocouples were used in the experiments where material resistivity and contact resistance were measured. Above 1300°C the thermocouples have an accuracy of ± 2°C.

SINTEF

CERTIFICATE OF CALIBRATION

FOR

THERMOMETERS

Certificate number : 231

Manufacturer, model :

Thermometer type : S

Identfication (s.no) : 1

Customer :

The total uncertainty assigned to the measurements is : +/-0.9°C up to 1100°C +/-2.0°C above. (Stated as 2 standard deviations)

Test equipment used in the calibration : Solartron Voltmeter 7061, Isotec Saturn Furnace, Ref TC SINTEF-1

The thermometers have been calibrated using standards whose accuracies are traceable to national and international standards, and the temperatures are determined in accordance to ITS-90.

Calibration temp.	Measured value	Calculated temp.	Deviation
°C	µV	°C	°C
1300.97	13170.18	1300.92	-0.05
1100.86	10765.20	1100.73	-0.13
900.41	8452.24	900.27	-0.14

Additional information : The calibration is carried out by comparison against a laboratory reference thermocouple type S

23. januar 2008 — Date of certification

Svend Grådahl — Certified by

SINTEF

CERTIFICATE OF CALIBRATION
FOR
THERMOMETERS

Certificate number : 232

Manufacturer, model :

Thermometer type : S

Identfication (s.no) : 2

Customer :

The total uncertainty assigned
to the measurements is : +/-0,9°C up to 1100°C +/-2,0°C above. (Stated as 2 standard deviations)

Test equipment used
in the calibration : Solartron Voltmeter 7061, Isotec Saturn Furnace, Ref TC SINTEF-1

The thermometers have been calibrated using standards whose accuracies are traceable to national and international standards, and the temperatures are determined in accordance to ITS-90.

Calibration temp.	Measured value	Calculated temp.	Deviation
°C	µV	°C	°C
1300.97	13175.33	1301.34	0.37
1100.86	10770.68	1101.19	0.33
900.41	8457.10	900.70	0.30

Additional information : The calibration is carried out by comparison
: against a laboratory reference thermocouple type S
:
:

23. januar 2008
Date of certification

Svend Grådahl
Svend Grådahl
Certified by

SINTEF

CERTIFICATE OF CALIBRATION
FOR
THERMOMETERS

Certificate number : 233

Manufacturer, model :

Thermometer type : S

Identfication (s.no) : 3

Customer :

The total uncertainty assigned
to the measurements is : +/-0.9°C up to 1100°C +/-2.0°C above. (Stated as 2 standard deviations)

Test equipment used
in the calibration : Solartron Voltmeter 7061, Isotec Saturn Furnace, Ref TC SINTEF-1

The thermometers have been calibrated using standards whose accuracies are traceable to national and international standards, and the temperatures are determined in accordance to ITS-90.

Calibration temp.	Measured value	Calculated temp.	Deviation
°C	µV	°C	°C
1300.97	13172.30	1301.09	0.12
1100.86	10768.07	1100.97	0.11
900.41	8454.93	900.51	0.10

Additional information : The calibration is carried out by comparison
: against a laboratory reference thermocouple type S
:
:

23. januar 2008
Date of certification

Svend Grådahl
Svend Grådahl
Certified by

Appendix 2

Appendix 3: Statistical Evaluation of Material Resistivity and Contact Resistance

Material resistivity of graphite

A linear regression analysis of the material resistivity data for all the whole graphite shapes was performed for the temperature region 1000°C to 1600°C. This region was chosen since this is the region of main interest. From the graphs it seems as though this region is close to linear and the graphite furnace control is most stable in this temperature region. The variables are, as mentioned in Chapter 4, the cross section area A_{neck} at the neck of the sample and the temperature rounded to the nearest 10°C, T^*. The latter is done to get replicates and thus be able to asses the goodness of the fit through a *Lack of fit test*. The regression equation is shown in Equations (4.2) and (4.3). The variables in Equation (4.2) have been standardized so that the impact of the variables on ρ_m can be compared. The regression equations are given below.

$$\rho_m = 8.38 \cdot 10^{-6} - 1.03 \cdot 10^{-6} \cdot \underbrace{\frac{T^* - 1300}{300}}_{\text{Standardized variable}} - 1.11 \cdot 10^{-6} \cdot \underbrace{\frac{A_{neck} - 356 \cdot 10^{-6}}{344 \cdot 10^{-6}}}_{\text{Standardized variable}} \quad (4.2)$$

$$\rho_m = 5.05 \cdot 10^{-6} + 3.44 \cdot 10^{-9} \cdot T^* - 3.22 \cdot 10^{-3} \cdot A_{neck} \quad (4.3)$$

The table of coefficients, Table A3.1, gives the standard error of the coefficients and the T and P values for Equation (4.2). Except for the coefficient values, the table is identical for Equation (4.3). It can be seen that the P value is 0 for all of the predictors. P has values from 0 to 1, and describes the possibility that the null hypothesis is correct. A P value of 0.5 tells us that there is a 50 % probability that the tested hypothesis is wrong. A cut-off value of 0.05 is often used, saying that if a variable has a higher P value, the variable is insignificant, and should thus, in most cases, be excluded from the regression analysis. This value can, however, be raised. Based on the P values in Table A3.1 it can be

seen that both of the variables and the constant term are significant, i.e. the neck cross section diameter influences the material resistivity.

Table A3.1: Table of coefficients for Equation (4.2). All variables are significant.

Predictor	Coef	SE Coef	T	P
Constant	8.38E-06	1.40E-07	59.48	0.000
T^* (stand.)	1.03E-06	1.90E-07	5.55	0.000
A_{neck} (stand.)	-1.11E-06	1.50E-07	-7.21	0.000
$R^2 = 62.8\%$	R^2adj = 61.2%			

The analysis of variance table (ANOVA) for Equations (4.2) and (4.3) is shown in Table A3.2. Based on the P values, it can be seen that the regression is significant, and that there are no significant lack of fit.

Table A3.2: Analysis of variance table (ANOVA) for Equations (4.2) and (4.3).

Source	DF	SS	MS	F	P
Regression	2	8.21E-11	4.11E-11	41.30	0.000
Residual Error	49	4.87E-11	9.94E-13		
Lack of Fit	16	1.05E-11	6.55E-13	0.57	0.887
Pure Error	33	3.82E-11	1.16E-12		
Total	51	1.309E-10			

A possible apparatus drift was assessed using the graphite cylinders, which had 7 replicate runs throughout the experimental series. It was discovered that the resistivity of the first experiment was significantly higher compared to those of the 6 last runs. This is most likely due to the fact that the first was made from a different batch of graphite compared to the six last samples. The evaluation of the drift was done based on the six last experiments. The results, shown in Table A3.3, show that the run order is not significant, i.e. there is no statistically significant drift in the apparatus.

Table A3.3: The run order is not a significant variable when the analysis is done on the six last graphite ϕ30 mm cylinders, which were made from the same batch of graphite.

Predictor	Coef	SE Coef	T	P
Constant	6.45E-06	6.40E-07	10.00	0.000
T^* (stand.)	1.16E-06	2.50E-07	4.64	0.000
Run order(stand.)	6.97E-07	8.10E-07	0.86	0.400

$R^2 = 51.4\%$ $R^2adj = 56.8\%$

The material resistivity of metallurgical cokes

A statistical evaluation was also done for all the whole sample shapes of the SSAB and Zdzieszowice cokes. Corus was not included due to the limited number of parallel experiments. The linear regression was also performed in the temperature region 1000°C to 1600°C. The variables T^*, A_{neck}, and a dummy variable, *type*, describing the *type* of material, was used. The regression equation with standardized variables is shown in Equation (A3.1).

$$\rho_m = 138.3 \cdot 10^{-6} - 20.1 \cdot 10^{-6} \cdot \frac{T^* - 1300}{300} - 11.1 \cdot 10^{-6} \cdot \frac{A_{neck} - 360 \cdot 10^{-6}}{340 \cdot 10^{-6}} - 4.44 \cdot 10^{-6} \cdot type \quad \text{(A3.1)}$$

In Table A3.1 the standard error of the coefficients and the T and P value is given. It can be seen that the standard error of the variable *type* is almost as large as the coefficient itself. The large P value tells us that a variable is insignificant or the chance of an expression being insignificant, as in Table A3.5. From this we see that the variable *type* is insignificant. The regression should then be redone without *type*.

Table A3.4: Table of coefficients for Equation (A3.1). The predictors or variables are standardized! The variable *type* is insignificant.

Predictor	Coef	SE Coef	T	P
Constant	0.0001379	4.29E-06	32.15	0
T^* (stand.)	-2.011E-05	5.99E-06	-3.36	0.001
A_{neck} (stand.)	-1.112E-05	4.86E-06	-2.29	0.026
type	-4.44E-06	4.29E-06	-1.04	0.304

$R^2 = 22.70\%$ $R^2adj = 18.90\%$

In Table A3.5 the Analysis of variance table (ANOVA) for Equation (A3.1) is shown. From the P values it can be seen that the regression is significant, but that there is no significant Lack of fit. To perform a *Lack of fit* test there must be genuine replicates in the data set. In the data sets analyzed here, the temperature was rounded to the nearest 10°C to obtain this. The advantages of a *Lack of fit* test is that it is not as easily manipulated as R^2. R^2 will be perfect if the noise is added.

Table A3.5: Analysis of variance table for Equation (A3.1). There is no significant lack of fit.

Source	DF	SS	MS	F	P
Regression	3	2.06E-08	6.88E-09	5.97	0.001
Residual Error	61	7.03E-08	1.15E-09		
Lack of Fit	26	2.64E-08	1.01E-09	0.81	0.711
Pure Error	35	4.39E-08	1.25E-09		
Total	64	9.09E-08			

The regression was redone with only the two significant variables, T^* and A_{neck}. The coefficient table and the ANOVA of Equations (4.4) and (4.5) are identical, except for the coefficient values. Only the tables of Equation (4.4) are thus shown below.

$$\rho_m = 138.3 \cdot 10^{-6} - 20.2 \cdot 10^{-6} \cdot \frac{T^* - 1300}{300} - 3.22 \cdot 10^{-3} \cdot \frac{A_{neck} - 360 \cdot 10^{-6}}{340 \cdot 10^{-6}} \qquad (4.4)$$

$$\rho_m = 237 \cdot 10^{-6} - 67.3 \cdot 10^{-9} \cdot T^* - 30.4 \cdot 10^{-3} \cdot A_{neck} \qquad (4.5)$$

Table A3.6 shows that all the variables are significant.

Table A3.6: Table of coefficients for Equation (4.4). All variables are significant.

Predictor	Coef	SE Coef	T	P
Constant	1.38E-04	4.27E-06	32.37	0.000
T^* (stand.)	-2.02E-05	5.99E-06	-3.37	0.001
A_{neck} (stand.)	-1.03E-05	4.81E-06	-2.15	0.036

$R^2 = 21.3\%$ $R^2adj = 18.80\%$

The ANOVA of Equation (4.4) shows that the regression is significant and that there is no significant lack of fit, see Table A3.7.

Table A3.7: ANOVA for Equations (4.4) and (4.5). The regression is significant and there is no significant lack of fit.

Source	DF	SS	MS	F	P
Regression	2	1.94E-08	9.69E-09	8.40	0.001
Residual Error	62	7.15E-08	1.15E-09		
Lack of Fit	15	1.06E-08	7.05E-10	0.54	0.901
Pure Error	47	6.09E-08	1.30E-09		
Total	64	9.09E-08			

Due to the cross section area of the neck being a significant factor, the double cones cannot be included when the material resistivity is determined. A further analysis has been done where only the cylinders are included. This statistical evaluation also includes Corus coke, and a variable describing the properties of the material is thus included to separate the three metallurgical cokes. Ash, fixed carbon, ash and the L_c value is used, separately, to describe the difference between the three metallurgical cokes. d_{002} is not used, since there is hardly any variation between the three metallurgical cokes. The variables are standardized to vary between -1 and 1, as shown in Chapter 4. The regression analysis where the L_c value is used to represent the difference between the three cokes is shown in Equation (A3.2). $\overline{L_c}$ is the *standardized* L_c variable. In standardized variables, SSAB is 1, Corus is -0.43 and Zdzieszowice coke is -1, the L_c values being 24.34, 22.87 and 22.28, respectively.

$$\rho_m = 130 \cdot 10^{-6} - 14.2 \cdot 10^{-6} \cdot \frac{T^* - 1300}{300} - 1.97 \cdot 10^{-6} \cdot \overline{L_c} \qquad \text{(A3.2)}$$

In Table A3.8 the P value tells us that L_c is insignificant. None of the other variables that was tried as a representative of the properties of the cokes turned out to be significant.

Table A3.8: Table of coefficients for Equation (A3.2).

Predictor	Coef	SE Coef	T	P
Constant	1.31E-04	5.16E-06	25.28	0.000
T^* (stand.)	-1.42E-05	6.53E-06	-2.17	0.035
Lc (stand.)	-1.97E-06	6.09E-06	-0.32	0.748
$R^2 = 10.0\%$	$R^2adj = 5.9\%$			

In Table A3.9 the ANOVA for Equation (A3.2) is shown. The regression is barely not significant if a P value of 0.1 is chosen as the cut-off value, i.e. there is a 10 % probability that the regression is wrong. The lack of fit is not significant.

Table A3.9: ANOVA for Equation (A3.2). Both the regression and the lack of fit are not significant.

Source	DF	SS	MS	F	P
Regression	2	5.01E-09	2.50E-09	2.40	0.103
Residual Error	43	4.49E-08	1.04E-09		
Lack of Fit	13	9.69E-09	7.45E-10	0.64	0.805
Pure Error	30	3.52E-08	1.17E-09		
Total	45	4.988E-08			

Contact resistance of metallurgical cokes

A statistical analysis was done to see if 1) the neck size is significant and 2) if there are any significant difference between the types of metallurgical coke. Since the temperature region between 1000°C and 1600°C is the most interesting region concerning the conditions in the furnace, the lower

temperatures were excluded from the analyses. Corus coke was also excluded from the analysis due to only two experiments with no parallels being performed. To get replicates so that the *pure error* could be calculated and thus the *Lack of Fit* test could be done, the temperature was rounded to the nearest 10°C, as in the statistical analysis of the material resistivity data. T^* is used as the modified temperature. The *Holm's radius* used in the metal contact theory states that the contact resistance is proportional to the inverse diameter of the apparent contact area if the contact spots are evenly distributed within this area and there is no thin film, thus $R_c \propto 1/2\alpha$ (Timsit 1999). The *Holm's radius*, α, is here assumed to be equal to the radius of the apparent contact area, $d_{neck}/2$. A dummy variable represented the type of coke, +1 representing SSAB coke and -1 representing Zdzieszowice coke.

The result of the standardized regression equation is shown in Equation (4.6), and the uncoded result is shown in Equation (4.7). All the predictors shown are significant, as shown in Table A3.10, and that there is no significant Lack of Fit, see Table A3.11. It can be seen, from Equation (4.6), that the *type* of coke has less influence on the contact resistance than both the temperature and the Holm's radius, α.

$$R_c = 61.2 \cdot 10^{-3} - 31.4 \cdot 10^{-3} \cdot \frac{T^* - 1300}{300} + 21.7 \cdot 10^{-3} \cdot \frac{1/d_{neck} - 117}{142} + 4.5 \cdot 10^{-3} \cdot type \qquad (4.6)$$

$$R_c = 167 \cdot 10^{-3} - 105 \cdot 10^{-6} \cdot T^* + 260 \cdot 10^{-6} \cdot 1/d_{neck} + 4.50 \cdot 10^{-3} \cdot type \qquad (4.7)$$

Table A3.10: Table of coefficient of the standardized variables in Equation (4.6).

Predictor	**Coef**	**SE Coef**	**T**	**P**
Constant	0.061239	0.002316	26.44	0
T^* (stand.)	-0.031373	0.00265	-11.84	0
$1/d_{neck}$ (stand.)	0.021677	0.003138	6.91	0
type	0.004499	0.001943	2.32	0.025

$R^2 = 80.5\%$ $R^2adj = 79.3\%$

Table A3.11: ANOVA for regression equations (4.6) and (4.7)

Source	DF	SS	MS	F	P
Regression	3	4.18E-02	1.39E-02	68.81	0
Residual Error	50	1.01E-02	2.03E-04		
Lack of Fit	30	5.76E-03	1.92E-04	0.88	0.636
Pure Error	20	4.38E-03	2.19E-04		
Total	53	0.051955			

Appendix 4: The Four Point Measurement Technique

Measuring the resistance by using a traditional handheld module can introduce a series of errors to the measurements. The hand held units usually operate with a two point measurement technique, where the measurement is performed by attaching two wires to two points of the ends of an iron rod, as shown in Figure A4.1. A measurement current is supplied by a power source, in this case a direct current power source. From the voltage, U, and the current, I, a resistance, R, is determined. The resistivity of the iron ρ_{iron} can be calculated according to Equation (A4.1). The two point measurement method is easy and fast to use, but the disadvantage is that there are contact resistances, R_c, in the loop, one of which is indicated in Figure A4.1. This increases the R calculated from U and I, thus increasing the estimated resistivity, ρ_{iron}.

$$R = \int \frac{\rho_{\text{iron}}(h)}{A(h)} dh \tag{A4.1}$$

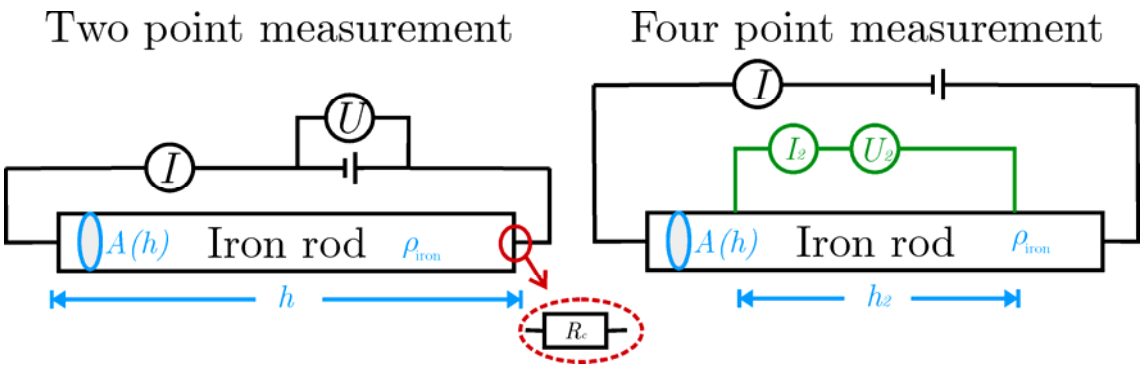

Figure A4.1: Electrical circuit diagrams illustrating the two and four point measurement technique, respectively.

The four point measurement has a measurement circuit (green) which is separate from the circuit that supplies the measurement current, I. Given that the voltage measurement is performed with a high resistance voltmeter, typically with a resistance of several MΩ, the current of the measurement circuit will be negligible, i.e. $I_2 \rightarrow 0$ A. The voltage drop over the sample is then

the only thing that will be measured, which is given by the iron rod and *not* the resistance of the measurement circuit. ρ_{iron} can then be calculated according to Equation (A4.1), but with R calculated as U_2/I, integrating over the distance between the two points of measurement, h_2.

Appendix 5: Charge Material Analyses

Two charge mixes were used in the one phase furnace experiments. One mix was used for the two FeMn experiments, where only the particle size range of the Corus coke was changed, and another set of both raw materials and mix was used for the SiMn experiment.

The charge mix used in the FeMn experiments is given in Chapter 6. The analyses of the Corus coke size fractions used are given in Chapter 3. The analysis of the ores, sinter and dolomite is given in Table A5.1.

The charge mix used for the SiMn experiment is also given in Chapter 6. The analysis of the raw materials, including the Corus coke, which was a different batch from the Corus coke used in the FeMn experiments, is given in Table A5.2.

Table A5.1: Chemical analysis of the ores and the dolomite used in the two FeMn experiments. All values are given as weight pct., dry basis.

Material	H2O	Mn	O_{Mn}	Fe	O_{Fe}	SiO2	P2O5	TiO2	C-Fix	C	XH2O	CO2	Al2O3
Comilog MMA	8.70	50.78	28.40	3.77	1.08	3.95	0.03	0.20			3.90	0.18	4.61
Comilog Sinter	1.80	56.65	19.98	3.71	1.06	8.54	0.28	0.29		0.18			7.14
Asman 46%	0.90	47.50	20.88	8.17	3.51	3.84	0.05	0.08				3.63	0.23
Dolomite	1.47					0.92	0.02			0.00	0.00	46.83	0.08

Material	MgO	CaO	BaO	K2O	Zn	Pb	Hg	Cd	Cu	B	Ni	S	Sum
Comilog MMA	0.18	0.12	0.15	0.82	$9.0 \cdot 10^{-3}$								106.9
Comilog Sinter	0.16	0.26	0.40	0.89	0.1200								101.5
Asman 46%	1.08	9.01	0.44	0.03	$1.0 \cdot 10^{-3}$					0.06			99.4
Dolomite	20.90	30.60	0.01	0.02	$2.0 \cdot 10^{-3}$	$35 \cdot 10^{-6}$	$0.5 \cdot 10^{-6}$	$37 \cdot 10^{-6}$	$120 \cdot 10^{-6}$	$190 \cdot 10^{-6}$	$2.7 \cdot 10^{-3}$	$4.5 \cdot 10^{-3}$	100.9

Table A5.2: The analyses of the charge materials used in the SiMn experiment. The values are given as weight pct.

Material	MnO2	MnO	Fe2O3	FeO	SiO2	P2O5	SO2	TiO2	Al2O3
CVRD Sinter	56.7	17.0	8.6	2.4	7.2	0.1	0.0	0.5	10.5
Asman	43.7	25.0	11.0	2.9	5.0	0.0	0.2	0.0	0.2
Quartz	0.0	0.0	0.1	0.0	98.8	0.0	0.0	0.0	0.7
Dolomite	0.0	0.0	0.1	0.0	0.0	0.0	0.0	0.0	0.1
Corus coke 5-20mm	0.0	0.0	0.4	0.2	6.5	0.0	0.0	0.1	3.4

Material	MgO	BaO	CaO	K2O	Fixed C	H2O	CO2	Volatiles	Total
CVRD Sinter	0.4	0.5	0.7	1.4	0.0	0.0	0.0	0.0	106.0
Asman	0.5	0.1	7.3	0.0	0.0	0.0	4.9	0.0	100.8
Quartz	0.0	0.0	0.0	0.0	0.0	0.2	0.0	0.0	99.8
Dolomite	20.4	0.0	30.1	0.0	0.0	0.0	51.0	0.0	101.7
Corus coke 5-20mm	0.0	0.0	0.4	0.1	83.1	0.0	0.0	1.3	95.5

Appendix 6: Bulk Resistivity T_{room}-1600°C

In this appendix the bulk resistivity measurements from room temperature to 1600°C is presented. In Chapter 5, where the bulk resistivity measurements are presented, the main focus is the temperature region above 1000°C, due to it's relevance in the aspect of the industrial coke bed.

In Figure A6-1 the measured bulk resistivity of the four SSAB coke size fractions are shown. The hump is quite marked for all the experiments.

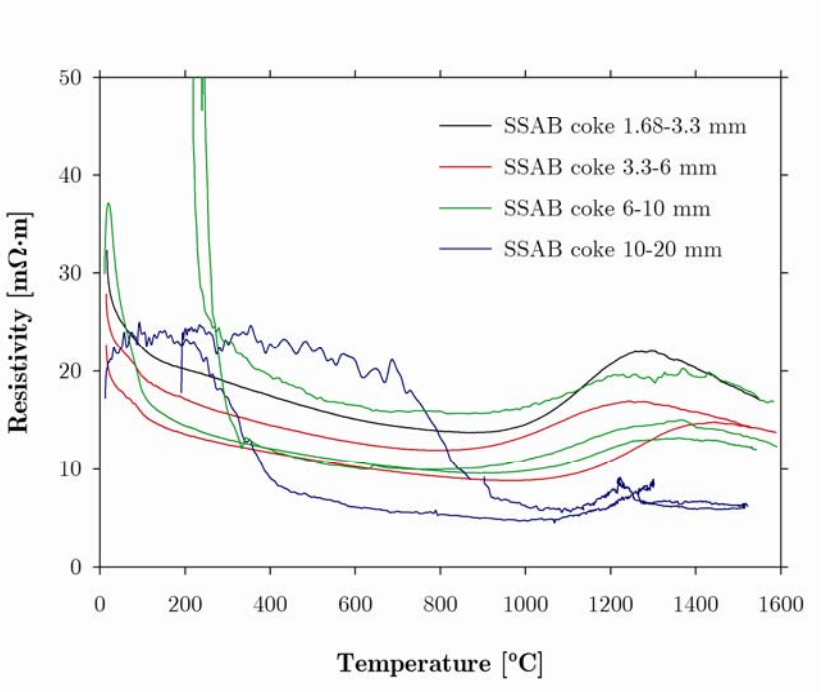

Figure A6-1: Bulk resistivity of the SSAB coke size fractions.

In Figure A6-2 the measured bulk resistivity of Magnitogorsk, Zdzieszowice and Corus metallurgical cokes are shown. For the Zdzieszowice coke experiments the furnace power has been switched off at approximately 700°C so that temperature gradients would equalize. The furnace stop is the reason for the break in the curve.

The hump is not as significant for the Magnitogorsk and the Corus coke as for the Zdzieszowice coke.

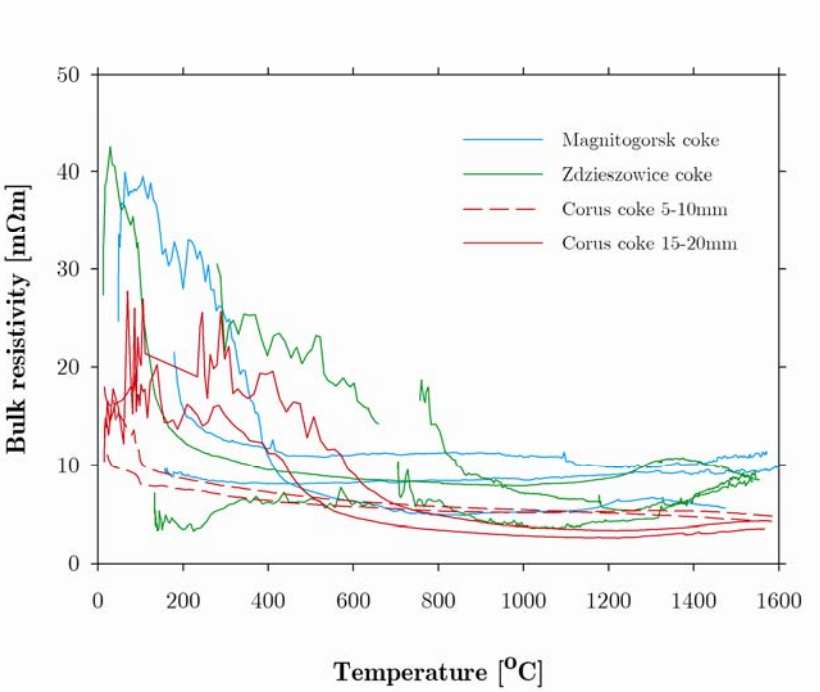

Figure A6-2: Measured bulk resistivity of the Magnitogorsk, Zdzieszowice and Corus metallurgical cokes. Two size fractions of Corus coke were tested.

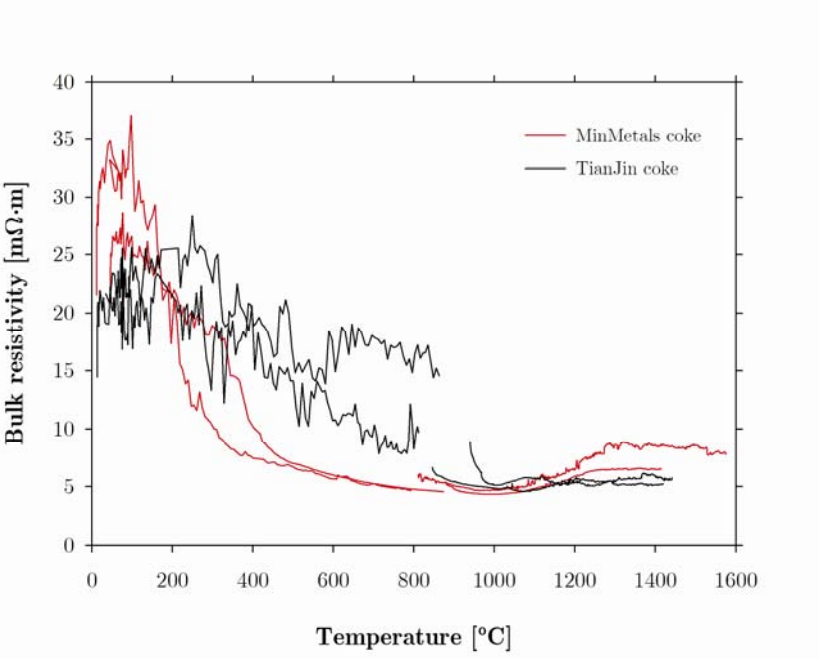

Figure A6-3: Bulk resistivity measurements of the MinMetal and TianJin metallurgical cokes.

In Figure A6-3 the bulk resistivity measurements of the MinMetal and TianJin metallurgical cokes are shown. The measurements are quite unstable up to approximately 800°C for the TianJin coke. The power was then turned off to allow the temperature gradients to equalize. After the power is turned on again, the measurements are more stable.

The hump is observed for both the TianJin and the MinMetal cokes.

In Figure A6-4 the bulk resistivity measurements of the Vietnamese and Siberian anthracites and the Chalmette and Marietta petroleum and sponge petroleum cokes are shown. The decrease in bulk resistivity with increasing temperature is steeper compared to the metallurgical cokes. This is, however, not observed for the calcined Marietta sponge petroleum coke. This indicates that the high bulk resistivity at lower temperatures may be due to the volatile content.

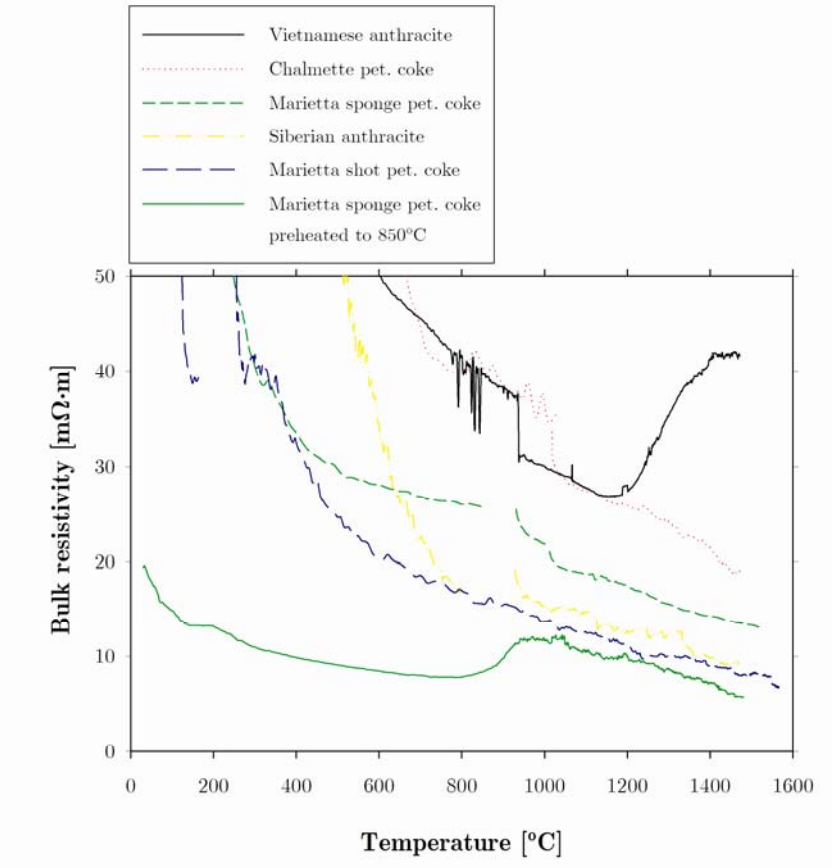

Figure A6-4: Bulk resistivity measurements of petroleum cokes and anthracites.